UNIVERSITY OF BIRMINGHAM

BIO-MECHANICAL BEHAVIOUR OF ARTICULAR CARTILAGE: CHARACTERISATION OF SURFACE DAMAGE, FRICTION AND REPLACEMENT

by

HUMAIRA MAHMOOD

A thesis submitted to
University of Birmingham
for the degree of
DOCTOR OF PHILOSOPHY

School of Engineering
Department of Mechanical Engineering
University of Birmingham
April 2020

ABSTRACT

The progression of cartilage damage has the potential to develop into the joint disease of osteoarthritis. Cartilage repair methodologies involve the implementation of biomaterials, for which the bio-mechanical characteristics should closely align with articular cartilage. To date, the frictional torque of articular cartilage has not been assessed, nor has the coefficient of friction of replacement biomaterials inserted within a defect. Additionally, cartilage damage inducing factors have not been considered for a likely dual effect.

Consequently, this thesis presents three novel developments to fulfil the lack of knowledge outlined above. The first novel outcome is the assessment of the dual impact of loading frequency and underlying substrate density, as a replication of bone mineral density, on resulting cartilage damage. The second novel development is a technique to determine the frictional torque of articular cartilage, corresponding to an inserted cartilage replacement biomaterial. The third novel development is a technique to assess the coefficient of friction of a cartilage replacement biomaterial, in line with osteochondral graft surgical procedures. Various approaches have been implemented to include three materials testing machines, Hertzian contact stress analysis and chemical hydrogel manufacture. For this thesis, bovine articular cartilage was modelled for human articular cartilage.

The results demonstrate significant cartilage off-bone damage with the multi-factorial effect of a loading frequency of 10 Hz, in combination with an increase in substrate density ($p < 0.05$). The torque range and characteristics have been identified for which a cartilage replacement biomaterial should adopt, followed by the prospect to assess the coefficient of friction of a biomaterial amongst a defect. The work presented in this thesis has implications on the contribution to osteoarthritis and the manufacture of cartilage replacement biomaterials.

.

ACKNOWLEDGEMENTS

I would like to begin with acknowledging and thanking my supervisors both Professor Duncan Shepherd and Dr Daniel Espino, for providing me the opportunity to accomplish the advanced outcome complied in this thesis. Their consistent ongoing guidance, support and expertise resulted in the successful achievement of the work presented.

I would like to thank the technical staff of the Mechanical Engineering department at the University of Birmingham, Mr Lee Gauntlett and Mr Peter Thornton, for manufacturing the components required for the experimental work of this thesis.

In addition, thanks to the Biomedical Engineering Research Group of the Mechanical Engineering department at the University of Birmingham, for the available advice as and when required.

Finally, I would like to thank my family for their continuous kind support and advice throughout my doctorate.

NOVEL ACADEMIC CONTRIBUTIONS

International Peer-reviewed Journal Publications

Mahmood H, Shepherd DET, Espino DM. Surface damage of bovine articular cartilage-off-bone: the effect of variations in underlying substrate and frequency. *BMC Musculoskeletal Disorders.* 2018;19:384-94.

Mahmood H, Eckold D, Stead I, Shepherd DET, Espino DM, Dearn KD. A method for the assessment of the coefficient of friction of articular cartilage and a replacement biomaterial. *Journal of the Mechanical Behaviour of Biomedical Materials*. 2020;103:103580

Mahmood H, Shepherd DET, Espino DM. A technique for measuring the frictional torque of articular cartilage and replacement biomaterials. *Medical Engineering and Physics*. 2020. *Accepted with revisions*

International and National Conference Presentations

H Mahmood, DET Shepherd, DM Espino. 2018. The surface failure of articular cartilage following variation in substrate density. *8th World Congress of Biomechanics, Dublin, Ireland.*

H Mahmood, DET Shepherd, DM Espino. 2018. Alterations in the underlying material density on the surface damage of bovine articular cartilage. *BioMedEng 18 Conference, Imperial College London, United Kingdom.*

TABLE OF CONTENTS

LIST OF FIGURES

LIST OF TABLES

ACRONYMS

OA…… Osteoarthritis

ECM…… Extracellular Matrix

DMA…… Dynamic Mechanical Analysis

BMD…… Bone Mineral Density

OP…… Osteoporosis

TJR…… Total Joint Replacement

ACI……Autologous Chondrocyte Implantation

HA…… Hyaluronic Acid

MSCs …… Mesenchymal Stem Cells

MeGC…… Methacrylated Gycol Chitosan

C-C…… Cartilage-Cartilage

C-G…… Cartilage/hydrogel-Cartilage

C-M…… Cartilage-Aluminium

IQR……Interquartile Range

PVA…… Polyvinyl Alcohol

1 INTRODUCTION

Articular cartilage is a highly specialised connective tissue to allow for the transmission of load during articulation (Fox *et al*., 2009). Damage to articular cartilage, if untreated, is known to progress into early osteoarthritis (OA), reported as complex and difficult to treat (Bhosale and Richardson, 2008). Several factors are addressed in literature for the association with cartilage damage, to include frequency and the condition of the underlying subchondral bone. The enhancement of the application of loading frequency has shown to advance cartilage damage, through increased crack propagation (Sadeghi *et al.,* 2018), as well as increased crack dimensions (Sadeghi *et al*., 2015). Additionally, the stiffened nature of the subchondral bone relates to cartilage damage (Radin *et al*., 1972), further reinforced by an inverse relationship between the condition of OA and osteoporosis (OP). The definition of OP is detailed as a skeletal disorder of the compromise of bone strength, leading to increased risk of fracture (Consensus Development Panel, 2001).

It is essential to consider such damage inducing factors, to enable the control of the initiation and progression of cartilage damage. Although the literature has presented various contributing factors to cartilage damage, the effects are assessed on a single basis, rather than as a multi-factorial evaluation on respective tissue damage. As a consequence of OA, surface fibrillation (Cooke *et al*., 2018) and fissures are experienced by the tissue, to include an irregular tidemark of the extracellular matrix (ECM), with enhanced blood vessels (Athanasiou, 2013). OA is further described by the correlation between biomechanical and biological factors (Pearle *et al*., 2005). This relationship is described by the process of cartilage damage, to initiate from silent alterations to the tissue, followed by a negative impact on the overall mechanical properties as a result of the destruction to the ECM (Athanasiou, 2013). The challenges associated with the repair of damaged cartilage relate towards the non-vascularised and limited capacity for self-repair of the tissue (Karuppal, 2017).

Bioengineering techniques have been implemented for the replacement of articular cartilage, particularly the use of biomaterials (Ansari and Eshghanmalek, 2019). For the design of an effective cartilage replacement biomaterial, the behaviour should closely mimic that of the tissue. Hence, it is crucial to assess the mechanical performance of the biomaterial in relation to that of articular cartilage, whilst subject to identical testing configurations.

A prominent function of articular cartilage is the maintenance of a joint articulating environment with a low coefficient of friction (Fox *et al.,* 2009). Therefore, the developed biomaterial should closely coincide with the low frictional properties of the tissue. Whilst the literature has addressed the effect of various factors on the coefficient of friction of articular cartilage (Drewniak *et al.,* 2012; Li *et al.,* 2010), the behaviour of articular cartilage subject to a rotational configuration remains limited in knowledge. Additionally, for the understanding of the frictional behaviour of a potential replacement biomaterial, literature determines the interaction with articular cartilage itself (Li *et al*., 2016). However, it remains unknown as to how a potential replacement biomaterial behaves on insertion within a cartilage defect, in articulation against articular cartilage, itself.

Consequently, the aim of this study was to characterise the surface failure of articular cartilage, followed by the development of novel techniques for the assessment in friction, of both cartilage and potential replacement biomaterials. The specific objectives were as follows:

1) Evaluate the dual effect of two damage inducing factors, that of frequency and bone mineral density on corresponding cartilage damage.
2) Design an innovative technique for the evaluation of the frictional torque for both articular cartilage and a replacement biomaterial.
3) Design an innovative technique for the assessment of the coefficient of friction of a replacement biomaterial incorporated within a cartilage defect, against articular cartilage, itself.

To fulfil the three aims outlined above, this thesis presents new knowledge that has been learned as the solution. For aim 1), the loading frequency and substrate density used as a surrogate for bone mineral density, has been assessed for the effect on cartilage damage. It has been discovered that a combination of a loading frequency at 10 Hz only, with an increase in substrate density, is required for significant off-bone cartilage damage. Further tested frequencies have failed to show significant cartilage damage, both on- and off-bone, in combination with substrate density.

For aim 2), a new technique has been developed to effectively assess the frictional torque of articular cartilage and a replacement biomaterial. Three test set-ups have been established for this technique, to include the torque assessment of articular cartilage alone, in combination with the inserted biomaterial, as well as of the biomaterial itself. The unknown range of the torque magnitude for articular cartilage has been discovered as 0.08 to 0.11 N m and 0.06 to 0.08 N m, using two analysis methods, respectively. This technique can be used as the baseline for future studies that assess the frictional torque of articular cartilage, in comparison to that of a potential cartilage replacement biomaterial.

For aim 3), a new technique has been developed to assess the coefficient of friction of a cartilage replacement biomaterial incorporated within a defect. The new knowledge gained from this technique is the ability to explore the unknown coefficient of friction between the inserted biomaterial amongst articular cartilage, in sliding against articular cartilage itself. This technique can be used as the baseline for future studies that assess the coefficient of friction of cartilage replacement biomaterials incorporated within a defect.

To summarise the novel discoveries obtained from this thesis, the publications and presentations are listed in the ‘Novel Academic Contributions’ section.

1.1 Thesis Overview

Chapter 2 outlines the background information required to understand the subsequent chapters in this thesis. The background details the bio-mechanical properties of articular cartilage, failure properties, the behaviour in friction, as well as the implementation of the use of biomaterials for the repair of damaged cartilage, focusing on the use of alginate. Several studies on the various works of articular cartilage are addressed in this section, to include critical assessment.

Chapter 3 details the design of an innovative study for the multi-factorial assessment of the effect of substrate density and frequency, on the associated surface damage to articular cartilage. Two techniques are presented in this chapter, to include experimental and Hertzian contact. The chapter is based on the work published in *BMC Musculoskeletal Disorders* titled – 'Surface damage of bovine articular cartilage-off-bone: the effect of variations in underlying substrate and frequency'; 2018, Volume Number 19, Pages 384 – 394. This work was also presented at both the World Congress of Biomechanics, Dublin, 2018, as well as the BioMedEng meeting, at Imperial College London, 2018.

Chapter 4 details the design of an innovative technique for the assessment of the unknown frictional torque of articular cartilage, and potential replacement biomaterials. In this chapter, the resulting torque was assessed in response to a varied load, whilst an identical testing configuration was performed on both articular cartilage and a calcium alginate hydrogel. The study in this chapter is based on the work accepted with revisions in *Medical Engineering and Physics* titled 'A technique for measuring the frictional torque of articular cartilage and replacement biomaterials'.

Chapter 5 details the design of a second innovative technique. The work presented in this chapter illustrates the novel evaluation of the coefficient of friction of articular cartilage and replacement biomaterials, whilst a sample calcium alginate biomaterial is incorporated within

a surface defect. This chapter is based on the work published in the *Journal of the Mechanical Behaviour of Biomedical Materials* titled - ‘A method for the assessment of the coefficient of friction of articular cartilage and a replacement biomaterial’; 2020, Volume Number 103, Page 103580.

Chapter 6 outlines the overall discussion, to include future work and conclusions.

2 BACKGROUND

2.1 Chapter Introduction

This chapter discusses the tissue of hyaline articular cartilage, as the principal focus for the biomechanical exploration presented in this thesis. To begin, a background is provided on subchondral bone in Section 2.2. Following this, the structure, composition and function of articular cartilage is described in Section 2.3, in joints and on a micro scale. The friction and various lubrication mechanisms of articular cartilage followed by the discussion of the gait-cycle and the Stribeck curve, are outlined in Section 2.4. Various experimental approaches to assess the bio-mechanical properties of articular cartilage are discussed in Section 2.5, to further include the material properties, failure properties and frictional properties. Section 2.6 outlines the clinical implications of cartilage damage. This is followed by a discussion of the use of biomaterials for cartilage repair in Section 2.7, with a focus on the use of alginate.

2.2 Subchondral bone

The subchondral bone is formed of two distinct regions. This includes the subchondral bone plate which acts as the compact bone segment. The second region is the trabecular bone (Stewart and Kawcak, 2018). The two regions give a varied architecture to the subchondral bone (Stewart and Kawcak, 2018), as well as varied mechanical properties from rigid to elastic (Mcllwraith, 2016). The thickness of the subchondral bone plate differs depending on the location, typically ranging from 10 µm to 3 mm below the tibial plateau centre (Mcllwraith, 2016). The thickened region beneath the tibial plateau is concentrated with osteons. This in contrast to the thinner bone formed of appositional layers consisting of trabeculae, with minimal haversian canals (Clark and Huber, 1990).

The alteration to the architecture of bone is described by Wolff's law, on application to loading (Frost, 1994). The mechanics of Wolff's law is defined by the process of bone remodelling on a load increase, or a shift in the homeostatic mechanisms towards the catabolic

state, with a load decrease (Teichtahl *et al*., 2015). The process of bone remodelling is comprised of three phases; resorption of old bone digestion by osteoblasts, reversal when mononuclear cells are observed on the surface, followed by formation of new bone by osteoblast action (Hadjidakis and Androulakis, 2006). The outcome of the bone remodelling process results in a thickened compact bone (Mcllwraith, 2016).

The subchondral bone is connected to overlying articular cartilage, which it supports. The connection is formed through a layer of calcified cartilage (Mcllwraith, 2016). This leads onto the discussion of hyaline articular cartilage in the next section.

2.3 Hyaline Articular Cartilage

2.3.1 Hyaline Cartilage in Joints

Hyaline articular cartilage is located at the bone ends with the prominent function of enabling minimal friction at the bearing surface ends during movement (Wang and Ateshian, 1997). The value reported in the literature for the coefficient of friction of articular cartilage is as low as 0.003, measured in sliding against glass in a linear reciprocating manner, of sliding velocity 1 mm/s at 1 Hz, of an initial offset load at 4.5 N (Krishnan *et al.,* 2004). This friction measurement was determined on intact bovine articular cartilage cylindrical plugs, with a diameter of 4.8 mm (Krishnan *et al.,* 2004). The underlying bone was removed from the deep zone of the specimens, resulting in a final thickness of 2.1 ± 0.43 mm (Krishnan *et al.,* 2004). Additionally, the existence of macromolecules such as lubricin (Flannery, 2015), a boundary lubricant, is known to maintain the low frictional behaviour of articular cartilage during motion (Jay and Waller, 2014). Cartilage typically has a surface roughness of 80-170 nm (Ghosh *et al.,* 2013). This is to create an environment resistant to wear (Wang and Ateshian, 1997), further associated with a load-bearing ability (Steinert *et al.,* 2007), enabling efficient gliding kinetics during joint movement (Houard *et al*., 2013).

The tissue is composed of a collagen fibre extracellular matrix (ECM) surrounded by a highly hydrated gel (Hukins *et al*., 1985). Subsection 2.2.2 of this chapter provides a detailed breakdown of the various components of the ECM of articular cartilage. In addition, articular cartilage is known for its behaviour as a viscoelastic material (Parsons and Black, 1977), given by the definition of a material displaying both viscous and elastic characteristics, whilst subject to a deformation. Section 2.5 of this chapter provides further analysis of the studies performed to evaluate the viscoelasticity of articular cartilage.

Articular cartilage can be identified by its smooth, shiny glossy appearance (Paterson *et al.,* 2015), as illustrated by the zoomed in segment of a bovine humeral head in Figure 2.1. Articular cartilage functions amongst the synovial joint. The synovial joint is surrounded by an articular capsule which contains the joint cavity, filled with synovial fluid, whilst a thin layer of articular cartilage aligns the bone ends (Betts, 2019) (Figure 2.2). There are six known variations of the synovial joint, to include pivot, hinge, condyloid, saddle, plane and ball-and socket (Betts, 2019) (Figure 2.3).

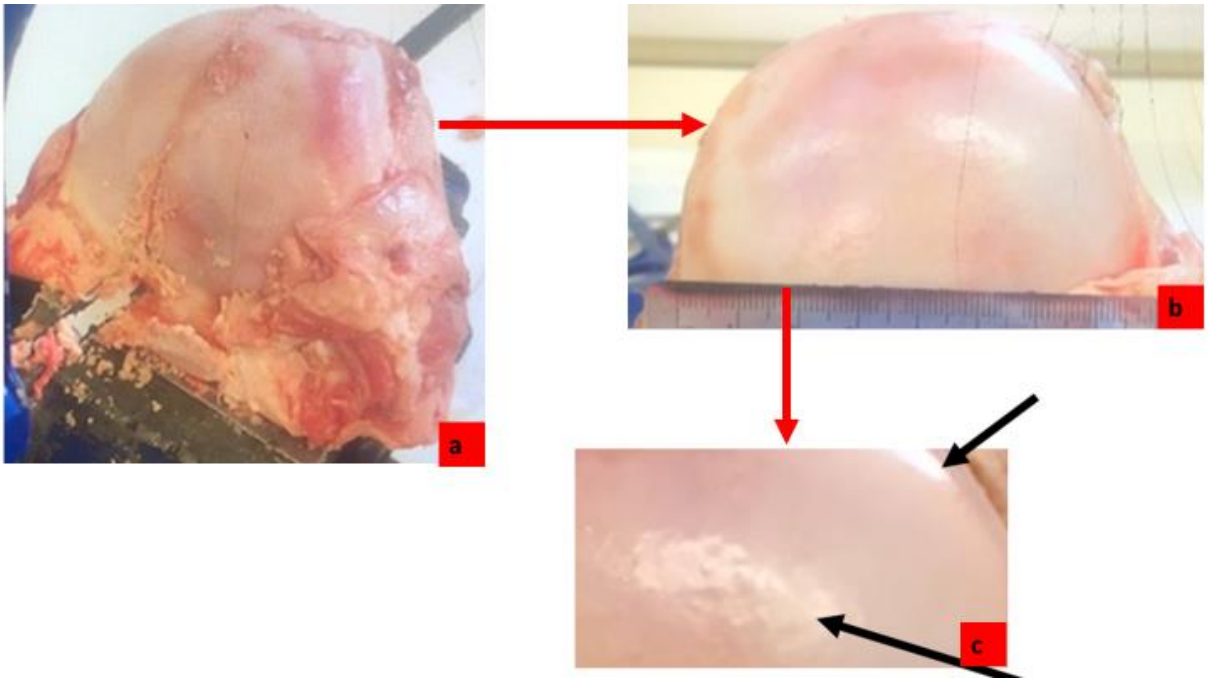

Figure 2.1: Photographic illustration to display the shiny and glossy appearance as outlined with the black arrows on the zoomed in segment of a bovine humeral head in part c). The site is zoomed in from the humeral head joint displayed in part a), zoomed further in part b).

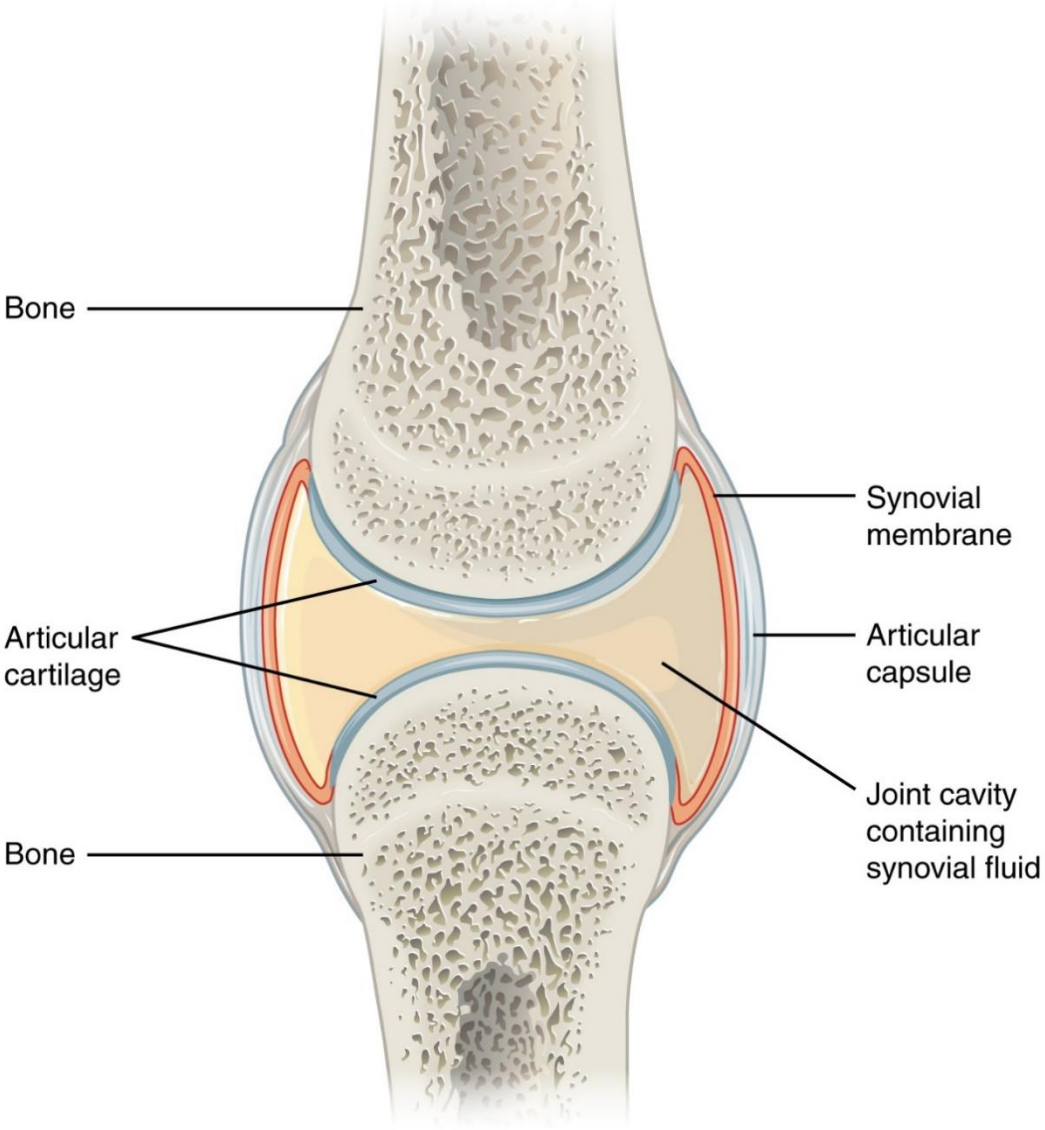

Figure 2.2: Illustration of the synovial joint. The articular cartilage is found to align the surface of two bone ends within a joint cavity, surrounded by synovial fluid, aligned by a synovial membrane. This entire segment is known as the articular capsule. (Reproduced from BC Open Textbook; Betts, 2019, which is distributed under the terms of the Creative Commons Attribution 4.0 International License (http://creativecommons.org/licenses/by/4.0/), which permits unrestricted use, distribution, and reproduction in any medium)

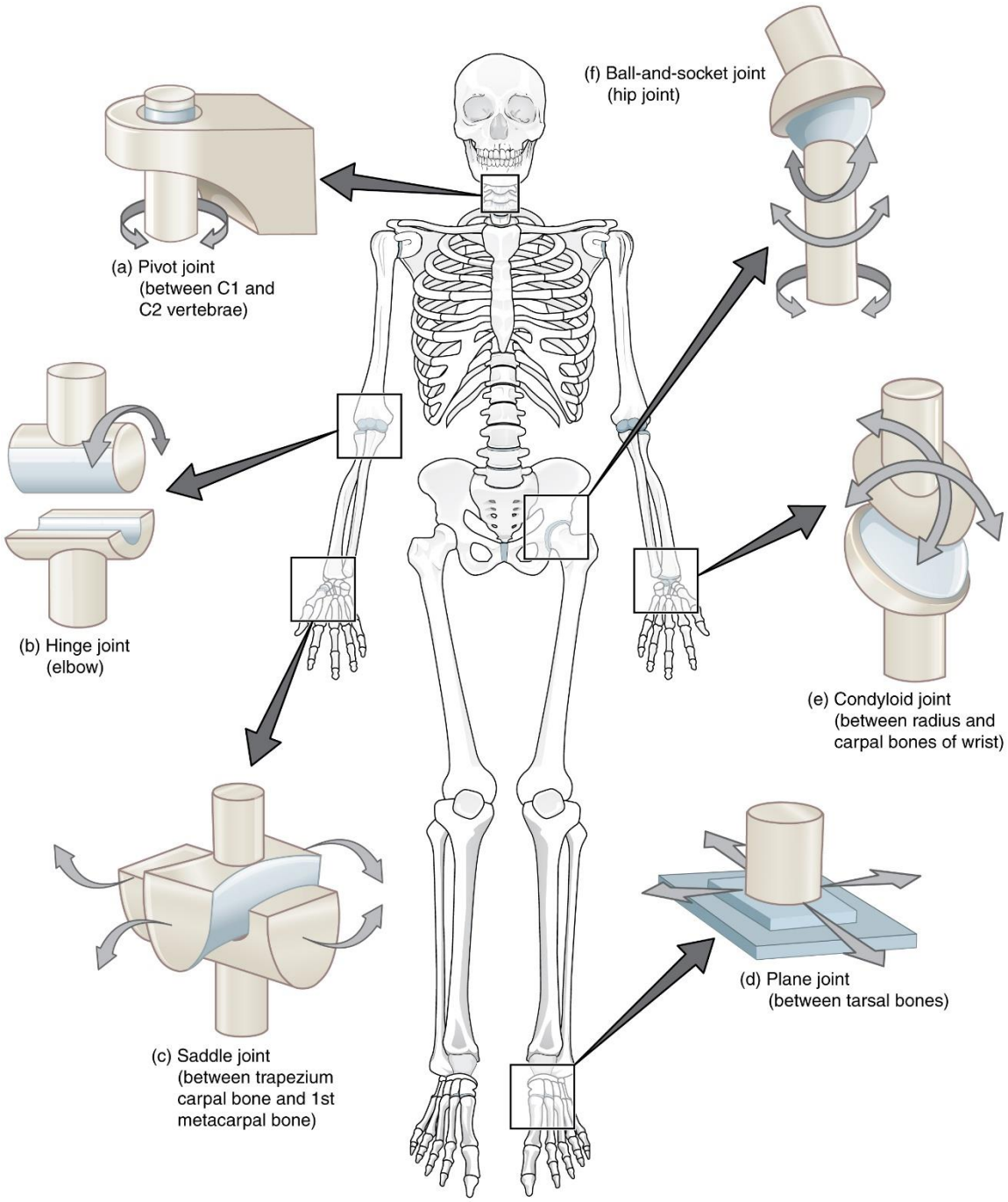

Figure 2.3: The six types of synovial joints. a) pivot joint allows for rotation around the axis such as side rotation of the head b) hinge joint works in accordance to a door hinge, such as the kinetic of the elbow c) saddle joint such as the base of the thumb articulation, d) plane joints such as between the bones of the feet, e) radiocarpal joint such as that located in the wrist and f) ball-and-socket joints located in the hip and shoulder only. (Reproduced from BC Open Textbook; Betts, 2019, which is distributed under the terms of the Creative Commons Attribution 4.0 International License (http://creativecommons.org/licenses/by/4.0/), which permits unrestricted use, distribution, and reproduction in any medium)

2.3.2 Microstructure

The structure of articular cartilage can be described by the corresponding zonal variations (Jeffery *et al.,* 1991), represented by the various constituents and layout amongst the ECM. This initiates at the superficial zone articulating surface, the transition zone (Kaab *et al.,* 1998), middle zone and through to the deep and underlying subchondral bone, at the calcified zone (Fox *et al.,* 2009). Articular cartilage prominently consists of approximately 70-80% water by weight, with solid constituents of the tissue includes collagen (50%-75%) and proteoglycans (15%-30%) (Athanasiou, 2013). Highly specialised cells specific to articular cartilage, known as chondrocytes (Tarafder and Lee, 2016) constitute a 2% of the overall tissue volume (Alford and Cole, 2005), whilst noncollagenous proteins and glycoproteins compose the outstanding areas (Fox *et al.,* 2009). Type II collagen represents 90%-95% of the collagen in the tissue (Fox *et al.,* 2009), characterised as the major collagen type (Alford and Cole, 2005).

The superficial zone contributes to approximately 10%-20% of the overall human cartilage tissue (Athanasiou, 2013). It has been reported that the relative thickness of this zone differs for other species, such as a thinner layer of approximately 3%-4% in rabbits (Kaab *et al*., 1998). This segment of the ECM is the closest to the synovial fluid, maintaining the tensile properties in particular of the tissue, to act in accordance with external forces of shear, tension and compression to the joint (Fox *et al.,* 2009). Specific to this zone, the collagen fibres tend to align in a parallel orientation to the articular surface (Figure 2.4a) (Hukins *et al.*, 1984), whilst the high quantity of chondrocytes are tightly packed in a manner also parallel to the upper cartilage surface (Figure 2.4a) (Fox *et al.,* 2009). The chondrocytes present in the superficial zone are known to have a disc shape or “leaf-like morphology”, (Figure 2.4b), whilst the chondrocytes in deeper zones are known to adopt spherical configurations (Mansfield *et al.*, 2015). Additionally, the leaf-like arrangement is also reported for the collagen fibres in the superficial zone (Kaab *et al.,* 1998). The chondrocytes are found within a pericellular matrix

(Figure 2.4c), also known to contain elastin (Mansfield *et al*., 2009). The superficial chondrocytes have further demonstrated a larger instantaneous modulus of 0.55 kPa, in comparison to 0.29 kPa of the chondrocytes present in the middle and deep zones (Darling *et al.,* 2006).

The transition zone is found directly beneath the superficial zone. The transition zone contains fewer spheroid-shaped chondrocyte cells with larger diameter collagen fibres (Figure 2.4a) (Bhosale and Richardson, 2008), known to adopt a leaf-like arrangement of a curved nature, as illustrated by freeze-fracture of human cartilage in previous work (Figure 2.5) (Kaab *et al*., 1998).

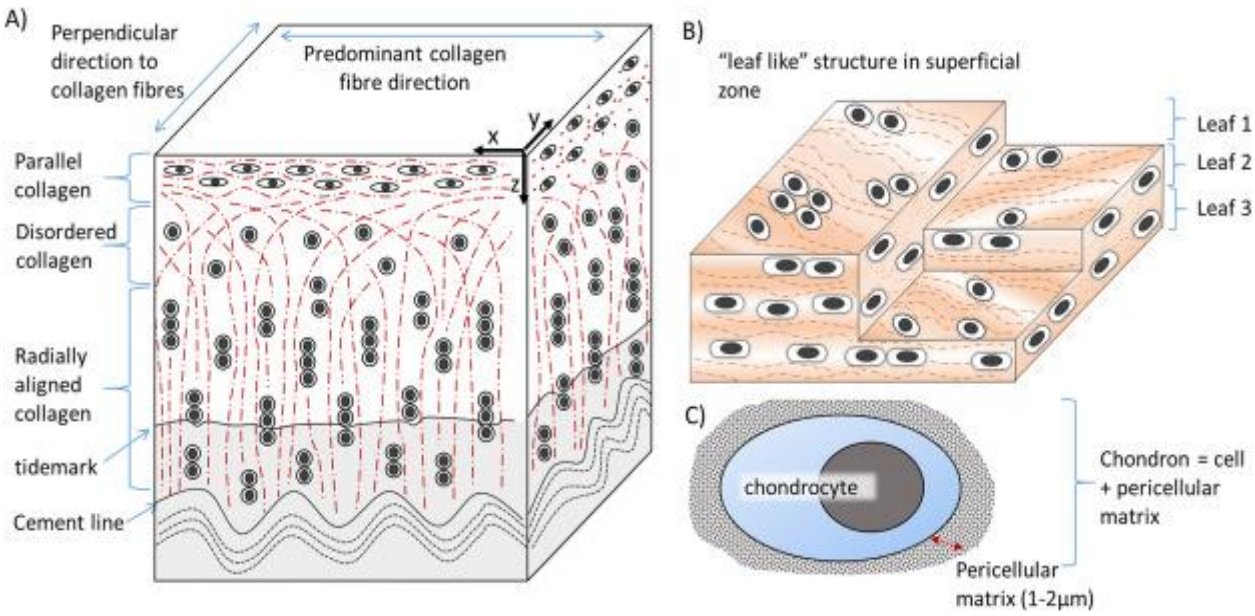

Figure 2.4: Illustration of the components of the extracellular matrix of articular cartilage. A) represents the variation in the layout of the chondrocytes shown by the black shapes and collagen fibres shown by the red dotted lines, found within the various zones of the extracellular matrix. The superficial zone is located at the upper surface, followed by the transitional zone directly beneath. The middle zone is then represented, followed by the deep zone and finally the calcified zone at the tidemark. B) The representation of the leaf-like structure of the chondrocytes observed at the surface superficial zone, followed by C) as the illustration of the chondron to contain the chondrocyte and the surrounding pericellular matrix. (Reprinted from 'The micromechanics of the superficial zone of articular cartilage', volume 23, J.C. Mansfield, J.S. Bell and C.P. Winlove, pp 1806-1816, 2015, with permission from Elsevier)

The middle zone contributes to ~40%-60% of the overall human cartilage tissue thickness (Athanasiou, 2013), to include chondrocytes of a lower amount to that of the upper superficial zone (Fox *et al.,* 2009). The collagen fibres in the middle zone are known to bend towards a perpendicular orientation, with respect to the surface (Figure 2.4a) (Julkunen *et al*., 2010), as further illustrated by the freeze-fracture imaging in Figure 2.5 (Kaab *et al*., 1998). The middle zone is known for the initial provision of the opposition to external compressive forces to a joint (Fox *et al*., 2009).

The deep zone provides the utmost opposition to external compressive forces, aided by an organised layout of collagen fibres aligned in a perpendicular manner to the joint surface (Figure 2.4a) (Julkunen *et al*., 2010), of a leaf-like arrangement (Kaab *et al.,* 1998). Whilst this segment of the ECM contributes to approximately 20%-50% of the overall human cartilage tissue (Athanasiou, 2013), the chondrocytes adopt a column-like configuration of a similar parallel alignment to the collagen fibres, and of a perpendicular arrangement to the upper cartilage surface (Fox *et al*., 2009) (Figure 2.4a).

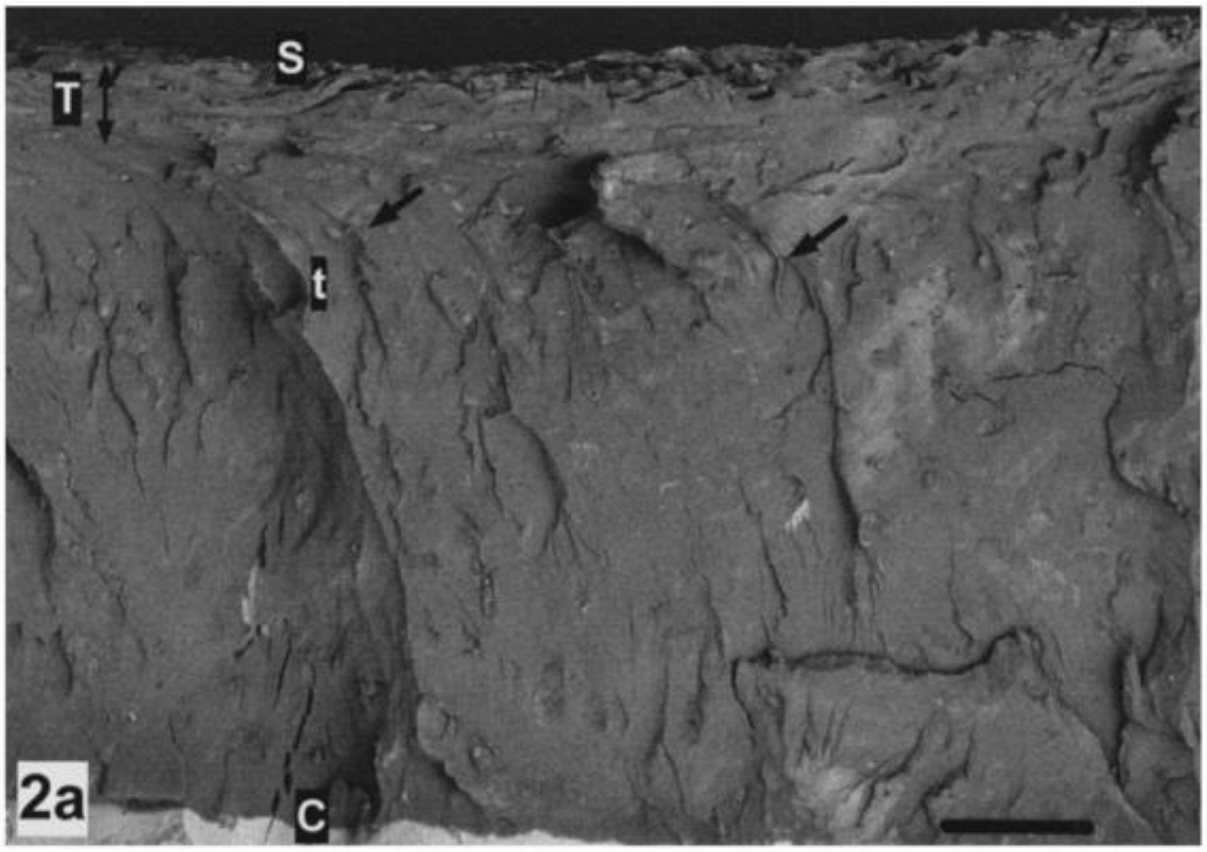

Figure 2.5: The freeze-fracture image of human cartilage to identify the arrangement of the collagen fibres in the various zones of the extracellular matrix. The superficial zone, 'S', displays fibres aligned in a parallel orientation to the surface, whilst the transition zone, 't' displays fibres that are curved towards the perpendicular direction, therefore leading to fibres aligned in the perpendicular direction to the cartilage surface in the middle zone, further identifying the collagen fibres in the calcified zone, 'C', referred to as leaves. (Reprinted from Collagen fibre arrangement in the tibial plateau articular cartilage of man and other mammalian species, volume 193, M.J. Kaab, I. AP. Gwynn and H.P. Notzli, pp 23-34, 1998, with permission from John Wiley and Sons)

The calcified zone of articular cartilage provides the attachment of cartilage to bone of which the "tidemark" differentiates between the junctions (Oegema *et al*., 1997). The prominent function of the calcified zone is to allow for the attachment of the articular cartilage to the underlying subchondral bone, via the anchorage of the collagen fibres (Fox *et al.,* 2009) (Figure 2.5). This is to enable the reduction in the varied gradient of stiffness amongst the bone and articular cartilage (Radin and Rose 1986).

A further three categories are used to describe the ECM. This includes the pericellular, territorial and interterritorial regions (Fox *et al.,* 2009). As described, the pericellular matrix

encompasses the chondrocyte (Mansfield *et al.*, 2015) to prominently contain proteoglycans and glycoproteins, whilst the territorial zone contains the pericellular zone (Guilak and Mow, 2000). The interterritorial zone exceeds in size in comparison to both the pericellular and territorial regions, acting as the major contributor to the biomechanical performance of the tissue (Guilak and Mow, 2000).

2.4 Friction and Lubrication Mechanisms

As highlighted in Section 2.3, a prominent function of articular cartilage is to allow for a minimal coefficient of friction at the bearing surface of the joint ends in contact. The low coefficient of friction of articular cartilage is associated with various lubrication methods (Jin and Dowson, 2013; McNary *et al*., 2012), dependent upon fluid forces due to synovial fluid pressure determined by joint motion (McNary *et al*., 2012). This is further reinforced by the normal and tangential forces acting upon the tissue, in accordance with time periods of loading and joint motion determined by the chemical and physical behaviour of the fluid (Forster and Fisher, 1996; Schmidt and Sah, 2007). Various lubrication mechanisms have been reported for articular cartilage, as outlined in the following subsections, which are important to consider for the understanding of the low frictional characteristic. In the following subsections, the lubrication mechanisms during the gait-cycle are also assessed, followed by the application of the Stribeck curve for analysis of the lubricant type present within a system.

2.4.1 Boundary Lubrication

The boundary lubrication mechanism of articular cartilage is defined as the mechanism of ‘molecular protection’ (Schmidt and Sah, 2007), where lubricant molecules within a surface film at the articular cartilage surface are known to facilitate load bearing (Schmidt *et al.,* 2007). Boundary lubrication allows for the support of an applied load via surface-to-surface contact (Wright and Dowson, 1976). The presence of the attachment of synovial fluid to the cartilage

surfaces prevents the joining of the surfaces for the maintenance of a reduced friction (Ali and Yousif, 2008). The boundary lubrication mechanism of articular cartilage is crucial for the inhibition of surface wear. However, this particular lubrication mechanism does not effectively perform when subject to increased loads, hence, it is vital for the adoption of further lubricating mechanisms within the synovial joint system (Ali and Yousif, 2008).

2.4.2 Hydrodynamic Lubrication

Hydrodynamic lubrication is defined by the constraining of the synovial fluid to induce a pressure adequate to carry the load, a further lubrication category of fluid-film lubrication (Ali and Yousif, 2008). During hydrodynamic lubrication, the pressure is generated due to the relative sliding motion of non-parallel opposing surfaces, contributing to keeping the joint surfaces apart (Singh, 2017). Pressure does not typically reach levels which induce significant elastic deformation during hydrodynamic lubrication (Singh, 2017).

2.4.3 Elastohydrodynamic Lubrication

For the case of a soft tissue such as cartilage, it is argued that the resulting pressure established during hydrodynamic lubrication leads to elastic deformation (Ali and Yousif, 2008). This highlights the definition of a further fluid-film lubrication mechanism, known as elastohydrodynamic lubrication (Wright and Dowson, 1976). Elastohydrodynamic lubrication is further defined as the maintenance of a sufficient layer of fluid between the joint surfaces in contact, of a fluid film thickness range of 0.0001 to 0.001 mm (Singh, 2017). The elastic distortion provides an increased geometrical conformity, contributing to a thicker lubricating film per load application (Singh, 2017).

2.4.4 Squeeze-film Lubrication

Squeeze-film lubrication is defined by the development of a hydrodynamic pressure (Hou *et al*., 1992) because of the viscosity of the synovial fluid between the surfaces in contact (Ali and Yousif, 2008) whilst approaching towards one other in the normal direction, enabling the support of a load (Yousif and Al-allaq, 2013). The formation of the pressure forces the low molecular weight components of the lubricant out, contributing to a thin layer of film lubricant whilst the joint surfaces come into contact (Ali and Yousif, 2008). The remaining fluid is increased in hyaluronate constituents, thereby increasing the viscosity of the fluid, whilst the low molecular weight components are returned to the joint interface via the hydrodynamic lubrication mechanism, enabling the joint to perform at its next loading series (Ali and Yousif, 2008).

2.4.5 Weeping Lubrication

The weeping lubrication mechanism described by McCutchen (1959), defines articular cartilage to adopt a “hydrostatic bearing” (McCutchen, 1959) process, whereby on load application the fluid enters the interface region between the surfaces in contact (Ali and Yousif, 2008; McCutchen, 1959; Wright and Dowson, 1976). The surfaces are held apart by the lubricant film that is maintained under pressure, induced by muscle contractions or as a consequence of weight bearing compression due to load application (Singh, 2017).

2.4.6 Lubrication during the Gait-Cycle

The gait cycle is referred to the sequence of functions as the body moves, whilst one limb provides support for the advancement in position by the other limb, further defined by two stages of stance and swing (Kharb *et al*., 2011). During the stance phase, the foot is reported for 60 % of ground contact of the gait cycle, whilst the remaining 40% of the gait cycle is referred to the swing phase, defined as the action of the forward swinging of the limb for

initiation of the next stride (Umberger, 2010). The gait-cycle can further be divided into three phases to describe i) first interval – from heel strike to flat foot, ii) second interval – as the body passes over the foot and iii) third interval – from heel lift to toe-off (Shetty and Bendall, 2011).

Various lubrication mechanisms are reported to occur throughout the different stages of the gait-cycle, as illustrated by the movement of the lubrication during both the swing and stance phase in Figure 2.6.

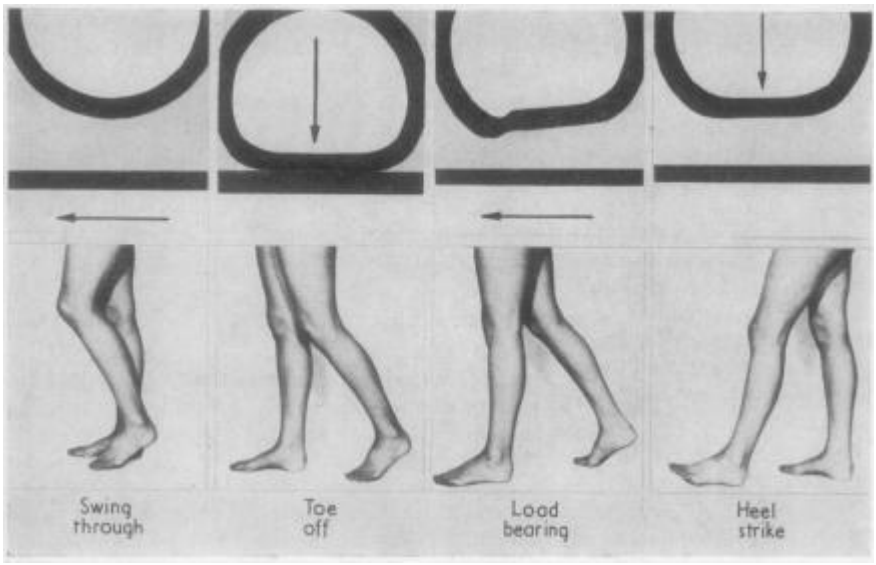

Figure 2.6: Schematic to represent the various lubrication mechanisms in response to the stages of the gait cycle. Positions at the gait cycle include swing through, toe off, load bearing and heel strike. (Reproduced from [Some new evidence on human joint lubrication, A. Unsworth; D. Dowson, V. Wright, 34, pp. 277-85, 1975, copyright notice year: 2020] with permission from BMJ Publishing Group Ltd).

The lubrication mechanisms during the gait cycle are based on the hip joint (Abdullah, 2019; Unsworth *et al*., 1975), whilst the descriptions have not referred to other lower limb joints such as the knee and ankle in the studies mentioned (Abdullah, 2019; Unsworth *et al*., 1975). The heel-strike phase is known to experience squeeze-film lubrication (Unsworth *et al*., 1975). At this stage, the weight of the body is applied when the heel strikes the ground, inducing rotation of the femoral head bearings relative to the acetabular cup (Abdullah, 2019). Squeeze-film lubrication is induced as a consequence of the increase in the external load in relation to

the spring load, for the full or partial separation of the articular cartilage surface (Abdullah, 2019).

During the stance phase, the force in a joint increase, leading to the development of elastohydrodynamic lubrication (Ramachandran, 2017). At this stage, both the film thickness and surface roughness are reported as high (Abdullah, 2019). As walking progresses, a lighter load is produced followed by sliding, inducing fluid to be drawn into the load-bearing area of the joint. It is reported at this point for the generation of a fluid-film for the maintenance of the surface separation (Unsworth *et al*., 1975). On entrance into the toe-off phase, whilst the leg reaches the peak posterior stance, the load is reported as over four times the body weight (Unsworth *et al*., 1975), hence, it is reported that both boundary and squeeze-film lubrication may occur at this stage (Abdullah, 2019). This is known to cause a decline in the film thickness (Unsworth *et al*., 1975).

With movement into the swing phase, as the load experienced declines followed by an increase in sliding speed, the film thickness is regenerated to allow protection of the surfaces through a further cycle (Unsworth *et al*., 1975) (Figure 2.6). The swing phase is also reported to experience hydrodynamic lubrication, followed by the prolonged stance to adopt boundary lubrication (Ramachandran, 2017). The lubrication mechanisms during the gait-cycle have been established from the friction measured on a hip-joint, using a pendulum machine. A load range of 135-1500 N was applied, before the oscillations began (Unsworth *et al*., 1975). The prediction of the lubrication mechanism is defined by the relationship between angular displacement and time (Unsworth *et al*., 1975).

2.4.7 Stribeck Curve

For the determination of a particular type of lubrication mechanism present within a system, a Stribeck curve is used. The Stribeck curve represents the resulting coefficient of

friction (μ), with respect to the product of the fluid viscosity (η) and fluid velocity (v), divided by the applied load (F) (Figure 2.7). This calculation is summarised by equation 2.1 and illustrated in Figure 2.7 (Mang and Dresel, 2007; Sotres and Arnebrant, 2013).

$$\mu = \frac{v.\eta}{F} \qquad (2.1)$$

The outcome is scaled equivalently with the fluid thickness, also dependent upon the surface roughness in addition to the friction and lubrication mechanisms (Mang and Dresel, 2007). The initial stationary position is subject to a thin molecular lubricant layer, determining the presence of boundary lubrication, where the friction is not affected by the properties of the lubricant (Sotres and Arnebrant, 2013).

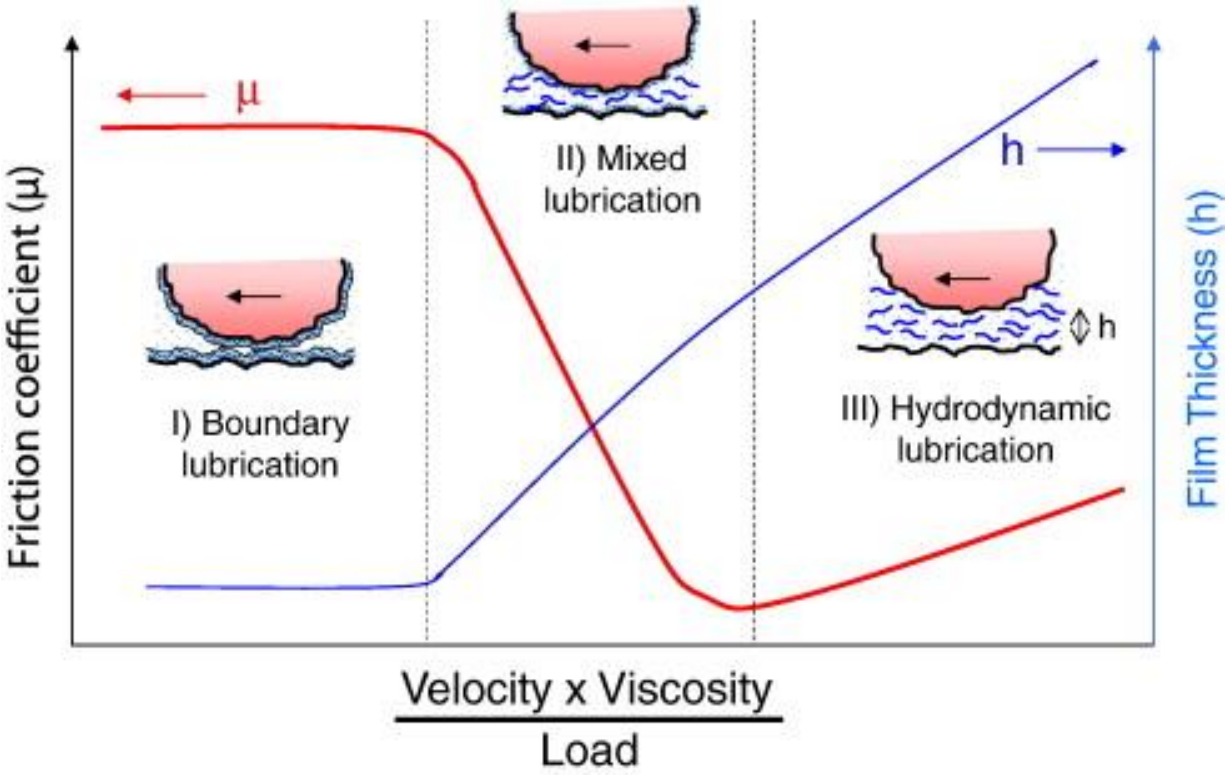

Figure 2.7: Schematic to represent the Stribeck curve, displaying the relationship between the friction coefficient as a function of fluid velocity and fluid viscosity divided by the load, in accordance with the lubrication film thickness. The three various lubrication mechanisms to correspond to the levels of friction coefficient are highlighted as boundary, mixed and hydrodynamic. (Reprinted from Molecular mechanisms of aqueous boundary lubrication by mucinous glycoproteins, volume 15, J.M. Coles, D.P. Chang and S Zauscher, pp 406-416, 2010, with permission from Elsevier).

As the speed of the moving surfaces in contact increase, the formation of a thick hydrodynamic lubricant film contributes to a mixed lubrication environment. At this point, a decline in the coefficient of friction is observed to reach its minimum value. Due to internal friction, the friction is then observed to increase through elastohydrodynamic and hydrodynamic lubrication mechanisms (Mang and Dresel, 2007).

Consequently, the Stribeck curve is based on bearings lubricated with oils, hence may raise questions for the application to a human joint system with varying lubrication mechanisms. However, the Stribeck curve takes into account key contributors to the resulting friction, providing a repeatable method for the lubrication analysis. In particular, the viscoelasticity of the adsorbed lubricant film is reported as a prominent influencer on the boundary lubrication mode, solely due to alterations to the contact area of the surfaces in question (Sotres and Arnebrant, 2013).

2.5 Mechanical Properties and Experimental Approaches

Various testing methods have been implemented to assess the bio-mechanical properties of articular cartilage. For instance, compression testing can be performed via unconfined, confined or indentation procedures (Korhonen and Saarakkala, 2011), with each scenario illustrated in Figure 2.8. Unconfined compression testing refers to the compression of a circular specimen of articular cartilage via two platens, therefore inducing the fluid exudation in the radial direction from the articular cartilage (Warner *et al.,* 2001). Confined compression uses a porous-permeable indenter for the compression of a cylindrical specimen of articular cartilage, fitted within an impermeable sleeve for the prevention of radial fluid exudation (Warner *et al*., 2001). Indentation allows for the compression of the tissue with a cylindrical, plane-ended or spherical-ended indenter, whilst fluid flow is feasible in both the lateral and axial directions (Korhonen and Saarakkala, 2011) (Figure 2.8). A typical output

result of unconfined, confined and indentation testing of articular cartilage is displayed in Figure 2.9.

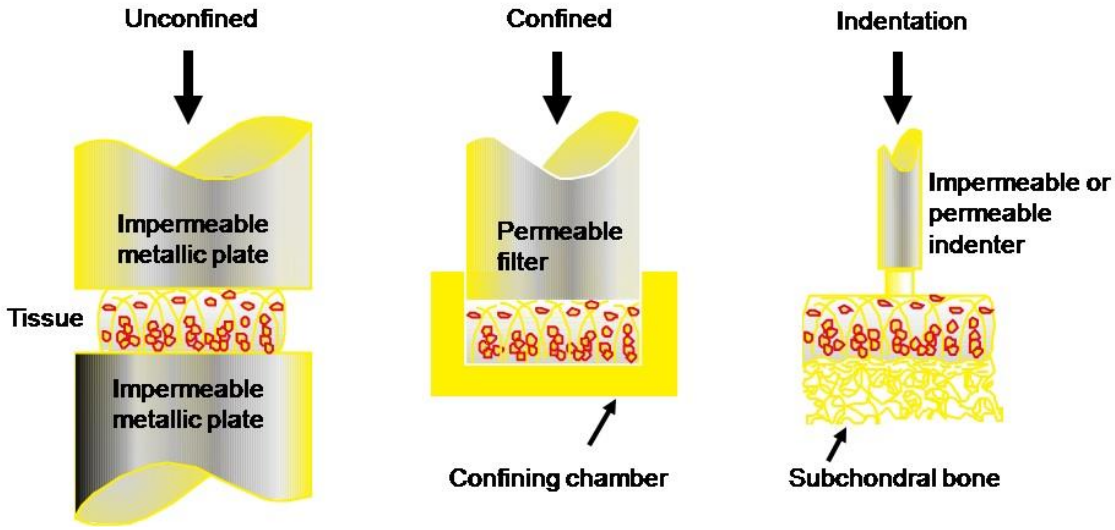

Figure 2.8: Schematic to demonstrate the three various categories of compression testing for articular cartilage. The categories can be observed as unconfined, confined and indentation. (Reproduced from InTechOpen; Korhonen, 2011, which is distributed under the terms of the Creative Commons Attribution 3.0 International License (http://creativecommons.org/licenses/by/3.0/), which permits unrestricted use, distribution, and reproduction in any medium)

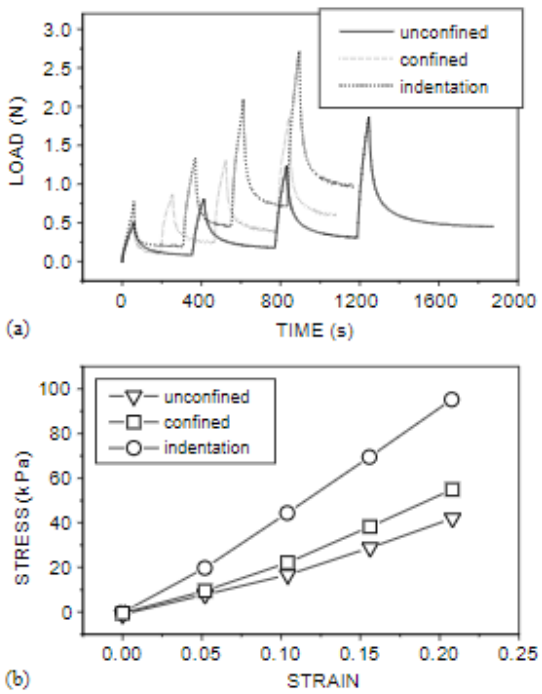

Figure 2.9: Schematic to represent a typical outcome for unconfined and confined compression testing as well as indentation of articular cartilage. Part a) of the figure displays the stepwise stress-relaxation behaviour and part b) demonstrates the equilibrium response of the relationship between stress and strain. (Reprinted from 'Comparison of the equilibrium response of articular cartilage in unconfined compression, confined compression and indentation', volume 35, R.K Korhonen, M.S Laasanen, J Toyras, J Rieppo, J Hirvonen, H.J Helminen and J.S Jurvelin, pp. 903-09, 2002, with permission from Elsevier)

Indentation is widely used to measure the compressive properties of articular cartilage (Mak *et al*., 1987; Mow *et al*., 1989), allowing for the calculation of both the elastic and viscoelastic properties of the tissue (Athanasiou, 2013). Indentation maintains the physiological structure of cartilage to closely mimic the clinical setting (Griffin *et al.,* 2016). Furthermore, a technique to identify the thickness of articular cartilage of a whole joint has been performed to involve a needle probe protocol (Shepherd and Seedhom, 1999).

The use of quasi-static loading confers limitations to the study of measuring the mechanical properties of articular cartilage. This is due to the slow rate at which the load is applied over a period. Therefore, the resulting impact is not large enough to affect the mechanical properties of the tissue. Although this is a disadvantage for extracting the mechanical properties of articular cartilage, the slow loading rate preserves the collagen

structure, therefore avoiding disruption to the matrix of the tissue. This may be particularly useful for scenarios when cartilage specimens are scarce and are to be re-used for testing. Furthermore, the application of quasi-static loading confers greater control due to the reduced speed of loading.

On the other hand, the use of impact loading is a dynamic approach. This technique uses a fast loading rate which in turn will influence the mechanical properties of the tissue. Thus, impact loading is advantageous as it can successfully be used to obtain data on the mechanical properties of articular cartilage. Yet, applying a fast impact to the tissue will induce damage, thus the specimen cannot be re-used. A further limitation of impact loading is the lack of control the technique allows, due to the free-falling approach.

The evaluation of true impact can perhaps only be determined in a scenario with a free-falling mass (Aspden *et al*., 2002). This is due to a lower time to peak load for impact loading, than the physiological range at 30 – 150 ms (Aspden *et al*., 2002). Therefore, the additional method used to determine the properties of articular cartilage subject to compression, is the releasing of a defined mass onto the surface of the tissue to allow for the direct measurement of the force of impact. For this protocol, it is common for the use of a custom-built drop tower for the independent variation of the mass and drop height. An accelerometer and force sensor are attached to the load carriage (Kaleem *et al*., 2017), enabling the measurement of the deceleration of the impactor at the time of impact, as well as the associated force transmitted through the specimen, for which the data is directly transferred to a computer for analysis (Burgin and Aspden, 2007). The internal process is described by the ability of the drop plate to contain the impact to move on a thread, with attachment to a timing pulley, as well as a spring-loaded locking pin mechanism to hold each impactor (Burgin and Aspden, 2007).

An example set-up for impact loading is displayed in Figure 2.10. A classic force-displacement curve following the impact testing of articular cartilage is also shown in Figure 2.11

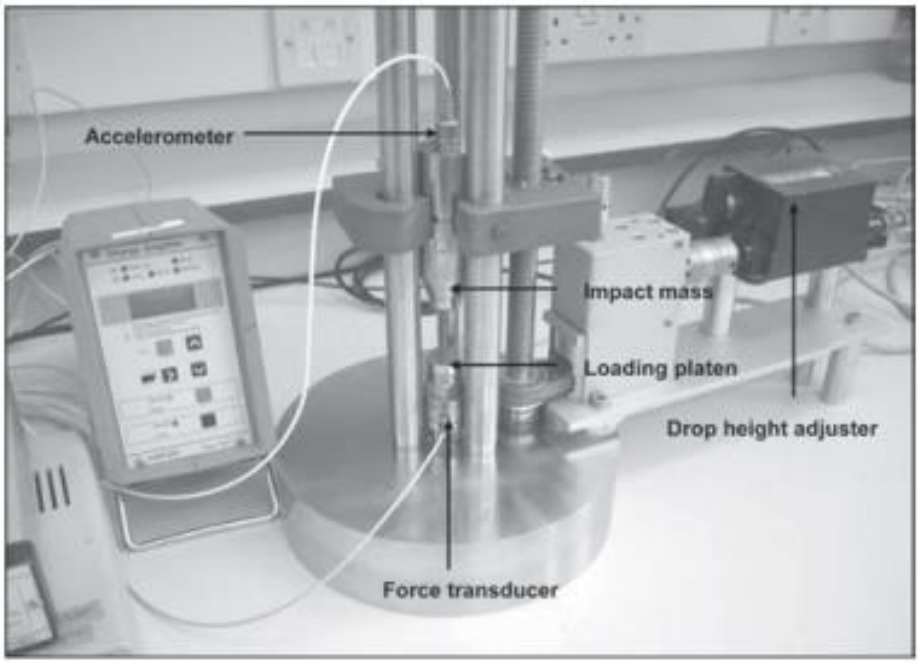

Figure 2.10: Typical set-up of a drop-tower impact loading apparatus. The components include the loading platen, impact mass, accelerator, force transducer and drop height adjuster. The specimen Is placed onto the loading platen and the mass released, at a height set by the drop height adjuster. The force is measured by the force transducer whilst the resulting displacement is measured with the accelerator. (Reprinted from 'The biophysical effects of a single impact load on human and bovine articular cartilage', volume 220, J.E. Jeffrey and R.M. Aspden, pp 677-86, 2006, where permission from SAGE Publishing is granted at no cost for use of content in a Master's Thesis and/or Doctoral Dissertation).

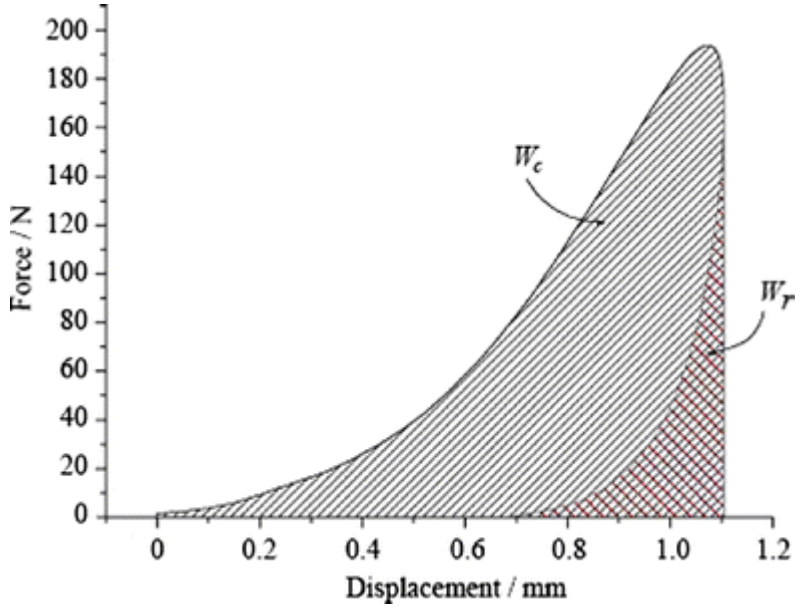

Figure 2.11: Schematic to represent a typical outcome result for the impact testing of articular cartilage. The force is shown with respect to displacement. Wc and Wr display the work done in compression and restitution, respectively. (Reprinted by permission from [Springer Nature] [Journal of Materials Science: Materials in Medicine] [Impact testing to determine the mechanical properties of articular cartilage in isolation and on bone, L.V. Burgin and R.M. Aspden, volume 19, pp. 703-11, 2008])

For the determination of the viscoelastic properties of articular cartilage, it is known for the practice of creep and stress relaxation tests (Keenan *et al.*, 2013; Li *et al.*, 2008). Creep is observed when the applied stress is held constant, whilst stress relaxation occurs on application of a constant strain (Li *et al.*, 2008). However, the use of such tests confers limitations to the measurement of the mechanical properties of articular cartilage, as previously defined by the variations in quasi-static and dynamic tests above. Additionally, the application of static loading is not the physiological scenario of a joint, as illustrated by the previous discussion of gait. Consequently, for better representation of the dynamic kinetics of a joint, this leads onto the consideration of alternative dynamic methods, for the assessment of the viscoelastic properties of articular cartilage. Both creep and stress relaxation can be measured with the indentation set-up displayed in Figure 2.8. A typical result for a creep and stress-relaxation test is displayed in Figure 2.12.

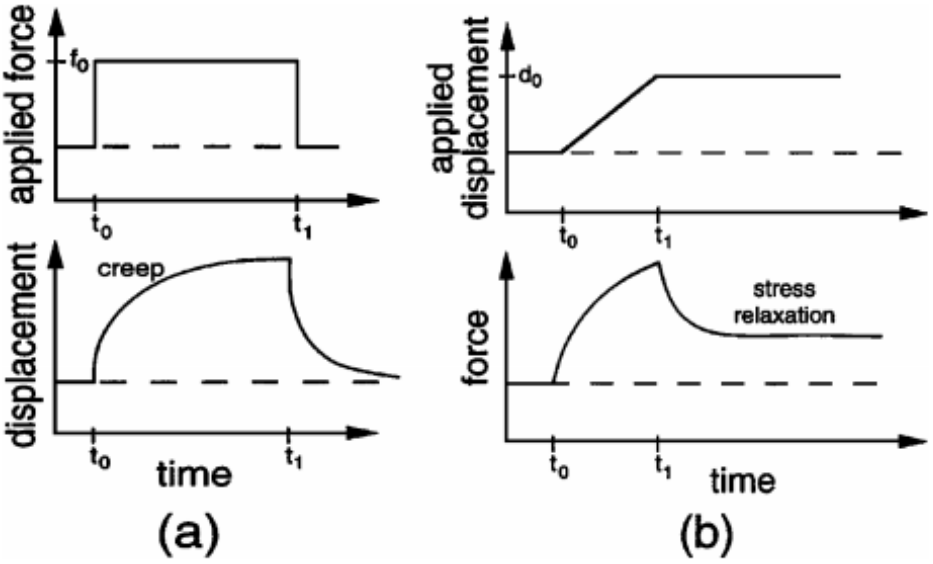

Figure 2.12: Schematic to represent a typical creep response of articular cartilage in part a). The step force is represented by f_0 and the resulting creep deformation behaviour is shown. Recovery of articular cartilage is shown on load removal at section t_1. A typical stress-relaxation response of articular cartilage is shown in part b). An increase in the force followed by stress-relaxation is shown in accordance with the applied displacement. (Reprinted by permission from [Annual Reviews, Inc.] [Annual Review of Biomedical Engineering] [Mechano-electrochemical properties of articular cartilage: Their inhomogeneities and anisotropies. M.C, Van and X.G, Edward, volume 4, pp. 175-209, 2002])

The viscoelastic properties of a material are characterised by the storage, *E'*, and loss moduli, *E''* (Hukins *et al*., 1999). The storage modulus signifies the elastic response, where energy is stored and used for the elastic recoil on stress removal, whilst the loss modulus represents the viscous response, determined by the dissipation of energy (Fulcher *et al*., 2009). The storage and loss moduli are derived from the storage, *k*', and loss stiffness, *k*'', with use of a shape factor (Fulcher *et al*., 2009).

A testing method known as Dynamic Mechanical Analysis (DMA) has previously been used for examining the viscoelastic properties of a range of natural tissues, not only limited to articular cartilage (Fulcher *et al*., 2009; Temple *et al.,* 2016), but also including the bladder (Barnes *et al*., 2015; Barnes *et al*., 2016), coronary arteries (Burton *et al.,* 2017) as well as orthopaedic implants (Lawless *et al*., 2017; Lawless *et al*., 2016). DMA is conducted through the application of a frequency sweep following a set pre-load to the specimen (Lawless *et al*., 2017). Next, the DMA software applies a Fourier analysis for each frequency, which quantifies

the magnitude of the load (*F**), magnitude of displacement (*d**) and the phase lag (*δ)* (Lawless *et al*., 2016). The angle *δ* is defined by the phase difference between the applied compressive force and displacement (Lawless *et al*., 2017). A set-up of a DMA experiment to assess the viscoelastic properties of articular cartilage is shown in Figure 2.13.

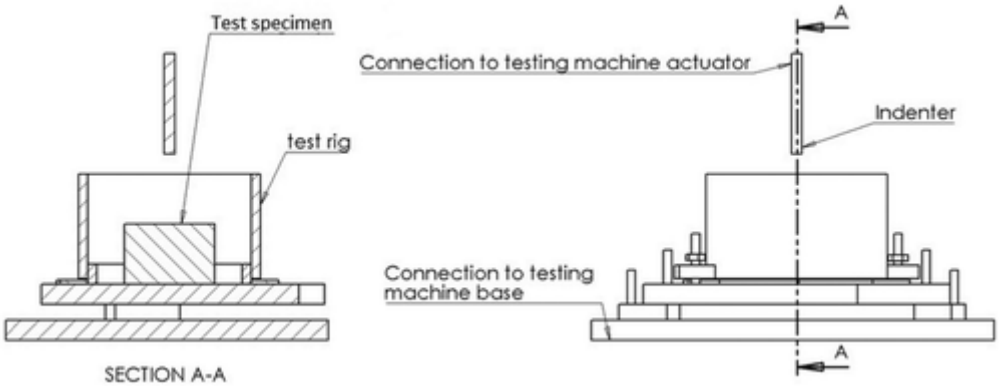

Figure 2.13: Schematic to represent an example test set-up for the dynamic mechanical analysis of articular cartilage. The dynamic mechanical analysis procedure is carried out with the indenter, which is applied onto the specimen contained within the test rig. (Reprinted from Proceedings of the Institution of Mechanical Engineers, Part H: Journal of Engineering in Medicine; Variation in viscoelastic properties of bovine articular cartilage below, up to and above healthy gait-relevant loading frequencies, H. Sadeghi, D.M, Espino, D.E.T, Shepherd, volume 229, pp. 115-23, 2015, which is distributed under the terms of the Creative Commons Attribution 3.0 International License (http://creativecommons.org/licenses/by/3.0/), which permits unrestricted use, distribution, and reproduction in any medium))

The magnitude of the load and displacement are obtained from the Fast Fourier Transform of the sinusoidal force and displacement waves, respectively. Using this information, the DMA software computes the complex (*k*),* storage (*k'*) and loss stiffness (*k"*), as shown in equations 2.2 to 2.4 below (Lawless *et al.,* 2016).

$$k^* = \frac{F^*}{d^*} \qquad (2.2)$$

$$k' = k^* \cos\delta \qquad (2.3)$$

$$k'' = k^* \sin\delta \qquad (2.4)$$

Figure 2.14a-b display an example outcome from DMA, for the storage and loss stiffness relationship with frequency, for bovine articular cartilage (Lawless *et al*., 2017). The ratio of storage to loss stiffness (Figure 2.15) relates to the amount of energy storage, thus a greater ratio provides more energy for failure (Espino *et al*., 2014).

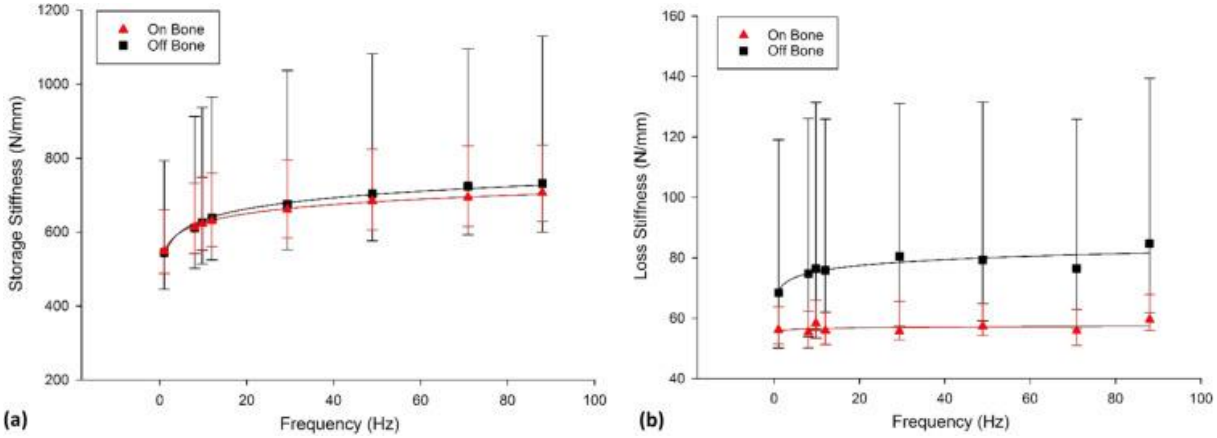

Figure 2.14: Result to display the (a) storage and (b) loss stiffness of articular cartilage both on- and off-bone. This displays an example outcome result from testing dynamic mechanical analysis on articular cartilage. The error bars are based on eight specimens. (Reprinted from the Journal of the Mechanical Behaviour of Biomedical Materials; Viscoelasticity of articular cartilage: Analysing the effect of induced stress and the restraint of bone in a dynamic environment, B.M, Lawless, H Sadeghi, D.K, Temple, H Dhaliwal, D.M, Espino, D.W.L, Hukins, volume 75, pp. 293-301, 2017, which is distributed under the terms of the Creative Commons Attribution 4.0 International License (http://creativecommons.org/licenses/by/4.0/), which permits unrestricted use, distribution, and reproduction in any medium))

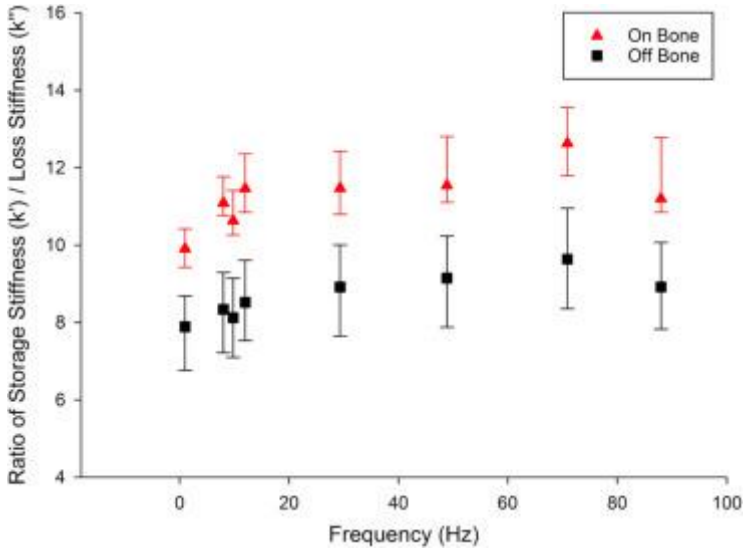

Figure 2.15: Result to display the ratio of the storage stiffness with loss stiffness for articular cartilage, both on- and off-bone. This is an example result from the outcome of applying dynamic mechanical analysis to articular cartilage. The error bars are based on the assessment of eight specimens. (Reprinted from the Journal of the Mechanical Behaviour of Biomedical Materials; Viscoelasticity of articular cartilage: Analysing the effect of induced stress and the restraint of bone in a dynamic environment, B.M, Lawless, H Sadeghi, D.K, Temple, H Dhaliwal, D.M, Espino, D.W.L, Hukins, volume 75, pp. 293-301, 2017, which is distributed under the terms of the Creative Commons Attribution 4.0 International License (http://creativecommons.org/licenses/by/4.0/), which permits unrestricted use, distribution, and reproduction in any medium))

The next step to DMA is the determination of the complex modulus (*E**), storage modulus (*E'*) and loss modulus (*E''*). For this step, a shape factor is calculated using the specimen diameter (*D*) and thickness (*t*) (Lawless *et al*., 2017). Equations 2.5 to 2.8 demonstrate this.

$$S = \frac{\pi D^2}{4t} \quad (2.5)$$

$$E^* = \frac{k^*}{S} \quad (2.6)$$

$$E' = \frac{k'}{S} \quad (2.7)$$

$$E'' = \frac{k''}{S} \quad (2.8)$$

The complex stiffness (*k**) and phase angle (*δ*) are associated to the storage and loss stiffness as shown in equation 2.9 and 2.10. An example outcome figure known as the Argand diagram (Lawless *et al*., 2017), is displayed in Figure 2.16.

$$|k^*| = \sqrt{k'^2 + k''^2} \qquad (2.9)$$

$$\delta = \tan^{-1}\left(\frac{k''}{k'}\right) \qquad (2.10)$$

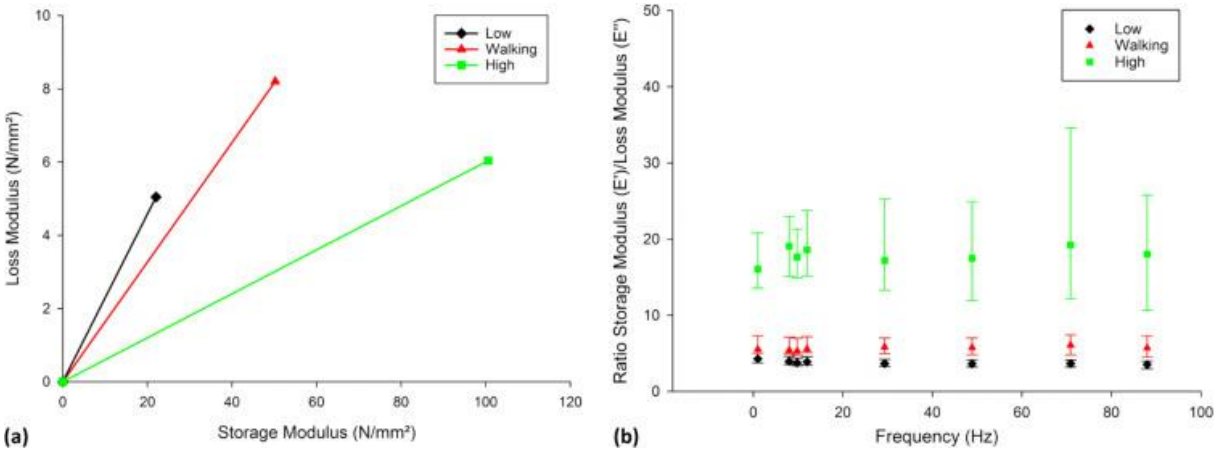

Figure 2.16: Schematic to represent an example Argand diagram of the relationship between the loss and storage moduli of articular cartilage, at various stresses is displayed in part (a). Part (b) of the figure displays the relationship between the ratio of storage modulus to loss modulus with respect to frequency. (Reprinted from the Journal of the Mechanical Behaviour of Biomedical Materials; Viscoelasticity of articular cartilage: Analysing the effect of induced stress and the restraint of bone in a dynamic environment, B.M, Lawless, H Sadeghi, D.K, Temple, H Dhaliwal, D.M, Espino, D.W.L, Hukins, volume 75, pp. 293-301, 2017, which is distributed under the terms of the Creative Commons Attribution 4.0 International License (http://creativecommons.org/licenses/by/4.0/), which permits unrestricted use, distribution, and reproduction in any medium))

Figure 2.17a-b display an example outcome from DMA, for the storage and loss modulus relationship with frequency, for bovine articular cartilage (Lawless *et al*., 2017).

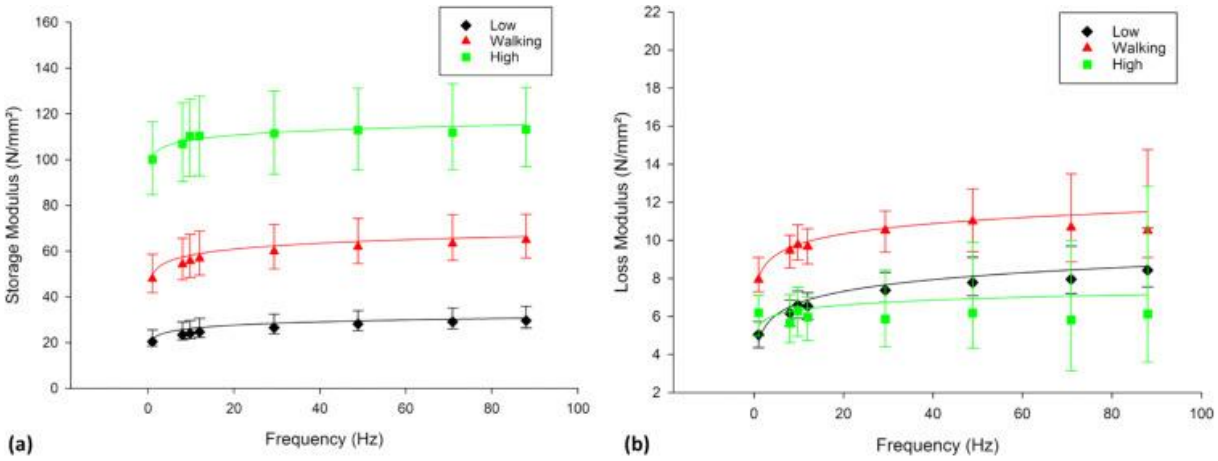

Figure 2.17: Result to display the (a) storage and (b) loss modulus of articular cartilage whilst subject to various stresses. This is an example result that can be obtained from the application of dynamic mechanical analysis to articular cartilage. (Reprinted from the Journal of the Mechanical Behaviour of Biomedical Materials; Viscoelasticity of articular cartilage: Analysing the effect of induced stress and the restraint of bone in a dynamic environment, B.M, Lawless, H Sadeghi, D.K, Temple, H Dhaliwal, D.M, Espino, D.W.L, Hukins, volume 75, pp. 293-301, 2017, which is distributed under the terms of the Creative Commons Attribution 4.0 International License (http://creativecommons.org/licenses/by/4.0/), which permits unrestricted use, distribution, and reproduction in any medium))

The viscoelasticity of articular cartilage has been demonstrated from frequencies of 1 to 92 Hz (Fulcher *et al*., 2009). The result is displayed in Figure 2.18.

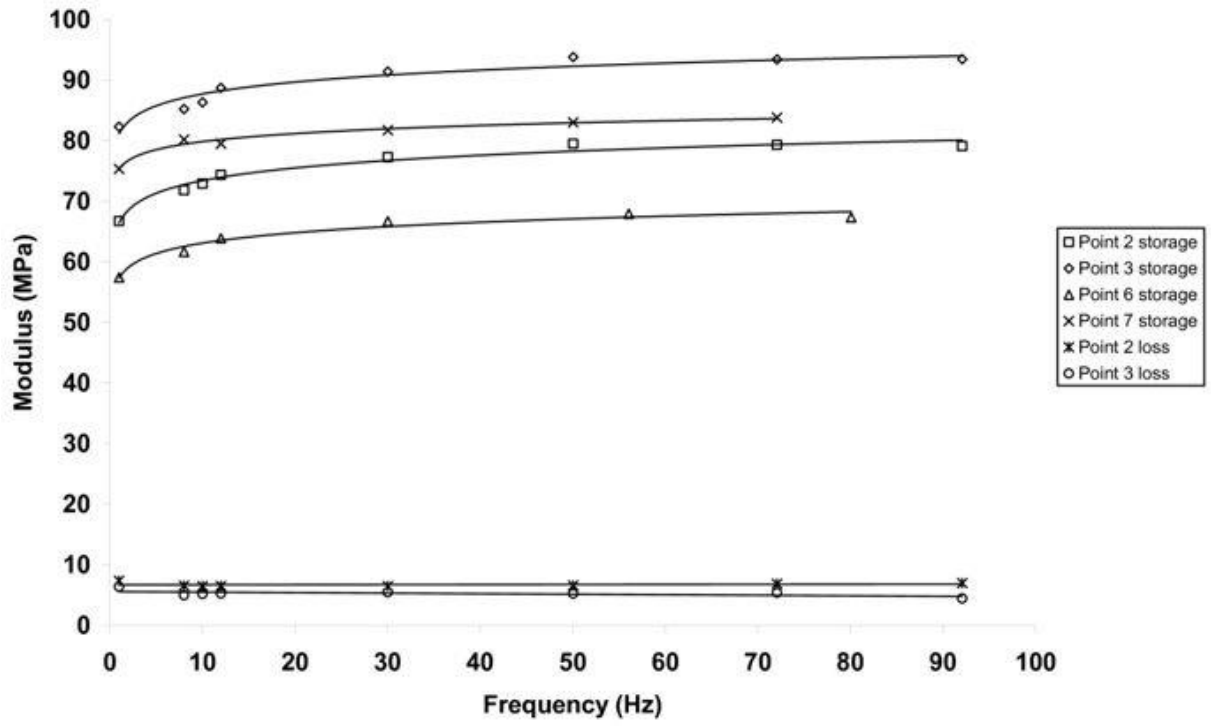

Figure 2.18: Schematic to represent the relationship between storage and loss moduli versus frequency tested up to 92 Hz. (Reprinted by permission from [Springer Nature] [BMC Musculoskeletal Disorders] [Viscoelastic properties of bovine articular cartilage attached to subchondral bone at high frequencies, G.R Fulcher, D.W.L, Hukins, D.E.T, Shepherd, volume 10, pp. 61, 2009]).

The frictional properties of articular cartilage are typically measured using a flat counterface contact of articular cartilage against an external material, in sliding. This underpins the field of tribology, the study of friction, lubrication and wear, whilst exposing the material to compression and sliding shear stress (Whitney *et al*., 2017). In fact, for the identification of the friction between two surfaces in sliding, known as the coefficient of friction, the most well-known method for the evaluation with articular cartilage is that of the plug-on-plate technique (Athanasiou, 2013), or plane-on-plane. This method involves a smaller diameter specimen as the upper component, in sliding against a larger diameter lower component, whilst both components adopt a flat configuration. A typical friction testing set-up is displayed in Figure 2.19.

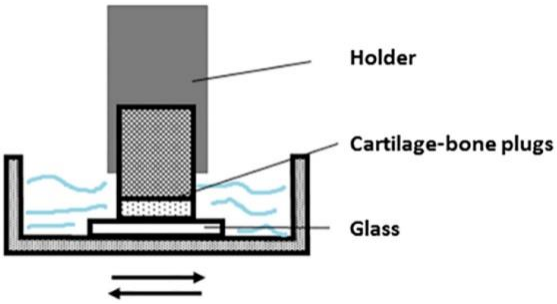

Figure 2.19: Schematic to represent the typical set-up of friction testing of articular cartilage against a counter-interface, which in this case is glass. The holder contains the cartilage specimen for sliding movement. (Reprinted by permission from [John Wiley and Sons] [Journal of Biophotonics] [Detection of depth-depend changes in porcine cartilage after wear test using Raman spectroscopy, L Tong, Z Hao, C Wan, S Wen, volume 11, 2017]).

In addition to a flat mount counterface, previous work has also implemented a hemicylindrical mount for both the articular cartilage and material in contact, for the representation of incongruent joint morphologies such as the knee (Whitney *et al.*, 2017). An example result for a typical coefficient of friction plot against time is shown for articular cartilage in Figure 2.20.

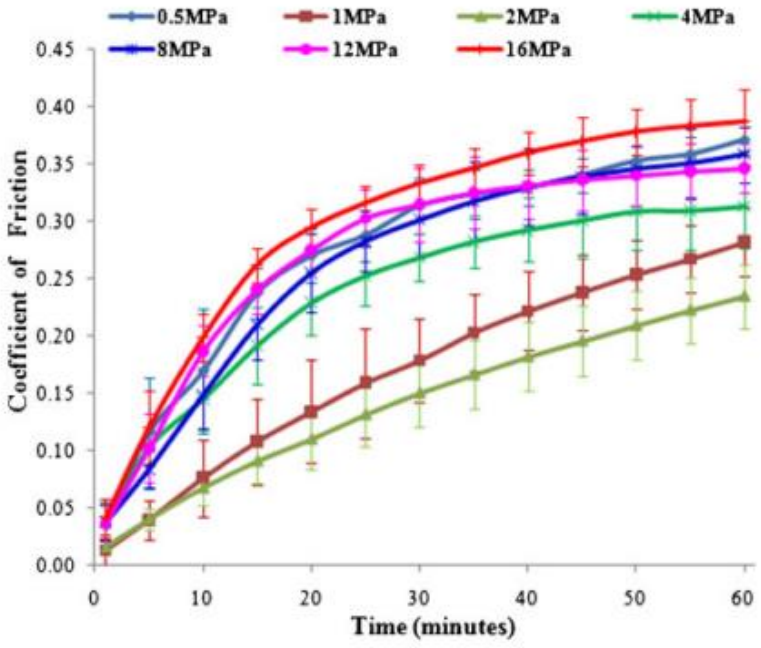

Figure 2.20: Schematic to represent the resulting coefficient of friction of articular cartilage with respect to time under various contact stresses. (Reprinted from 'The effect of contact stress on cartilage friction, deformation and wear', volume 225, J Lizhang, J Fisher, Z Jin, A Burton and S Williams, pp. 461-75, 2010, where permission from SAGE Publishing is granted at no cost for use of content in a Master's Thesis and/or Doctoral Dissertation).

Microdamage is commonly observed in calcified cartilage of osteoarthritic joints (Burr and Schaffler, 1997). There are two forms to microdamage, known as linear microcracks and diffuse damage (Herman *et al.,* 2010). The measurements of linear microcracks range in length from tens to a few hundred microns, while diffuse damage adopts a patch-like appearance of clusters of sublamellar-sized cracks (Herman *et al*., 2010). Specific to linear microcracks, the process of bone remodelling is suggested to initiate from microdamage present in calcified cartilage (Kawcak *et al*., 2001). Subsequently, the advancing tidemark leads to cartilage thinning (Li *et al*., 2013). Alternatively, diffuse microdamage is not reported to relate to the remodelling process nor the activation of resorption by osteocytes. Such differences in the measurements of the various types of microdamage may be due to the reduced focal injury response (Herman *et al.,* 2010). A previous study has observed enhanced bone porosity through the depth of the bone, as a potential result of microdamage to articular cartilage (Lacourt *et al.,* 2012).

2.5.1 Material Properties

To begin this section, previous work to evaluate the compressive modulus, and dynamic modulus of articular cartilage via both indentation and impacting techniques are outlined. This discussion is followed by a selection of previous studies that have characterised the viscoelastic properties of articular cartilage. A summary is provided in Table 2.1.

The relationship between the instantaneous compressive modulus of articular cartilage has been explored in relation to its deformation response to cyclic loading, to identify a compressive modulus within the range of 1 – 19.5 MPa (Barker and Seedhom, 2001). This is of a similar outcome to the mean compressive creep modulus observed in previous work, identified as 8.47 ± 1.49 MPa, 9.48 ± 1.55 MPa, 6.81 ± 0.92 MPa and 8.59 ± 1.62 MPa, for the lateral and medial condyle of the femoral surface of the knee, and the lateral and medial condyle of the tibial surface of the knee, respectively (Swann and Seedhom, 1993). The age

range of the specimen donors were of 21 to 59, from the age data available (Swann and Seedhom, 1993).

Additionally, the work of Shepherd and Seedhom (1997) has identified a range of 2.6 – 18.6 MPa calculated at a compressive modulus of 2 seconds after initial loading (Shepherd and Seedhom, 1997). Similarly, previous work has identified a mean compressive modulus of 6.80 MPa and 7.10 MPa for the lateral and medial tibial surface covered by the meniscus, respectively. For the tibial surface not covered by the meniscus, the compressive modulus was reported at 3.92 MPa and 4.80 MPa, for the lateral and medial areas, respectively (Yao and Seedhom, 1993). The results recorded in the literature for the compressive modulus of articular cartilage align with the typical stresses during walking of an approximate range of 1 to 6 MPa (Brown and Shaw, 1983; Hodge *et al*., 1989), and the increase to 18 MPa for the action of rising from a chair (Hodge *et al.,* 1989). The stresses in the work of Brown and Shaw (1983) have been obtained from indentation testing on the femoral head of cadavers. Both the load cell and transducer output were recorded. Hip specimens were held at a neutral extension position, as well as 10, 20 and 30° of flexion (Brown and Shaw, 1983). To examine the stresses experienced at walking, oscillatory joint loadings were applied at a frequency of 1 Hz (Brown and Shaw, 1983). The contact pressures in the work of Hodge *et al*. (1989) were obtained from implanting a pressure-measuring endoprosthesis in a seventy-year old patient.

Consequently, limitations are associated with the studies mentioned, such that the work of Barker and Seedhom (2001) is limited to the assessment of the stiffness of each specimen in relation to a 50-millisecond compressive modulus, determined 50-milliseconds post initial contact of the indenter with the cartilage. Whereas, a wider loading rate range would provide a fuller analysis of kinetics (Barker and Seedhom, 2001). Whilst the work of Swann and Seedhom (1993) performs an interesting topographical representation to form numerical maps of the cartilage stiffness, sample size was small, up to a maximum of 13 joints, potentially reducing the reliability of the data (Swann and Seedhom, 1993). 20, 50 and a maximum of 40

indentation tests were performed on the ankle, femoral condyle and tibial condyle, respectively (Swann and Seedhom, 1993). Thus, the lack of consistency in the number of experiments performed on each location certainly creates questioning, as to the accuracy in comparing the data presented. Similarly, in the work of Shepherd and Seedhom (1997), the small sample size of five knee joints confers limitations to the assessment of the technique, for which validation would improve with a larger number of specimens for assessment. Further, the method for analysis of the compression modulus is determined across a mesh drawn across the cartilage surface. Although this provides a thorough assessment of the surface, it may be difficult to provide repeatability in the technique due to differences in the division of the mesh area/location.

The effective modulus of articular cartilage has also previously been explored, to involve three substrate variations of brass, nylon and cork, whilst a mass of 100 g was released from a height of 50 mm, onto each specimen (Burgin and Aspden, 2008). As detailed in Table 2.1, the study outcome determined a positive correlation of the effective modulus of the substrate with the articular cartilage, as a combined structure, with that of the modulus of the substrate. When in combination with the higher substrate modulus, brass, the effective modulus reached approximately 580 MPa, whilst when in combination with cork, the effective modulus was observed to reach approximately 20 MPa (Burgin and Aspden, 2008).

In the work of Burgin and Aspden (2008), the cartilage alone was further assessed with an impactor mass of 100 or 500 g, released from drop heights of 25, 50, 80, 100 mm, or 25 and 50 mm, respectively. A different sample diameter was assessed for the cartilage alone, and on a substrate, of 5 and 9 mm, respectively. It is worth noting that an identical sample diameter would improve the accuracy of the comparisons. Similarly, a further study has explored the variation in the biophysical properties of human and bovine articular cartilage, with the release of a single impact load of mass 500 g, released from a height of either 25, 50 or 75 mm onto the specimen (Jeffrey and Aspden, 2006). Both an impact and indent protocol

were used for which the values are presented in Table 2.1, comparable to those obtained from the study of Burgin and Aspden (2008). The work of Jeffrey and Aspden (2006) identifies the difference in the biophysical properties of human and bovine cartilage, particularly due to the lesser damage observed on human cartilage in relation to bovine (Jeffrey and Aspden, 2006). Arguably, for the consideration of the use of bovine in replace of human articular cartilage for experimental studies, a previous study has clarified the consistent frequency-dependent viscoelastic trends of bovine articular cartilage with that of human (Temple *et al.,* 2016).

The viscoelastic properties of bovine articular cartilage have been assessed relevant to loading frequencies to represent below, up to and above normal gait, with use of a stainless-steel indenter 5.2 mm in diameter, identifying the storage and loss stiffness (Sadeghi *et al.,* 2015). This study has indicated a linear increase in the storage stiffness with the logarithm of frequency, from 367 N/mm at 0.001 Hz to 1460 N/mm at 10 Hz (Sadeghi *et al.,* 2015) (Figure 2.21).

The outcome for the loss stiffness was not so clearly defined in relation to the logarithm of frequency, as it was observed to increase from 148 to 247 N/mm, at 0.001 and 0.01 Hz, respectively, followed by a decline with the increase in frequency up to 10 Hz, from 170 to 128 N/mm (Sadeghi *et al*., 2015). The result is provided in Figure 2.21.

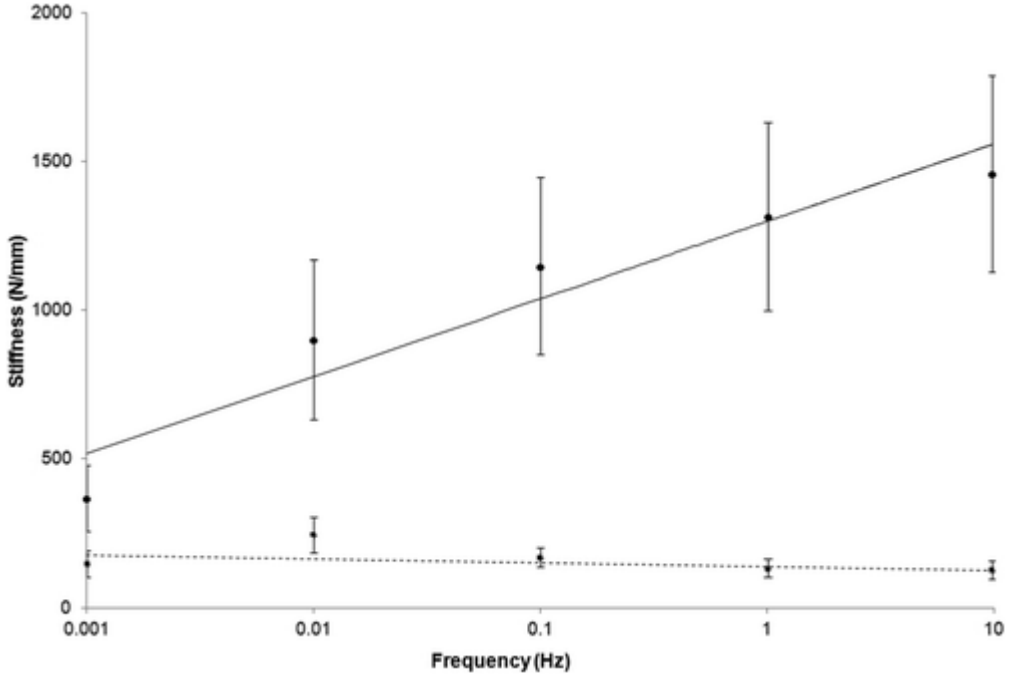

Figure 2.21: Schematic to display the result of the relationship between the mean storage and loss stiffness of articular cartilage and frequencies between 0.001 and 10 Hz. The solid line displays the storage stiffness while the dashed line represents the loss stiffness. The frequency is displayed in logarithm. (Reprinted from Proceedings of the Institution of Mechanical Engineers, Part H: Journal of Engineering in Medicine; Variation in viscoelastic properties of bovine articular cartilage below, up to and above healthy gait-relevant loading frequencies, H. Sadeghi, D.M, Espino, D.E.T, Shepherd, volume 229, pp. 115-23, 2015, which is distributed under the terms of the Creative Commons Attribution 3.0 International License (http://creativecommons.org/licenses/by/3.0/), which permits unrestricted use, distribution, and reproduction in any medium))

A similar outcome of the increase in the storage modulus of articular cartilage was observed in the work of Fulcher *et al*. (2009), from 82 to 93 MPa, at frequencies of 1 and 92 Hz, respectively, whilst a plateau was further observed in the storage modulus with an increase in frequency (Fulcher *et al*., 2009) (Figure 2.22). Disagreement in the result of the work of Fulcher *et al*. (2009) to that of Sadeghi *et al.* (2015) was identified by the frequency-dependent loss modulus of articular cartilage, across the frequencies tested, in the range 3.2 to 6.7 MPa (Fulcher *et al*., 2009). This result is displayed in Figure 2.22.

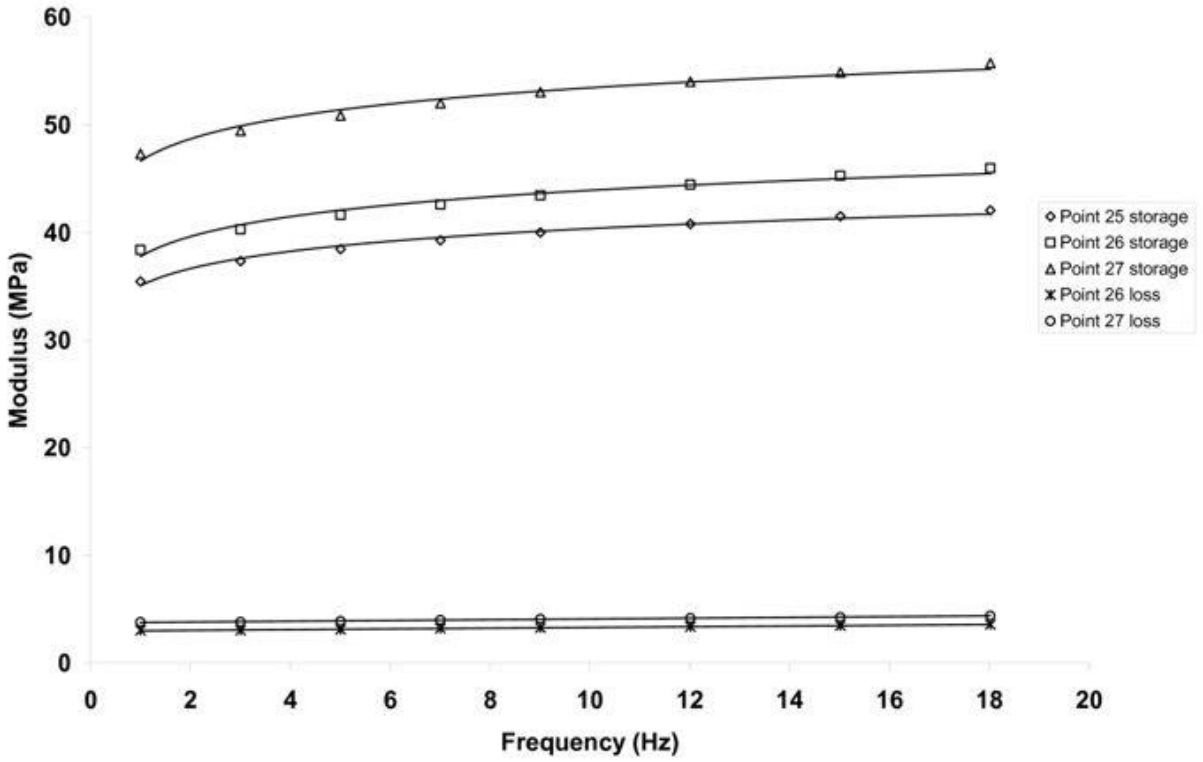

Figure 2.22: Schematic to represent the result of the relationship between storage and loss moduli with frequency tested up to 18 Hz. (Reprinted by permission from [Springer Nature] [BMC Musculoskeletal Disorders] [Viscoelastic properties of bovine articular cartilage attached to subchondral bone at high frequencies, G.R Fulcher, D.W.L, Hukins, D.E.T, Shepherd, volume 10, pp. 61, 2009]).

A more recent study has also identified a significant logarithmic trend in the storage stiffness of articular cartilage, alone, with respect to frequency, whilst 17 of 24 cartilage specimens demonstrated the identical relationship for loss stiffness (Fell *et al*., 2019), (Figure 2.23) again displaying a varied outcome to the work of Sadeghi *et al*. (2015). Further, the osteochondral core has displayed an identical relationship to that seen in the work of Sadeghi *et al*. (2015), identified by the significant logarithmic trend of storage stiffness with frequency, reaching an approximate maximum of 1430 N/mm. Additionally, the loss stiffness was determined as frequency independent, of approximately 100 N/mm across the frequencies assessed (Fell *et al*. 2019) (Figure 2.23).

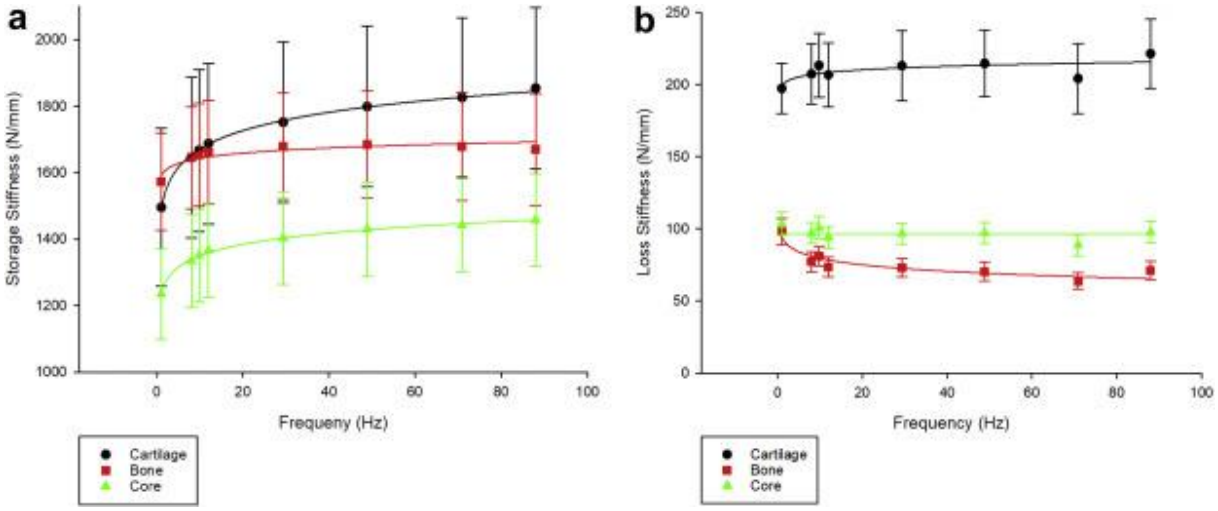

Figure 2.23: Schematic to represent the resulting storage and loss stiffness with respect to frequency for cartilage, bone and the combination of both in the osteochondral core. Error bars are based on 24 specimens. (Reprinted from Osteoarthritis and Cartilage; The role of subchondral bone, and its histomorphology, on the dynamic viscoelasticity of cartilage, bone and osteochondral cores, N.L.A, Fell, B.M, Lawless, S.C, Cox, M.E, Cooke, N.M, Eisenstein, D.E.T, Shepherd, D.M, Espino, volume 27, pp. 535-43, 2019, which is distributed under the terms of the Creative Commons Attribution 4.0 International License (http://creativecommons.org/licenses/by/4.0/), which permits unrestricted use, distribution, and reproduction in any medium))

This study has effectively identified the storage and loss stiffness of the separate regions of the osteochondral core, providing unknown data on the behaviour of the articular cartilage alone. Further novel findings from this study include the linear relationship between the loss modulus of articular cartilage and the bone mineral density (BMD) of the subchondral bone, as well as of between the cartilage thickness and subchondral bone plate thickness (Fell *et al*., 2019). However, it is argued that the data may be misleading due to the averaging of viscoelastic properties across four varied regions for assessment, that being the meniscus covered as well as the meniscus uncovered from both the medial and lateral tibial plateau (Fell *et al*., 2019).

The frequency-dependency of the storage modulus as demonstrated in previous work (Fulcher *et al*., 2009), further relates to a recent study that has identified the increase in storage modulus by 3.8 (88 Hz) to 4.9 (1 Hz) times, with applied stress (Lawless *et al*., 2017) (Figure 2.17). This study has further effectively identified a frequency-dependent logarithmic trend for

loss modulus at low and walking stress ranges, similar to the work of Fulcher *et al*. (2009), yet not at the application of high stress (Lawless *et al*., 2017), similar to the relationship with frequency obtained in the work of Sadeghi *et al.* (2015). The impact of the presence of the underlying subchondral bone has demonstrated a frequency-independent loss stiffness, whilst off-bone cartilage has resulted in a frequency-dependent loss stiffness (Lawless *et al.,* 2017) (Figure 2.14). This outcome is interesting to relate to the previous study, which identifies a frequency-dependent loss stiffness of bone, observed to decline with frequency (Fell *et al*., 2019) (Figure 2.23). Therefore, the bone alone and in combination with cartilage has shown varied viscoelastic properties, which should be taken into consideration when experimenting with on- and off-bone articular cartilage. Critically evaluating, the experiments in the work by Lawless *et al*. (2017) are performed on two different joints. As different joint locations possess varying mechanical properties, this may limit the accuracy in combining the conclusions across the anatomy.

The loss and storage modulus of articular cartilage has further been analysed in a previous study, in which cartilage was subject to 1200 consecutive compressive load cycles, prior and post-impaction, at a stress of 1.5 MPa at 1 Hz, followed by a stress of 7 MPa, at 2 Hz (Verteramo and Seedhom, 2007). At an impact energy of both 1.472 J and 1.962 J, the results identified an increase in the storage modulus with the number of loading cycles (Verteramo and Seedhom, 2007) (Figure 2.24; Figure 2.25). This outcome is similar to the observed increase in storage modulus with frequency (Sadeghi *et al*., 2015), as well as sinusoidal stress (Lawless *et al*., 2017). Similarly, the loss modulus was also demonstrated to increase with the number of loading cycles (Verteramo and Seedhom, 2007). This study has effectively identified the threshold of the stress applied to the cartilage at impact, to determine at what point the variation in the mechanical properties are induced. However, a clearer representation of the raw data for the loss modulus, as represented for the storage modulus, would improve the clarity for the reader.

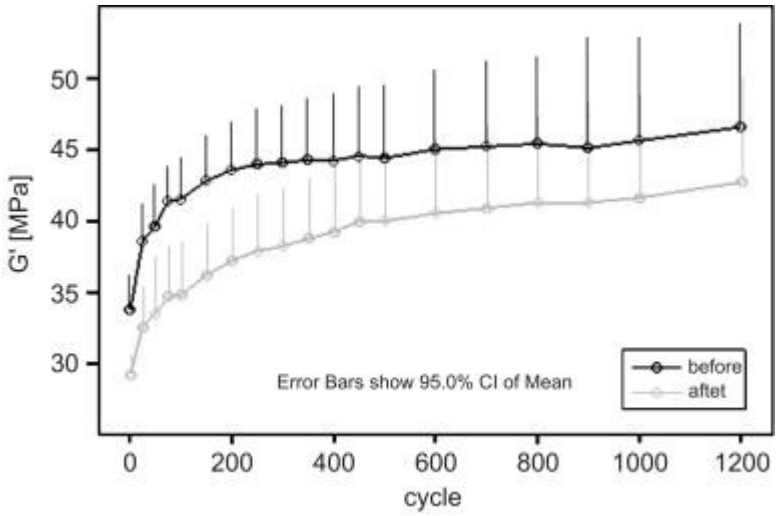

Figure 2.24 Schematic to represent the result for the resulting compressive storage modulus of articular cartilage at an impact energy of 1.472 J. Both the scenario before and after impact at running are shown. (Reprinted from 'Effect of a single impact loading on the structure and mechanical properties of articular cartilage', volume 40, A Verteramo and B.B, Seedhom, pp. 3580-89, 2007., with permission from Elsevier)

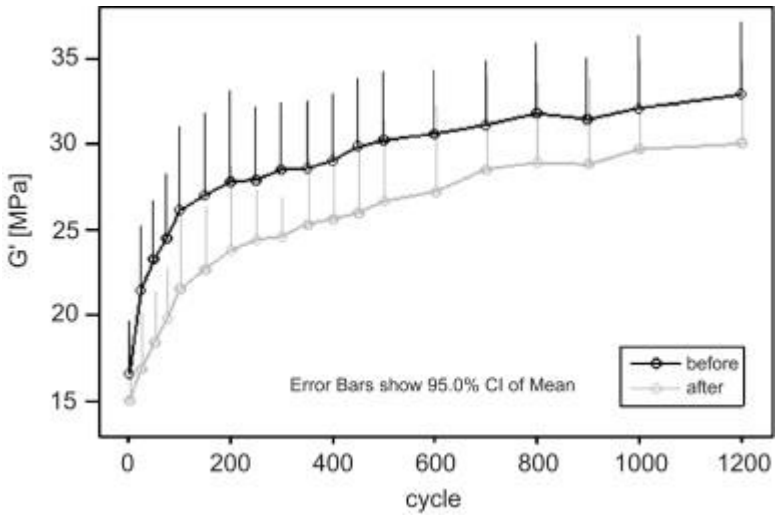

Figure 2.25: Schematic to represent the result for the resulting compressive storage modulus of articular cartilage at an impact energy of 1.962 J. Both the scenario before and after impact at walking are shown. (Reprinted from 'Effect of a single impact loading on the structure and mechanical properties of articular cartilage', volume 40, A Verteramo and B.B, Seedhom, pp. 3580-89, 2007., with permission from Elsevier)

Table 2.1: Summary of material properties described in Section 2.5.1.

a) Compressive Modulus (MPa)						
Anatomical Site	**Species**	**Number of Measurements**	**Measurement**	**Test Method**	**Study Key Limitations**	**Reference**
Knee	Human	1 – cartilage deformation after 50 ms loading 2 – applied load after 50 ms loading 3 – cartilage thickness	**1 – 19.5**	Indentation	Assessment limited to 50-millisecond compressive modulus	Barker and Seedhom, (2001)
Knee Ankle	Human	Knee femur: 50 indentation Knee tibia: 30-40 indentation Ankle talus: 20 indentation Ankle tibia: 15 indentation	**10.07, 8.98** and **7.70** for ankle tibia, femoral condyle and tibial condyle of knee	Indentation	Varied number of indentation tests raises questions for comparisons	Swann and Seedhom, (1993)
Knee	Human	Five joints	**2.6 – 18.6** at 2 seconds, **4.4 – 27** at 20 milliseconds	Indentation	Small sample size and mesh repeatability	Shepherd and Seedhom, (1997)
Knee Ankle	Human	Six areas: 1 – ankle talar 2 – ankle tibial 3 – knee tibial with menisci 4 - knee tibial without menisci 5 – femoral condylar 6 – femur patellar	**6.80** and **7.10** for lateral and medial tibial surface covered by meniscus, respectively. **3.92** and **4.80** for lateral and medial tibial surface not covered by meniscus, respectively	Indentation	Assessment required in animal models for further clarification	Yao and Seedhom, (1993)

b) Dynamic Modulus (MPa)						
Anatomical Site	**Species**	**Number of Measurements**	**Measurement**	**Test Method**	**Study Key Limitations**	**Reference**
Metacarpal	Cow	108 samples of 5 mm diameter 10 samples of 9 mm diameter	**580** (cartilage + brass), **20** (cartilage + cork) **86 - 128** at 100 g impact **195 - 237** at 500 g impact	Impact	Different sample diameters limit the accuracy for data comparison	Burgin and Aspden, (2008)
Femoral head	Human Cow	1 – plane-ended impact 2 – indentation	**85.1 at** 500 g impact (human), **170** at 500 g impact (bovine) **14.4** (human),	Impact Indentation	Damage not quantified nor are images provided of the cartilage prior to testing for	Jeffrey and Aspden, (2006)

			8.3 (bovine)		confirmation of damage absence	

c) Storage Stiffness (N/mm)						
Anatomical Site	**Species**	**Number of Measurements**	**Measurement**	**Test Method**	**Study Key Limitations**	**Reference**
Femoral head	Cow	3 test regions per half femoral head	**367 – 1460**	Dynamic Mechanical Analysis	Assessment of viscoelastic properties not representative of physiological loading conditions	Sadeghi *et al*. (2015)
Knee	Cow	24 – two specimens (with and without meniscus) extracted from medial and lateral site	Maximum at **~1825**	Dynamic Mechanical Analysis	Viscoelastic data extracted from different regions	Fell *et al*. (2019)

d) Loss Stiffness (N/mm)						
Anatomical Site	**Species**	**Number of Measurements**	**Measurement**	**Test Method**	**Study Key Limitations**	**Reference**
(see column above)	(see column above)	(see column above)	**128 – 247**	Dynamic Mechanical Analysis	(see column above)	Sadeghi *et al*. (2015)
(see column above)	(see column above)	(see column above)	**~225**	Dynamic Mechanical Analysis	(see column above)	Fell *et al*. (2019)

e) Loss Modulus (MPa)						
Anatomical Site	**Species**	**Number of Measurements**	**Measurement**	**Test Method**	**Study Key Limitations**	**Reference**
Knee	Cow	29 points; 6-9 sites on central region of four tibial plateau	**3.2 – 6.7**	Dynamic Mechanical Analysis	No presentation of raw data of limits data analysis	Fulcher *et al*. (2009)
Femoral head Humeral head	Cow	16 specimens 3 test protocols: 1 – air/Ringer's solution 2 – varied stress 3 – on/off-bone	**5 – 11**	Dynamic Mechanical Analysis	Assessment on more than one joint type limits accuracy for data comparison	Lawless *et al*. (2017)

f) Storage Modulus (MPa)						
Anatomical Site	**Species**	**Number of Measurements**	**Measurement**	**Test Method**	**Study Key Limitations**	**Reference**
(see column above)	(see column above)	(see column above)	**20 – 117**	Dynamic Mechanical Analysis	(see column above)	Lawless *et al*. (2017)

(see column above)	(see column above)	(see column above)	**82 – 93**	Dynamic Mechanical Analysis	(see column above)	Fulcher *et al.* (2009)
Knee	Cow	16 specimens 1 – 1200 cycles compression deformation response 2 – compared to pre-tests 3 – damage checks	**~15 – 33**	Impact and Cyclic Compressive Loading	Trauma induced stresses provide measurements of damaged cartilage	Verteramo and Seedhom, (2007)

Note, it is clear from Table 2.1 that the studies have been performed on both human and cow species. Thus, the cow model is an accepted surrogate for representing human articular cartilage. However, it is important to note that key differences in the morphology and cell concentration have been reported for bovine and human articular cartilage. For instance, it has previously been identified for an increased thickness of human cartilage in comparison to bovine, as well as a greater birefringence in the superficial and deep zones of human articular cartilage (Rieppo *et al.,* 2003). Furthermore, human articular cartilage has a reduced proteoglycan concentration in the superficial zone, in comparison to bovine articular cartilage (Rieppo *et al.,* 2003). Overall, the total proteoglycan concentration is shown to be less in bovine articular cartilage than human (Rieppo *et al.,* 2003). Thus, of course, the use of human articular cartilage provides an accurate representation of the scenario *in vivo*.

2.5.2 Failure Properties

Failure of articular cartilage has been assessed in the literature with respect to both *in vitro* and *in vivo* circumstances. Factors such as frequency, repeated loading and the nature of the underlying subchondral bone are associated with cartilage surface damage. This subsection outlines studies that have addressed the failure of articular cartilage in such manners, whilst a summary of the data is provided in Table 2.2.

In vitro testing allows for the assessment of cartilage damage initiation or explant effects, generally up to a maximum period of several weeks (Nickien *et al*., 2018). A previous study has identified the effect of impact load on articular cartilage *in vitro*, with respect to the resulting matrix integrity and chondrocyte viability (Jeffrey *et al*., 1995), for which a linear relationship was observed for chondrocyte viability and impact energy (Jeffrey *et al*., 1995). Similar work for the identification of chondrocyte cell death and the variation in matrix properties was conducted in a previous *in vitro* study, for the application of injurious compression to bovine articular cartilage discs (Loening *et al*., 2000). The traumatic loading was applied via six repeated on and off cycles at a strain rate of 1000 μm/s, within a strain range of 30-50 %, maintained for 5 minutes, followed by the release of compression for 25 minutes (Loening *et al*., 2000). The results indicated chondrocyte cell death at peak stresses as low as 4.5 MPa, whilst observed to increase with peak stress (Loening *et al*., 2000), as identified in the work of Jeffrey *et al*. (1995) with an increase in impact energy.

Similar to 40 % chondrocyte viability observed at high impact in the work of Jeffrey *et al.* (1995), the study performed by Loening *et al*. (2000) identifies a minimum of 50 % cell apoptosis in relation to a high peak stress greater than 20 MPa. This work has been performed on immature bovine cartilage. The use of immature tissue is advantageous for increased cellular repair (Khan *et al*., 2008) and quantity (Szeparowicz *et al*., 2006). In addition, the potential for a higher proliferation rate for chondrocytes is associated with young tissue (Szeparowicz *et al*., 2006). Thus, the use of immature cartilage for this study formed a crucial aspect to assess cell viability at its peak.

Previous work identifies a correlation between the peak-stress, stress-rate and loading-duration on the resulting compositional and metabolic changes of canine articular cartilage (Chen *et al*., 1999). A lower identified peak stress to the work of Loening *et al*, (2000), of 2.5 MPa has been associated with matrix damage and the increase in water content (Chen *et al*., 1999). Similar to the outcome of Loening *et al.* (2000), having identified 50 % cell apoptosis at

a peak stress greater than 20 MPa, this study has identified damage to the cartilage visualised macroscopically, when subject to impact loads greater than or equal to 20 MPa (Chen *et al*., 1999). Further, the study has identified an increase in damage to the collagen network, across a 10-day culturing period post impact loading, with a further conclusion of stress-rate determining cartilage damage of at least 30 MPa/s for 2 minutes (Chen *et al*., 1999).

In the work of Jeffrey *et al*. (1995), the fissures observed for specimens removed from the bone were generally at an approximate angle of 45° to the cartilage surface, penetrating as far as the transition zone, resulting in a delaminating effect for the loose attachment of the surface-zone cartilage to the remainder of the tissue (Jeffrey *et al*., 1995). Similarly, the work of Chen *et al.* (1999), identifies denatured collagens located near the articular surface (Chen *et al*., 1999). However, to improve the understanding of the resulting cartilage damage, macroscopic images could be provided, particularly of the breakage of the entire cartilage core to pieces, reported at a load of 60 MPa (Chen *et al*., 1999). For critical assessment of the work of Jeffrey *et al*. (1995) the lack of specimens extracted with the bone remaining, in comparison to bone removal, fails to provide an equal evaluation for both specimen variations. A solution would have involved the purchase of further bovine joints for the increased extraction of cartilage on-bone specimens.

Whilst the application of *in vitro* techniques for the assessment of cartilage damage allows for i) a repeatable and controlled protocol (Nickien *et al*., 2018), ii) the systematic exploration of a range of stresses or strains, and iii) the quantitative exploration of the effect of predetermined injurious loading parameters on tissue biomechanical/biological properties (Loening *et al*., 2000), the complex three-dimensional loading system of a human joint provokes difficulty in the mimicking of *in vitro* systems (Bader *et al*., 2011; Loening *et al*., 2000).

In vivo testing allows for the determination of cartilage overloading on the inducement of post-traumatic osteoarthritis (OA), commonly through impact loading, supply of matrix-

degrading substances or the alteration of joint kinematics, with assessment conducted from months up to a year (Nickien *et al*., 2018). Previous work demonstrates an *in vivo* study on a rabbit knee joint with exposure to cytokine to induce damage, identifying up to 50 % of proteoglycan loss from the matrix. In the work of Thomas *et al.* (1991), the inhibition of glycosaminoglycan synthesis was observed at one day post injection, which was shown to reduce one week later in the patellar and femoral cartilages of the rabbit knee joint (Thomas *et al*., 1991). A similar outcome of proteoglycan loss is also demonstrated in later work, identifying the damaging effect to the ECM, by a single high-energy impact load on the development of posttraumatic OA in rabbits (Borrelli *et al*., 2008).

Consequently, the results of *in vitro* and *in vivo* testing complement one another, as demonstrated by similar damage methods such as chondrocyte loss and collagen de-structuring (Nickien *et al*., 2018). Therefore, the use of *in vitro* models to replicate the study of *in vivo* testing should be encouraged, reducing the use of animals, based on an ethical perspective (Nickien *et al*., 2018). In particular, a joint motion simulator provides an effective middle ground between *in vitro* and *in vivo* testing, allowing for increased controlled loading than *in vivo* testing. Also, the application of loading in a joint simulator is closer to physiological regimes than explored in *in vitro* testing (Nickien *et al*., 2018). Thus, the use of a joint simulator was implemented for the assessment of cartilage bio-mechanical properties, in Chapter 4 of this thesis.

In addition, the surface damage of articular cartilage is important to assess for the determination of the damage inducing factors, to allow for the investigation into the control of cartilage damage initiation and development. The outcome of such research has implications on the joint disease of OA.

Concerning the effect of frequency, in particular on the surface damage of articular cartilage, previous studies have identified a positive correlation with the applied frequency of

loading, and corresponding cartilage damage. The study of Sadeghi *et al*. (2015), explores the resulting surface defects of articular cartilage whilst subject to a sinusoidal load via a stainless-steel indenter (Sadeghi *et al*., 2015). The results identified a positive correlation with the applied frequency of loading and respective crack and fissure length, demonstrated by the increase in mean total crack length by 1.1, 2.4 and 5.1 mm, at the respective loading frequencies of 1, 10 and 100 Hz (Sadeghi *et al.,* 2015). This outcome is similar to a previous study that determines an increase in crack length propagation with frequency, identifying a maximum crack growth of 0.6, 0.8 and 1.1 mm, at frequencies of 1, 10 and 100 Hz, respectively (Sadeghi *et al*., 2018). An additional study has also identified the reduction in the fracture resistance of cartilage, with an increase in loading frequency, on performing cyclic three-point bend tests at 1, 10 and 100 Hz (Sadeghi *et al.*, 2017). Again, the impact of frequency in the study of Sadeghi *et al*. (2017), is similar to the effect of frequency on the increase in cartilage damage, as shown previously (Sadeghi *et al*., 2015; 2018).

Such studies have effectively developed a repeatable protocol for the assessment of cartilage surface damage under various testing configurations, yet with respect to a central factor of frequency. All the studies discussed show an increase in cartilage surface damage with frequency. However, the large difference in the time frame corresponding to each frequency, such as 2 hours and 47 minutes and 100 seconds at a frequency of 1 and 100 Hz, respectively (Sadeghi *et al*., 2017), may raise questions as to the equality of damage inducement. This is due to the under prediction of failure at 100 Hz as a result of the lower time of loading, in comparison to the application of 1 Hz.

In terms of the effect of repeated loading on the assessment of cartilage surface damage, the study by Kerin *et al*. (2003) induces failure via an indenter, similar to previous work (Sadeghi *et al*., 2015), identifying the effect of cyclic loading on specimens at 40% of the failure stress (Kerin *et al*., 2003). It was observed in this work for cartilage surface fractures to increase in length with cyclic loading (Kerin *et al.*, 2003), therefore illustrating as an additional

factor to the frequency explored in previous work (Sadeghi *et al*., 2015; 2017; 2018). Fissures in this study were identified as the surface damage, shown to rapidly increase during the initial 75 cycles, with a prominent parallel orientation (Kerin *et al*., 2003), as observed in previous work (Sadeghi *et al*., 2015), to the direction of the split line pattern.

Earlier work demonstrates human cartilage surface fibrillation in response to fatigue testing via indentation, set at a frequency of 6 cycles min^{-1} for a loading duration of 1 second (Weightman *et al*., 1973). On completion of 90,000 load cycles at nominal stress of 2 MN m^{-2}, the results illustrate surface cracks and fibrillation in response to the fatigue mechanism (Weightman *et al*., 1973), similar to the outcome from previous studies (Kerin *et al*., 2003; Sadeghi *et al*., 2015). This study provides great knowledge of human articular cartilage surface failure (Weightman *et al*., 1973), an area which the previously described studies do not address (Kerin *et al*., 2003; Sadeghi *et al*., 2015; 2017; 2018). However, the study does not provide details on specimen preparation for repetition of the protocol, whilst only one test specimen is identified for surface cracking and fibrillation, thus, further details are arguably required here.

The nature of the underlying subchondral bone is also reported in the literature for the negative impact on the damage to articular cartilage. The work of Radin and Rose has proposed the hypothesis of the effect of impulse loading on the association between bone stiffening and cartilage breakdown, leading to degeneration of the joint, due to increased stresses acting upon the cartilage (Radin *et al*., 1972). This hypothesis is supported by previous work that has identified a stiffer bone in patients suffering from OA, in comparison to those with osteoporosis (OP), at 356 and 247 MPa, respectively (Li and Aspden, 1997).

The work of Day *et al.* (2001) identifies a reduced bone tissue stiffness in accordance with mild cartilage damage. This study has further considered an increased bone volume fraction for the potential association with cartilage damage (Day *et al*., 2001). This study was performed on the proximal tibia, for which both the medial and lateral sites were assessed

(Day *et al*., 2001). Previous work is in support of this outcome, having identified a significant increase in bone volume fraction and the trabecular thickness of the cancellous bone from OA patients, in comparison to cancellous bone from OP patients (Li *et al*., 2012). This study was performed on the femoral head of the hip joint (Li *et al*., 2012).

Literature reports an inverse relationship between OA and OP. This relates to the relationship between an increase in BMD and the occurrence of OA. For instance, the Chingford Study demonstrates the increased BMD in the hands, knees and lumbar spine of middle-aged women. In these locations, OA is present (Hart *et al*., 1994). Similarly, the work of Hordon *et al*. (1993) observes the increased BMD in the spine and distal forearm for women with OA (Hordon *et al*., 1993). This relationship is also supported by a previous study that observes a higher BMD in the hip of women with moderate to severe hip OA (Nevitt *et al*., 1995).

Conversely, the inverse relationship between OA and OP has raised controversy amongst authors (Shen *et al*., 2013), such that previous studies have identified the correlation not only between OA and increased BMD, yet also the relationship between the additional factor of increased bone loss and OA (Burger *et al.,* 1996).

Table 2.2: Summary of the failure properties described in Section 2.5.2

In Vitro			
Method	**Result**	**Study Key Limitations**	**Reference**
Impact loading 500 g release from 20 cm height	Linear relationship between chondrocyte viability and impact energy 40 % chondrocyte viability	Varied specimen type preparation: cartilage on- and off-bone creates questioning as to a fair comparison	Jeffrey *et al.* (1995)
Injurious compression 1000 µm/s 30-50% strain	Increase in chondrocyte death with peak stress; 50 % cell apoptosis > 20 MPa; cell death at 4.5 MPa	Young, immature cartilage may confer different stress threshold to adult articular cartilage	Loening *et al*. (2000)
Repeated impact loading	Cartilage matrix damage at repeated impacts of 2.5 MPa	Lack of microscopical image detail, particularly of entire cartilage core damage	Chen *et al.* (1999)
In Vivo			
Method	**Result**	**Study Key Limitations**	**Reference**
Injection with catabolin/interleukin 1	50 % proteoglycan loss with cytokine	Caution to be taken for comparison to human articular cartilage	Thomas *et al*. (1991)
High-energy impact loading	Proteoglycan loss, decreased type II collagen and chondrocyte loss for posttraumatic osteoarthritis cartilage appearance	Quantitative assessment of % proteoglycan loss not provided to allow for detailed evaluation – based on histological staining	Borrelli *et al.* (2008)
Surface Damage: Effect of Frequency			
Method	**Result**	**Study Key Limitations**	**Reference**
Indentation at frequencies 1, 10 and 100 Hz	Increased crack length formation with loading frequency	Large variation in loading time-frame limits equality in damage inducement; associated with 1, 10 and 100 Hz; ranging from 100 s to 2 hr and 47 mins	Sadeghi *et al*. (2015)
Cyclic tensile strain on pre-existing crack	Increased crack length propagation with frequency		Sadeghi *et al*. (2018)
Three-point bending at frequencies 1, 10 and 100 Hz	Reduced fracture resistance with frequency		Sadeghi *et al*. (2017)
Surface Damage: Effect of Repeated Loading			
Method	**Result**	**Study Key Limitations**	**Reference**
Fatigue testing	Increase in cartilage fissure length and height loss with cyclic loading; mean increase at 353 % and 360 %, respectively	Use of saline for hydration may affect height loss measurements	Kerin *et al*. (2003)
Fatigue testing	Surface cracking and fibrillation with fatigue testing	A minimal of one specimen result presented for surface cracking and fibrillation	Weightman *et al*. (1973)
Underlying Subchondral Bone			
Method	**Result**	**Study Key Limitations**	**Reference**
Impulse loading	Bone stiffening associated with cartilage breakdown	Limited hypothesis of the relationship simply between bone stiffness and cartilage breakdown	Radin *et al.* (1972)

Unconstrained compression testing 20%/minute	Stiffer bone for osteoarthritic patients	Clear quantitative final values would improve ease of understanding for extractions of conclusions	Li and Aspden (1997)
Finite element models Compressive mechanical testing	Increase in bone volume fraction associated with cartilage damage and osteoarthritic patients	Selection of Caucasian/Chinese donors limits representation of results across other populations	Day *et al*. (2001); Li *et al*. (2012)
The Chingford Study – radiographs and bone densitometry (Hart *et al*., 1994) Dual energy X-ray absorptiometry (Hordon *et al*., 1993) Radiography (Nevitt *et al.,* 1995)	Increased bone mineral density associated with OA	Representation of final results not provided on overall figure for clear trend observation in the work of Hart *et al.* (1994) and Hordon *et al.* (1993) Healthy subjects not representative of all women with OA in the work of Nevitt *et al.* (1995)	Hart *et al*. (1994); Hordon *et al.* (1993); Nevitt *et al.* (1995)
Radiographs for osteoarthritis assessment Kellgren score for bone loss assessment	Increased bone loss associated with osteoarthritis	Small axis provided in the figures create difficulties for assessment	Burger *et al*. (1996)

Consequently, the studies discussed in this section do not focus on a multi-factorial contribution to the onset of cartilage surface damage, yet are limited to the evaluation of a single mechanical factor, such as frequency, number of loading cycles or an increased BMD. Therefore, research is required on the resulting effect of the combination of damage inducing factors to articular cartilage.

2.5.3 Frictional Properties

When applying an external load, the interstitial fluid of articular cartilage is known to pressurise, from which the fraction of the total load supported by the fluid pressurisation is known as the fluid load support (Ateshian, 2009). Providing the interstitial fluid support remains elevated, the maintenance of the low friction of articular cartilage is achieved (Krishnan *et al.,* 2004). This phenomenon is described by the exudation of interstitial fluid into the unloaded areas and joint capsule, leading to the reduction of the stresses supported by the solid matrix (Ateshian, 2009; Forster and Fisher, 1996). This behaviour is in line with the enhanced fluid

load support, leading to the decline in the coefficient of friction as a result of load transfer between the solid and fluid phases (Krishnan *et al*., 2004).

A previous study has performed friction tests of articular cartilage against glass at 1 mm s^{-1} across a distance of 56 mm in each direction (Whitney *et al.,* 2015). Following on from the rectification of the raw coefficient of friction data, the result for native cartilage was observed to reach an approximate maximum friction of 0.38 at 10000 seconds (Whitney *et al.,* 2015). This result differs to the coefficient of friction obtained in a previous study at approximately 0.12, for cartilage sliding at 5.0 mm at 1 mm/s against glass, over a four-hour period (Oungoulian *et al.,* 2015). In the work of Whitney *et al*. (2015) histology was performed to analyse the resulting damage to the articular cartilage as “damaged” or “internally damaged”. The term “damaged” was used to describe greater than 5 % of observed surface damage, and the term “internally damaged” was used to describe less than 5 % of observed surface damage (Whitney *et al.,* 2015).

A measurement of the exact quantity of damage to the surface, would provide a quantifiably comparable representation of the damage present, rather than categorical statements as often used (Whitney *et al.,* 2015). The study by Whitney implements the use of a support vector machine, where the support vectors are used to generate the decision boundary of the classification of damaged and undamaged samples, post friction testing, as marked by red or green circles, respectively. The support vector machine was selected for the analysis of the generated friction signal features that were specific to the raw coefficient of friction signal, to allow for the identification of damaged specimens incurred during the friction tests. The support vector machine identified specimens falling within the region of two boundaries as damaged, whilst those appearing outside the boundaries as undamaged. The support vector machine was successful in the ability to detect damaged samples with a median accuracy of 90 %, whilst undamaged samples were detected with a median accuracy of 82 % (Whitney *et al.,* 2015). However, the study is limited to the absence of the information on the

exact time period of the occurrence of the damage, as is the visual characterisation of damage within the two categories, certainly an area of subjection (Whitney *et al.,* 2015).

The work by Oungoulian *et al.* (2015) further characterised the friction between bovine articular cartilage and implant materials, to include cobalt chromium; low and high carbon, as well as 316 low vacuum melt stainless steel. On completion of the four-hour test period, the coefficient of friction was observed to reach approximately 0.16, 0.12 and 0.25, for the friction tests of cartilage against cobalt chromium; high and low carbon, as well as stainless steel, respectively (Oungoulian *et al.,* 2015). In addition, this study has identified the greatest damage in the form of delamination to the cartilage surface layer, post-sliding, against 316 low vacuum melt stainless-steel, further reinforced by the largest coefficient of friction for this material interface (Oungoulian *et al.,* 2015). This study is particularly important for this thesis, as it highlights the two-way interaction between the cartilage and implant material. This indicates the requirement to undertake research to explore the three-way interaction, not only between the cartilage and implant material, yet also against that of articular cartilage itself.

A further study has explored the effect of loading time and lubricant type on the resulting coefficient of friction of articular cartilage (Forster and Fisher, 1996). Protocol set-ups included sliding at 4 mm/s with a 30 N normal load, of cartilage against metal, metal against cartilage as well as cartilage against cartilage, using either synovial fluid, Ringer's solution or no lubrication (Forster and Fisher, 1996). For all testing groups, the results indicated an increase in the coefficient of friction up to approximately 0.30 at the 45-minute testing point (Forster and Fisher, 1996). Particularly for the cartilage against cartilage testing configuration, the results identified a decline in the friction with use of synovial fluid in comparison to Ringer's solution, attributed to an enhanced boundary lubrication mechanism (Forster and Fisher, 1996). Thus, this study has effectively identified two key influencers on the coefficient of friction, that being loading time and lubricant type (Forster and Fisher, 1996).

The study by Forster and Fisher regards the biphasic theory of articular cartilage as the explanation for the observed increase in friction, described by the rise in the load carried by the solid phase (Forster and Fisher, 1996). However, it has been reported that the fluid pressure takes approximately 15 minutes to reach the peak (Fick *et al*., 2011), thus, the biphasic theory raises questions as to the amount of time required for internal fluid pressure to take precedence, creating controversy in the ideas (Fick *et al.,* 2011).

The measurement of the coefficient of friction of articular cartilage is important to study, whilst research has further identified the influence of the zones within the tissue. A previous study has concluded that approximately 100 µm of the uppermost superficial zone of articular cartilage, fails to withhold specific properties that correlate to a direct effect on the frictional properties of the tissue (Krishnan *et al*., 2004). This conclusion has been identified through unconfined compression creep tests of sliding cartilage against glass, prior and post-removal of the superficial zone, as well as upon complete surfaces of the tissue, including the deep zone (Krishnan *et al*., 2004). Although the rationale to explore the varying effects of the zones of the tissue with respect to the frictional properties certainly implies importance, as determined in this study (Krishnan *et al*., 2004), the sliding of cartilage against cartilage would certainly provide enhanced accuracy in the evaluation.

It is key to underpin that the central concept of the friction studies of articular cartilage in the literature, concern the measurement of the coefficient of friction in relation to a kinetic in sliding, thus confer a limitation in the analysis of the physiological movement of a joint (Schenau, 1989). The particular response of the resulting friction of articular cartilage in relation to a rotation, known as torque, is in fact unknown data. Torque is particularly important to measure as the underlying kinetic to this measurement closely mimics joint movement *in vivo.* Further, the response of articular cartilage subject to a rotational movement can allow for investigation of its specific boundary lubrication mode (Accardi *et al*., 2011), representing the lubrication present at the cartilage-cartilage boundary *in vivo* (Cilingir, 2015). Consequently,

Chapter 4 of this thesis considers the development of a technique to assess the frictional torque of articular cartilage.

2.6 Clinical Applications of Cartilage Damage

2.6.1 Mechanical Implications

In terms of the effects of loading, the resulting impact energy following on from a single traumatic loading case (Huser and Davies, 2006) and repeated loading (Cooper *et al.,* 1994), are considered as risk factors for cartilage damage. Additionally, the type of loading is associated with cartilage damage, as demonstrated by the increased resistance to damage when subject to dynamic loading, in comparison to static loading (Flachsmann *et al.,* 2001 & 2005), whilst an increase in the number of cycles has further identified cartilage softening and damage (Vazquez *et al.,* 2019). As previously highlighted, the increase in loading frequency has demonstrated enhanced damage to articular cartilage (Sadeghi *et al.,* 2015; 2017; 2018), as well as the relative position adjacent to a lesion of articular cartilage to have established enhanced rupture (Flachsmann *et al*., 2005).

To determine the peak forces on physiological loading of the human knee, the value is reported to be of the range of 1.9 to 7.2 multiplied by the body weight of the individual (Komistek *et al.,* 2005). This measurement range has been obtained from various approaches in literature. The measurements have been extracted across various activities to include walking, stair climbing as well as jogging (Komistek *et al*., 2005). The two common techniques are experimental and mathematical modelling (Komistek *et al*., 2005). Experimental techniques to directly measure the forces in a joint involved the use of a transducer (Kaufman *et al*., 1996; Morris *et al*., 2001). The use of strain gauges is a further experimental approach for peak force measurements (Burny *et al*., 2000). Alternatively, mathematical modelling techniques predict the contact forces and torques at a joint (Komistek *et al*., 2005). To develop the model of a human joint, three rigid bodies are to be represented (Komistek *et al*., 2005). The use of *in vivo*

data to construct computational models for the measurement of forces in a joint has recently been implemented (Komistek *et al*., 2005). For this model, a free-body diagram was developed, after which position vectors were applied to foot and ground contact (Komistek *et al*., 2005).

Three conditions define the specific impact loads that contribute to articular cartilage damage, to include a millisecond order of peak load, as well as one of either the three conditions outlined below (Aspden *et al*., 2002). Though, as a limitation to such conditions, damage to articular cartilage is also possible with repeated loading, alone (Athanasiou, 2013).

1) *Stress rate* ***> 1000 MPa/s***
2) *Strain rate* ***> 500 s^{-1}***
3) *Loading rate* ***> 100 kN/s***

Articular cartilage has been evaluated for damage under shear. That study found that a compressive strain rate of 0.1 to 1.0 s^{-1} up to 50 % strain, reduced the viability of the chondrocytes (Kurz *et al*., 2001). A similar outcome is observed on the suggested outcome concerning the decline in proteoglycan synthesis, on strain application of 0.1 s^{-1} at 40 % (Ryan *et al*., 2009), thus, both studies are in accordance with one another. In the normal direction to shear, it is reported that articular cartilage is weaker in tension (Kempson *et al.,* 1972), which has implications for damage under torsion (Kempson *et al.,* 1972). However, any conclusions would require further testing to indicate whether this were indeed the case (Kempson *et al.,* 1972).

2.6.2 Clinical Implications/Osteoarthritis

The Outerbridge classification is a common technique used by orthopaedic surgeons for the identification of the level of severity of cartilage lesions (Outerbridge, 1961). The four various grades are described below (Outerbridge, 1961). An image to represent the cartilage at each grade is provided in Figure 2.26.

1) **Grade 0:** Normal cartilage

2) **Grade 1:** Softened cartilage with no apparent damage
3) **Grade 2:** Surface fibrillation with diameter < 1.5 cm of extension to subchondral bone
4) **Grade 3:** Surface fibrillation with diameter > 1.5 cm extension to subchondral bone
5) **Grade 4:** Subchondral bone exposure

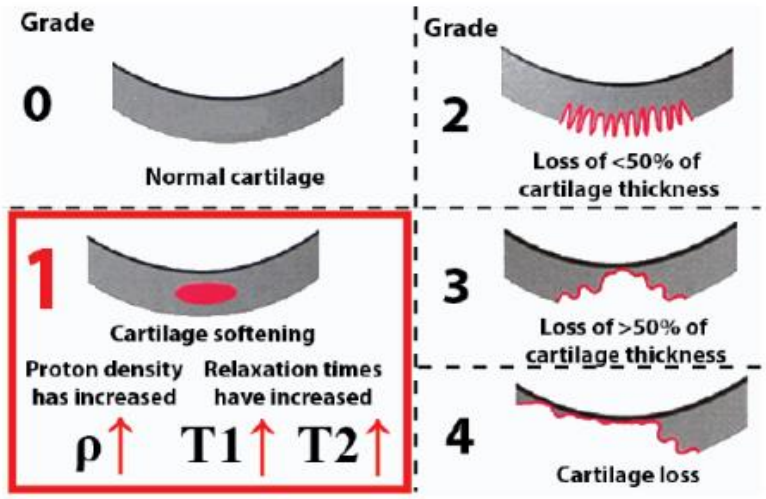

Figure 2.26: Schematic to represent the condition of articular cartilage at each of the four grades of the Outerbridge Classification. (Reprinted from IOP Conference Series: Journal of Physics: Conference Series: 2016 Congress on Industrial and Applied Life Sciences and Mathematics; Development of methods for analysis of knee articular cartilage degeneration by magnetic resonance imaging data, A Suponenkovs, A Glazs and A Platkajis, volume 818, 2017, which is distributed under the terms of the Creative Commons Attribution 3.0 International License (http://creativecommons.org/licenses/by/3.0/), which permits unrestricted use, distribution, and reproduction in any medium))

A later histological-histochemical grading system was introduced in 1971, known as the MANKIN system, extensively used for the assessment of OA cartilage (Rutgers *et al*., 2010). The MANKIN system evaluates four key areas, that of i) cartilage structure, ii) cellularity, iii) Safranin O staining and iv) tidemark integrity, for the summation of scores of each category, resulting in a total score determinant of 'normal' at 0, to 'severe OA' at a total score of 14 (Pauli *et al.,* 2012).

The type of arthritis associated with the destruction and abnormality to the tissue is known as osteoarthritis (OA) (Medvedeva *et al*., 2018; Tiku and Sabaawy, 2015). OA is reported to affect approximately 3.3 % to 3.6 % of the global population, whilst 43 million people

are known to suffer from moderate to severe stages of the disease (Sen and Hurley, 2019). Consequently, OA is ranked as the 11th distressing disease on a world-wide scale (Sen and Hurley, 2019). Whilst the condition of OA is regarded as a degenerative joint disease (Litwic *et al*., 2013), specific definition is given by the "progressive damage to articular cartilage" (Athanasiou, 2013), such that factors concerning obesity (King *et al*., 2013) and ageing (Anderson and Loeser, 2010) contribute to the rise of the disease incidence.

A patient suffering with severe stages of OA would typically be referred for total joint replacement (TJR) (Medical Advisory Secretariat, 2005). TJR would be expected to last for approximately 10-20 years (Athanasiou, 2013), taken as the end-of-line scenario treatment option (Medical Advisory Secretariat, 2005). Three variations exist for the knee replacement, to include i) non-constrained which uses the patient's ligaments for stability of the prosthesis, ii) semi-constrained not wholly relying on the patient's ligaments for stability, and iii) constrained, where the patient's ligaments are insufficient for the provision of stability (Medical Advisory Secretariat, 2005). Note, the TJR is discussed here due to its widespread practice. The knee in particular is not a central focus of this thesis.

The studies developed in this thesis use the humeral head of the shoulder joint. A similar approach to the TJR is applied for total shoulder arthroplasty. The TJR can be extrapolated to total shoulder arthroplasty of first assessing the situation of the joint, the rotator cuff and glenoid cavity. This information is used to determine the implant. Only with the presence of an intact glenoid socket can shoulder arthroplasty take place, to allow for successful implantation of the glenoid part. A hemi-arthroplasty, alike to partial TJR, is the most suitable option when the glenoid is misaligned. For the resurfacing prosthesis, the technique involves measuring the humeral head prior to its preparation. A neck resection is carried out prior to implantation of the prosthesis. For implantation of the humeral head, a collar is inserted. Sutures are then used to repair the anterior capsule and tendons (Merkle *et al.,* 2016). Therefore, the final stages of repair to damaged articular cartilage display similarities across different joints.

As for any surgical intervention, several disadvantages and risks are associated with total joint replacements, to include wear, leading to the failure of the implant, the instability as well as loosening (Medical Advisory Secretariat, 2005). Consequently, this creates the importance for the development of alternative techniques, of a non-surgical nature for the treatment of damaged articular cartilage. In fact, the avascular characteristic of articular cartilage leads to great difficulty in the natural healing response of the tissue (Karuppal, 2017). It has been reported that articular cartilage defects have the potential to develop into OA (Hjelle *et al.,* 2002). Consequently, this leads to the discussion of the available treatment techniques to provide a solution for the repair of such a tissue, absent with blood vessels, nerves or lymphatics (Fox *et al.*, 2009).

2.6.3 Cartilage Defect Repair

Articular cartilage defects can be divided into chondral or osteochondral, depending on the defect depth, whilst chondral defects are further categorised as full thickness (to subchondral bone), or partial thickness (cartilage flap) (Figure 2.27 – 'E'). The osteochondral defect is known to extend to the underlying subchondral bone (Figure 2.27 – 'F'), to cross the tidemark (Bhosale and Richardson, 2008).

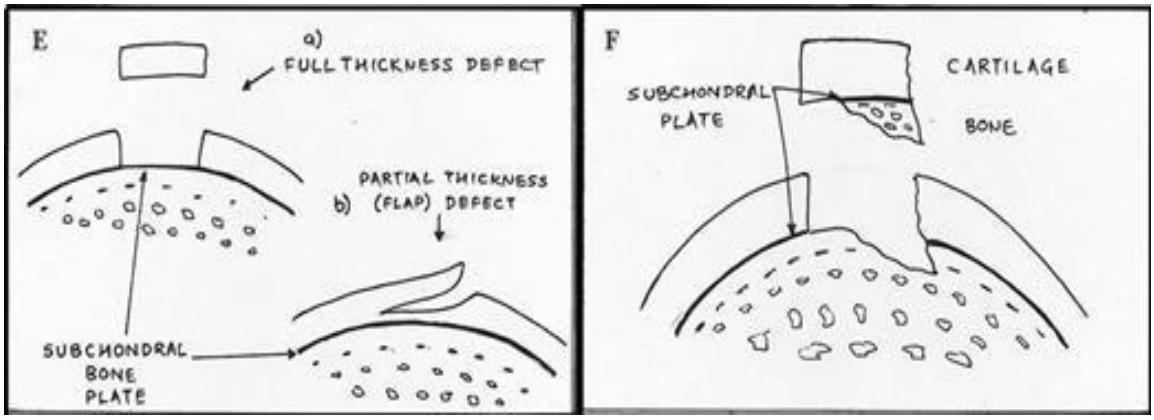

Figure 2.27: The division of cartilage defects into 'E') full thickness or partial thickness as the two categories of chondral defects. The full thickness defect is shown to expose the subchondral bone plate, whilst the partial thickness defect results in cartilage flapping, rather than subchondral bone exposure. Osteochondral defects are illustrated by segment 'F' of the schematic, shown to impact both the cartilage as well as underlying subchondral bone. (Reprinted from Articular cartilage: structure, injuries and review of management, volume 87, A.B. Bhosale and J.B. Richardson, pp 77-95, 2008, with permission from Oxford University Press).

The technique of microfracture initiated in the early 1980s, with advantages of the low cost, lack of complications as well as the low rate of related patient morbidity (Steadman *et al.,* 2010). Microfracture is implemented for small to medium sized chondral and osteochondral defects (Kuroda *et al*., 2007). The procedure involves the removal of unstable articular cartilage for the exposure of a defect surrounded by normal cartilage, following which multiple fracture holes are induced into the subchondral bone plate, at 3 to 4 mm apart, whilst ensuring maintenance of the integrity of the subchondral bone plate (Bhosale and Richardson, 2008). Clotting occurs within the defect site, for the end-result amongst a fibrin clot as the formation of fibrocartilage, which, however, does not resist compression and shear loads as effectively as hyaline cartilage (Lewis *et al*., 2006).

Advances in the microfracture method include the use of the periosteal flap, demonstrated in previous work by the harvesting of the periosteal flap from the medial part of the proximal tibia, for placement over the defect. This was followed by the suturing of the flap via approximately five sutures to the defect rim, glued with Tisseal glue (Aroen *et al*., 2003).

Autologous chondrocyte implantation (ACI) is a further approach used for the repair of damaged tissue, as initially highlighted in 1994 (Brittberg *et al*., 1994). The technique involves three phases, to include i) the extraction of healthy cartilage tissue via arthroscopy, ii) chondrocyte culture and iii) transplantation of the chondrocytes into the defect-site, forming articular cartilage, close to that of the hyaline type (Na *et al*., 2019). Of course, there are several disadvantages associated with this treatment method, to include the limitation of the articular cartilage available for extraction, which must be absent of the condition of OA, as well as the inability to withstand the mechanical properties if extracted from a non-loaded region (Athanasiou, 2013). As a limitation, both microfracture and ACI techniques do not lead to the formation of pure cartilage of the hyaline type, but rather of the fibrocartilage type (Hu and Nukavarapu, 2019).

Allograft procedures differ to autologous implants, in that the extraction of articular cartilage is of deceased donors, thus, allowing for extraction of larger quantities of articular cartilage (Athanasiou, 2013), for ease and convenience for use by surgeons (Giedraitis *et al.,* 2014). However, there are limitations with such a procedure, namely the potential of immune rejection, transmission of disease (Athanasiou, 2013) or a reaction to the sterilization process (Giedraitis *et al.,* 2014). Recent studies have demonstrated a high success rate for osteochondral allograft procedures. For femoral procedures, this includes a 96% survival at 2 years (McCulloch *et al*., 2007), a 76% survival at 15 years (Emmerson *et al*., 2007), as well as a 66% survival at 20 years (Levy *et al*., 2013). The success rate for tibial osteochondral allografts has been reported as 95% at 5 years (Gross et al., 2005) and 68% at 10 years (Getgood *et al*., 2015). Kaplan-Meier follow-up survival of osteochondral allograft transplantation in the humeral head, projected to arthroplasty, is reported at 80% (Riff *et al*., 2017).

2.7 Biomaterials for use in Cartilage Repair

The application of biomaterials is derived from the field of tissue engineering, described by the use of cells, engineered materials/scaffolds and biochemical factors for the improvement or replacement of biological functions (Akter, 2016; O'Brien, 2011). Biomaterials form the crucial component from which the scaffold is manufactured (O'Brien, 2011), and are commonly associated with three variations, to include natural, synthetic as well as composites (Hu and Nukavarapu, 2019). Natural based scaffolds are located within living organisms and on extraction can form useful biomaterials, for instance hydrogels (Athanasiou, 2013), as used for demonstration in the techniques developed in Chapter 4 and 5 of this thesis. A hydrogel can be defined as a polymer network, formed by the cross-linking of monomers, allowing for characteristics of swelling and the ability to retain water (Ahmed, 2015). Of the development of cartilage repair biomaterials, particular attention is required for the adoption of suitable

mechanical properties according to the defect site (O'Brien, 2011), allowing for the scaffold to withstand the mechanical loading environment *in vivo* (Athanasiou, 2013).

Previous studies have implemented the use of various natural biomaterials as the scaffold for cartilage repair. A study demonstrates the use of collagen type II mixed with chondrocytes extracted from New Zealand white rabbits, in a gel form, injected within a defect site (Funayama *et al*., 2008). The results from that study indicate a successful integration of the injected gel within the surrounding articular cartilage, as well as bone; thus, demonstrating that the collagen biomaterial is an effective natural scaffold material for use with chondrocyte transplantation (Funayama *et al*., 2008). A positive outcome for the use of collagen type II is also illustrated by the mixing with collagen type I, demonstrating the 3:1 ratio of collagen type I to type II, to display the improved ability to tolerate compressive forces (Portalatin *et al*., 2016). Further work demonstrates the use of hyaluronic acid (HA) hydrogels to work in combination with transforming growth factor-beta and human mesenchymal stem cells (MSCs) (Bian *et al*., 2011), identifying the success in the formation of neocartilage (Bian *et al*., 2011). HA is further utilised in combination with methacrylated glycol chitosan (MeGC), for the synthesis of a hydrogel, via photocrosslinking (Park *et al*., 2013), demonstrating chondrocyte viability of up to 90 % (Park *et al*., 2013). Further, the compressive modulus has shown to increase to 17 kPa with incorporation of HA with the MeGC, in comparison to the absence of HA, of MeGC alone, at 11 kPa (Park *et al*., 2013).

2.7.1 Alginate Biomaterial for use in Cartilage Repair

Alginate is a natural scaffold biomaterial, extracted from algae (Hu and Nukavarapu, 2019). It is a linear copolysaccharide, constituted of monomers β-D-mannuronate (M) and α-L-guluronate (G) (Li *et al*., 2007), known for application as an implanted or injected hydrogel for use in cartilage repair (Hu and Nukavarapu, 2019). The use of alginate has shown further success in the development of a chondrocyte seeded scaffold via a microfluidic device,

demonstrating chondrocyte viability through functional phenotypes (Wang *et al*., 2012). The novel manufacturing technique of 3D bioprinting has also demonstrated a positive output for the design of a nanofibrillated cellulose composite bionk, with the incoporation of alginate (Guyen *et al.*, 2017). The results have identified the suitability of the composite for the bioprinting of human-derived induced pluripotent stem cells, enabling cartilage generation (Guyen *et al.*, 2017). Thus, such studies have utilised complex technologies for the implementation of alginate, in light of developing effective cartiage repair techniques.

A further study demonstrates the ability of a combined calcium/cobalt alginate bead to promote chondrogenesis without the requirement of growth factors (Focaroli *et al*., 2016), thus, initiating a cost-effective protocol for the production of chondrocytes to enable cartilage repair (Focaroli *et al*., 2016). Success in the implementation of calcium gluconate with alginate for the manufacture of an injectable hydrogel, has also revealed effective defect and chondrocyte repair, identifying promising use for cartilage tissue engineering (Liao *et al*., 2017).

There are several advantages in using alginate, to include biocompatibility (Venkatesan *et al*., 2015) and a suitable environment for the distribution of MSCs to closely mimic the *in vivo* cartilage environment (Kurth *et al*., 2007). Further advantages include variable tensile properties (Drury *et al.,* 2004) and ease of manufacture of gel formation (Venkatesan *et al*., 2015). Thus, this has formed the foundation for selection of alginate as the base biomaterial for assessment, in Chapter 4 and 5 of this thesis.

3 EVALUATION OF THE EFFECTS OF SUBSTRATE DENSITY ON SURFACE DAMAGE OF ARTICULAR CARTILAGE

3.1 Introduction

Articular cartilage, as discussed in the Background section, is a connective tissue attached to subchondral bone, to allow for joint articulation of low friction via a smooth surface (Fox *et al*., 2009). Damage experienced by articular cartilage has been linked to the mechanism of loading, such as the effects of loading rates (Lawless *et al*., 2017; Shepherd *et al.*, 1997), impact loading (Burgin *et al*., 2008; Jeffrey *et al.,* 2006), and frequency independent of load (Sadeghi *et al*., 2015; Sadeghi *et al*., 2017; Sadeghi *et al*., 2018). In addition, the association between an enhanced stiffness of the subchondral bone and the advances in cartilage impairment (Radin *et al*., 1972), concerns the alterations in the underlying bone that are key to diagnosing osteoarthritis (OA). Further, there is a relationship between a high bone mineral density (BMD) and cartilage degradation (Dequeker *et al*., 2003; Teichtahl *et al*., 2017).

Bone remodelling has been hypothesised in the onset of OA, by the relationship between impulse loading of the bone at the joint experiencing fracture, to result in a stiffened base for the cartilage. Consequently, this exposes the cartilage to greater stress, leading to the enhancement of its rate of damage development (Radin *et al*., 1972). It is unknown as to whether, a potential 'mechanical' effect exists between the process of bone remodelling, in combination with a high BMD on the predisposition to articular cartilage failure. This concerns the effect of frequency as the mechanical cause for cartilage failure (Sadeghi *et al*., 2015; Sadeghi *et al.,* 2017; Sadeghi *et al*., 2018), in combination with a stiffened bone base, to enhance the development of cartilage damage (Radin *et al*., 1972). This is further reinforced by the concept of an increase in BMD and the occurrence of OA (Dequeker and Mbuyi-Muamba 1996; Foss and Byers 1972; Nevitt *et al.*, 1995; Burger *et al*., 1996). Thus, it is unknown as to whether a direct effect exists of the two damage inducing factors, to include

frequency of loading and the density of the underlying bone. To date, the literature has not addressed whether such factors act in combination on potential articular cartilage damage.

The aim of the work presented in this chapter was to investigate a potential relationship between frequency of loading of articular cartilage, and the density of its underlying substrate on corresponding cartilage damage. Thus, this chapter explores controlled evaluation of the density of an underlying substrate under isolated articular cartilage. An experimental approach was taken to explore the combined effect of substrate density and frequency on the resulting surface damage of bovine articular cartilage, both on- and off-bone. This was followed by the evaluation of the Hertzian contact stress at the cartilage-substrate interface, with relevance to the assessment of the surface damage of articular cartilage in this chapter.

3.2 Experimental Materials and Methods

3.2.1 Articular cartilage storage and handling

For the comparison between the effects of substrate density on the surface damage of articular cartilage, both on- and off-bone cartilage were evaluated. Twelve bovine humeral heads were obtained from a supplier (Dissect Supplies, Kings Heath, Birmingham, UK) from animals of the approximate age range of 18-30 months old at slaughter. Bovine articular cartilage was selected based on the previously established relationship of the frequency-dependent viscoelastic properties, consistent with that of human articular cartilage (Temple *et al.*, 2016). The humeral heads were covered in tissue paper, coated with Ringer's solution prepared to a full-strength mass concentration by dissolving 4.83 g of Ringer's tablets (Oxoid Ltd., Hampshire, UK), per 500 ml of distilled water, and separately stored in double heat-sealed plastic bag at - 40°C (Espino *et al*., 2014; Lawless *et al*. 2017). To prepare the bovine humeral heads for testing the samples were thawed (Temple *et al*., 2016). The freeze-thaw process does not affect the mechanical properties of articular cartilage (Szarko *et al*., 2010). India ink (Daler-Rowney, Bracknell, UK) was applied to the cartilage surface to ensure that humeral

head cartilage surfaces were free from lesions ahead of the selection of areas for dissection, both for off- and on-bone cartilage sample preparation (Meachim, 1972; Sadeghi *et al.,* 2017; Lawless *et al*., 2017). This procedure was applied before coring described for off- and on-bone cartilage extraction described below.

3.2.2 Cartilage-off-bone specimens

A hand cork-borer was used to create circular dents on the surface of the articular cartilage, and through to the underlying bone. The illustration provided in Figure 3.1 is for representation purposes of the equipment, rather than exact positioning of the cork-borer. Caution was taken during the harvesting process to obtain undamaged cartilage specimens. A surgical scalpel with blade size 10A (Swann-Morton, Sheffield, UK) was used to isolate the cartilage core from the underlying subchondral bone (Burgin and Aspden, 2008; Edelsten *et al*., 2010; Lawless *et al*., 2017; Lewis *et al*., 1998; Temple *et al*., 2016). Typically, the cartilage off-bone cores were of an approximate thickness of 1 mm and a diameter of 11 mm. On harvesting of the cartilage cores from the underlying bone, they were immediately immersed in Ringer's solution to prevent dehydration. Each specimen was immersed in Ringer's solution for 30 minutes (Barker and Seedhom, 2001) before testing (Temple *et al*., 2016). The extraction procedure was as follows:

1) The extraction position was controlled by selecting identical locations for all specimens, namely at the thicker central region, ensuring the cartilage surface was complete and undamaged (Temple *et al*., 2016).
2) The cork borer was positioned in an orientation of the normal direction to the central extraction surface of the humeral head.
3) On positioning in the normal loading direction relative to the surface of the humeral head, the loading direction was applied from right to left in a twisting movement
4) Quality checks were performed on each specimen to determine the selection for testing. This involved ensuring the cartilage core was of an equal all-rounded thickness

and flatness, absent of tears and breakages and displayed a smooth all-rounded circumference.

After coring and prior to testing, India ink (Daler-Rowney, Bracknell, UK) was used to confirm the absence of damage from each cork-bored specimen, clarified through its application following removal by rinsing. Images of the surfaces of test specimens were captured (i.e. without damage) using an Apple iPhone version 6 (Apple Inc, California, USA), operated with iOS 10.3.3 and iSight camera (8-megapixel, 1.5µ focus pixels). The image obtained for each specimen was compared with the image taken post-testing for an evaluation of the induced damage.

Figure 3.1: Cork boring procedure for the preparation of cartilage off-bone specimens. The cork borer is applied with force onto the surface of the cartilage humeral head, in the normal direction to the cartilage surface. This schematic is for representation purposes of the equipment rather than exact positioning of the cork-borer relative to the cartilage surface. This procedure is followed by the removal with a surgical scalpel.

3.2.3 Cartilage-on-bone specimens

Preparation of cartilage on-bone specimens differed compared to off-bone cartilage, in that initially the surrounding bone and unwanted tissue was removed with a 300 mm bi-metal hacksaw blade (RS Components Ltd, Corby, UK), with the joint held in a vice (Figure 3.2-a). The obtained humeral head was further dissected into segments for sample preparation

(Figure 3.2-b; 3.2-c). To prepare on-bone cartilage specimens, a diamond core drill (Makita UK Ltd, Milton Keynes, UK) was used to create cylindrical cores on the segments dissected from the central region of the humeral head. The central segments were drilled so that specimens obtained had a flat surface, necessary for testing. Further, the central region of the joint was from the mid-position at physiological joint contact (Clare *et al.,* 2008). Specimens were prepared to approximately 8 mm in diameter (Burgin and Aspden 2008; Lawless *et al*. 2017), using the drill set-up displayed in Figure 3.3-a, to prepare samples as shown in Figures 3.3-b and 3.3-c. Note, the specimens displayed in Figure 3.3-c do not represent the actual specimens used for testing. This image is for the purpose of displaying the extraction procedure only. Hence, to clarify, the specimens were extracted from the central region of the humeral head to ensure both the subchondral bone and overlying articular cartilage were flat, and therefore reliable specimens for testing. This formed the selection criteria for the on-bone cartilage specimens, as all slanted specimens were excluded from testing. The subchondral bone of the cores was trimmed to approximately 10 mm in thickness; to match the thickness of the underlying Sawbone substrate (see Section 3.2.2). The cartilage layer was typically 1 mm thick. In addition, to allow for positioning of the on-bone specimen within the Sawbone substrate during testing, an approximate 2 mm deep indent was drilled within the substrate. Similarly, to the preparation of cartilage-off-bone cores, each specimen was left to soak in Ringer's solution for 30 minutes before testing (Temple *et al*., 2016).

As described for the cartilage off-bone procedure above, an image was captured of the on-bone cartilage specimen without damage with an Apple iPhone version 6 (Apple Inc, California, USA), operated with iOS 10.3.3 and iSight camera (8-megapixel, 1.5µ focus pixels). This image was compared with the image taken post-testing for an evaluation of the induced damage. This procedure is described in Section 3.2.5. Note, the repeatability is to be checked as this is classed as a qualitative assessment as highlighted in the overall discussion of the chapter.

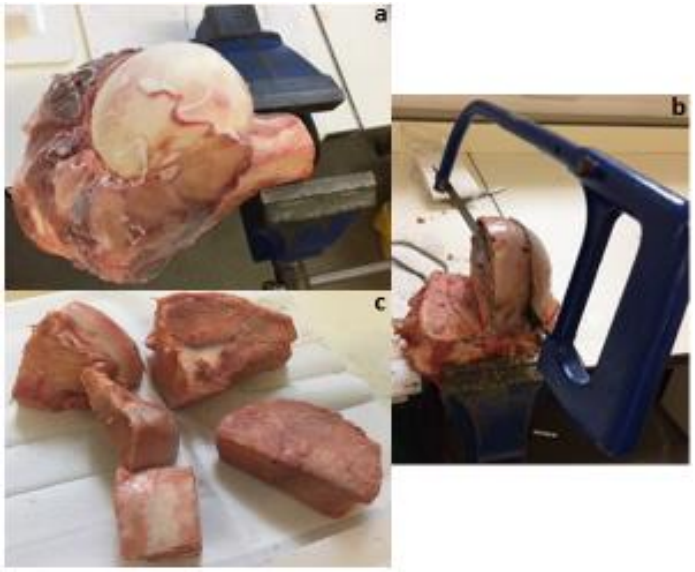

Figure 3.2: Dissection procedure of the bovine humeral head. a) the positioning of the entire bovine humeral head within the vice for dissection. b) the dissection procedure of the humeral head into segments with a hacksaw blade. c) the final prepared dissected segments of the humeral head.

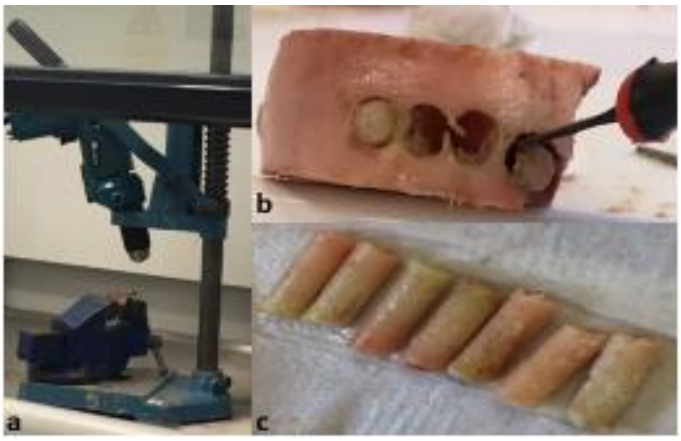

Figure 3.3: Preparation of cartilage-on-bone cores. a) the drill-set up for the preparation of cartilage on-bone specimens with securement in the vice. b) the release of the drilled on-bone cartilage cores. c) final prepared cartilage on-bone cores for representation of the procedure only. Slanted specimens are not used for testing.

3.2.4 Substrate design and mechanical loading

Specimens were positioned on the substrate blocks (Sawbones, Washington, USA) as shown in Figure 3.4-a and Figure 3.4-b, for the on- and off-bone cartilage set-up, respectively, for testing. A simple schematic of the various layers of the experimental set-up are displayed in Figure 3.5-a and Figure 3.5-b, for the on- and off-bone cartilage set-up, respectively. Four Sawbone densities were tested, which were 0.1556, 0.3222, 0.5667 and 0.6000 g/cm^3. The

substrate with the lowest density, substrate one, was used as an osteoporotic representation of bone (Patel *et al*., 2008). The highest density substrate was the closest to osteoarthritic bone, previously reported with a density of 1.69 g/cm^3, in comparison to normal bone, at 1.79 g/cm^3, measured as the mean value across five varied loading regions from the human femoral head (Li and Aspden, 1997). The Sawbone was prepared using a vertical band saw (Startrite Volant 24, UK) into blocks with dimensions 30 mm × 30 mm × 10 mm. The Young's modulus of each substrate was obtained from compression tests using a Bose Electroforce 3300 testing machine via Bose WinTest software (Bose Corporation, ElectroForce Systems Group, Minnesota, USA; updated to: TA Instruments, New Castle, DE, USA). Force-displacement plots were produced at 0.02 mm/s with compression from a metal plate, 81 mm in diameter, onto the substrate block; shown in Figure 3.6-a for substrate one. From this data the associating stress-strain plot was produced. To obtain the Young's modulus of the substrate, a quadratic curve fit on Sigmaplot Version 12.5 (Systat Software Inc., London, UK), was applied at the region of the variation in the gradient of the stress-strain curve, induced by the loading of the cartilage (Figure 3.6-b). Equation (3.1) represents the quadratic curve fit:

$$\sigma = \sigma_0 + a\varepsilon + b\varepsilon^2 \qquad (3.1)$$

where σ is the stress in MPa, ε is the strain and σ_0, a and b are empirically derived constants. To calculate the Young's modulus, *E*, equation (3.1) was differentiated as displayed in equation (3.2):

$$E = \frac{d\sigma}{d\varepsilon} = a + 2b\varepsilon \qquad (3.2)$$

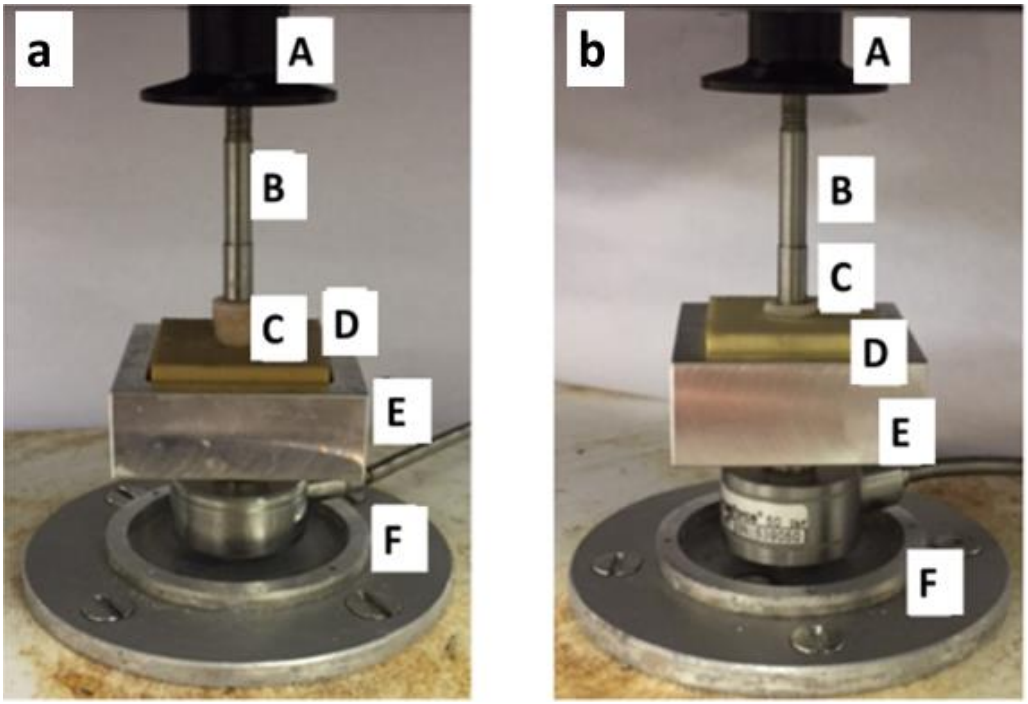

Figure 3.4: Experimental set-up for a) on-bone and b) off-bone cartilage investigations. In each case, A: actuator of testing machine, B: stainless-steel indenter, C: cartilage specimen; on- and off-bone on part a and b, respectively, D: underlying substrate, E: aluminium test-rig and F: load cell of testing machine.

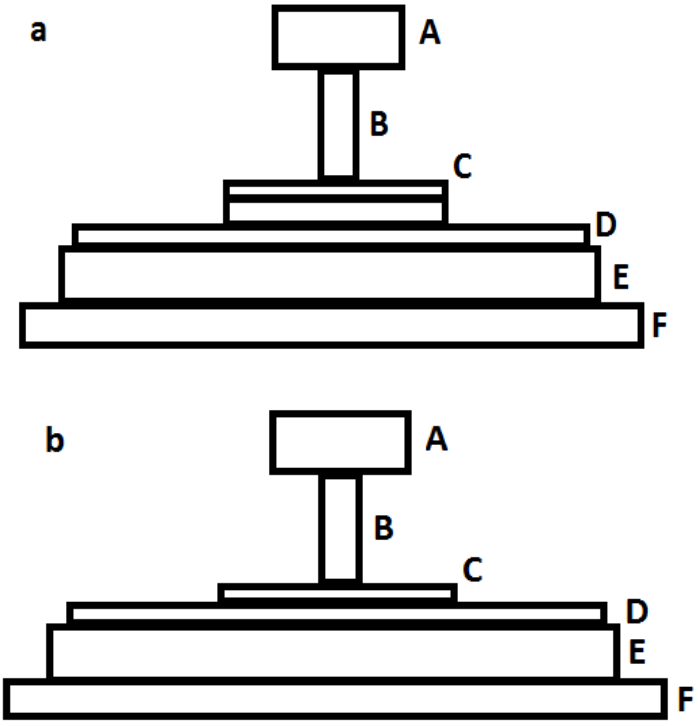

Figure 3.5: Simple schematic to represent the layers of the experimental set-up shown in Figure 3.4 for a) on-bone cartilage and b) off-bone cartilage. In each case, A: actuator of testing machine, B: stainless-steel indenter, C: cartilage specimen, D: underlying substrate, E: aluminium test-rig and F: load cell of testing machine

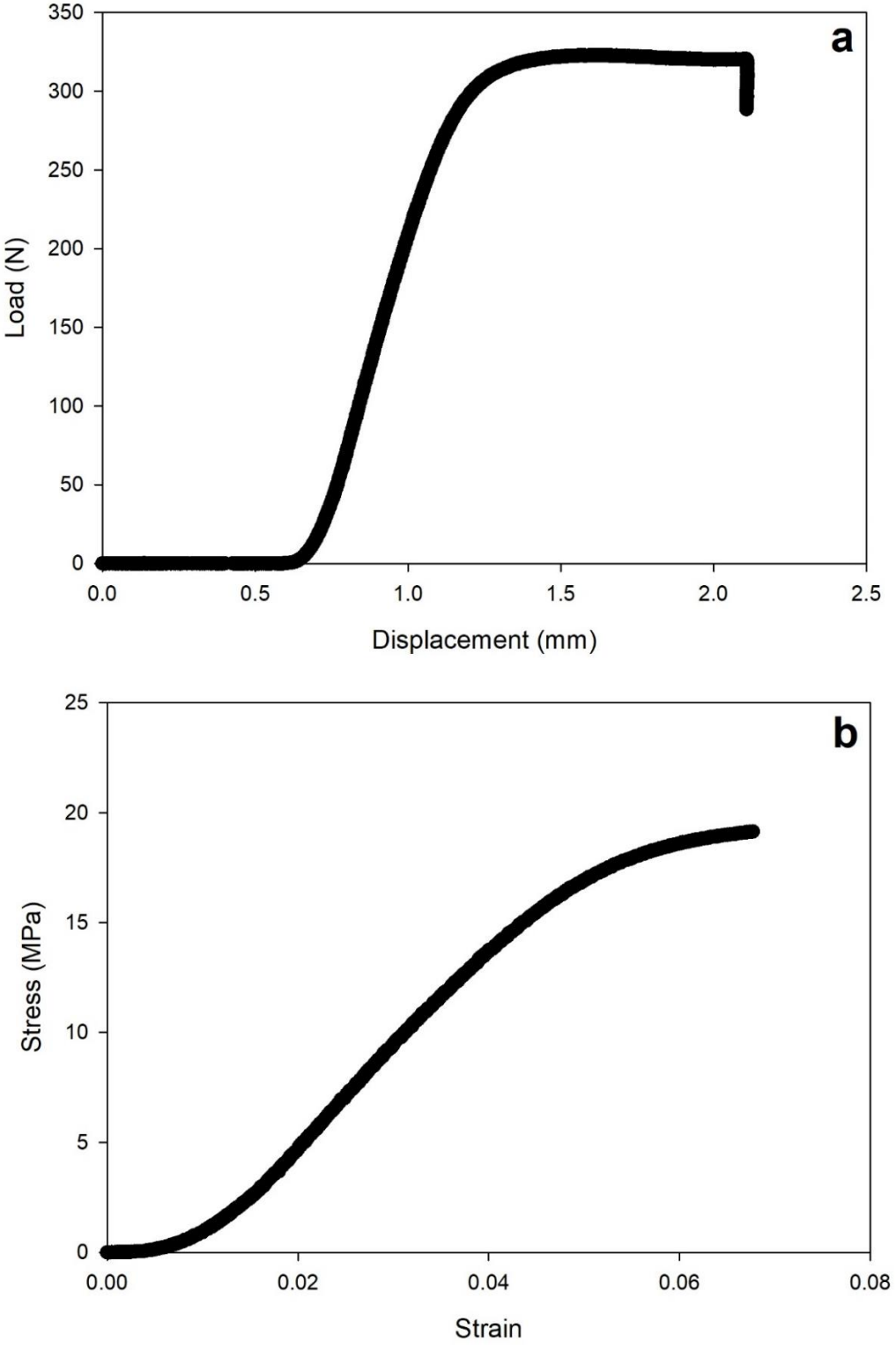

Figure 3.6: Representative illustration with substrate one for the method of extraction of the Young's modulus for each substrate. a) force-displacement plot obtained from the compression test. b) region of the associating stress-strain curve utilised for the evaluation with a quadratic curve fit as represented by eq. (3.1). Final values of the Young's modulus are summarised in Table 3.1. Note, the force-displacement plot in part a) is adjusted to commence from 0 displacement and 0 force. This is for improved presentation and transfer to the stress-strain plot shown in part b). This segment represents the initial contact of the indenter with the substrate.

Following on from the compression testing of the substrate blocks to produce the stress-strain plot, a strain value observed for all four substrates was inserted into equation (3.2), extracted as a common strain of 0.0157. The calculation of the Young's Modulus was computed in conjunction with the derived values of the coefficients: σ_0, a and b as determined from the quadratic curve fit. This method was utilised for all substrates, with the final values presented in Table 3.1. It is worth noting however, the calculated Young's modulus may be underestimated. This is due to the large distance between the actuator and the specimen on the set-up (Figure 3.4), leading to underestimated displacement measurements. However, although this is a limitation, the Young's modulus is not used for the determination of final conclusions in this chapter, where rather the focus is given to the presence of cartilage damage in relation to the frequency and substrate density. Further, a consistent number of cycles is applied to each specimen for damage quantification. The mass of each substrate was measured with a weighing balance (A & D Weighing, Oxfordshire, UK), enabling the density to be calculated by dividing this measured value by the substrate volume. The substrate volume was determined by the product of the measured length, width and height of the block, obtained with a ruler (Fisher Scientific, Leicestershire, UK). The output value is of a nominal state due to the controlled preparation of the size of the substrate blocks. The Poisson's ratio of the substrates were obtained from the Sawbones company site (available at www.sawbones.com). See Table 3.1 for details.

Table 3.1: Material properties of the four underlying substrates utilised to represent varied bone mineral densities positioned beneath each cartilage specimen during testing, allowing for investigation of the effect of substrate density on the damage to articular cartilage.

Substrate	**Density (g/cm^3)**	**Mass (g)**	**Young's Modulus (*E*) (MPa)**	**Volume (cm^3)**	**Poisson's ratio**
1	0.1556	1.4	407.33	9	0.30
2	0.3222	2.9	930.04	9	0.30
3	0.5667	5.1	2090.87	9	0.30
4	0.6000	5.4	3310.22	9	0.30

A square aluminium test rig was designed with dimensions 41 mm × 41 mm × 16 mm into which the Sawbone substrate was placed (Figure 3.7). A stainless-steel flat circular faced indenter, with a 0.5 mm bevelled edge to avoid stress concentration at its edges, 5.2 mm in diameter (Sadeghi *et al*., 2015) was fixed to the actuator of the testing machine and used to induce damage through indentation to the surface of the cartilage specimen. This procedure was similar to a previous study for on-bone cartilage (Sadeghi *et al*., 2015). A Bose ElectroForce 3200 testing machine controlled via the Bose WinTest 4.1 software (Bose Corporation, ElectroForce Systems Group, Minnesota, USA; updated to: TA Instruments, New Castle, DE, USA) was used for testing; the set-up configuration displayed in Figure 3.8. The stainless-steel indenter was used to load the cartilage specimen.

Figure 3.7: Aluminium test-rig customly designed to securely contain the substrate, above which the cartilage specimen is placed for testing.

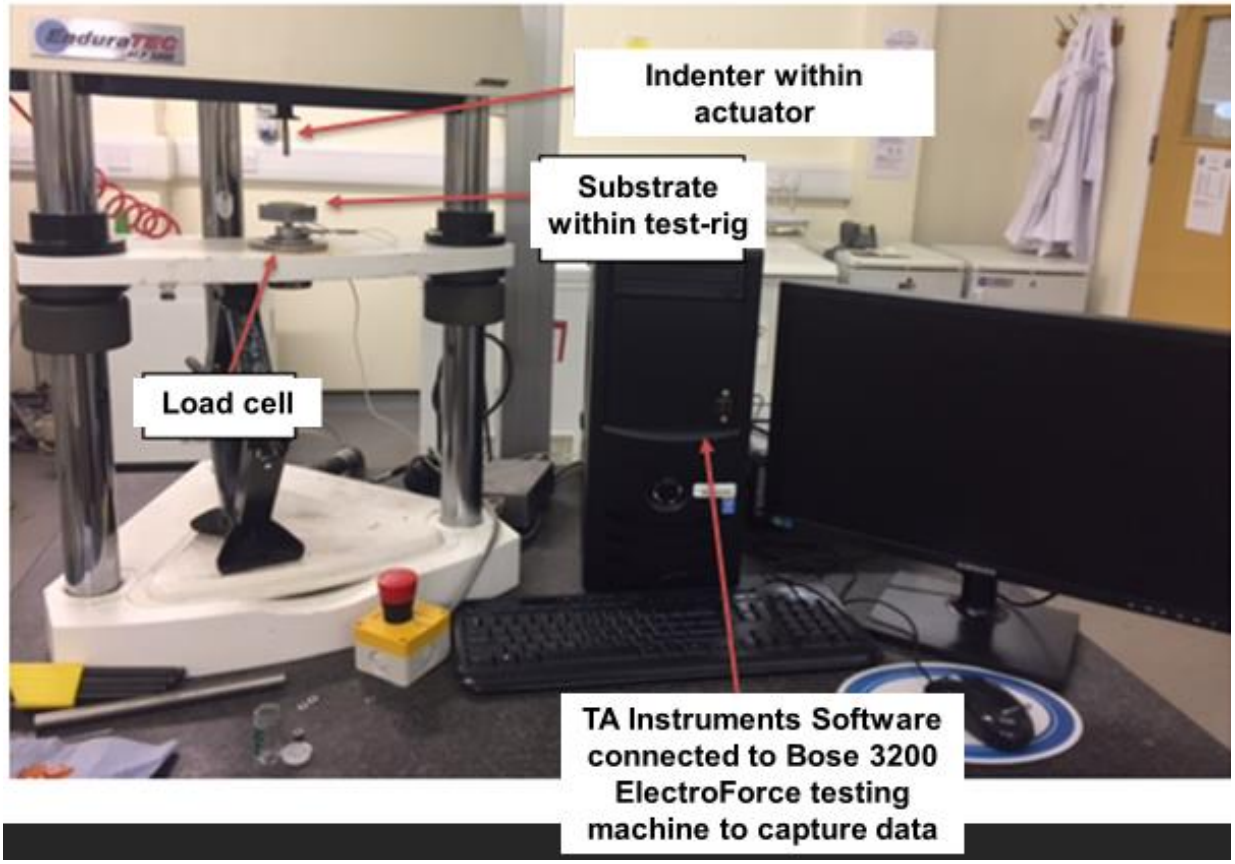

Figure 3.8: The experimental set-up illustrating as labelled the position of the 'indenter within actuator', above the 'substrate within test rig', which is secured above the 'load cell'. The image displays the use of the BOSE 3200 ElectroForce testing machine connected to the TA Instruments software.

Six cartilage specimens were tested per substrate, at a given frequency. The cartilage specimens were manually positioned on the underlying substrate, without the use of adhesive treatment prior to testing. Specimens were not observed to move during testing. For the instance of cartilage off-bone, this placement replicates the effect of the soft-on-hard construct but may not replicate the restriction of collagen at the cartilage calcified zone, due to the removal of the underlying bone (Edelsten *et al.,* 2010). With reference to preliminary tests (see Appendix A for details), a sinusoidally varying force under unconfined compression between 5 and 50 N was applied to the specimens for 10,000 cycles (Sadeghi *et al*., 2015). Repeated loading has previously been found to induce disruption to the articular cartilage surface (Kerin *et al*., 2003; Sadeghi *et al*., 2015; Weightman *et al.,* 1973).

The frequencies applied at testing were selected to represent normal-gait (1 Hz) and above (10 and 50 Hz), based on previous work (Sadeghi *et al.,* 2015; Sadeghi *et al*., 2017; Sadeghi *et al.,* 2018). Three different frequencies at loading were applied to the cartilage-off-bone specimens. These were 1, 10 and 50 Hz. In total, 72 individual tests were completed for off-bone cartilage. For cartilage on-bone it was observed following preliminary tests that at 50 Hz there was no difference in comparison to 10 Hz. Therefore, it was decided to complete tests at 1 and 10 Hz for on-bone cartilage, only, resulting in a completion of 48 individual tests.

At 5000 cycles, the halfway point during testing, the articular cartilage specimens were irrigated with Ringer's solution (Sadeghi *et al.,* 2017; Sadeghi *et al.,* 2018), to ensure hydration of the cartilage. Further, recent work has also confirmed the similarity in the behaviour of articular cartilage when tested in air or Ringer's solution (Lawless *et al*., 2017).

3.2.5 Quantification of changes to the cartilage surface

India ink was used to identify alterations to the cartilage surface following testing (Meachim, 1972; Sadeghi *et al*., 2015; Weightman *et al*., 1973). For evaluation of the damage

present, ImageJ software (version 1.48, Rasband, W.S., U.S. National Institutes of Health, Bethesda, Maryland, USA) was used. Firstly, the area indented following testing was highlighted (i.e. a non-damaged measurement). Secondly, the total length of cracks was measured using an existing method, and this was considered as a damage measurement (Sadeghi *et al*., 2015). A known distance on the scale was identified to allow for calibration of the image (Figure 3.9). The area of indentation (mm^2) and total crack length (mm) were analysed as two separate conditions for each specimen.

For reproducibility of the crack length for damage quantification, the following criterion was developed:

1) The specimen is placed on a flat surface
2) Cracks that run parallel to the outer circumference of the cartilage core are included in the measurement for damage quantification
3) The cracks that form at the outer edge at the periphery that are 1 mm away from the border are excluded from damage quantification. This is the region clearly exempt from contact with the indenter.
4) An iPhone is used to capture the images and the procedure takes place within an identical laboratory environment. This identical set-up for all image capturing contributes to a reproducible method.
5) A well-lit space for capturing the image is incorporated. The lighting is provided by a single fluorescent tube commonly found within a laboratory environment. The lighting is not provided at a specific angle, but rather directly from the ceiling above.
6) The camera is held over the entire specimen so that the sample is positioned within the centre of the image. This enables maximum lighting to reach the specimen for image capturing.

For reproducibility of the indented area measurement, the following criterion was developed:

1) The specimen is placed on a flat surface
2) The larger indented area is captured as the measurement. The smaller stained regions surrounding this large segment are disregarded as artefacts from application of the India ink.
3) An iPhone is used to capture the images and the procedure takes place within an identical laboratory environment. This identical set-up for all image capturing contributes to a reproducible method.
4) A well-lit space for capturing the image is incorporated. The lighting is provided by a single fluorescent tube commonly found within a laboratory environment. The lighting is not provided at a specific angle, but rather directly from the ceiling above.
5) The camera is held over the entire specimen so that the sample is positioned within the centre of the image. This enables maximum lighting to reach the specimen for image capturing.

Figure 3.10 displays the protocol on ImageJ utilised to quantify the resulting indented area on an off-bone cartilage sample. The freehand tool was used to highlight this area across each of the six specimens. The mean indented area was then calculated and plotted against substrate density. Figure 3.11 displays the method to quantify the total crack length on an off-bone cartilage sample. The straight-line tool was used to measure the length dimension of each crack present, for which the total crack length was recorded per specimen. Across the six specimens, the mean total crack length value was then calculated and plotted against substrate density. Similarly, the use of the straight-line tool to measure the total crack length, as well as the freehand tool to quantify the area left by the indenter at the on-bone cartilage specimens, is displayed in Figure 3.12 and 3.13, respectively. Image measurements were repeated twice per sample and the mean value reported. It is worth noting the extent of limitations in the criteria for measuring both the crack length to represent damage, as well as

the area of indentation. Further details on this are highlighted in the overall discussion of the chapter.

Sigmaplot Version 12.0 (Systat Software Inc., London, UK) was used to perform regression analysis on the relationship between the variables of the area of indentation and crack length, at a given frequency and substrate. A linear regression fit was assessed as the most appropriate representation of the statistically significant derived relationships ($p < 0.05$). The linear regression was performed on the mean value for crack length and indented area per substrate density (n = 4). Additionally, One-Way ANOVA was performed between each substrate group at a given frequency, as well as between each frequency at a given substrate. Statistically significant differences were identified by $p < 0.05$.

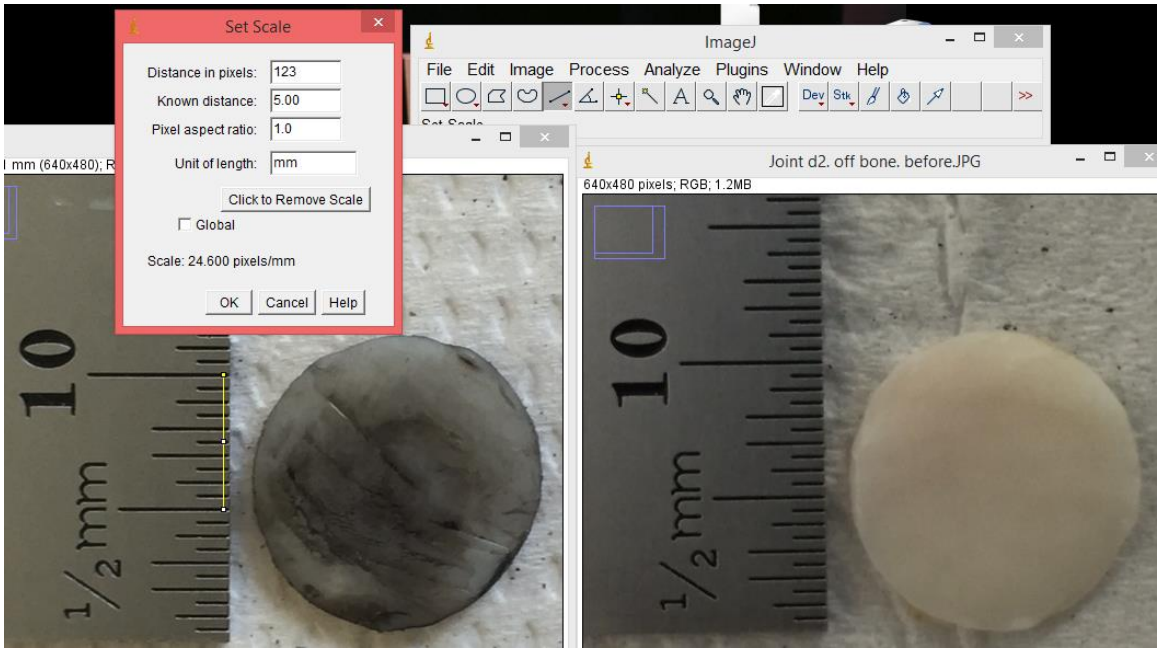

Figure 3.9: Method of calibration for off-bone cartilage. A known dimension on the scale bar highlighted in yellow is reported in the 'Set Scale' option. Right-hand side image displays the specimen prior to testing, left-hand side image displays the specimen post-test. This calibration method is utilised for all cartilage specimens

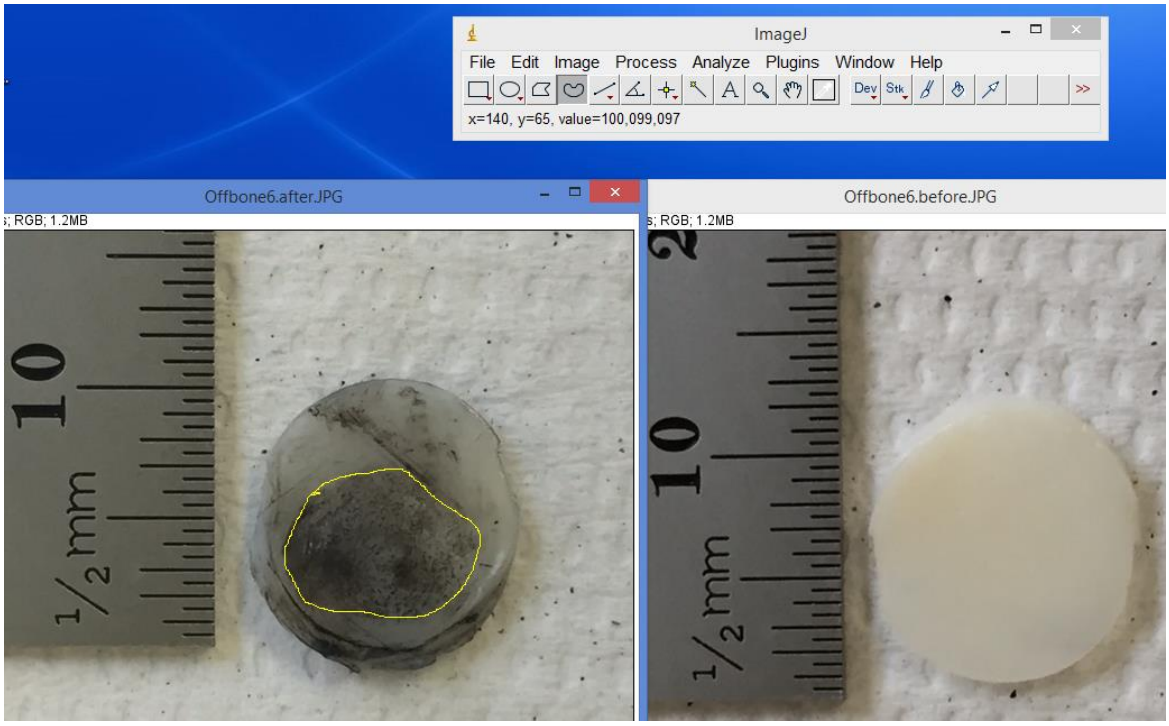

Figure 3.10: Use of the freehand tool highlighted in yellow to quantify the area left by the indenter on the surface at off-bone cartilage. The result is extracted as the 'Area' in mm^2. Right-hand side image displays the specimen prior to testing, left-hand side image displays the specimen post-test.

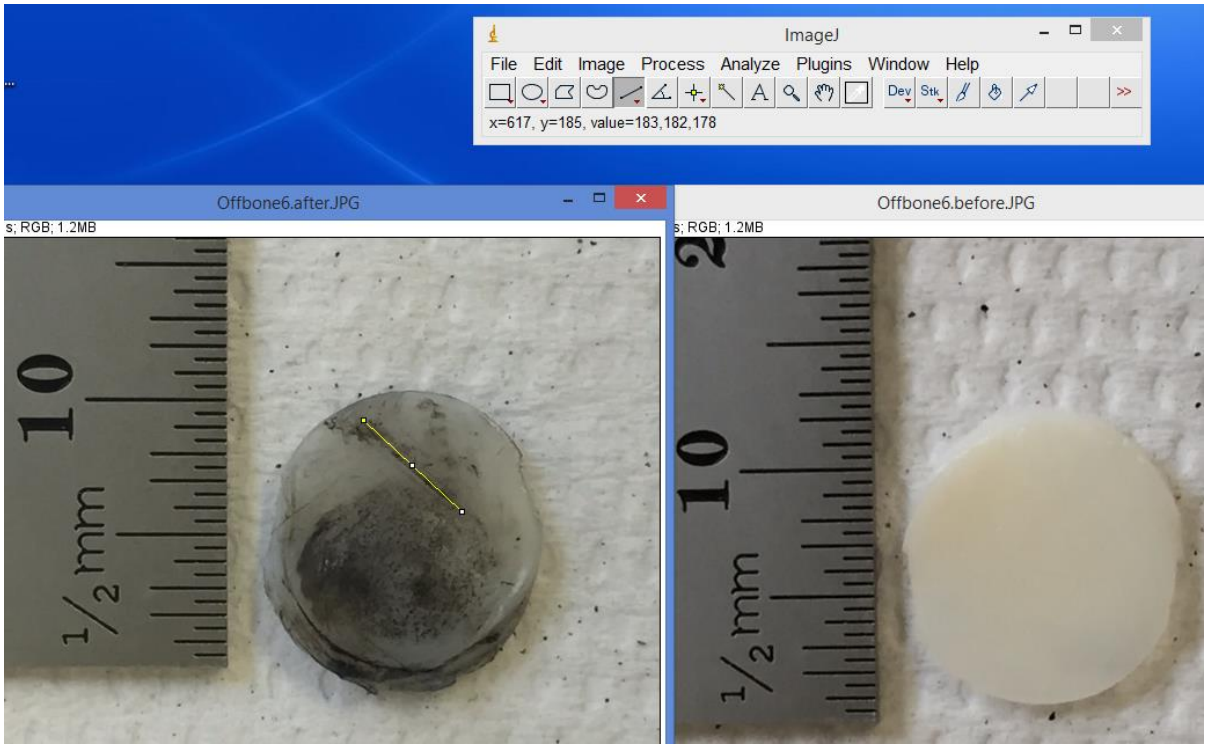

Figure 3.11: Use of the straight-line tool highlighted in yellow to measure total crack length at the surface of a cartilage off-bone specimen. The result is extracted as the sum of 'Length' in mm. Right-hand side image displays the specimen prior to testing, left-hand side image displays the specimen post-test.

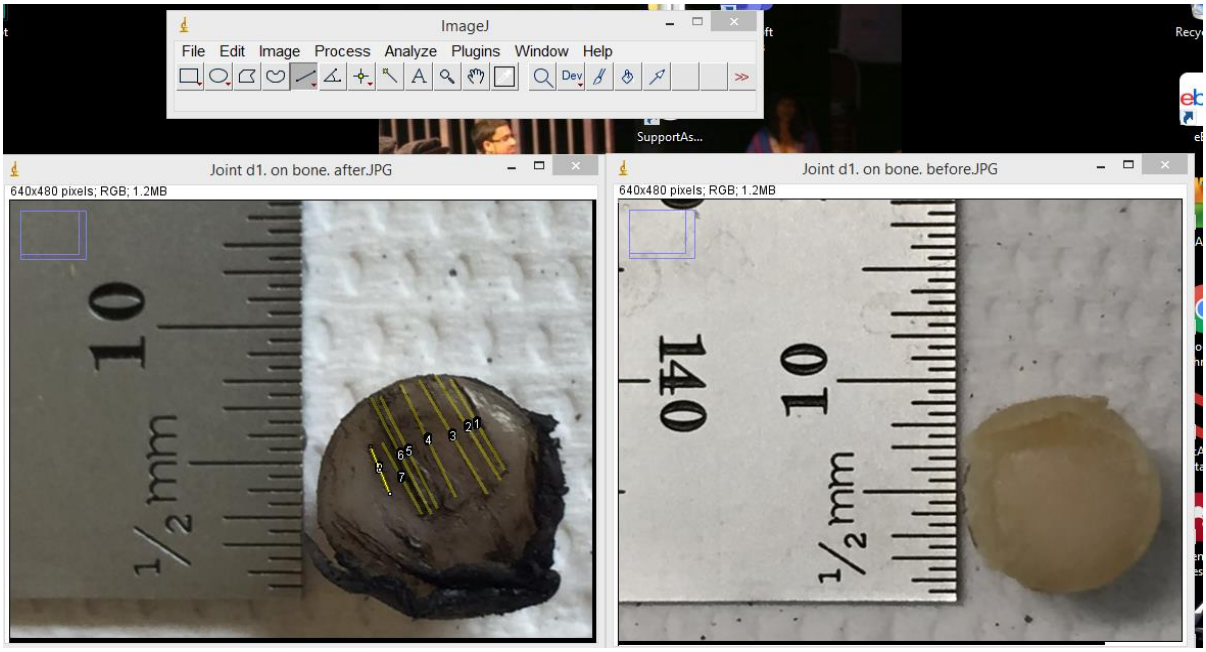

Figure 3.12: Use of the straight-line tool highlighted in yellow to measure all parallel crack lengths at the surface of a cartilage on-bone specimen. The result is extracted as the sum of 'Length' in mm. Right-hand side image displays cartilage on-bone specimen before testing, left-hand side image displays cartilage on-bone specimen post-test.

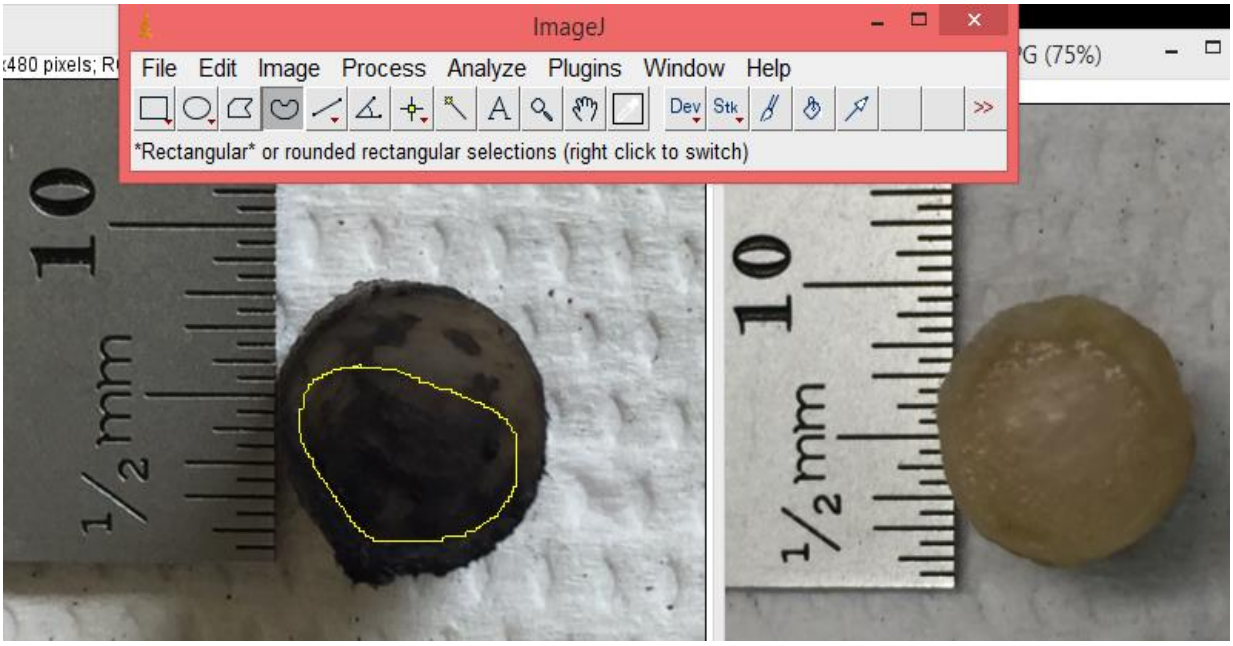

Figure 3.13: Use of the freehand tool highlighted in yellow to quantify the larger area left by the indenter on the surface of an on-bone cartilage specimen. The result is extracted as the 'Area' in mm^2. Note, the smaller stained regions are not accounted for as a result of staining artefacts away from the indented region. Right-hand side image displays the specimen prior testing, left-hand side image displays the specimen post-test.

3.3 Experimental Results

3.3.1 Cartilage off-bone surface assessment

Representative images of cartilage off-bone specimens after testing are shown for 1, 10 and 50 Hz, in Figure 3.14, Figure 3.15 and Figure 3.16, respectively; using all four substrates investigated of 0.1556, 0.3222, 0.5667 and 0.6000 g/cm^3, as shown by part a-d, respectively. The damage observed as crack formation is clearly indicated with a black outlined ellipse. Figure 3.17 and Figure 3.18 display the relationship between substrate density and the mean crack length and mean indented area, respectively, at all three frequencies investigated. See Appendix B for the remaining photographic images of cartilage off-bone results, at all frequencies and substrates studied.

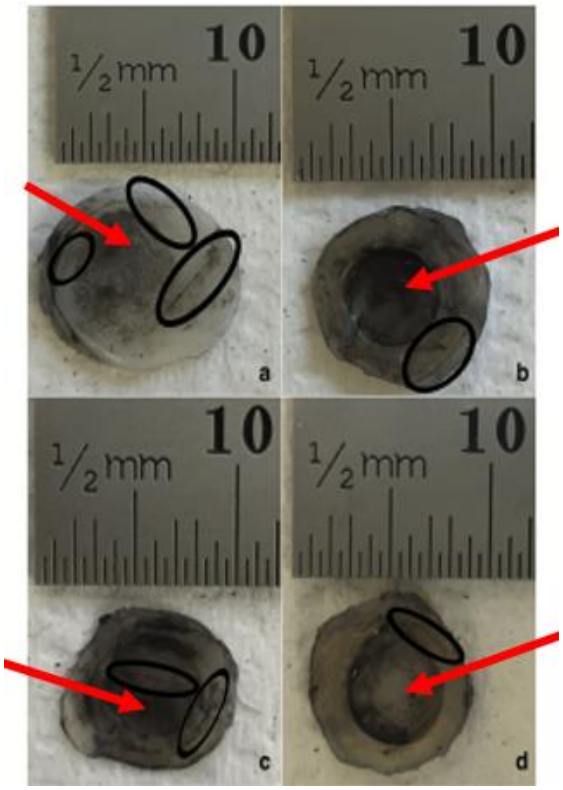

Figure 3.14: Representative images of bovine articular cartilage-off-bone samples after testing, at 1 Hz frequency of loading. Image **a**-**d** display a sample result of the highest to the lowest substrate density, identified by the densities of 0.1556, 0.3222, 0.5667 and 0.6000 g/cm^3, respectively. Damage as cracks and indentation were identified with application of India ink. Cracks formed are highlighted with the black ellipse for clear observation. The indented region is identified with the red arrow for each specimen. Indentation can be observed across most of the cartilage-off-bone specimen surface, at this frequency of loading. Scale bar (mm) included for quantifying results

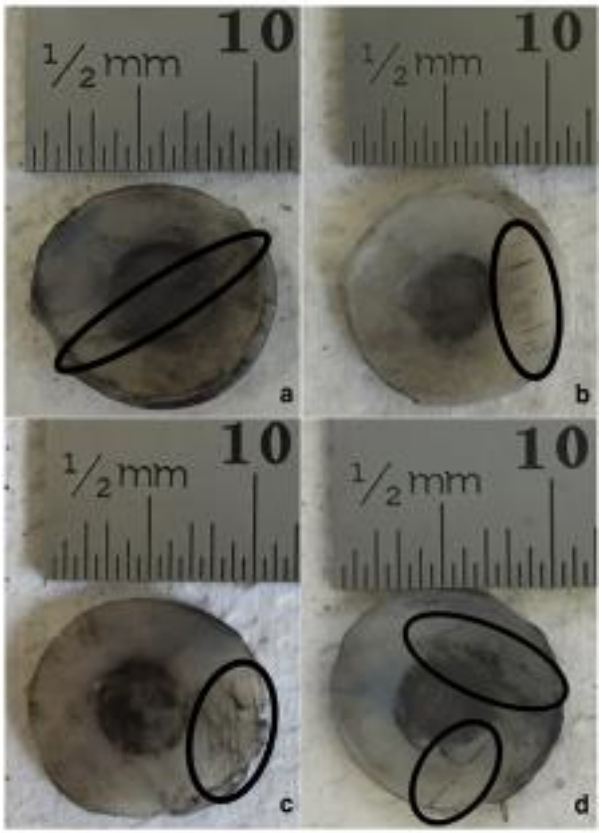

Figure 3.15: Representative images of bovine articular cartilage-off-bone samples after testing, at 10 Hz frequency of loading. Image **a**-**d** display a sample result of the highest to the lowest substrate density, identified by the densities of 0.1556, 0.3222, 0.5667 and 0.6000 g/cm^3, respectively. Damage as cracks and indentation were identified with application of India ink. Cracks formed are highlighted with the black ellipse for clear observation, notably of multiple parallel straight-lines. Scale bar (mm) included for quantifying results

Figure 3.16: Representative images of bovine articular cartilage-off-bone samples after testing, at 50 Hz frequency of loading. Image **a**-**d** display a sample result of the highest to the lowest substrate density, identified by the densities of 0.1556, 0.3222, 0.5667 and 0.6000 g/cm^3, respectively. Damage as cracks and indentation were identified with application of India ink. Cracks formed are highlighted with the black ellipse for clear observation, notably of single-line configurations of varying lengths. Scale bar (mm) included for quantifying results

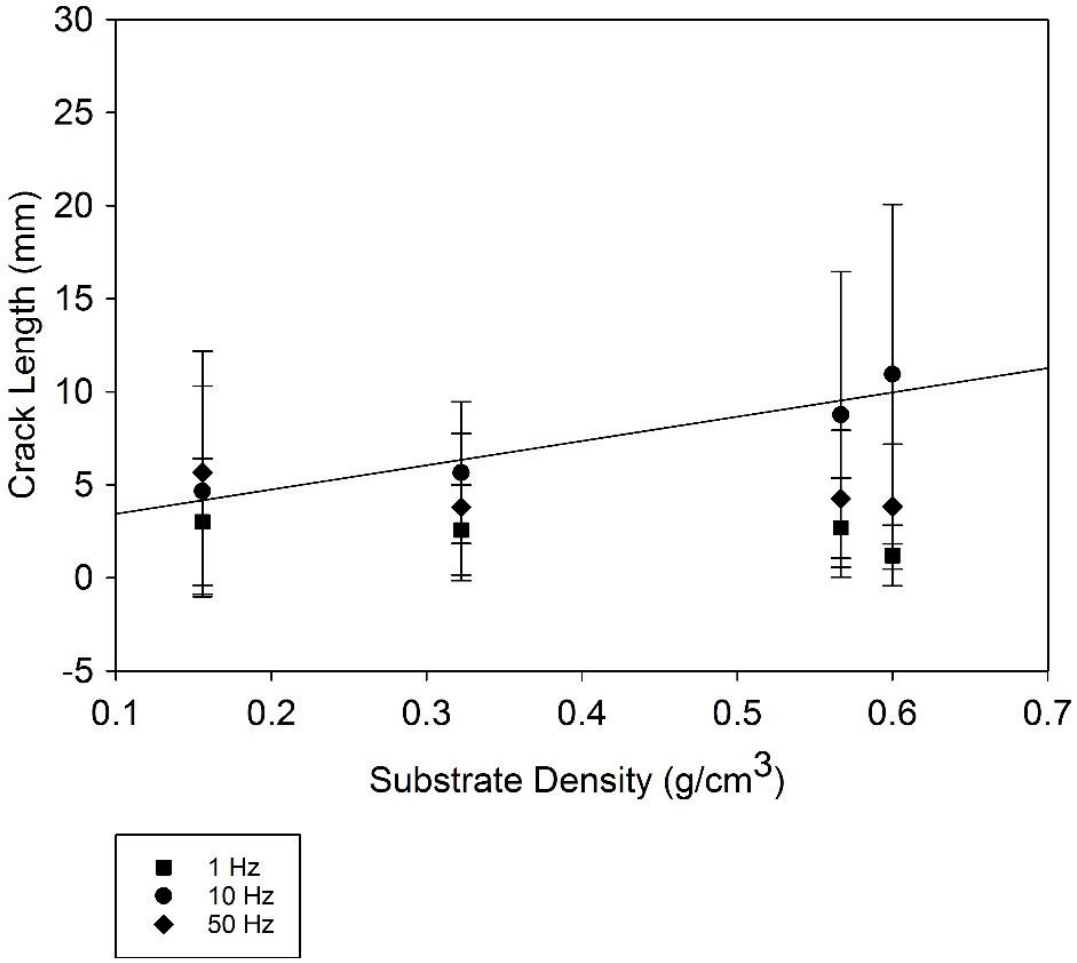

Figure 3.17: Mean crack length plotted with substrate density at 1, 10 and 50 Hz for off-bone articular cartilage, represented by the square, circle and diamond, respectively. Linear regression displayed by eq. (3.3) fit the data at R^2 value of 0.91 at 10 Hz. Error bars represent standard deviations for which there are six repeat points across six specimens.

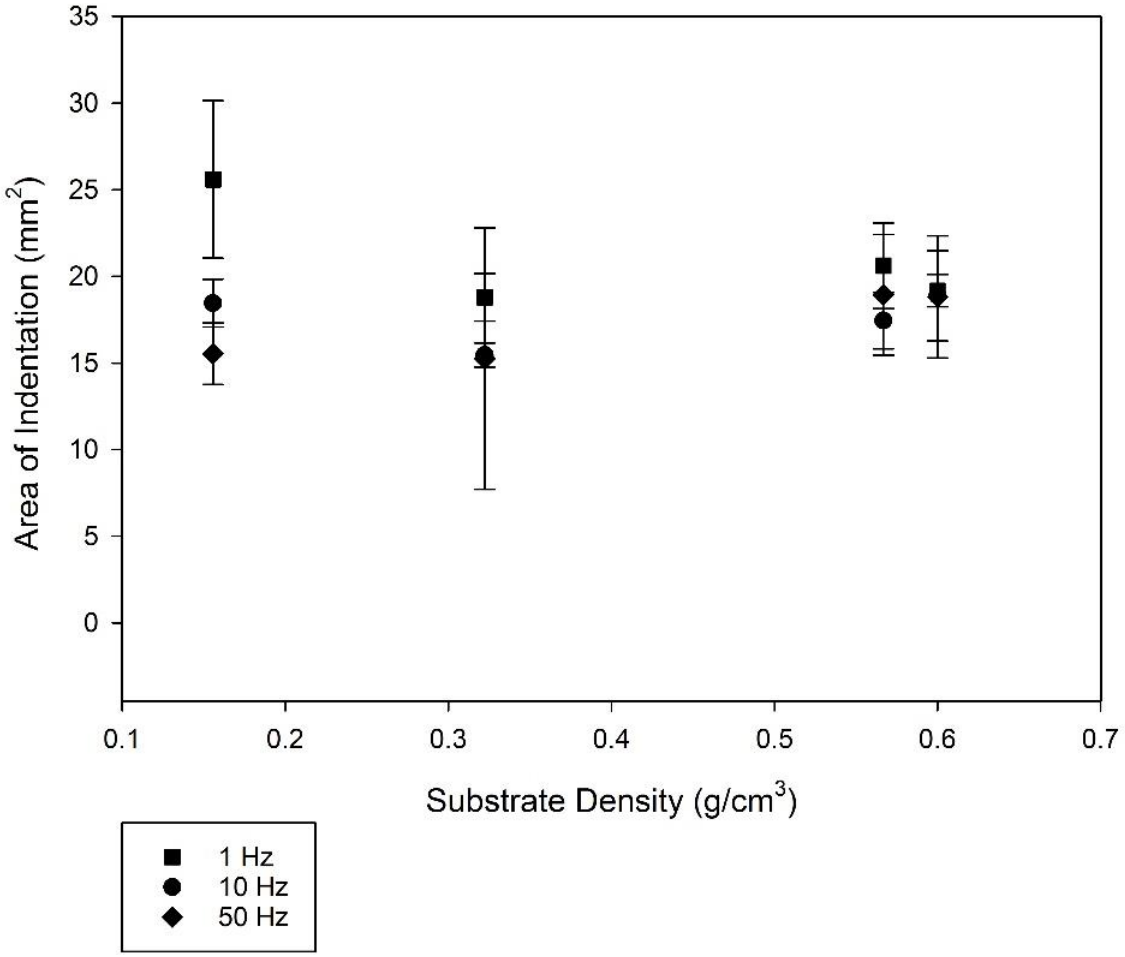

Figure 3.18: Mean area of indentation plotted with substrate density at 1, 10 and 50 Hz for off-bone articular cartilage, represented by the square, circle and diamond, respectively. Error bars represent standard deviations for which there are six repeat points across six specimens.

Crack length for cartilage off-bone was significantly correlated to substrate density at 10 Hz ($p < 0.05$) (Figure 3.17; Table 3.2), described by equation (3.3), for which the combined variables of frequency at 10 Hz with increasing substrate density, led to an increase in crack length with density ($p < 0.05$) (Figure 3.17; Table 3.2).

$$c = D + AB \qquad (3.3)$$

where c is the crack length mean total, A is the gradient of the slope, B is the substrate density and D is the intercept; D and A are empirically derived constants. However, crack

length for cartilage off-bone was not significantly associated with substrate density at 1 or 50 Hz ($p > 0.05$) (Figure 3.17; Table 3.2). The associated details are summarised in Table 3.2, at all three frequencies tested.

Frequency of loading in combination with substrate density had no effect on the area of indentation for off-bone cartilage when samples were tested at 1, 10 and 50 Hz ($p > 0.05$) (Figure 3.18; Table 3.2). Equation (3.4) was evaluated for which no significant relationship was found between substrate density and the indented area:

$$a = Z + mB \qquad (3.4)$$

where a is the mean indented area, m is the gradient of the slope, B is the substrate density and Z is the intercept; Z and m are empirically derived constants. The associated details are summarised in Table 3.2, at all three frequencies tested. One-Way ANOVA results for off-bone cartilage are displayed in Table 3.3 and Table 3.4, for assessments of the differences between a given frequency and substrate, respectively. A significant difference was shown between all substrate densities at 1 and 10 Hz for the indented area of cartilage-off-bone ($p < 0.05$) (Table 3.3). A significant difference was also shown for the indented area at substrates 1 and 2 between all frequencies tested for cartilage-off-bone ($p < 0.05$). In addition, a statistical difference was identified for substrate 4 between all frequencies tested for the crack length of cartilage-off-bone ($p < 0.05$) (Table 3.4).

Table 3.2: Statistical details derived from mean crack length and area of indentation with substrate density plots of Figure 3.17 and 3.18, at frequencies 1, 10 and 50 Hz; for cartilage off-bone. *A* and *m* are the constants from the curve fits. R^2, the squared correlation coefficient indicates the extent of the data and regression line fit for the crack length at 10 Hz. A *P*-value less than or equal to 0.05 confirms statistically significant data, as displayed at 10 Hz of loading frequency for crack length, only.

Frequency (Hz)	**Total crack length linear fit details for cartilage-off-bone**				**Total area of indentation linear fit details for cartilage-off-bone**		
	A	**D**	**R^2**	***P***	**m**	**Z**	***P***
1	(-)2.65	3.45	-	0.30	(-)10.39	25.31	0.30
10	(+)13.08	2.12	0.91	0.05	(+)1.42	16.98	0.80
50	(-)3.00	5.61	-	0.28	(+)8.81	13.51	0.08

Table 3.3: Statistical details derived from One-Way ANOVA tests for crack length and area of indentation for cartilage-off-bone. Results are shown for comparisons between each of the four substrate densities at a given frequency. A *P*-value less than or equal to 0.05 confirms statistically significant data

	Cartilage-off-bone crack length	**Cartilage-off-bone area of indentation**
Frequency (Hz)	***P***	
1	0.607	0.003
10	0.389	0.012
50	0.975	0.153

Table 3.4: Statistical details derived from One-Way ANOVA tests for crack length and area of indentation for cartilage-off-bone. Results are shown for comparisons between frequencies of 1 and 10 Hz at each substrate tested. A *P*-value less than or equal to 0.05 confirms statistically significant data

		Cartilage-off-bone crack length	**Cartilage-off-bone area of indentation**
Substrate Density (g/cm^3)	**Substrate Number**	***P***	
0.1556	1	0.836	<0.001
0.3222	2	0.327	0.013
0.5667	3	0.141	0.071
0.6000	4	0.053	0.967

When evaluating the effect of frequency alone, on the area of indentation, an increase in the frequency resulted in a decrease in the indented area (Figure 3.18). The post-test recovery following the testing of the cartilage off-bone specimens varied for each frequency. Testing at 1 Hz of frequency resulted in the least recovery of the articular cartilage specimen; with a larger indented area observed. This is represented by the observations where the indented area, as clearly highlighted by the black circular staining of India ink, extended to the majority of the cartilage specimen surface at 1 Hz (Figure. 3.14), in comparison to the lesser surface indented at 10 (Figure 3.15) and 50 Hz (Figure 3.16). For cartilage-off-bone, the mean indented area varied from 18.79 to 25.59 mm^2 at 1 Hz, 15.46 to 18.88 mm^2 at 10 Hz, and 15.25 to 18.94 mm^2 at 50 Hz (Figure 3.18; Table 3.5).

Sample images displayed at 1 Hz (Figure 3.14) illustrate cracks that were of a single-line configuration, notably through the specimen periphery, parallel to the specimen circumference, observed at a maximum mean of 3.01 mm (Figure 3.17; Table 3.6). As the applied frequency at testing increased to 10 Hz, mean crack length at this frequency increased to its maximum by 7.94 mm (Figure 3.17; Table 3.6).

Table 3.5: Mean area of indentation values with standard deviation for cartilage-off-bone samples, following testing, at all frequencies and substrates investigated, as a combined study

	Cartilage off-bone mean area of indentation (mm^2) ± SD			
Frequency (Hz)	**Substrate 1 density: 0.1556 g/cm^3**	**Substrate 2 density: 0.3222 g/cm^3**	**Substrate 3 density: 0.5667 g/cm^3**	**Substrate 4 density: 0.6000 g/cm^3**
1	25.59 ± 4.54	18.79 ± 1.37	20.62 ± 2.47	19.17 ± 0.93
10	18.45 ± 1.38	15.46 ± 0.70	17.44 ± 1.63	18.88 ± 2.60
50	15.53 ± 1.78	15.25 ± 7.55	18.94 ± 3.49	18.81 ± 3.52

Table 3.6: Mean total crack length values with standard deviation for cartilage-off-bone samples, following testing, at all frequencies and substrates investigated, as a combined study

	Cartilage off-bone mean total crack length (mm) ± SD			
Frequency (Hz)	**Substrate 1 density: 0.1556 g/cm^3**	**Substrate 2 density: 0.3222 g/cm^3**	**Substrate 3 density: 0.5667 g/cm^3**	**Substrate 4 density: 0.6000 g/cm^3**
1	3.01 ± 3.41	2.57 ± 2.42	2.69 ± 2.66	1.19 ± 1.63
10	4.65 ± 5.66	5.65 ± 3.80	8.76 ± 7.70	10.95 ± 9.12
50	5.65 ± 6.54	3.80 ± 3.95	4.25 ± 3.68	3.82 ± 3.36

Representative images of 10 Hz in applied frequency at each substrate (Figure 3.15), illustrate crack formation predominantly observed as multiple parallel straight-line

arrangements, of various lengths. This finding is similar to previous studies (Kerin *et al.,* 2003; Sadeghi *et al.*, 2015), with failure commonly observed at the periphery of the cartilage specimen. At 50 Hz, the maximum mean crack length reduced by 5.30 mm from 10 Hz (Figure 3.17; Table 3.6), where crack formation was primarily located across the diameter of the sample. The cracks were observed as single-line conformations, of various lengths, parallel to the specimen circumference (Figure 3.16).

3.3.2 Cartilage on-bone surface assessment

Representative images of cartilage on-bone specimens after testing are shown for 1 and 10 Hz, in Figure 3.19 and Figure 3.20, respectively; at all four substrates investigated of 0.1556, 0.3222, 0.5667 and 0.6000 g/cm^3, as shown by part a-d, respectively. The damage observed as crack formation is clearly indicated with a black outlined ellipse. Figure 3.21 and Figure 3.22 display the relationship between substrate density and the mean crack length and mean indented area, respectively, at all three frequencies investigated. See Appendix C for the remaining photographic images of cartilage on-bone results, at all frequencies and substrates studied.

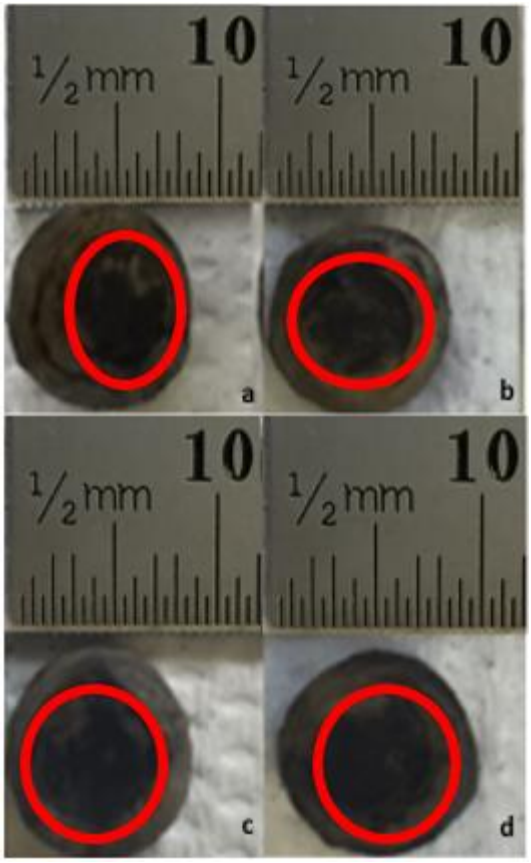

Figure 3.19: Representative images of bovine articular cartilage-on-bone samples after testing, at 1 Hz frequency of loading. Image **a**-**d** display a sample result of the highest to the lowest substrate density, identified by the densities of 0.1556, 0.3222, 0.5667 and 0.6000 g/cm^3, respectively. Damage as cracks were predominantly absent at this frequency. The majority of the specimen was subject to an indented area post-testing, identified with application of India ink as highlighted by the red outline. Scale bar (mm) included for quantifying results

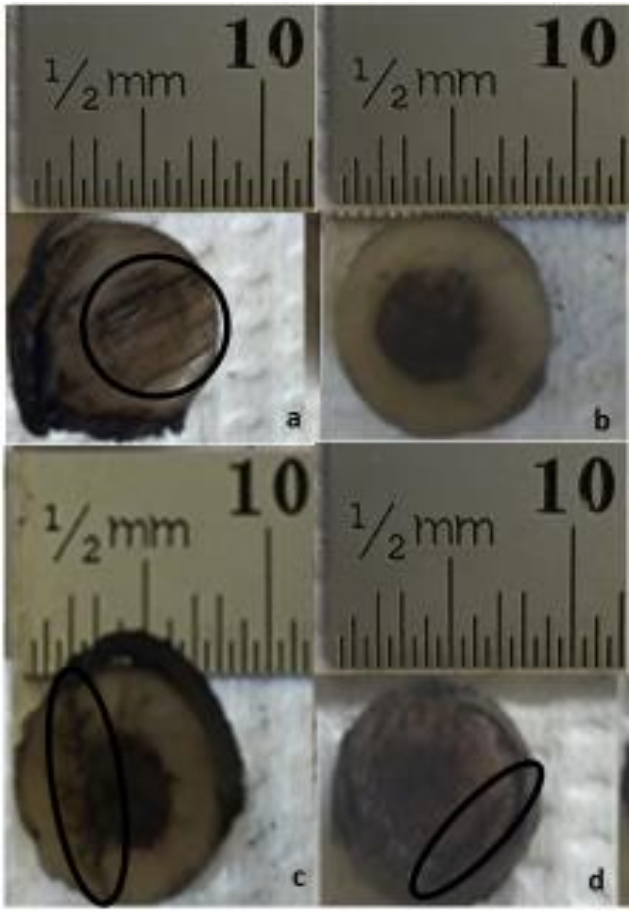

Figure 3.20: Representative images of bovine articular cartilage-on-bone samples after testing, at 10 Hz frequency of loading. Image **a**-**d** display a sample result of the highest to the lowest substrate density, identified by the densities of 0.1556, 0.3222, 0.5667 and 0.6000 g/cm^3, respectively. Damage as cracks and indentation were identified with application of India ink. Cracks formed are highlighted with the black ellipse for clear observation. Scale bar (mm) included for quantifying results

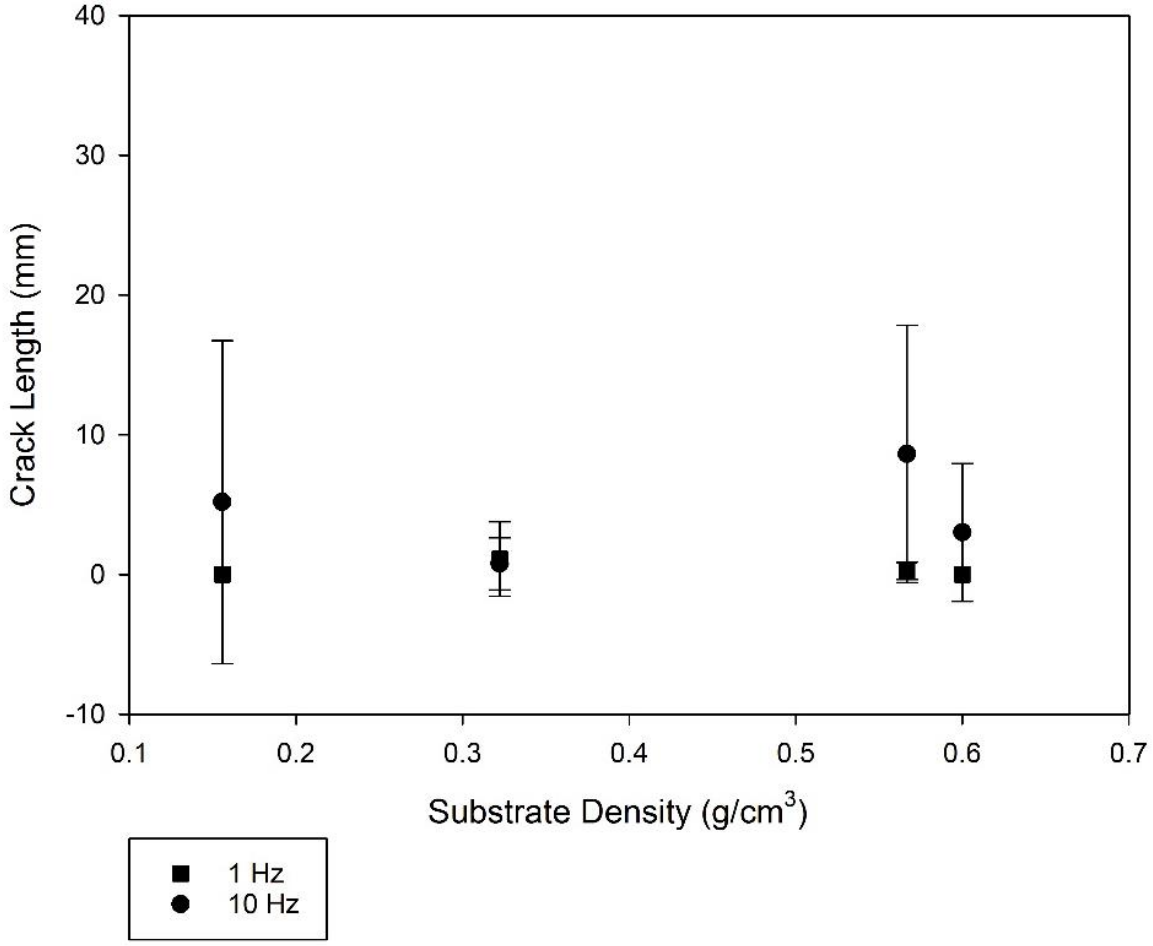

Figure 3.21: Mean crack length plotted with substrate density at 1 and 10 Hz for on-bone articular cartilage, represented by the square and circle, respectively. Error bars represent standard deviations for which there are six repeat points across six specimens.

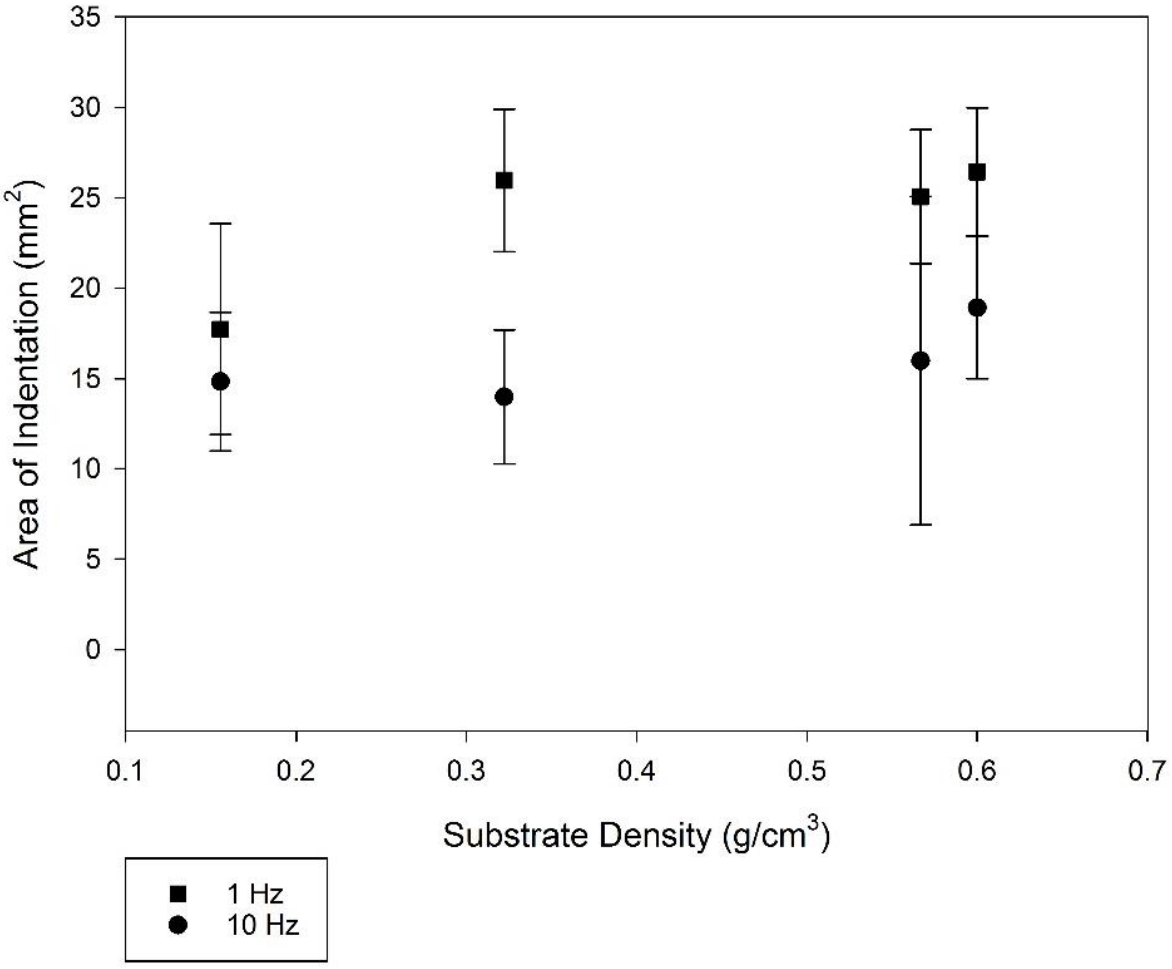

Figure 3.22: Mean area of indentation plotted with substrate density at 1 and 10 Hz for on-bone articular cartilage, represented by the square and circle, respectively. Error bars represent standard deviations for which there are six repeat points across six specimens.

Crack length for on-bone cartilage was not significantly correlated to substrate density at either 1 or 10 Hz ($p > 0.05$) (Figure 3.21; Table 3.7), as shown by the evaluation of equation (3.3). The associated details are summarised in Table 3.7, at the two frequencies tested for on-bone cartilage.

Frequency of loading in combination with substrate density had no effect on the area of indentation for on-bone cartilage when samples were tested at 1 and 10 Hz ($p > 0.05$) (Figure 3.22; Table 3.7), as shown by the evaluation of equation (3.4). The associated details are summarised in Table 3.7, at the two frequencies tested for on-bone cartilage. Further, when

evaluating the effect of frequency alone, on the area of indentation, an increase in the frequency resulted in a decrease in the indented area (Figure 3.22). One-Way ANOVA results for on-bone cartilage are displayed in Table 3.8 and Table 3.9, for assessments of the differences between a given frequency and substrate, respectively. A significant difference was shown between all substrate densities at 1 Hz for the indented area of cartilage-on-bone ($p < 0.05$) (Table 3.8). A significant difference was also shown for the indented area at substrates 2, 3 and 4 between all frequencies tested for cartilage-on-bone ($p < 0.05$). In addition, a statistical difference was identified for substrate 3 between all frequencies tested for the crack length of cartilage-on-bone ($p < 0.05$) (Table 3.9).

Table 3.7: Statistical details derived from mean crack length and area of indentation with substrate density plots of Figure 3.21 and 3.22, at frequencies 1 and 10 Hz; for cartilage on-bone. *A* and m are the constants from the curve fits. *P*-value less than or equal to 0.05 confirms statistically significant data, for which no *P*-value displays statistical significance.

Frequency (Hz)	**Total crack length linear fit details for cartilage-on-bone**			**Total area of indentation linear fit details for cartilage-on-bone**		
	A	**D**	***P***	**m**	**Z**	***P***
1	(-)0.43	0.51	0.82	(+)15.45	17.45	0.21
10	(+)3.91	2.79	0.75	(+)7.73	12.75	0.25

Table 3.8: Statistical details derived from One-Way ANOVA tests for crack length and area of indentation for cartilage-on-bone. Results are shown for comparisons between each of the four substrate densities at a given frequency. A *P*-value less than or equal to 0.05 confirms statistically significant data

	Cartilage-on-bone crack length	**Cartilage-on-bone area of indentation**
Frequency (Hz)	***P***	
1	0.553	0.007
10	0.144	0.467

Table 3.9: Statistical details derived from One-Way ANOVA tests for crack length and area of indentation for cartilage-on-bone. Results are shown for comparisons between frequencies of 1 and 10 Hz at each substrate tested. A *P*-value less than or equal to 0.05 confirms statistically significant data

		Cartilage-on-bone crack length	**Cartilage-on-bone area of indentation**
Substrate Density (g/cm^3)	**Substrate Number**	***P***	
0.1556	1	0.394	0.334
0.3222	2	0.937	<0.001
0.5667	3	0.041	0.047
0.6000	4	0.394	0.006

Sample images displayed at 1 Hz (Figure 3.19) for on-bone cartilage demonstrate that for most of the specimen surfaces there was an absence of cracking, observed at a maximum mean length of 1.09 mm (Figure 3.21; Table 3.10). As the applied frequency at testing increased to 10 Hz, mean crack length at this frequency increased to a maximum of 8.63 mm (Figure 3.21; Table 3.10). At this frequency, the cracks were observed as long multiple cuts through the diameter of the specimen surface (Figure 3.20), highlighted with the black ellipse.

Surface morpology results observed for cartilage on-bone at 1 Hz appeared to show the majority of the surface area left indented, observed for most of the specimens that underwent testing (Figure 3.19). Thus, similar to off-bone cartilage, testing at 1 Hz of frequency resulted in the least recovery of the on-bone cartilage specimen, with a larger indented area observed (Figure 3.19; Table 3.11). This is represented by the observations where the indented area, as clearly highlighted by the black circular staining of India ink, extended to the majority of the cartilage on-bone specimen surface at 1 Hz (Figure 3.19), in comparison to the lesser surface indented at 10 Hz (Figure 3.20).

Table 3.10: Mean total crack length values with standard deviation for cartilage-on-bone samples, following testing, at all frequencies and substrates investigated, as a combined study

	Cartilage on-bone mean total crack length (mm) ± SD			
Frequency (Hz)	**Substrate 1 density: 0.1556 g/cm^3**	**Substrate 2 density: 0.3222 g/cm^3**	**Substrate 3 density: 0.5667 g/cm^3**	**Substrate 4 density: 0.6000 g/cm^3**
1	0 ± 0	1.09 ± 2.67	0.25 ± 0.62	0 ± 0
10	5.18 ± 11.56	0.76 ± 1.86	8.63 ± 9.22	3.01 ± 4.93

Table 3.11: Mean area of indentation values with standard deviation for cartilage-on-bone samples, following testing, at all frequencies and substrates investigated, as a combined study

	Cartilage on-bone mean area of indentation (mm^2) ± SD			
Frequency (Hz)	**Substrate 1 density: 0.1556 g/cm^3**	**Substrate 2 density: 0.3222 g/cm^3**	**Substrate 3 density: 0.5667 g/cm^3**	**Substrate 4 density: 0.6000 g/cm^3**
1	17.72 ± 5.84	25.97 ± 3.94	25.07 ± 3.70	26.44 ± 3.53
10	14.82 ± 3.84	13.98 ± 3.72	15.98 ± 9.09	18.92 ± 3.92

3.4 Hertzian Contact Analysis

The Hertzian contact stress between each substrate and off-bone cartilage was calculated, with a point-contact approach (Taylor, 2016) as illustrated by the simple schematic

in Figure 3.23. Equations (3.5) – (3.7) below describe the various steps required for determination of the maximum contact stress (Taylor, 2016):

$$P_o = \frac{3F}{2\pi a^2} \quad (3.5)$$

$$\left[\frac{1}{E^*} = \frac{1-V_1^2}{E_1} + \frac{1-V_2^2}{E_2}\right] \quad (3.6)$$

$$a = \left(\frac{3FR_e}{4E^*}\right)^{\frac{1}{3}} \quad (3.7)$$

where F = applied load (N), a = radius of area of contact (mm), R_e = reduced radius (mm), E^* = contact modulus (MPa), E_1 and E_2 = Young's modulus of the cartilage and substrate, respectively (MPa), V_1 and V_2 = Poisson's ratio of the cartilage and substrate, respectively, and P_o = maximum contact pressure (MPa) (Taylor 2016). Note, the Young's modulus of the cartilage was taken as 10 MPa, which is comparable to literature (Barker and Seedhom, 2001; Edelsten *et al*., 2010; Shepherd and Seedhom, 1999). The Poisson's ratio of articular cartilage was taken as 0.44, as an average from the range stated in literature of 0.37 - 0.50 (Jurvelin *et al*., 1997). The Young's modulus of each substrate was taken as the values obtained from the compression testing, described in Section 3.2.4 and detailed in Table 3.1. Similarly, the Poisson's ratio of the substrate was taken from the Sawbones website as previously described in Section 3.2.4 and detailed in Table 3.1.

For calculation, the radius of the off-bone cartilage was 5.5 mm (Figure 3.23). The substrate was modelled as a flat plane (Figure 3.23); thus $R_2 = \infty$, therefore $R_e = R$, as represented in equation 3.8 (Taylor 2016). Equation (3.5) highlights the overall equation for determining the maximum contact pressure; the Hertzian contact stress, deriving the contact area radius, a, from equations (3.6) and (3.7).

$$\left[\frac{1}{R_e} = \frac{1}{\mathrm{R}_1} + \frac{1}{\mathrm{R}_2}\right] \quad (3.8)$$

The applied load, F (N) is taken as the maximum of 50 N used in the mechanical testing. A summary of the calculations is provided in Appendix D. Final values of the Hertzian contact for each case are detailed in Table 3.12.

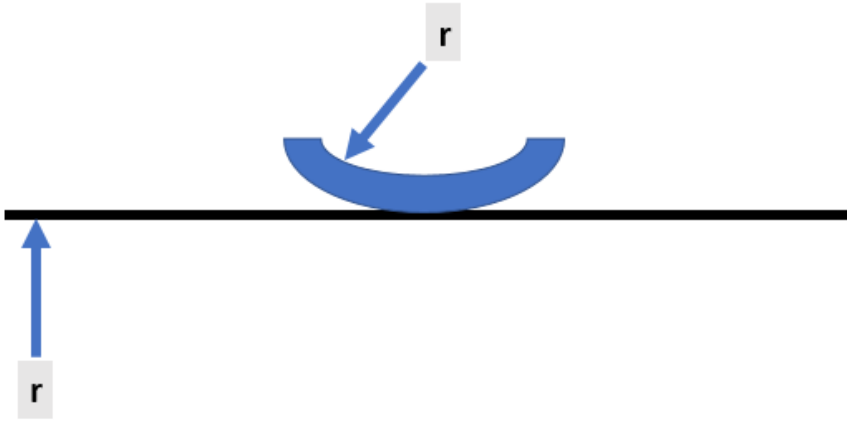

Figure 3.23: For calculation of the point contact Hertzian contact stress between cartilage-off-bone and underlying substrate, a simple illustration is displayed of the cartilage-off-bone specimen (arc) in point contact with the underlying substrate (horizontal line). The ‘r’ in each case defines the radius.

3.5 Hertzian Contact Results

Table 3.12: The values of the calculated Hertzian contact between the off-bone cartilage specimen and the underlying substrate. Values are presented in MPa. The corresponding contact modulus and contact area radius utilised for each calculation are also displayed.

Surface in contact	Contact modulus; E^* (MPa)	Contact area radius; a (mm)	Hertzian contact stress (MPa)
Substrate 1 with off-bone cartilage	12.07	2.58	3.59
Substrate 2 with off-bone cartilage	12.25	2.56	3.64
Substrate 3 with off-bone cartilage	12.33	2.56	3.64
Substrate 4 with off-bone cartilage	12.36	2.56	3.64

3.6 Discussion

In this chapter the measured surface damage experienced by articular cartilage was independent of substrate density, as a single variable. Increased damage due to greater energy absorption is expected with a stiffer substrate, with reference to the previously hypothesised bone remodelling concept of bone stiffening leading to cartilage breakdown (Radin *et al.,* 1972). However, this was not observed statistically for substrate density alone, using the experimental protocol in this chapter. It was observed from this chapter that a loading frequency of 10 Hz is required, in combination with an increase in substrate density to observe increased damage (total crack length), specifically for the scenario of cartilage off-bone. Thus, it is suggested that the combination of BMD and above normal gait frequencies (e.g. 10 Hz), predisposes articular cartilage to damage. Nevertheless, the linear regression has been performed on four values; that of the mean of both crack length and indented area for each of

the four substrates. Thus, it is worth noting as a limitation that the statistical outcome is based on a low number of points.

The study presented in this chapter demonstrates an evaluation of the effect of substrate density on the impact on cartilage damage, for which a direct effect has not been established. The substrate has been used as a surrogate for bone mineral density. This finding is in contrast to previous work, that has identified a significant linear relationship between the increased thickness of cartilage and BMD (Fell *et al*., 2019). This is interesting to note, as an earlier study has demonstrated thicker cartilage in the tibial plateau not covered by the meniscus as more likely to show signs of damage (Espino *et al*., 2014). Thus, combining the work of Fell *et al*. (2019) and Espino *et al*., (2014) a relationship has been established between an increase in BMD and the thickness of cartilage, which in turn is related to enhanced damage. Alternatively, the work presented in this chapter identifies the requirement of a loading frequency at 10 Hz in combination with the physical property of BMD, for a direct significant effect on cartilage damage.

The loss stiffness of on-bone articular cartilage has been determined to be frequency-independent, but frequency-dependent for off-bone articular cartilage (Lawless *et al*. 2017). The findings concerning damage presented in this chapter coincide with such findings. This is illustrated by the damage for off-bone cartilage that varies with a change in frequency and substrate density; frequency-dependent, whilst the on-bone cartilage trend for crack length remains at approximately 0 mm, with frequency and substrate density, frequency-independent. Such a trend with cartilage damage explored in this chapter is also in agreement with the previous findings of a frequency independent loss modulus of on-bone cartilage (Fulcher *et al*., 2009), and a frequency dependent loss modulus for off-bone cartilage (Aspden 1990; Temple *et al*., 2016). Furthermore, the observed near to nil damage of on-bone cartilage in accordance to substrate density at 1 and 10 Hz, relates to the previously detected trend of the effect of frequency on the loss stiffness of on-bone cartilage (Lawless *et al*., 2017).

Additionally, for cartilage off-bone, the data shows the overall crack length was the greatest at 10 Hz, reaching a maximum of 10.95 mm. Conversely, the least damage with the lowest crack length, was observed at 1.19 mm for 1 Hz. Cartilage damage on-bone in this chapter also appeared to follow the same trend, as an increase in crack length was observed from a minimum of 0 mm at 1 Hz, to a maximum of 8.63 mm at 10 Hz. The finding for cartilage-on-bone in this chapter illustrates the equivalent trend previously seen of greater cartilage damage with an increase in frequency (Sadeghi *et al*., 2015; Sadeghi *et al*., 2017; Sadeghi *et al*., 2018). Overall, the results from this chapter have identified greater cartilage damage off-bone, in comparison to on-bone. This finding is discussed further on in this section, evaluating the expected outcome.

For off-bone cartilage there was no increase in damage when loading at 50 Hz, unlike for the on-bone study of loading (Sadeghi *et al.,* 2015; Sadeghi *et al*., 2017; Sadeghi *et al*., 2018). Thus, it is worth noting the differences in the behaviour of cartilage on- and off-bone, as a result of the presence or absence, respectively, of the restraining effect provided by the underlying bone (Edelsten *et al*., 2010). This may be due to the loss stiffness being frequency-dependent for off-bone articular cartilage (Lawless *et al.,* 2017), but not for on-bone cartilage (Fulcher *et al*., 2009). Therefore, off-bone articular cartilage is more able to dissipate energy, at 50 Hz, potentially preventing damage to the cartilage itself (i.e. via dissipating the energy through the formation of cracks); this ability to dissipate energy is greater at higher frequencies, particularly at 50 Hz, potentially reducing the extent to which cartilage undergoes damage at 50 Hz (which may not happen when cartilage is on-bone).

Within the region of and beyond 10 Hz, it is thought that cartilage enters a glass transition phase (Sadeghi *et al*., 2018). Therefore, a change in cartilage material properties is noticed from behaving as a deformable (‘soft’) material to one which is hard but brittle (Fulcher *et al*., 2009). Due to this alteration in the physical behaviour of articular cartilage, it may affect the

extent of damage. This description could be used to describe the significance of cartilage off-bone damage observed at 10 Hz only in this chapter. This is further supported by the results shown in this chapter, as maximum cartilage off-bone damage is observed at 10 Hz, in comparison to 1 and 50 Hz. The reduction in damage observed above the application of 10 Hz, such as 50 Hz as in this chapter for off-bone cartilage, could be due to the recently established relationship such that the loss stiffness of off-bone articular cartilage is dependent upon frequency (Lawless *et al*., 2017). Thus, articular cartilage may be better able to dissipate energy at 50 Hz which might explain why, off-bone, the extent of damage to the tissue is reduced as compared to 10 Hz of loading.

Due to the nature of biological material, the results for crack length and indented area for both off- and on-bone cartilage have displayed expected variation. This may be due to differences within the ECM of the specimen, such as amongst the biological behaviour of the proteoglycans and glycosaminoglycans. For the on-bone specimens, differences within the bone mineral density may also contribute to the variation. Disparities across the thickness of the specimen could have also impacted the variation in the results. Further, disparities within the positioning of the specimen on the substrate leads to different contact positions of the indenter on the cartilage surface, hence introducing variability to the data.

The outcome from the One-Way ANOVA tests have identified a common significant difference for the indented area at 1 Hz for on- and off-bone cartilage. This is expected due to the lowest elastic recovery of the specimen at this frequency. Substrates with a lower density resulted in a significant difference for the area of indentation for cartilage off-bone (Table 3.4). This could be explained by the decreased stress absorbed by the substrate, and therefore a greater impact on the surface of the cartilage to result in reduced elastic recovery. This result is in contrast to the higher density substrates resulting in a significant difference on the indented area for on-bone cartilage (Table 3.9). This may be due to the subchondral bone taking precedence over the lower density substrates. It is also an expected outcome for

statistical significance between the highest density substrate and the crack length for off-bone cartilage (Table 3.4), due to the increased absorbed stress and therefore exposing the cartilage to greater damage.

Interestingly, at 1 Hz, the results identify the absence of crack length for on-bone cartilage at substrates one and four, that of the lowest and highest substrate density. This may be explained by the maximum absorption of stress by the substrate of the highest density, resulting in the absence of damage to the cartilage. Similarly, for the substrate of the lowest density, the maximum absorption of stress could predominantly occur in the subchondral bone, resulting in the absence of damage to the cartilage. Further, an increased area of indentation is observed for on-bone cartilage, particularly at 1 Hz for substrates two to four. This may be due to the greater exposure of stress to the cartilage at a greater underlying density, resulting in the reduced recovery.

It is worth noting that off-bone cartilage cores have been removed from the adjacent regions of cartilage, therefore, weakening the cartilage due to the disruption of its extracellular matrix. Thus, this may provide an explanation for the greater damage observed for off-bone cartilage in this chapter. This is important to note, as although the results from this chapter have demonstrated greater damage for cartilage off-bone, it is expected, however, that on-bone cartilage experiences greater damage than off-bone cartilage; as previously hypothesised that the resulting energy may be released as cracks (Lawless *et al.*, 2017). This is primarily as a result of the rationale of the presence of the underlying bone that provides constriction to the cartilage, increasing the induced stress (Edelsten *et al*., 2010; Lawless *et al.*, 2017; Aspden, 1990). This concept is further reinforced by the deep zone of articular cartilage restricted in its ability to deform laterally (Park *et al*., 2004). The ability of bone to dissipate more energy after an applied load than cartilage (Malekipour *et al*., 2013) is also in support of increased damage for on-bone cartilage. However, the removal of the articular cartilage off-bone specimens in this chapter was kept consistent throughout the investigation,

thus, specifically concerning the unknown relationship between underlying substrate density and cartilage, at a varied frequency.

It is further worth highlighting the potential limitation of testing off-bone cartilage, due to the absence of the restrictive attachment provided by the underlying subchondral bone that is found in the natural environment *in vivo* (Aspden, 1990). The removal of the subchondral bone creates an alteration in the load transfer properties of the cartilage-off-bone specimen, notably the absence of the calcified cartilage layer with a stiffness in-between that of articular cartilage and the subchondral bone (Radin and Rose, 1986). Despite this, however, the substrates used in this study have acted as the underlying bone of a controlled density, to allow for evaluation of the effects of the density of the underlying substrate alone, on the associated cartilage damage.

The reproducibility of the ImageJ damage measurement may confer limitations due to the requirement of a laboratory environment, specific lighting, specimen positioning and subjectivity of crack and area formation. However, a clear protocol has been defined in Section 3.2.5 to ensure consistent measurements for this chapter. For development in future work, it would be ideal to implement an intra- and inter-specimen operator study to know the exact uncertainty in the measurements.

The use of an indentation test with articular cartilage is an established method previously developed to closely represent the physiological loading conditions of articular cartilage *in vivo* (Lu *et al*., 2004), as well as for damage inducing to the surface of articular cartilage (Sadeghi *et al*., 2015), having the advantage of being highly repeatable. Despite the hardness as well as the smaller diameter of the indenter in comparison to the cartilage specimen, a 0.5 mm radius bevelled edge was used to prevent artificial damage induced through stress concentrations at the edge. Further, the use of an indenter with a diameter smaller than the cartilage specimen, enables the deformation behaviour by the collagen matrix of the

surrounding cartilage specimen (Korhonen *et al*., 2002) outside of the indentation area. Ultimately, this protocol has enabled a controlled evaluation of the effect of substrate density on cartilage failure.

The calculated Hertzian contact stress vary from 3.59 to 3.64 MPa, a 1.39 % increase, of the off-bone articular cartilage at the lowest and highest substrate density, respectively (Table 15). This finding of a rise in the stress at contact between the bone-mimicking substrate and cartilage, can be used to explain the relationship between an increase in BMD and the occurrence of OA, as reviewed (Hardcastle *et al*., 2015) and extensively described previously (Dequeker and Mbuyi-Muamba 1996; Foss and Byers 1972; Nevitt *et al.*, 1995; Burger *et al*., 1996). Further, the hypothesis of an enhanced stiffness of the subchondral bone (Radin *et al*., 1973), relating to the occurrence of cartilage damage via greater stress absorption with an increase in BMD, additionally links to the finding of a greater Hertzian contact at substrate four, in comparison to that at substrate one. This finding also coincides with previous summaries that have established a negative relationship of OA with osteoporosis (Cooper *et al.*, 1991; Dequeker *et al*., 2003), as the osteoporotic substrate, substrate one, displays the lowest Hertzian contact.

Furthermore, although there was an observed increase in the Hertzian contact stress between substrate one and four; it is further worth noting that the calculated Hertzian contact stress was constant between substrate two and four. This result can be linked to the experimental outcome from this chapter, such that within the range of substrate densities examined, substrate density alone, is insufficient to cause large stress variations that could otherwise independently induce cartilage damage. As an extra evaluation, a preliminary computational model has been developed to assess the static effect of a variation in substrate density, on the internal stresses and displacement of the cartilage and substrate. This preliminary finite element analysis is presented in Appendix E.

3.7 Chapter Summary

The conclusions determined from this chapter are detailed below:

1) Damage to articular cartilage, off-bone in particular, is determined by a combination of damage inducing factors. Specifically, this chapter highlights the combination of an increase in the underlying substrate density, with an above-normal gait frequency of loading, that of 10 Hz, which contributes to significant off-bone cartilage damage. No statistical significance was found at 1 and 50 Hz, with substrate density, for both the crack length and area of indentation for cartilage off- and on-bone. Thus, a combination of damage inducing factors to articular cartilage should be taken into consideration when evaluating the onset of OA.
2) The Hertzian contact stress was calculated as the lowest between substrate one and cartilage off-bone. The Hertzian contact stress was observed to remain constant between substrates two to four. This lack of variation in the calculated Hertzian contact stress coincides with the experimental finding that substrate density alone, is not sufficient to cause statistically significant cartilage damage.
3) Overall, greater cartilage damage is experimentally observed for off-bone in comparison to cartilage on-bone.

4. A TECHNIQUE FOR MEASURING THE FRICTIONAL TORQUE OF ARTICULAR CARTILAGE AND REPLACEMENT BIOMATERIALS

4.1 Introduction

Articular cartilage is the bearing surface in synovial joints. The low friction characteristic of articular cartilage is an essential feature to ensure wear is reduced to a minimum (McNary *et al*., 2012; Fox *et al*., 2009). The lubrication mechanisms of synovial joints contribute to its low friction (McNary *et al*., 2012; Jin and Dowson, 2013), as highlighted in Section 2.3 of the Background. Further, as previously discussed, osteoarthritis (OA) is a disease that can affect synovial joints (Sandell and Aigner, 2001), inducing a rough, fibrillated exterior to the surface of the cartilage, that greatly differs from its original smooth surface configuration (Chiang *et al*., 1997). The advancement of OA is induced by the phenotypic modification of chondrocyte cells, leading to the destruction of articular cartilage (Goldring, 2012).

Consequently, as previously outlined in Section 2.6 of the Background, cartilage repair methodologies are required for the treatment of damaged articular cartilage tissue (Gomoll and Minas, 2014; Cao *et al*., 2014). Hydrogels, defined as a network of polymers of a hydrophilic gel (Ahmed, 2015), are commonly used as tissue replacements (Drury and Mooney, 2003), particularly due to the biocompatible nature (Jhon and Andrade, 1973) and biodegradability (Ahmed, 2015). Those with a polysaccharide origin have been specifically associated with the absence of toxicity (Ahmed, 2015), for instance, the calcium alginate hydrogel. The calcium alginate hydrogel is well-known for its use in several biomedical applications (Drury and Mooney, 2003; Wands *et al*., 2008; Shang *et al*., 2017), particularly for use as a suitable biomaterial for cartilage tissue engineering (Liao *et al.,* 2017; Chen *et al*., 2010). The viscoelastic properties of calcium alginate display similar characteristics to articular cartilage. This is shown by a frequency-dependent storage modulus of calcium alginate (Wands *et al*., 2008) and storage stiffness of articular cartilage (Sadeghi *et al*., 2015). Further, the storage stiffness is greater than the loss stiffness for articular cartilage (Sadeghi *et al*., 2015), similar

to a greater storage modulus in comparison to loss moduli for calcium alginate (Wands *et al*., 2008). In addition, the loss moduli and stiffness for calcium alginate and cartilage respectively, display frequency-dependency at lower frequencies only (Sadeghi *et al*., 2015; Wands *et al*., 2008). Although mechanically calcium alginate is reported for its low stiffness (Wands *et al.*, 2008), attempts have been made to reinforce the structure with cross-linking (Lee and Mooney, 2012) as well as particle reinforcement (Wands *et al.*, 2008).

The successful development of cartilage replacement biomaterials requires an understanding of the frictional characteristics of articular cartilage (Northwood and Fisher, 2007). Literature has reported the effect of sliding speed (Burris and Moore, 2017; Moore and Burris, 2017), time (Li *et al*., 2010) as well as cyclic loading (Drewniak *et al*., 2012) on the coefficient of friction of articular cartilage. However, the previously measured coefficient of friction is limited to the movement in sliding, therefore, dismissing the rotational motion of articular cartilage. The response of the resulting friction of articular cartilage in relation to a rotation, known as the frictional torque, has not been previously reported in the literature. The frictional torque is important to measure as the underlying kinetic to this measurement closely mimics joint movement *in vivo*. Further, the response of articular cartilage subject to a rotational movement can allow for investigation of its specific boundary lubrication mode (Accardi *et al*., 2011), representing the lubrication present at the cartilage-cartilage boundary *in vivo* (Cilingir, 2015). Consequently, for the development of a successful cartilage replacement biomaterial, one of the aspects is for the biomaterial to have a similar frictional torque to articular cartilage.

The aim of the work presented in this chapter was to develop a technique for the evaluation of the unknown frictional torque of articular cartilage, to which a biomaterial for the replacement of damaged cartilage can be compared. The use of calcium alginate in several biomedical engineering applications, particularly for that of cartilage tissue engineering, formed the selection basis for the assessment of this biomaterial presented in this chapter. The torque has been evaluated experimentally with an axial-rotation testing configuration, varying the

applied load of contact stresses associated with physiological behaviour. Following on from the assessment of the torque of articular cartilage, a small defect was induced on the surface of articular cartilage, to enable the insertion of the hydrogel for its investigation. The assessment was performed with two experimental variations; the calcium alginate hydrogel, alone, as well as the calcium alginate hydrogel in combination with articular cartilage. To enable a direct comparison of the frictional torque, an identical diameter region was tested for all specimen variations, as were testing parameters kept consistent.

4.2 Materials

4.2.1 Articular Cartilage Specimen Preparation

See Section 3.2.1 for the process of attaining bovine humeral heads for articular cartilage specimen preparation. For this Chapter, twelve different bovine humeral heads to those used for Chapter 3 were obtained from a supplier (Dissect Supplies, Kings Heath, Birmingham, UK). The underlying subchondral bone was used for the secure fixation of the specimen for the friction measurements in this study. Prior to testing, all specimens were immersed in Ringer's solution for 30 minutes (Temple *et al.,* 2016).

To evaluate the frictional torque of articular cartilage, the specimens were extracted from the central area of the humeral head (Figure 4.1-a; Figure 4.1-b), as performed for the preparation of the cartilage on-bone specimens described in Section 3.2.3. This region was selected as it is typically flat. Also, the central segment acts as a central point of contact within the shoulder joint. Six rectangular shaped cartilage specimens were dissected across six humeral heads with use of a 300 mm bi-metal hacksaw blade (RS Components Ltd, Corby, UK) (Figure 4.2-a). Similarly, for the evaluation of a 2 mm calcium alginate insert, six rectangular shaped cartilage samples were extracted from the central region of a further six humeral heads (Figure 4.2-b). To evaluate the torque of the calcium alginate hydrogel itself, a

further six cartilage on-bone specimens were extracted, each across six humeral heads of the twelve used in this study (Figure 4.2-c). This resulted in the preparation of eighteen specimens in total. Figure 4.2 illustrates the specimen extraction from each humeral head per testing group.

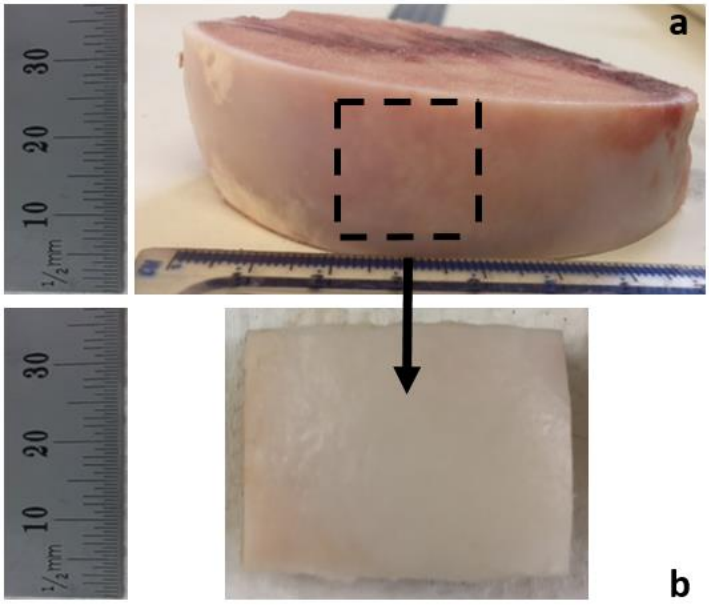

Figure 4.1: Dissection Procedure: a) schematic outline of a central segment of the humeral head utilised for the extraction of a rectangular-shaped specimen. b) dissected rectangular-shaped cartilage on-bone specimen for testing

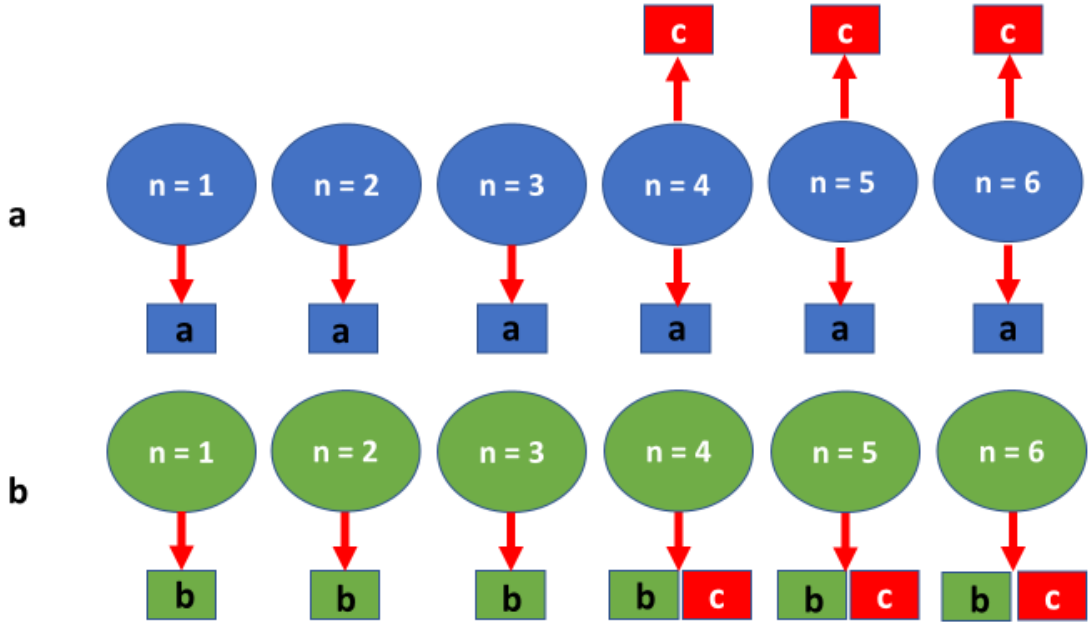

Figure 4.2: Schematic to represent the extraction procedure from humeral heads for testing. Group a) displays the extraction of six specimens across six different humeral heads for the cartilage-on-bone tests (n = 6). Group b) displays the extraction of six specimens across another different humeral heads to group a) for the 2-mm calcium alginate insert tests (n = 6). Group c) displays the extraction of six specimens from across six previously used humeral heads for groups a) and b) (n = 6).

All specimens were approximately 11 mm thick, with a cross-section of 26 mm × 21 mm. The three torque tests described in this chapter focused on the frictional torque of: i. cartilage alone, ii. cartilage with a 2 mm insert of calcium alginate, iii. cartilage with a 10 mm insert of calcium alginate. Future development of this preparation method to address the curvature and roughness measurements are discussed in the overall discussion.

To prepare the 2 mm inserts for calcium alginate, a 2 mm diameter drill head (EW Equipment, Stockport, UK) attached to a drill (Makita UK Ltd, Milton Keynes, UK), was used to create a cavity within the surface of the cartilage specimen (Figure 4.3-a). For the evaluation of the biomaterial alone, a 10 mm diameter drill head (EW Equipment, Stockport, UK) attached to a drill (Makita UK Ltd, Milton Keynes, UK), was used to create a cavity within the surface of the cartilage specimen (Figure 4.3-b). The cavity for all specimens was of an approximate depth of 3 mm. The induced defect cavity allowed for the insertion of the biomaterial. For all

testing groups, a simple schematic is provided in Figure 4.4 to display the various specimen surfaces.

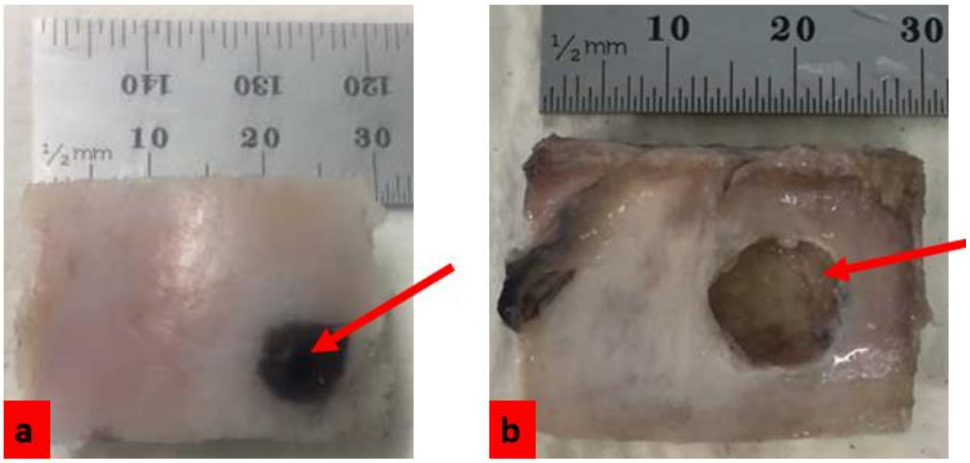

Figure 4.3: Cavity created within articular cartilage specimen for biomaterial insertion: a) the 2 mm perforated insert is highlighted with the red arrow. The black staining surrounding the biomaterial insert is of India ink utilised for identifying the location of the indenter in contact with the specimen surface. This is to enable detection of the region to insert the biomaterial for testing. b) 10 mm perforation insert highlighted by the red arrow.

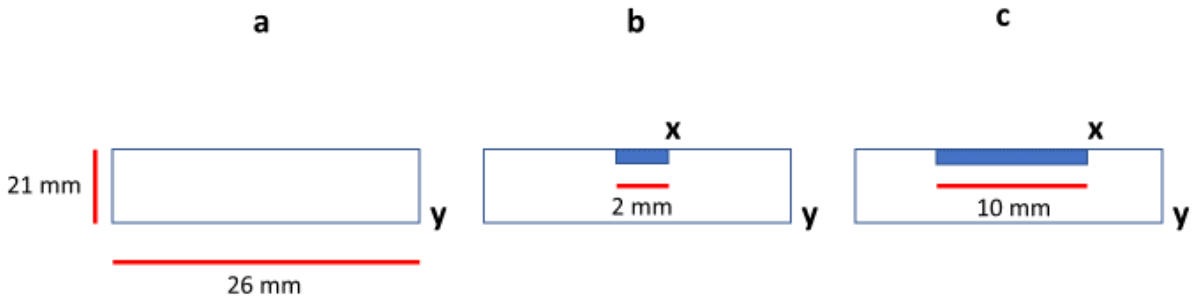

Figure 4.4: Schematic to represent the articular cartilage specimen for each testing group. a) cartilage on-bone alone, b) 2-mm calcium alginate insertion specimen, c) 10-mm calcium alginate insertion specimen. 'y' represents the cartilage specimen for each case. The insertions for both the 2- and 10-mm calcium alginate hydrogels are shown by the blue shaded area highlighted by 'x'. Key dimensions are shown with a scale bar

4.2.2 Preparation of Calcium Alginate

Calcium alginate hydrogel was formed by mixing 7.5 g of sodium alginate (Sigma-Aldrich, Dorset, UK) with 125 ml of deionised water (Wands *et al*., 2008). The mixing was performed overnight using a magnetic stirrer (Stuart Equipment, Staffordshire, UK), ensuring the glass beaker (Fisher Scientific, Leicestershire, UK) was covered to avoid dehydration.

Next, 12.5 g of calcium chloride dihydrate (EMD Millipore, Darmstadt, Germany) was mixed with an additional 125 ml of deionised water, which dissolved after a few minutes whilst using the magnetic stirrer. The formed calcium chloride dihydrate solution was transferred into the sodium alginate mixture. The mixture was left for 48 hours in a sealed container (Wands *et al.,* 2008). An image of the formed calcium alginate hydrogel is presented in Figure 4.5.

For the direct comparison of the frictional torque between the articular cartilage and calcium alginate biomaterial, an identical 5 mm diameter region was tested with a single indenter across all specimens; a 5 mm diameter region of articular cartilage, as well as two calcium alginate inserts, one of 2 mm with surrounding 3 mm of articular cartilage and another of 10 mm. Thus, both a 2 and 10 mm in diameter calcium alginate biomaterial insert, were assessed with a single indenter, 5 mm in diameter. Testing of the calcium alginate smaller in diameter size of 2 mm, in comparison to the 5 mm articular cartilage, enabled the evaluation of the combination of the biomaterial with articular cartilage to be assessed. Further, the assessment of the 10 mm calcium alginate biomaterial enabled the direct comparison between the torque of the identical diameter of 5 mm, across both the biomaterial and cartilage.

To prepare the specimen with the 2 mm insertion, a cork-borer with a diameter of 5 mm was inserted within the calcium alginate hydrogel, for the release of a core of the biomaterial (Figure 4.6-a). From the core, a segment 2 mm in diameter was obtained, and inserted within a cavity perforated at the surface of the articular cartilage (Figure 4.6-b). Similarly, for the preparation of the 10 mm insert specimen, a hand cork-borer with an inner diameter of 10 mm was inserted within the calcium alginate hydrogel (Figure 4.7-a), for the release of a core of the biomaterial, 10 mm in diameter. For testing, the core was inserted within a cavity created at the surface of the articular cartilage specimen (Figure 4.7-b). As previously illustrated, Figure 4.4 displays a simple schematic to outline the various specimens used in this chapter.

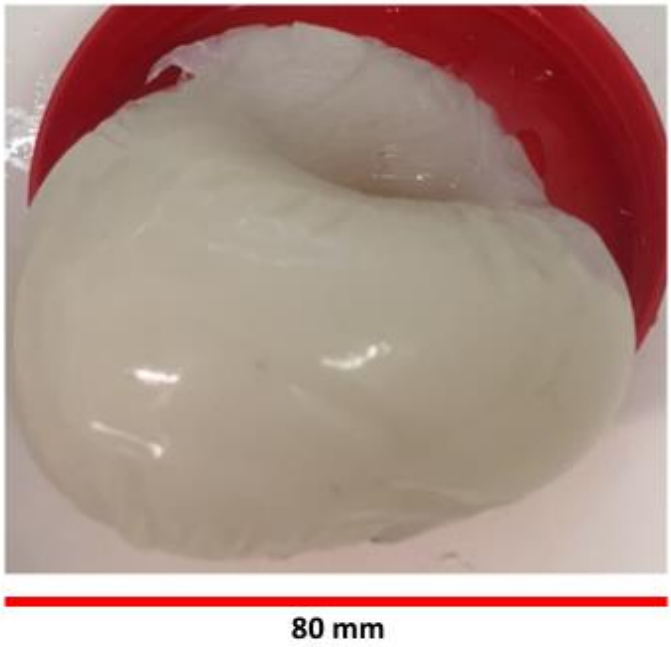

Figure 4.5: Calcium Alginate Hydrogel: synthesised result post 48-hours of setting. Scale bar is included

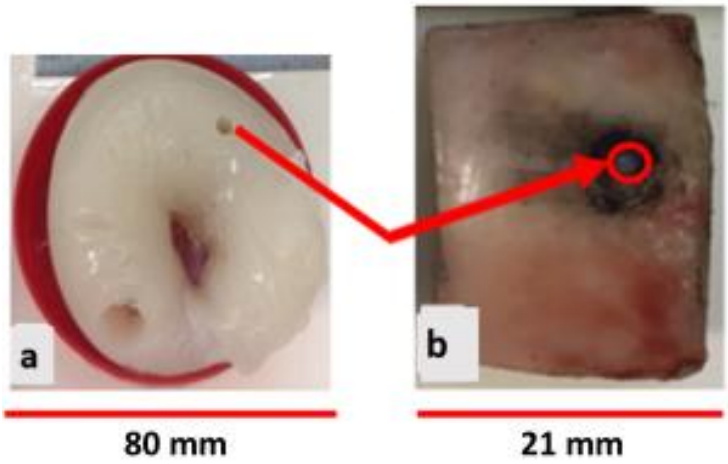

Figure 4.6: Illustration of the 2 mm insertion procedure of the calcium alginate hydrogel within the cartilage on-bone specimen: a) 2 mm hydrogel extraction inserted into the cartilage on-bone specimen as shown in part b)**.** The black surrounding circular staining of the hydrogel insert in part b) is the use of India ink to locate the insertion location for the biomaterial. The inserted biomaterial is highlighted with a red outline. Scale bar is included

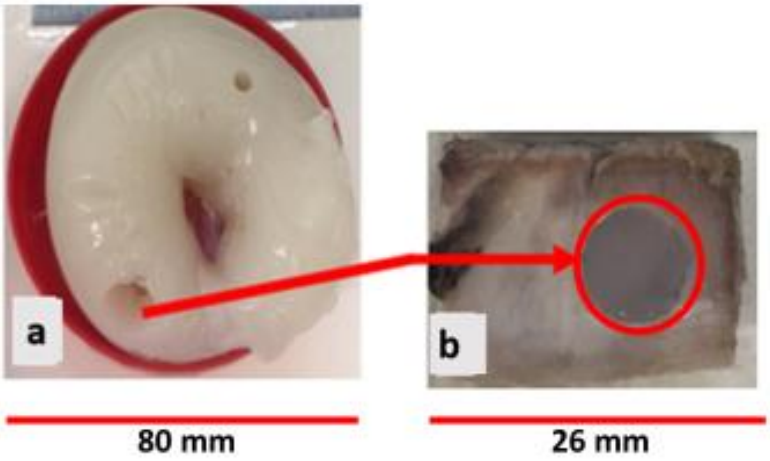

Figure 4.7: Illustration of the 10 mm insertion procedure of the calcium alginate hydrogel within the cartilage on-bone specimen: a) 10 mm hydrogel extraction inserted into the cartilage on-bone specimen as shown in part b). The inserted biomaterial is highlighted with a red outline. Scale bare is included

4.3 Experimental Methods

To assess the frictional torque of each of the eighteen individual specimens (six specimens of articular cartilage and six specimens each of the 2 and 10 mm calcium alginate inserts), a Bose ElectroForce SDWS testing machine operated with the Bose WinTest 4.1 software (Bose Corporation, ElectroForce Systems Group, Minnesota, USA) was used (Figure 4.8). Testing involved compressing a stainless-steel indenter against the specimen surface and applying an axial-rotation to determine the resulting frictional torque. Stainless-steel was selected based on previous studies that have extensively used stainless-steel on cartilage for frictional evaluations (Li *et al.,* 2010; Northwood and Fisher, 2007; Wang and Ateshian, 1997). The specimen curvature was controlled by extraction from the central segment of the humeral head, and therefore the flattest. Visual observation ensured the curvature was minimal and therefore suitable for testing. As mentioned in Section 4.2.1, future work is required for addressing the limitation of the curvature assessment. This is outlined in the overall discussion to the chapter.

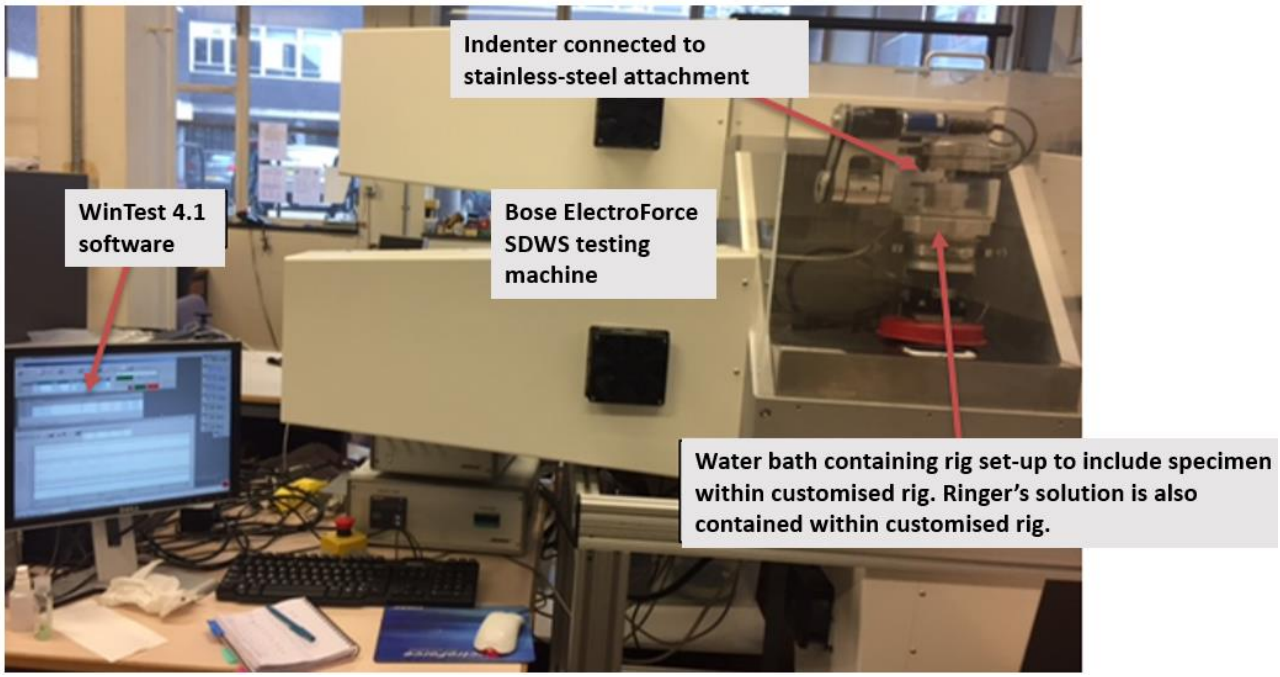

Figure 4.8: Overall schematic of the testing apparatus of the Bose ElectroForce SDWS testing machine: labelled components include the WinTest software, indenter connection to stainless-steel attachment and location of customised rig for the containing of the specimen and Ringer's solution.

For all testing groups, a simple schematic is displayed in Figure 4.9 to represent the application of force at testing.

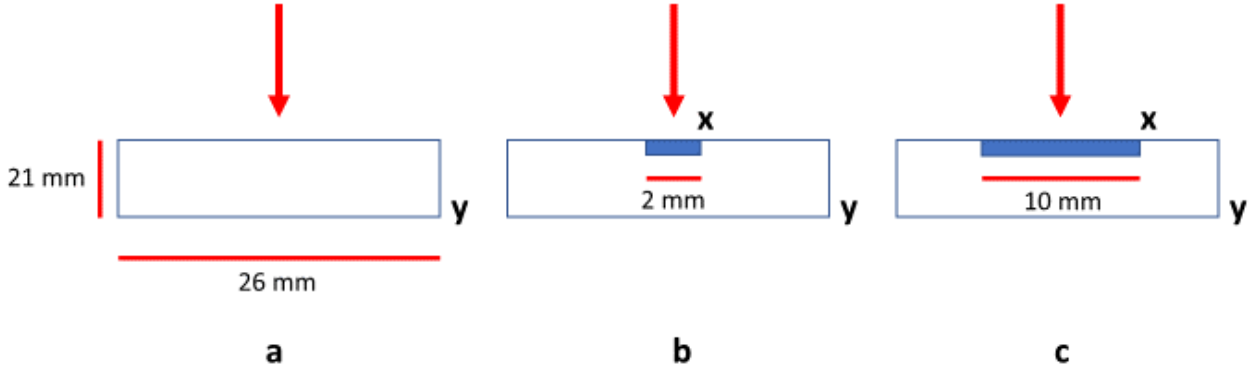

Figure 4.9: Schematic to display the testing set-up for each group. a) cartilage on-bone, b) 2 mm calcium alginate insertion specimen, c) 10 mm calcium alginate insertion specimen. The red arrow indicates the load applied with the indenter for testing. 'x' displays the 2- and 10-mm calcium alginate insertions, 'y' displays the cartilage on-bone sample. Key dimensions are included.

The indenter was designed with a diameter of 5 mm, 7.5 mm in length and with a 0.5 mm chamfered end to prevent damage to the cartilage (Mahmood *et al.,* 2018; Sadeghi *et al.,* 2015). The chamfered-polished end ensured a smooth surface for the assessment of the frictional torque in this chapter. The indenter was attached to a stainless-steel plate with a diameter of 110 mm (Figure 4.10-a) which was secured to the upper plate of the testing machine. The indenter was manufactured from polished stainless-steel to match previous studies which reported the Ra as 0.02 μm (Forster and Fisher, 1999; Northwood and Fisher, 2007).

All specimens were secured within a customised circular aluminium test rig (Figure 4.10-b), via two screws either side of the rig that were positioned through the subchondral bone to enable fixation. The rig was designed with a diameter of 63 mm and a thickness of 13.5 mm (Figure 4.10-b). Similar to previous work to determine the frictional characteristics of articular cartilage (Forster and Fisher, 1996), in this chapter, Ringer's solution was also used as the lubricant. The Ringer's lubricant in the bath solution was prepared to a full-strength mass concentration via the dissolving of 4.83 g of Ringer's tablets (Oxoid Ltd., Hampshire, UK), per 500 ml of distilled water (Mahmood *et al*., 2018). For the preservation of the tissue during testing, the Ringer's solution was inserted within the test rig, ensuring the cartilage/hydrogel/cartilage-hydrogel specimen was hydrated at all times throughout the testing procedure (Fulcher *et al*., 2009; Kerin et al., 2003; Sadeghi *et al*., 2015). The test rig was secured on a stainless-steel fixture (Moghadas *et al*., 2012), followed by the insertion within a water bath for mounting onto the machine (Moghadas *et al*., 2012). The overall experimental set-up is shown in Figure 4.10-c.

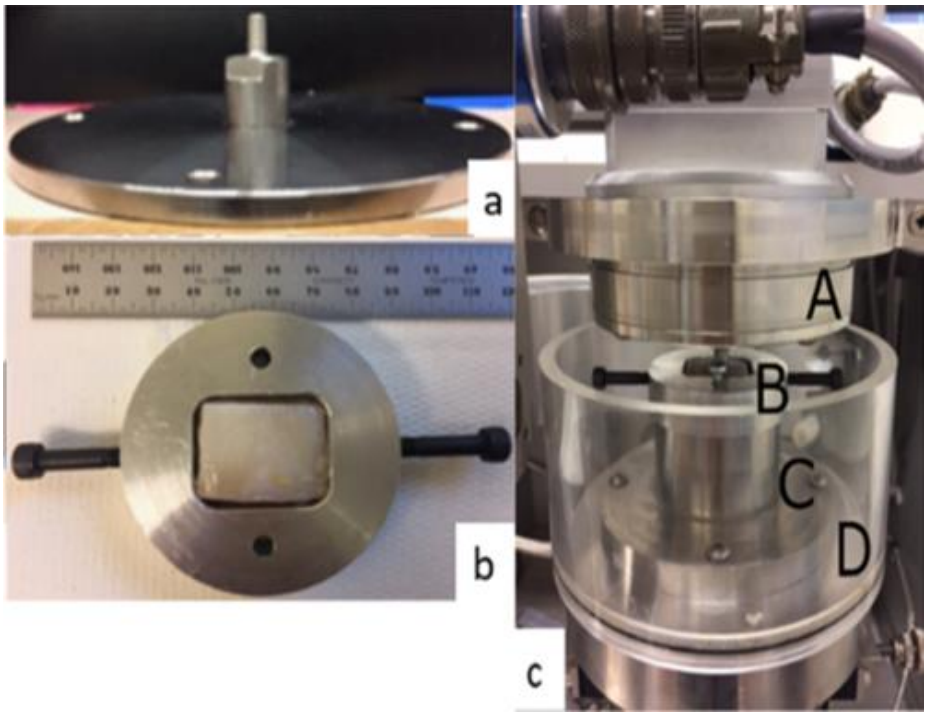

Figure 4.10: Testing Apparatus: a) stainless-steel indenter b) test-rig for the specimen which is secured with side screws. Ringer's solution is added to the rig to ensure cartilage hydration throughout testing. c) Experimental set-up of the testing configuration on Bose ElectroForce SDWS; A: stainless-steel indenter attachment to machine. B: aluminium test-rig containing specimen and Ringer's solution. C: lower metal-rig. D: water bath.

A static load of 10 N was applied onto the specimen, followed by a rotation from 0° to 2° to 0°, completed in one second, for 100 cycles. The rotation range of 0° to 2° to 0° was selected based on the physiological range of the hip for the internal rotation of specific movements (Hyodo *et al.,* 2017). This testing method was repeated for a further nine static loads from 20 to 100 N, evaluating the effect of an induced stress range from 0.51 to 5.09 MPa (across the ten loads examined) (Table 4.1). The load range of 10 – 100 N was selected based on preliminary tests, whilst the rotation range was chosen to mimic physiological conditions (See Appendix F for preliminary test details). All frictional torque tests were completed at a testing frequency of 1 Hz. Initially, the frictional torque of articular cartilage on-bone was evaluated, to include six repeat tests per load, on each of six cartilage specimens, resulting in the completion of 360 individual experiments. Following on from this, the torque of the 2 and 10 mm calcium alginate inserts was evaluated, for which the 2 mm insert was located below the centre of the

stainless-steel indenter. For this test type, six repeat tests were performed across a separate six cartilage specimens per insert type, at each load. Based on a 1 minute load removal for friction measurements in a previous study (Forster and Fisher, 1996), cartilage specimens were left to recover for 5 minutes between each increase in load, ensuring a consistent inner fluid recovery of the specimen between tests. The load removal between tests was further incorporated with the hydrogel/cartilage-hydrogel specimens for consistent comparisons in the torque.

Table 4.1: Testing parameters utilised for the evaluation of axial load on the frictional torque study when subject to a rotational configuration. Details include the applied load as well as corresponding peak induced stresses with respect to a fixed rotation

Applied axial load (N)	10	20	30	40	50	60	70	80	90	100
Induced peak stress (MPa)	0.51	1.02	1.53	2.04	2.55	3.06	3.57	4.08	4.58	5.09
Angle of rotation (°)	0-2-0	0-2-0	0-2-0	0-2-0	0-2-0	0-2-0	0-2-0	0-2-0	0-2-0	0-2-0

4.3.1 Quantification of the Frictional Torque Magnitude

The magnitude of the frictional torque was evaluated for the final 10 cycles from each 100-cycle test for every given load, based on torque analysis from previous work (Moghadas *et al*., 2012; Moghadas *et al.*, 2013). This enabled stable and repeatable dynamic data to be recorded. MATLAB (Version R2017a, MathWorks, Cambridge, UK) software was used to fit a sinusoidal wave to the last 10 cycles of the frictional torque generated with respect to time. This resulted in a fitted smooth curve fit from the original frictional torque plot, as illustrated by the red and blue curves, respectively, in both Figure 4.11 and Figure 4.12. Note, the torque data obtained for this chapter was directly extracted from the testing machine. It was therefore not required to calculate the torque, in relation to the applied force and distance from the rotation point.

For comparison, the frictional torque magnitude was measured by two different methods. These were:

Analysis Method 1)

- With reference to Figure 4.11, the absolute maximum and minimum curve points, annotated as '*a*' and '*b*', respectively, were used to obtain two distinct torque values. The calculated absolute difference was reported as the torque magnitude for the tested load. For the analysis of the cartilage on-bone, this process was repeated for each of the six repeats per load, and for all six specimens. Similarly, for the evaluation of the 2- and 10-mm calcium alginate insert, this process was repeated for the six specimens tested per load.
- For the overall analysis for cartilage on-bone, firstly the mean torque magnitude was calculated for a given load across the six repeats for each specimen. The overall mean value of the initial mean was then calculated for all loads across each of the six specimens. Linear regression was performed between the mean of mean value and load, therefore across ten data points.
- For the overall analysis for the 2- and 10-mm calcium alginate inserts, the mean torque magnitude was calculated across the six repeats from the six specimens. Linear regression was performed between the mean value across the six specimens and load, therefore across ten data points.

Analysis Method 2)

- With reference to Figure 4.12, all maximum and minimum points from the fitted curve at the last 10 cycles was extracted for each load and specimen. Across the 10 cycles, the torque magnitude was calculated as the difference between the mean maximum and mean minimum frictional torque. This procedure was repeated for all eighteen specimens; six each of cartilage, and 2 and 10 mm calcium alginate hydrogels. The procedure was applied to all ten loads.

- For the overall analysis of each test group, the mean of the torque magnitude mean was calculated across the six specimens. Linear regression was performed on this final mean value in relation to load.

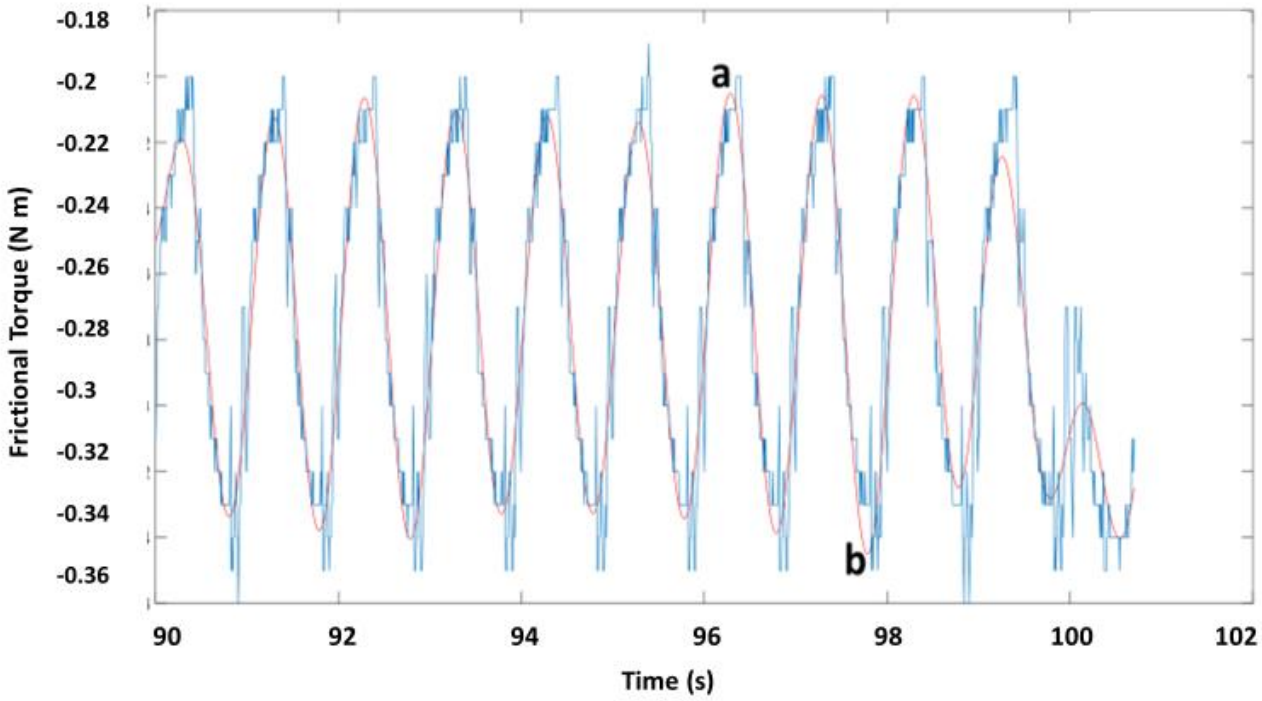

Figure 4.11: MATLAB analysis: the evaluation of torque magnitude calculated as the difference between the absolute positive maximum and minimum torque points on the resulting smooth curve fit (red curve), as points a and b, respectively. This is established from the original torque plot directly extracted from the testing machine, in response to time (blue curve). This plot represents the last 10 cycles from a representative test. This represents analysis method one.

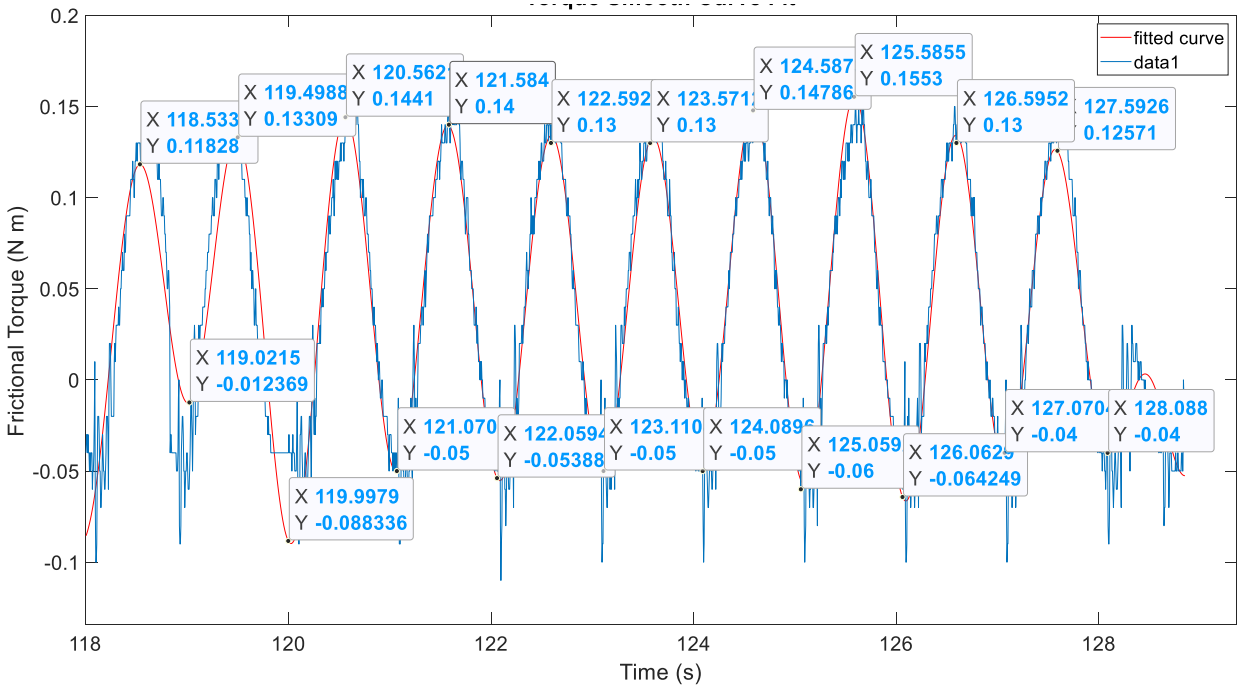

Figure 4.12: MATLAB analysis: the evaluation of torque magnitude calculated as the difference between the mean absolute positive maximum and mean absolute positive minimum torque points on the resulting smooth curve fit (red curve). This is established from the original torque plot directly extracted from the testing machine, in response to time (blue curve). This plot represents the last 10 cycles from a representative test. This represents analysis method two.

4.3.2 Data Analysis

For the obtained data of both analysis methods, linear regression was used to assess the relationship between the axial load and the resulting mean frictional torque magnitude for all specimens (Sigmaplot Version 12.0 (Systat Software Inc., London, UK)). Statistical significance was $p < 0.05$. The linear approach was selected based on the observed linear trend of the data in each case. The linear regression statistical test was performed on the final mean torque magnitude value for each scenario described for both analysis methods. Thus, all repetitions are considered. This result was in relation to each load from 10 to 100 N, therefore across ten data points.

Simple surface analysis of the specimens post-test was carried out with an InfiniteFocus, Alicona (Alicona Imaging GmbH, Raaba/Graz, Austria). The outcome is displayed in Appendix G.

4.4 Results

4.4.1 Effect of Axial Load on the Frictional Torque Magnitude

Individual torque against load plots for each of the six articular cartilage specimens are represented by parts a-f, of Figure 4.13, respectively. These plots have been produced in accordance with analysis method 1).

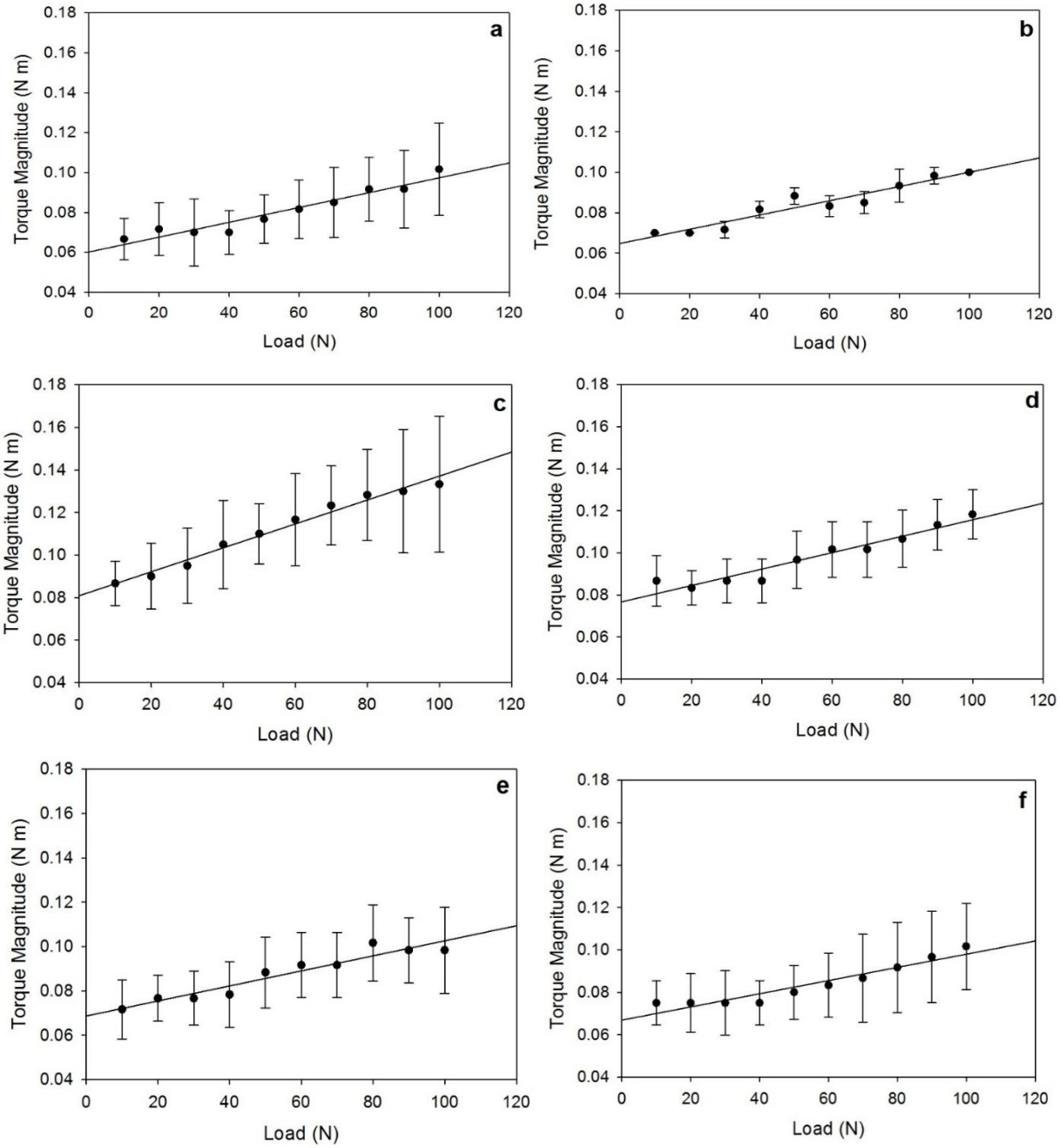

Figure 4.13: Individual articular cartilage specimen frictional torque magnitude as the mean torque calculated from six repeats at each load per specimen; a-f represents specimen 1-6, respectively. The variation with load from 10-100 N is demonstrated for each specimen. Error bars represent standard deviation. Data has been extracted according to analysis method 1)

As described in Section 4.31, using analysis method 1), the mean torque magnitude with respect to a variation in the axial load, across all six specimens is presented in Figure 4.14-a, 4.14-b 4.14-c for cartilage on-bone, and the 2 and 10 mm calcium alginate inserts, respectively. Alternatively, the result for the relationship between the mean torque magnitude and load analysed with method 2) is presented in Figure 4.15-a, 4.15-b 4.15-c for cartilage on-bone, the 2- and 10-mm calcium alginate inserts, respectively.

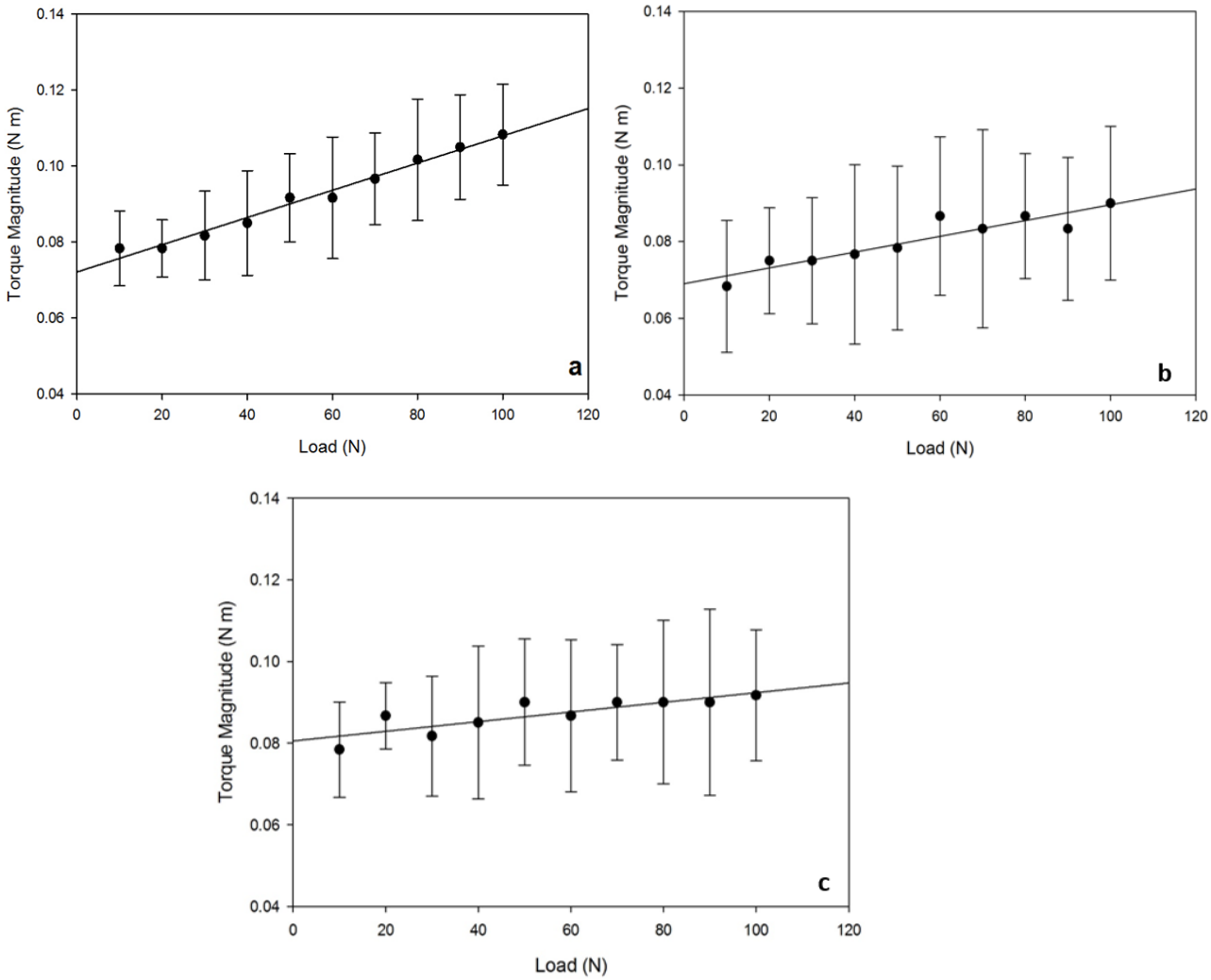

Figure 4.14: Mean frictional torque with respect to axial load: a) cartilage on-bone; mean of 36 data points calculated across six specimens (n=6). b) 2 mm calcium alginate insert; mean of 6 data points calculated across six specimens (n=6). c) 10 mm calcium alginate insert; mean of 6 data points calculated across 6 specimens (n=6). Error bars represent standard deviation. These plots are produced in accordance with data analyis method 1)

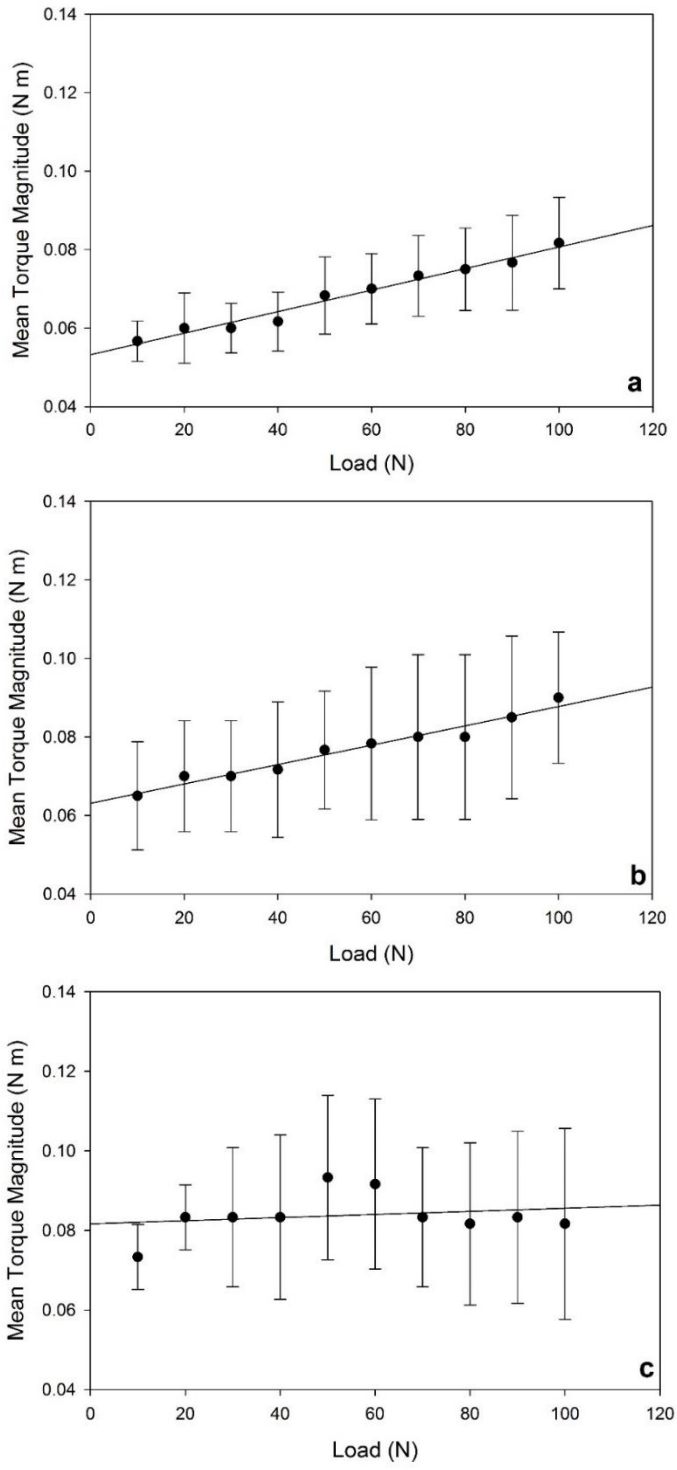

Figure 4.15: Mean frictional torque with respect to axial load: a) cartilage on-bone; mean of 6 mean data points calculated across six specimens (n=6). b) 2 mm calcium alginate insert; mean of 6 mean data points calculated across six specimens (n=6). c) 10 mm calcium alginate insert; mean of 6 mean data points calculated across 6 specimens (n=6). Error bars represent standard deviation. These plots are produced in accordance with data analyis method 2)

Based on the predominant linearity that is observed for the relationship between torque magnitude and load (Figure 4.13; 4.14; 4.15), the relationship between torque magnitude and axial load is represented by a linear regression line of best fit as described by equation 4.1:

$$T = D + AL \qquad (4.1)$$

where T is the frictional torque magnitude in N m, L is the load (in N), A and D are constants. Using analysis method 1), across all six cartilage on-bone specimens, the mean frictional torque magnitude with respect to all loads tested, ranged from 0.08 to 0.11 N m (Figure 4.14-a). The range for the 2 mm calcium alginate insert combined with cartilage was of 0.07 to 0.09 N m (Figure 4.14-b), whilst the range for the 10 mm calcium alginate insert was of 0.08 to 0.09 N m (Figure 4.14-c), at 10 and 100 N, respectively.

Alternatively, using analysis method 2), across all six cartilage on-bone specimens, the mean frictional torque magnitude with respect to all loads tested, ranged from 0.06 to 0.08 N m (Figure 4.15-a). The range for the 2 mm calcium alginate insert combined with cartilage was of 0.07 to 0.09 N m (Figure 4.15-b), as demonstrated using analysis method 1). The range for the 10 mm calcium alginate insert was also of 0.07 to 0.09 (Figure 4.15-c).

For analysis method 1, the linear regression fits of the overall mean torque magnitude and load curves indicated statistical significance for all three frictional torque tests, $p < 0.05$, that of the articular cartilage as well as both the 2 and 10 mm calcium alginate biomaterial inserts (Figure 4.14-a; 4.14-b; 4.14-c; respectively). The associated details for the individual cartilage specimen plots in accordance with equation 4.1 are presented in Table 4.2. Using analysis method 1), for each individual cartilage specimen it is apparent that statistical significance exists between frictional torque and load ($p < 0.05$) (Table 4.2). Further, the details

for the plots assessed with analysis method 1) for the articular cartilage specimen, the 2 and 10 mm calcium alginate inserts, are detailed in Table 4.3.

On the other hand, using analysis method 2), the linear regression fit of the mean torque magnitude and load curve did not indicate statistical significance for the 10 mm calcium alginate insert; $p > 0.05$. Statistical significance between frictional torque and load was identified for the cartilage and 2 mm calcium alginate insert specimens, $p < 0.05$. The statistical details are presented in Table 4.4.

Table 4.2: Corresponding statistical details extracted from linear regression fits of the variation in torque magnitude with load (Fig. 4.13), for individual articular cartilage specimens. Details are listed for each of the six specimens tested in this study. All data show statistical significance as shown by a P-value less than 0.05. High R^2 values indicate close regression line fits between torque magnitude and load. A and D are derived constants from the associating plots for each specimen.

Articular Cartilage Specimen Number	**A (10^{-4} m)**	**D (N m)**	**R^2**	***P***
1	3.45	0.0620	0.903	<0.001
2	3.64	0.0640	0.880	<0.001
3	5.03	0.0853	0.945	<0.001
4	3.70	0.0787	0.874	<0.001
5	3.27	0.0700	0.920	<0.001
6	2.42	0.0727	0.758	0.001

Table 4.3: Corresponding statistical details extracted from linear regression fits of the variation in mean torque magnitude with load (Fig. 4.14), for all specimen variations examined in this study. This assessment is provided with analysis method 1). All specimen types show statistical significance as shown by a *P*-value less than 0.05. High R^2 values indicate close regression line fits between torque magnitude and load. A and D are derived constants from the associating plots for each specimen.

Specimen	A (10^{-4} m)	D (N m)	R^2	*P*
Cartilage on-bone	3.70	0.0727	0.932	<0.001
2 mm Calcium Alginate and 3 mm Cartilage on-bone	2.06	0.0690	0.854	<0.001
10 mm Calcium Alginate	1.19	0.0804	0.708	0.002

Table 4.4: Corresponding statistical details extracted from linear regression fits of the variation in mean torque magnitude with load (Fig. 4.15), for all specimen variations examined in this study. This assessment is provided with analysis method 2). Statistical significance is identified for the cartilage on-bone and 2 mm calcium alginate insert, as shown by a *P*-value less than 0.05. For these specimens, high R^2 values indicate close regression line fits between torque magnitude and load. A and D are derived constants from the associating plots for each specimen.

Specimen	A (10^{-4} m)	D (N m)	R^2	*P*
Cartilage on-bone	2.75	0.0532	0.975	<0.001
2 mm Calcium Alginate and 3 mm Cartilage on-bone	2.46	0.0631	0.960	<0.001
10 mm Calcium Alginate	0.394	0.0817	0.0470	0.548

4.4.2 Relationship between the Frictional Torque and Rotation Angle

The frictional torque was observed to follow a similar sinusoidal trend with respect to the rotation angle of 0 to 2 to 0°, for all specimen types examined: cartilage on-bone, 2 and 10 mm calcium alginate insert. The frictional torque for each specimen type, cartilage on-bone, 2 and 10 mm calcium alginate insert in parts a-c of Figure 4.16, respectively, is displayed for the last 10-cycle period of the test, as a representative section of the entire test.

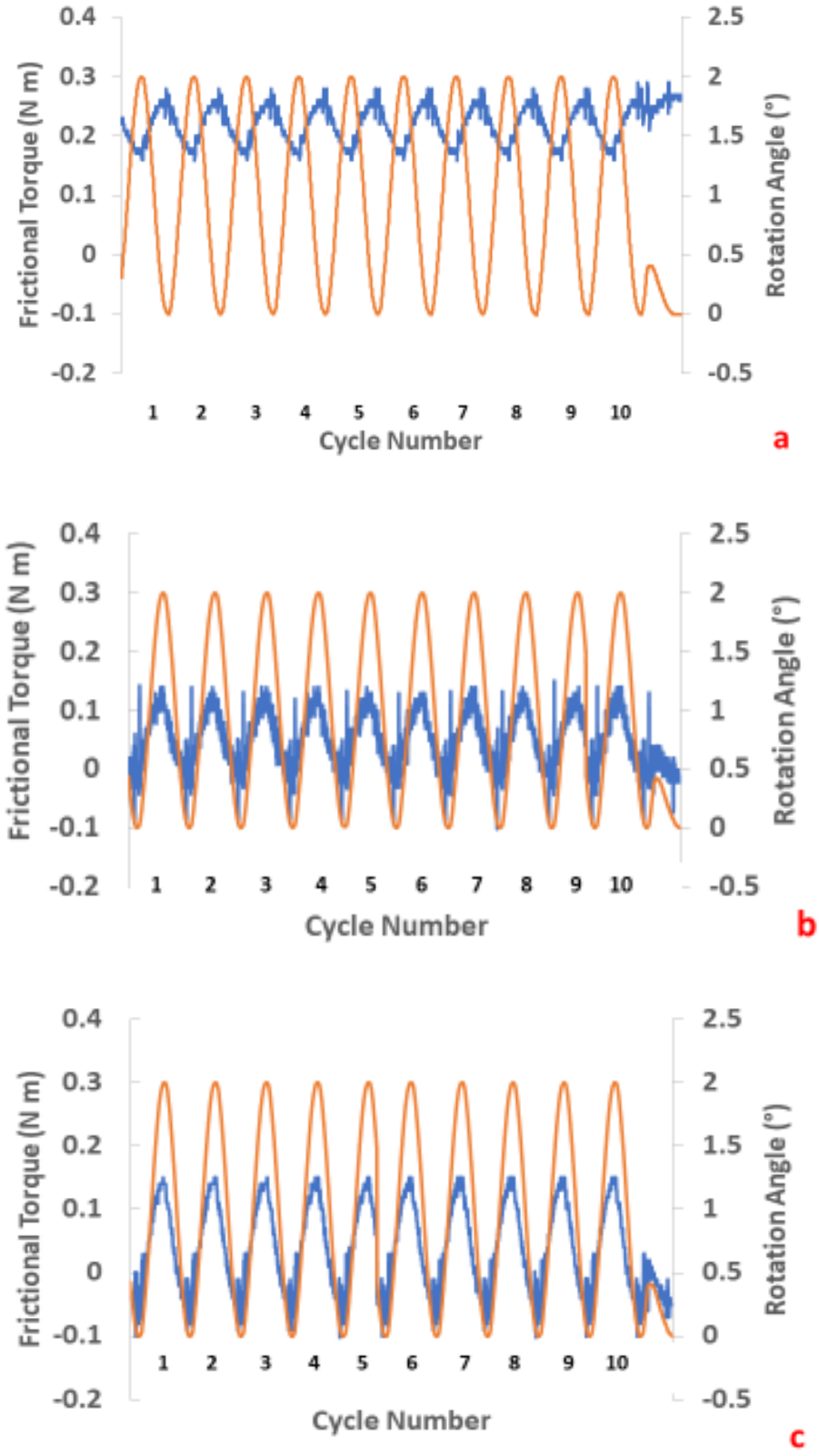

Figure 4.16: A combined plot extracted from the last 10 cycle period of the test is presented for frictional torque and rotation angle; a) cartilage on-bone, b) 2 mm calcium alginate insert and c) 10 mm calcium alginate insert. Data is extracted from testing at 100 N, as a representative result.

4.5 Discussion

The study presented in this chapter is the first to have developed a technique to evaluate the frictional torque of articular cartilage. This study has explored the effect of axial load on this relationship, to have further developed a method for the comparable assessment of potential replacement biomaterials. The results from this investigation build on existing studies by quantifying the frictional torque of articular cartilage during axial-rotation. For analysis method one, the frictional torque magnitude of articular cartilage increased with load, ranging from 0.08 to 0.11 N m across axial loads of 10 and 100 N, respectively. Analysis method two displayed a frictional torque magnitude range of 0.06 to 0.08 N m for articular cartilage. This chapter has further explored the frictional torque magnitude of calcium alginate for use as a replacement biomaterial, which was also observed to increase with load from 0.08 to 0.09 N m, and 0.07 to 0.09 N m, for analysis methods 1) and 2), respectively. Both analysis methods have shown a frictional torque magnitude of 0.07 to 0.09 N m for the combined calcium alginate and cartilage specimen. Overall, comparable ranges were identified across both analysis methods.

In the current study presented in this chapter, ten static loads from 10 to 100 N were applied to the surface of each specimen via a single stainless-steel indenter, 5 mm in diameter, inducing peak stresses ranging from 0.51 to 5.09 MPa of a physiological range (Brown and Shaw, 1983; Shepherd and Seedhom, 1997). Further, the 0 to 2 to 0° range of rotation applied to each specimen in this study, reflects the internal rotation of the hip at standing of 1° when putting on lower garments, and of the right hip at 2° when tying shoe laces and picking up objects (Hyodo *et al.,* 2017). Note, the method developed in this study establishes a controlled and repeatable approach, whilst not with the aim to replicate complete joint movement.

The linear increase in the frictional torque with load of articular cartilage, as assessed in this work, indicates the relationship which a suitable biomaterial for cartilage repair should adopt, from a tribology perspective. This outcome is further reinforced by the statistical

significance of the torque magnitude with load for all six individual cartilage specimens assessed, as well as of the mean torque magnitude of articular cartilage with respect to load ($p < 0.05$). The calcium alginate individually, as well as in combination with articular cartilage, both display a linear regression increase in the torque, with load ($p < 0.05$). Hence, with specific reference to the frictional torque behaviour itself, the calcium alginate replacement biomaterial closely matches that of the articular cartilage. In addition to this, the torque magnitude of a replacement biomaterial should be no greater than the range identified in this chapter, of 0.08 to 0.11 N m (cylindrical sample 5 mm in diameter within the test parameters used). Note, within the test parameters of 100 N and a rotation of 0 to 2°, this range would act as target values. For future studies, loading may vary beyond 2° and 100 N, and as a result of the evaluation of a wider range, this chapter provides a broader test protocol which can be used to evaluate 'baseline' data. The requirement for a low frictional torque magnitude range is similar to the necessity for engineered cartilage to adopt a low coefficient of friction (Sánchez-Téllez *et al*., 2017), as well as hydrogels to have a low surface friction for implementation as effective artificial articular cartilage (Gong *et al.,* 2001).

Several studies on the assessment of articular cartilage have shown similar trends to the outcome of the study presented in this chapter, such that an increase in the frictional properties of cartilage are observed; commonly with a variation in load, time and sliding speed. A study utilising a pin-on-plate set-up to evaluate the frictional properties of bovine articular cartilage, displayed an increase in the friction coefficient of cartilage against stainless-steel, under both uni- and multi-directional testing configurations (Northwood and Fisher, 2007).

Previous work has also reported an increase in the coefficient of friction of bovine articular cartilage against stainless-steel, with respect to time (Forster and Fisher, 1999). That study was conducted under a reciprocating motion, with an observed rise in the coefficient of friction from 0.005 to 0.50 when testing with synovial fluid, and up to 0.57 for Ringer's solution (Forster and Fisher, 1999). It is interesting to compare the estimated coefficient of friction for

cartilage against stainless-steel that can be inferred from this chapter, to existing literature. For this chapter, at a normal force of a defined indenter radius, the coefficient of friction is estimated as shown below:

1) Analysis method one:
    - Maximum estimated coefficient of friction at 100 N: 0.32 to 0.44 (0.08 N m and 0.11 N m, respectively)
    - Minimum estimated coefficient of friction at 10 N: 0.03 to 0.04 (0.08 N m and 0.11 N m, respectively)
2) Analysis method two:
    - Maximum estimated coefficient of friction at 100 N: 0.24 to 0.32 (0.06 N m and 0.08 N m, respectively)
    - Minimum estimated coefficient of friction at 10 N: 0.02 to 0.03 (0.06 N m and 0.08 N m, respectively) 0.025

Thus, the values inferred from this study are close to the range observed in previous work described above (Forster and Fisher, 1999). In addition, the estimated coefficient of friction from this chapter is also comparable to previous work that identifies a coefficient of friction range of approximately 0.01 to 0.28, of cartilage against metal, in Ringer's solution (Forster and Fisher, 1996). Similarity is also shown to previous work that demonstrates a coefficient of friction of approximately 0.22 of cartilage against stainless-steel, on completion of 20 minutes of testing (Lizhang *et al*., 2010)**,** as well as a value of 0.25 on completion of 4-hours of testing for cartilage against stainless-steel (Oungoulian *et al.*, 2015). Interestingly, the maximum estimated coefficient of friction inferred from Chapter 4 is comparable to the result obtained in Chapter 5. This is demonstrated by a coefficient of friction of 0.32 of cartilage against aluminium, in Ringer's solution (Mahmood *et al*., 2020a). See Chapter 5 for full details.

Additionally, previous work has explored the coefficient of friction of bovine articular cartilage subject to sliding against glass, at varied frequencies from 0.05 to 1 Hz (Krishnan *et al.*, 2005) for which the coefficient of friction is reported to increase with time at 1 Hz (Krishnan *et al*., 2005). Therefore, both the time in that study (Krishnan *et al*., 2005), and the load in the study presented in this chapter, have resulted in the increase in the frictional properties of articular cartilage. With reference to the previous study (Krishnan *et al.*, 2005), when the loading frequency is lowered from 1 Hz to 0.05 Hz, the friction coefficient is observed to increase (Krishnan *et al.*, 2005). Therefore, it is anticipated that the frictional torque would also follow this trend on application of a lower frequency (e.g. 0.05 Hz).

Further, previous work has explored the coefficient of friction of bovine articular cartilage tested under a pin and plate set-up, tested under both sliding and rotation at a constant load with varying lubricants (Cilingir, 2015). The results present an increase in the coefficient of friction of articular cartilage in the absence of lubrication, under rotation (Cilingir, 2015). Hence, again, both the effect of lubrication (whether present or not) in that study (Cilingir, 2015), and the load in the study presented in this chapter, have demonstrated an increase in the frictional properties of articular cartilage.

Previous studies on articular cartilage have noted an increase of the coefficient of friction of articular cartilage (Cilingir, 2015), linking their results to rotation movement and postulating that interstitial fluid leaves the surfaces in contact, with implications for the extracellular matrix and its loading (Cilingir, 2015; Lizhang *et al*., 2011). However, in this study it was observed for a linear increase in the frictional torque with normal load, which aligns directly to standard equations for calculating friction and torque (regardless of the type of material or whether fluid is present/absent). It is important, though, to highlight the link between the fluid lubrication mechanisms and the increase in frictional properties, particularly for testing under a rotational configuration. Previous work also suggests testing in multi-directional configurations can lead

to the decline in the boundary lubricants at the surfaces in contact, and, therefore, increase the resulting friction (Northwood and Fisher, 2007).

For the evaluation of the calcium alginate biomaterial, it is worth highlighting the importance of the completion of the identical torque test under axial-rotation, as assessed for the articular cartilage. This allowed for the calcium alginate biomaterial to mimic the action of the investigation of the boundary lubrication mode of articular cartilage, considering the cartilage-cartilage interface. Hence, this enables the assessment of the biomaterial as it would perform with respect to this specific lubrication mode *in vivo*, providing an accurate evaluation for its effectiveness as a replacement material for that of articular cartilage. Peak torque coincides with peak angle of rotation for both calcium alginate inserts (Figure 4.16-b; 4.16-c), mimicking the behaviour observed for the articular cartilage in this study.

It was also observed for the hydrogel specimens to react with reduced sensitivity to load, in comparison to the articular cartilage. This was shown by the decline in the derived constants from the linear regression, for both analysis methods. The decline in the constants for the hydrogel specimens may primarily be due to the differences in the depth of the gap at the hydrogel surface, amongst the surrounding cartilage specimen. This alters the positioning of the indenter at the hydrogel surface, positioning deeper with an increase in load, thus resulting in reduced sensitivity to load. Differences in specimen curvature may also contribute to the observed variations in the derived constants, as a result of the positioning of the indenter with the specimen surface.

This discussion further relates to the observed inter-specimen variations. In particular, where reduced variability is shown for the outcome at lower load applications, this can relate to the expected decreased deformation on application of a lower load. For the variations across each specimen, this can further relate to differences in specimen curvature and flatness.

In vivo, the surrounding ligaments and tendons, as well as the attachment to bone, may alter the resulting frictional torque to cartilage tested as an isolated tissue sample, as in the work presented in this chapter. However, cartilage specimens extracted from a joint allows for direct friction measurements (or indeed frictional torque), with enhanced control of the tribological protocol (Forster and Fisher, 1996), thus, supporting the procedure developed in this chapter. Further, although the metal testing configuration utilised in this work is not a physiological representation, previously an increase in the start-up coefficient of friction for both cartilage-cartilage and cartilage-metal with stationary loading time was identified (Forster and Fisher, 1996), suggesting that no difference in the relationship between coefficient of friction and loading time were observed between the use of metal and cartilage (Forster and Fisher, 1996). Hence, this has been taken into consideration for the evaluation of the frictional torque in this chapter.

A further potential limitation may be the existence in error of misalignment of the cartilage surface, as a result of the extent of the surface flatness. However, misalignment error has been controlled in this chapter by the extraction of cartilage specimens from the central, and therefore flattest region of the humeral head. Although an error in misalignment may still have occurred, for which an exact figure would be difficult to estimate, a previous study demonstrates the feasibility in obtaining sheets of cartilage (40 × 20 mm), from which curvature was not observed visually (Sadeghi *et al.,* 2018).

The use of bovine articular cartilage in replace of human cartilage may be a further potential limitation. Yet, to confirm the differences in the behaviour of the frictional torque magnitude between bovine and human cartilage, future testing would be required. For instance, the consistency in the frequency-dependency of the viscoelastic properties of human and bovine cartilage has been demonstrated (Temple *et al.*, 2016), forming the basis for selection of bovine cartilage as the model for human in this study. Consequently, the technique presented in this study acts as a baseline for the development with human cartilage in future

work. A further limitation may be the use of Ringer's solution instead of synovial fluid, restricting the physiological representation *in vivo*. However, previous work has identified the absence in the statistical significance in the coefficient of friction between use of synovial fluid and Ringer's solution, whilst a reduction in the coefficient of friction of cartilage against metal is observed with use of synovial fluid, at short testing times only (Forster and Fisher, 1996). It has also been demonstrated that a significantly lower coefficient of friction exists for cartilage contact against cartilage, with use of synovial fluid (Forster and Fisher, 1996). Consequently, as previously mentioned, the technique developed in this chapter acts as the baseline to which further physiological conditions can be introduced. This could include the use of human cartilage contact with cartilage, with use of synovial fluid as the lubricant.

It is also worth noting that within the test parameters outlined in this chapter at a load of 100 N and a rotation of 0 to 2°, this range would act as target values. For future work, loading may vary beyond 2° and 100 N, and as a result of the evaluation of a wider range, this chapter provides a broader test protocol which can be used to evaluate 'baseline' data". Furthermore, the low acquisition rate applied for data collection in this chapter, acts as a baseline which can be enhanced for future development.

A further potential limitation is the absence of a protocol to evaluate both the surface roughness and flatness of each specimen. Currently, the specimen is visually observed to confirm the specimen is flat and suitable for testing. However, in order to introduce a more accurate method, future work could involve confocal microscopy as well as surface roughness and surface 3D angle measurements.

The use of an indentation procedure is controlled and reproducible and has previously been utilised for the evaluation of the mechanical behaviour of articular cartilage (Lu *et al*., 2004). Note, although the homogeneity in stress cannot be confirmed below the indenter as it is expected for a different spatial stress distribution to exist amongst the specimens, the forces

have been applied equally to each specimen. This ensures a comparable assessment of the torque. Thus, despite a limitation, the conclusions presented in this chapter are not affected.

Although the measurement of frictional torque is not a material property, but rather limited to the specimen size, it is important to note that the work presented in this chapter has developed a technique for an accurately consistent comparison of the torque, between that of articular cartilage, and a given potential replacement biomaterial. The new method developed in this chapter is advantageous in comparison to the pin-on-disc set-up, due to the direct extraction of the unknown frictional torque of articular cartilage, with respect to a rotation.

4.6 Chapter Summary

The conclusions determined from this chapter are detailed below:

1) The technique developed in this study can be implemented in future studies for the evaluation of potential cartilage replacement biomaterials, specifically from a frictional torque perspective.
2) Using analysis method 1), the frictional torque magnitude of bovine articular cartilage is 0.08 to 0.11 N m, at 10 to 100 N, respectively. With analysis method 2), the frictional torque magnitude of bovine articular cartilage is 0.06 to 0.08 N m, at 10 to 100 N, respectively. A statistical difference exists between torque magnitude and load ($p < 0.05$), for articular cartilage. The work in this chapter presents the torque range for potential replacement biomaterials for articular cartilage. Statistical significance is displayed between torque magnitude and load for the 10 mm calcium alginate insert using analysis method 1) ($p < 0.05$), yet not for the relationship observed with analysis method 2) ($p > 0.05$). Similar to the outcome for articular cartilage, for both analysis methods a statistical difference exists between the torque magnitude and load for the 2 mm calcium alginate insert ($p < 0.05$). Overall, with respect to the frictional torque,

the calcium alginate biomaterial is observed to closely coincide with the results obtained for articular cartilage.

3) The frictional torque magnitude for the 2 mm calcium alginate biomaterial is also observed to increase with load for both analysis methods. From testing at 10 through to 100 N, the mean frictional torque observed is of 0.07 to 0.09 N m for both analysis methods. The frictional torque magnitude for the 10 mm calcium alginate biomaterial is of 0.08 to 0.09 N m and 0.07 to 0.09 N m for analysis methods 1) and 2), respectively.

5. A METHOD FOR THE ASSESSMENT OF THE COEFFICIENT OF FRICTION OF ARTICULAR CARTILAGE AND A REPLACEMENT BIOMATERIAL

5.1 Introduction

As outlined in Chapter 4, there are promising results for the use of hydrogels for the replacement of natural tissue (Li *et al*., 2016), including articular cartilage. As discussed, calcium alginate has potential uses in cartilage repair (Liao *et al.,* 2017). The coefficient of friction of calcium alginate has not been previously addressed in the literature, whilst it is crucial to assess its tribological performance for use as a cartilage replacement biomaterial (Cilingir, 2015).

Current techniques evaluate the coefficient of friction of a replacement biomaterial against articular cartilage (Li *et al.,* 2016), or against replacement counterparts, e.g. cobalt chromium molybdenum (Milner *et al.*, 2018) or alumina (Yarimitsu *et al.,* 2016). However, such measurements do not assess the interaction of the replacement biomaterial with cartilage when it is used to repair a defect in the articulating surface. As previously stated, such analysis of the frictional behaviour of the potential replacement biomaterial would more closely mimic the scenario of a surgical procedure. In particular, that of osteochondral grafting, for the transplantation of osteochondral plugs from a non-weight-bearing region to the defect site (Hattori *et al*., 2007).

The aim of the work presented in this chapter was to develop a technique for the evaluation of the coefficient of friction of articular cartilage, against an articular cartilage defect repaired with a biomaterial. As implemented in the technique presented in Chapter 4, this chapter also illustrates the use of calcium alginate as the sample biomaterial. For this chapter, three test groups were assessed in a reciprocating sliding configuration with a pin-on-plate set-up. A cartilage pin against a cartilage plate test group was the standard to compare the result of the biomaterial. The second friction test group consisted of a cartilage pin sliding against a cartilage plate induced with the biomaterial. The third friction test group was that between a

cartilage pin and aluminium plate, for which the aluminium acted as a base metal for testing future implant metals. Thus, the selection of aluminium for this chapter does not represent the material choice for an implant due to its toxicity. Rather, aluminium was selected as a base metal, solely due to the ease of manufacture and the non-susceptibility to corrosion.

5.2 Materials and Methods

5.2.1 Articular Cartilage Specimen Preparation

See Section 3.2.1 for details on obtaining the eighteen bovine humeral heads required for this chapter, up to the final stage of the application of India ink to select defect-free areas for testing. Note, the humeral heads used for this chapter were different to those used for Chapter 3 and 4.

5.3 Experimental Methods

For this chapter, eighteen friction tests were performed, including six of each of the following: i) cartilage against cartilage, ii) cartilage/hydrogel against cartilage and iii) cartilage against aluminium. Tests were performed using a TE/77 pin on disc tribometer (Phoenix Tribology, Hants, UK), in connection to Compend (Phoenix Tribology, Hants, UK), the data collection software (Figure 5.1). The positioning of the tribometer motor and sensor in accordance with the specimen set-up is displayed in Figure 5.2-a. The test set-up comprised an upper specimen holder into which a cartilage-on-bone core was located and a lower specimen holder into which the plate was located (Figure 5.2-b). For testing groups i) and ii), the lower specimen was either a cartilage-on-bone sheet alone, or with the biomaterial placed within a central surface perforation (mimicking a defect). Test group iii) consisted of an aluminium sheet as the lower specimen. Prior to the test start in sliding, caution was exercised to ensure the upper specimen was positioned at the centre of the lower specimen.

For each testing group, six different lower and upper specimens were prepared, each extracted from six different humeral heads. Figure 5.3 illustrates the location of specimen extraction amongst the eighteen bovine humeral heads. For both the upper specimen cartilage cores and lower specimen cartilage sheets, the extraction occurred from the central and therefore flattest region of the humeral head. Thus, flat specimens were used for testing only, and so the criteria of central extraction was used to ensure the curvature of the specimens was controlled.

All tests were conducted for 20 minutes, at a frequency of 1 Hz to represent the loading frequency during normal gait (Fulcher *et al.*, 2009; Sadeghi *et al.,* 2015). A normal force of 5 N was applied, corresponding to an induced stress of 0.06 MPa. The force for testing was determined following preliminary tests of compression to the calcium alginate hydrogel (see Appendix F for the outcome, to include preliminary friction tests). The friction tests were completed at 37°C to represent physiological conditions. Prior to the start of testing, the sample was loaded until 5 N with ramp loading of 1 N/s, whilst the temperature simultaneously equilibrated to reach the desired level.

The cartilage specimens were kept hydrated throughout testing using Ringer's solution as the lubricant (Forster and Fisher, 1996). Ringer's solution was held within an automated syringe (KD Scientific Inc., Holliston, USA) (Figure 5.1) and released into the lubricant bath, via tubing at a rate of 0.1 ml per minute throughout the entire 20-minute test. The lubricant bath comprises a rectangular segment attached to the machine, to which the aluminium jig of the test set-up (Figure 5.2-b) to encompass the lower articular cartilage specimen, is bolted against. In addition to this, 5 ml of Ringer's solution was inserted onto the surface of the articular cartilage specimen prior to testing.

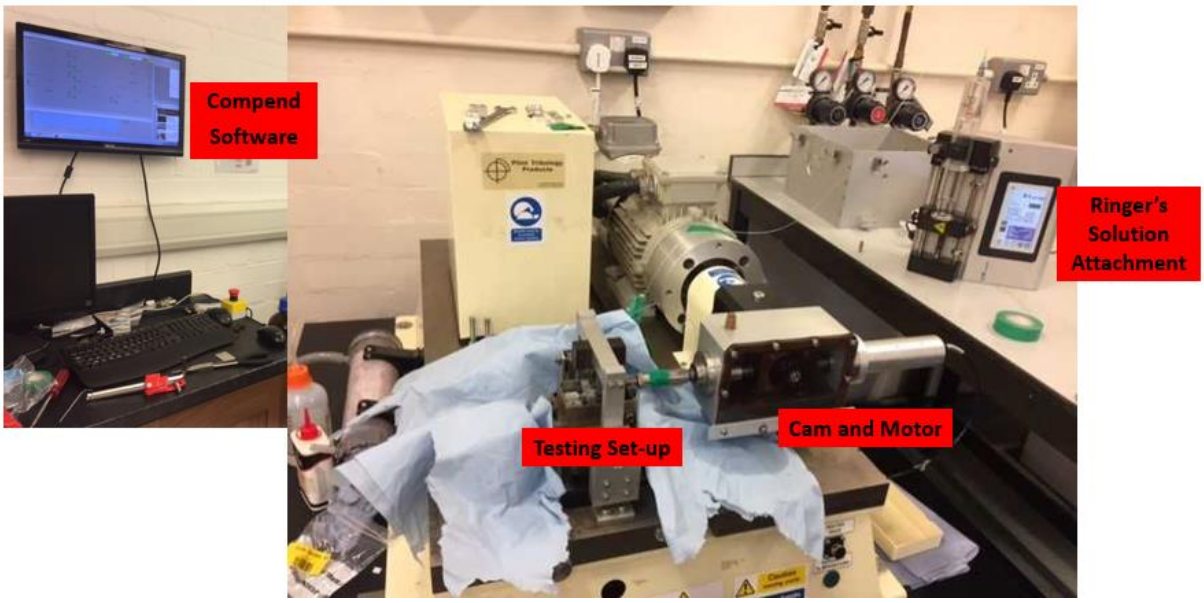

Figure 5.1: Schematic to represent the overall set-up of testing performed on the TE/77 Tribometer. The region of the test set-up is displayed, the cam and motor component as well as the syringe connection for the release of Ringer's solution lubricant, for maintenance of the hydration of cartilage specimens during testing. The Compend software in connection to the TE/77 Tribometer is also displayed. The tissue paper is placed for the prevention of contamination from potential dispersion of Ringer's solution lubricant during testing.

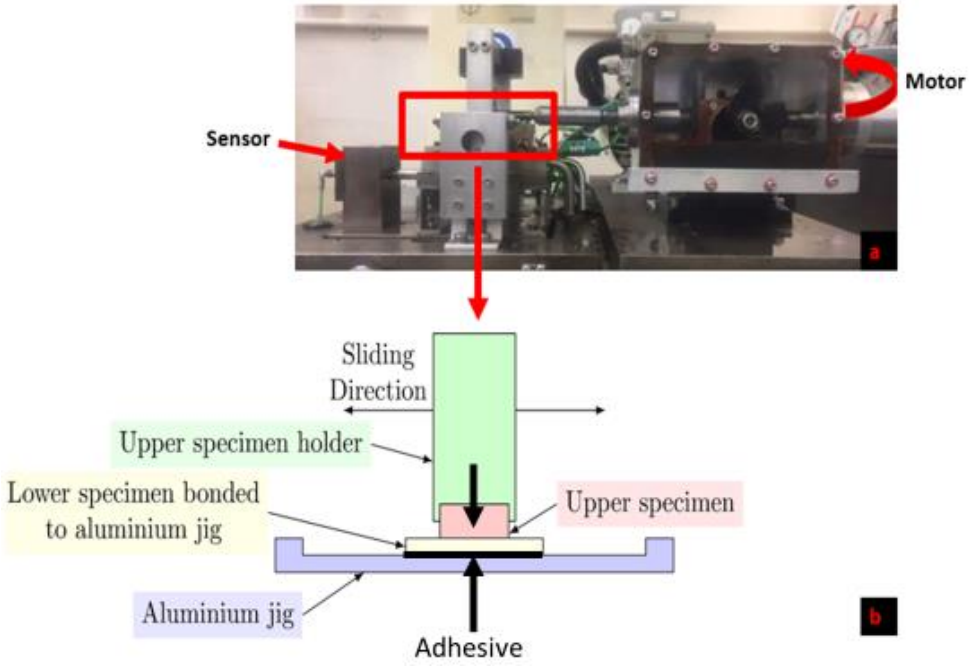

Figure 5.2: Experimental set-up of the TE/77 tribometer: a) photographic representation of the motor and sensor in position to the upper and lower specimens, as shown in the zoomed in segment of part b). The prominent components of the set-up illustrated in segment b), include the upper specimen holder placed over the upper specimen as indicated by the black arrow. The lower specimen is bonded to the aluminium jig with adhesive.

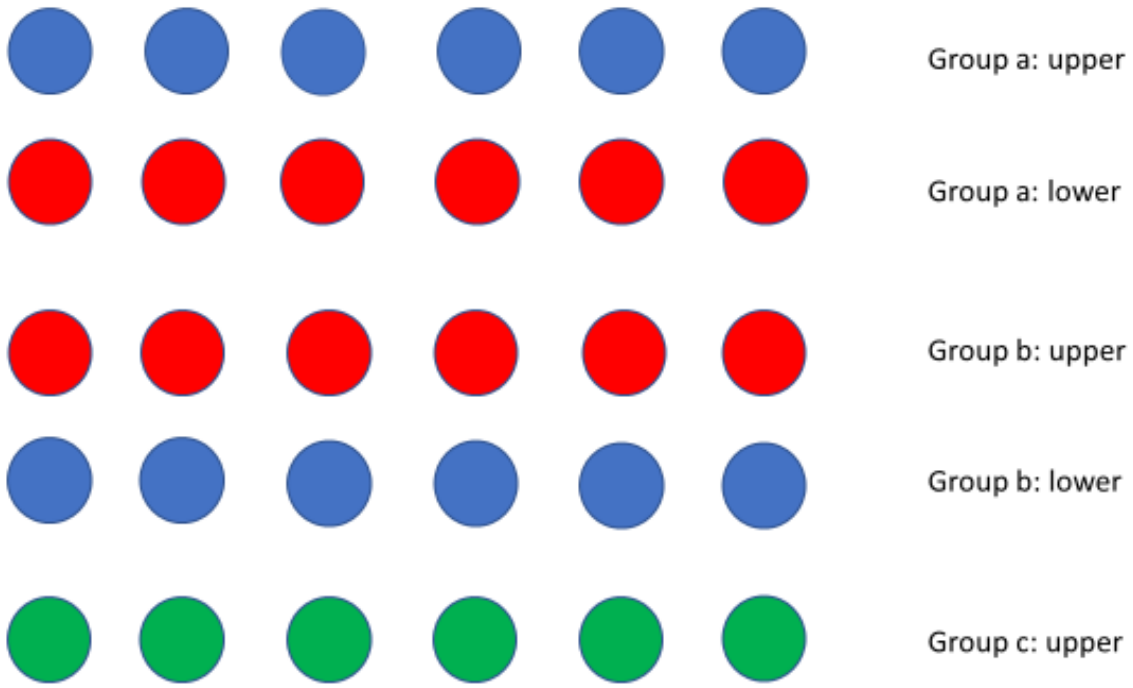

Figure 5.3: Schematic to illustrate the location of specimen extraction across eighteen bovine humeral heads for each testing group. Blue, red and green circles indicate the different sets of six humeral heads. Group a) cartilage-cartilage test, group b) cartilage/hydrogel-cartilage test and group c) cartilage-aluminium test. The upper and lower refer to the upper specimen cartilage core and lower specimen cartilage sheet for each set-up.

Based on the mechanics of the tribometer, the sliding motion was determined by an eccentric cam fitted onto an eccentric splined shaft (Figure 5.1). Rotation of the cam to a defined angle corresponds to an approximate stroke. Following preliminary tests, it was determined for this study to set the cam to 36°, which corresponds to an approximate sliding length of 3.832 mm, and a maximum velocity of 12.039 mm/s. As illustrated in Figure 5.4, for one overall sliding reciprocation, the sliding length of 3.8 mm was the total movement of the upper specimen from the centre to right of the lower specimen, and then from the centre to the left of the lower specimen.

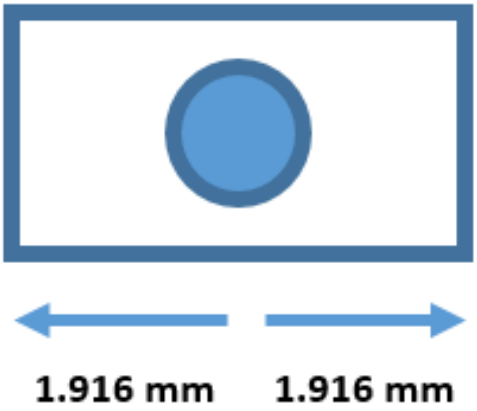

Figure 5.4: Reciprocating sliding movement: the direction of the upper specimen (circle) across the lower specimen (rectangle) of 1.916 mm from centre to right, and 1.916 mm from centre to left. The total sliding length for one full reciprocating sliding cycle is 3.8 mm.

A summary of the testing parameters are detailed in Table 5.1. High speed data was captured for all friction tests at 0.2 s every 10 s, at a sample rate of 20 kHz. This data represents the absolute value of the signal at the point of signal capture, extracted as a vector. The positive component of the vector corresponds to the direction closest to the motor, whilst the negative element is that closer to the sensor (Figure 5.2-a). Figure 5.5 outlines a simple sketch to illustrate the location on the high-speed data curve relative to the position of the upper specimen.

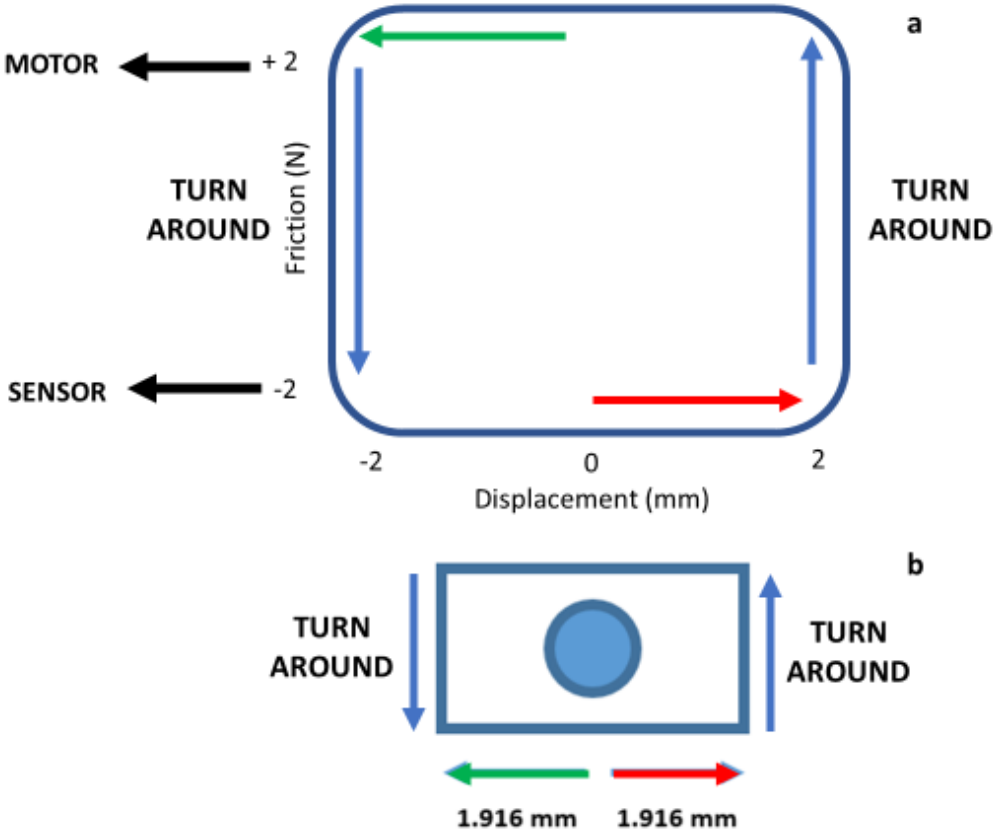

Figure 5.5: Schematic to display the position on the resulting high-speed data plot in part a), in accordance to the sliding direction of the upper specimen shown in part b). From the centre at 0 mm displacement, the upper specimen moves to the right and this is shown by the red arrow from 0 to 2 mm displacement. The turn-around point of the upper specimen is shown by the blue arrow. The return stroke of the upper specimen is identified by the green arrow, from 0 to -2 mm displacement. This represents the movement of the upper specimen from the centre to the left hand-side. A negative friction indicates a positioning of the specimen closer to the sensor, whilst a positive friction indicates a positioning closer to the motor.

The extraction of high-speed data enabled the quantification of the frictional energy as well as lubrication mechanisms to be assessed. Low speed data was extracted at a sample frequency of 10 Hz, extracted for the analysis of the median and maximum values of the entire 20-minute data set. Section 5.6 Data Analysis further outlines the information obtained from high and low speed data.

Table 5.1: A summary of the testing parameters used for all three friction tests in this study

Testing Parameters	
Load (N)	5
Frequency (Hz)	1
Sliding length (mm)	3.8
Maximum sliding velocity (mm/s)	12.039
Temperature (°)	37
Time (mins)	20
Lubricant	Full strength Ringer's Solution

5.4 Lower specimen preparation

5.4.1 Cartilage against cartilage and cartilage/hydrogel against cartilage friction test

For the lower specimen preparation of both i) cartilage against cartilage (C-C) and ii) cartilage/hydrogel against cartilage (C-G) tests, the mid-segment of the humeral head was dissected with a 300 mm bi-metal hacksaw blade (RS Components Ltd, Corby, UK) (Figure 5.6). This region was selected for the representation of the central contact area at the shoulder joint (Canal *et al*., 2009). Of the lower specimen preparation for the cartilage against cartilage test, six articular cartilage-on-bone specimens were trimmed using a 300 mm bi-metal hacksaw blade extracted across six bovine humeral heads. A further six cartilage-on-bone specimens were dissected from six separate humeral heads, for the cartilage with hydrogel insert against cartilage test. The specimens were of an approximate cross-section of 22.5 × 20 mm and a thickness of 2 mm. For insertion of the calcium alginate hydrogel, a 4 mm diameter end mill (RS Components Ltd, Corby, UK), was attached to a pillar drill and used to create a cavity within the centre of the articular cartilage specimen (Figure 5.7-a). Appendix F details the various hydrogel synthesis methods for which initiated the development of the technique presented in this chapter.

Soudal Superglue High Viscosity (Soudal, Tamworth, UK), a cyanoacrylate adhesive, was used to fix the lower specimens for both test groups: i) cartilage against cartilage and ii) cartilage/hydrogel against cartilage, to an aluminium test rig for testing. For maximum bonding strength the glue was left to bind to the subchondral bone at 6° within a refrigerator, for a minimum of 24-hours curing time prior to testing. Following curing, the specimen was fixated to the aluminium rig, demonstrated by the inability to move. Consequently, the presence of fluid, such as the Ringer's solution amongst the test set-up, did not influence the cured adhesive. Preceding testing, all specimens were immersed in Ringer's solution for 30 minutes (Barker and Seedhom, 2001).

The calcium alginate hydrogel used for this chapter was prepared with the method presented in Section 4.2.2. A 5 mm hand cork-borer was used to create the hydrogel inserts for the articular cartilage. The hydrogel was then inserted within the cavity created at the surface of the articular cartilage specimen (Figure 5.7-b) for testing.

Figure 5.6: Articular cartilage specimen dissection procedure: method to obtain the central region of the humeral head for extraction of lower cartilage specimen sheets, for testing

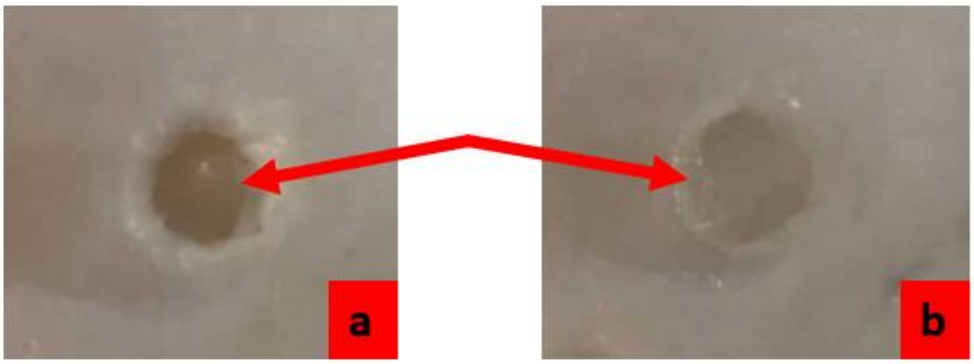

Figure 5.7: Insertion of biomaterial within the articular cartilage: a) 4 mm was created within the surface of articular cartilage specimen. b) calcium alginate insertion into the created hole

5.4.2 Cartilage against aluminium friction test

For the third friction test group, iii) cartilage against aluminium (C-M), the lower specimen was selected as a smooth sheet of aluminium, with an average surface roughness of 0.65 µm, with reference to literature (Yang *et al*., 2017). The aluminium sheets were prepared with a cross-section of 60 × 41 mm and a thickness of 2 mm. Six different aluminium sheets were prepared for each test.

5.5 Upper specimen preparation

For preparation of the upper specimen for each of the three friction test groups, six different articular cartilage-on-bone cores were extracted. The extraction procedure was carried out by drilling six humeral heads (Figure 5.5), with a pillar drill attached to a 12 mm outer diameter diamond coated drill head (10 mm inner diameter) (Fell *et al.*, 2019). The eighteen cartilage-on-bone cores were prepared to an approximate diameter of 10 mm and thickness of 4 mm. Representative drilled upper specimens prepared in this manner are illustrated in Figure 5.8. The specimens were immersed in Ringer's solution for 30 minutes prior to testing (Barker and Seedhom, 2001). For testing, the upper cartilage core was held within a custom-made upper specimen rig, as illustrated in Figure 5.9.

Figure 5.8: Illustration of prepared upper cartilage-on-bone specimens drilled and cut to precise dimensions for testing

Figure 5.9: Upper specimen holder: a) the upper articular cartilage specimen core held by the upper specimen holder illustrated in part b

An image of the set-up of each friction test; i) cartilage-cartilage, ii) cartilage/hydrogel-cartilage and iii) cartilage-aluminium, to include the lower and upper specimen is displayed in Figure 5.10-a; b and c, respectively. The subchondral bone faces upwards for the upper cartilage specimen, whilst the cartilage interface is in direct contact with the lower specimen in each case (Figure 5.10-a; b; c). Further, this image set-up provides a photographic representation of the upper and lower specimens only, and it is not the exact positioning prior to the start of testing.

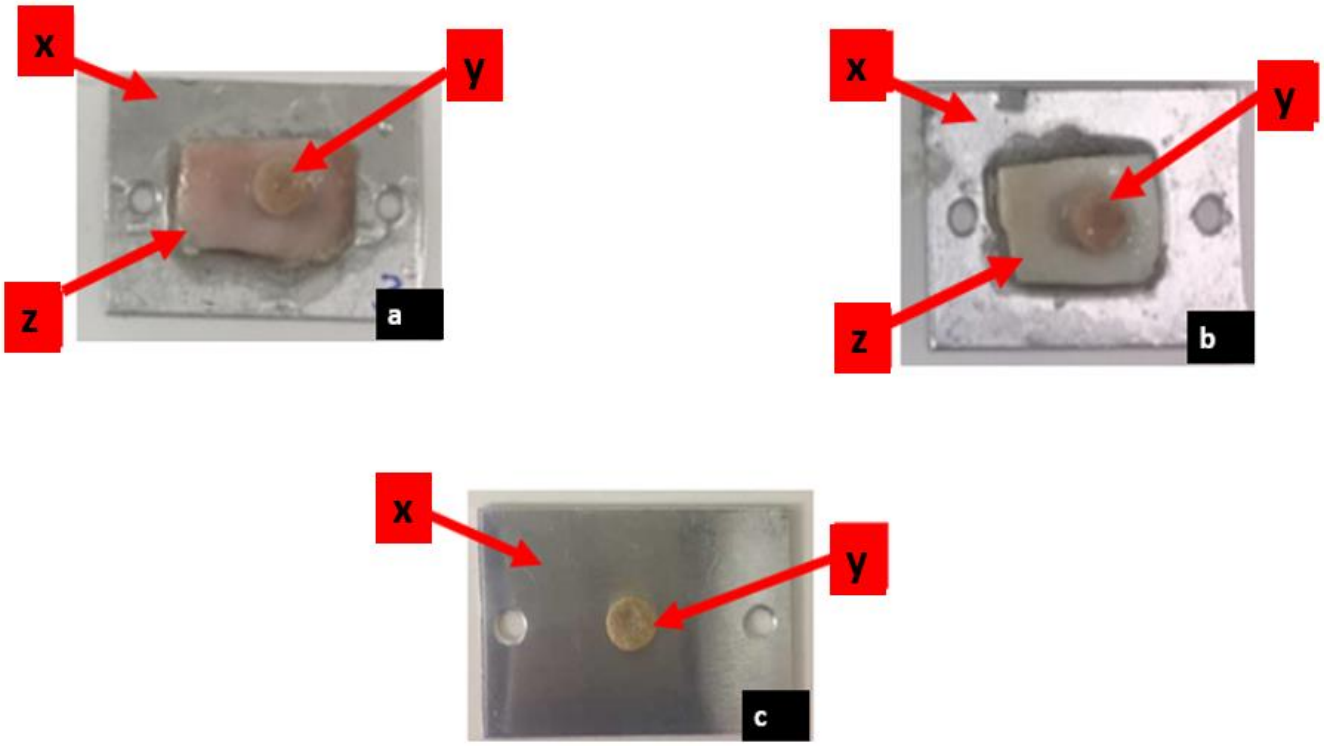

Figure 5.10: Upper and lower specimen illustration for the three friction tests assessed in this study: a) cartilage against cartilage friction test. b) cartilage with hydrogel insertion against cartilage friction test. c) cartilage against aluminium friction test. For each set-up, x: aluminium test-rig, which forms the lower specimen for test c, y: upper articular cartilage specimen and z: lower articular cartilage specimen. The red arrows indicate the component in each case. The images do not represent the exact positioning of the upper specimen on the lower specimen prior to the start of testing.

5.6 Data Analysis

Three measurements of the coefficient of friction for each test type, for every repeat of six, were extracted: i) the median coefficient of friction of the entire 20-minute data set, ii) the median coefficient of friction obtained from the last five minutes of the test and iii) the maximum coefficient of friction of the entire 20-minute test. The median data was selected based on the most stable friction position, taking into account the observed variations in both the start-up and steady-state friction. A similar analysis method has been established in recent work, for the use of the median for comparisons of frictional data across the meniscus, tibial and femoral articular cartilage, as well as a scaffold (Warnecke *et al.,* 2019). A box plot was produced for

the assessment in each case. The error bars to represent a 95% confidence interval were analysed for which the absence of error bar overlap was associated with statistically significant data ($p < 0.05$) (Alnaimat *et al.,* 2016). To further confirm the statistical outcome, a spearman rank correlation test was performed between all three test groups. Statistical significance was identified by $p < 0.05$.

A useful descriptor in analysis of friction and wear is the frictional energy encompassed within one stroke. Physically, this energy dissipation is represented by the area encompassed by the curve of the coefficient of friction with respect to the displacement of the upper specimen. The definition is shown in equation 5.1, where *E* denotes frictional energy and *F(s)* is the force as a function of the displacement (*s*).

$$E = \oint_0^S F(s)ds \qquad (5.1)$$

5.7 Results

5.7.1 Coefficient of friction

The results for the median coefficient of friction extracted from the entire dataset for six repeats (Figure 5.11) are as follows:

- Cartilage against cartilage (C-C): 0.36 ($p > 0.05$)
- Cartilage/hydrogel against cartilage (C-G): 0.38 ($p > 0.05$)
- Cartilage against aluminium (C-M): 0.32 ($p > 0.05$)

For all assessments of the coefficient of friction (Figure 5.11; 5.12; 5.13), the largest interquartile range (IQR) was displayed for the C-C test, followed by the C-G test, whilst the smallest IQR was observed for the C-M test (Figure 5.11; 5.12; 5.13). This is an expected

outcome due to the advanced flatness of the aluminium sheet lower specimen, in comparison to the articular cartilage biological material.

The results for the overall median coefficient of friction extracted from the final five minutes of testing across all repeats (Figure 5.12), are as follows:

- Cartilage against cartilage (C-C): 0.35 ($p > 0.05$)
- Cartilage/hydrogel against cartilage (C-G): 0.36 ($p > 0.05$)
- Cartilage against aluminium (C-M): 0.28 ($p > 0.05$)

The results for the maximum coefficient of friction (Figure 5.13) are as follows:

- Cartilage against cartilage (C-C): 0.43 ($p > 0.05$)
- Cartilage/hydrogel against cartilage (C-G): 0.48 ($p > 0.05$)
- Cartilage against aluminium (C-M): 0.41 ($p > 0.05$)

It is clear from the data that for all analysis scenarios a statistical difference failed to exist ($p > 0.05$). However, trends are noticed between each group. The observed statistical insignificance is further conformed by the spearman rank correlation test between the three combinations of testing groups ($p > 0.05$), for all performed assessments of the coefficient of friction (Table 5.2).

Table 5.2: The obtained *p*-value following on from assessment with the spearman rank correlation test for all test groups; C-C: cartilage against cartilage friction test, C-G: cartilage with hydrogel insertion against cartilage friction test, C-M: cartilage against aluminium friction test, in accordance with the three various analysis methods for the coefficient of friction. Statistical insignificance is displayed for all combinations; $p > 0.05$

Median from entire dataset		**Median from final five minutes**		**Maximum coefficient of friction from entire dataset**	
Test group combination	**Spearman rank test *p*-value**	**Test group**	**Spearman rank test *p*-value**	**Test group**	**Spearman rank test *p*-value**
C-C with C-M	0.242	**C-C with C-M**	0.103	**C-C with C-M**	0.242
C-C with C-G	0.803	**C-C with C-G**	0.419	**C-C with C-G**	0.497
C-G with C-M	0.242	**C-G with C-M**	0.103	**C-G with C-M**	0.242

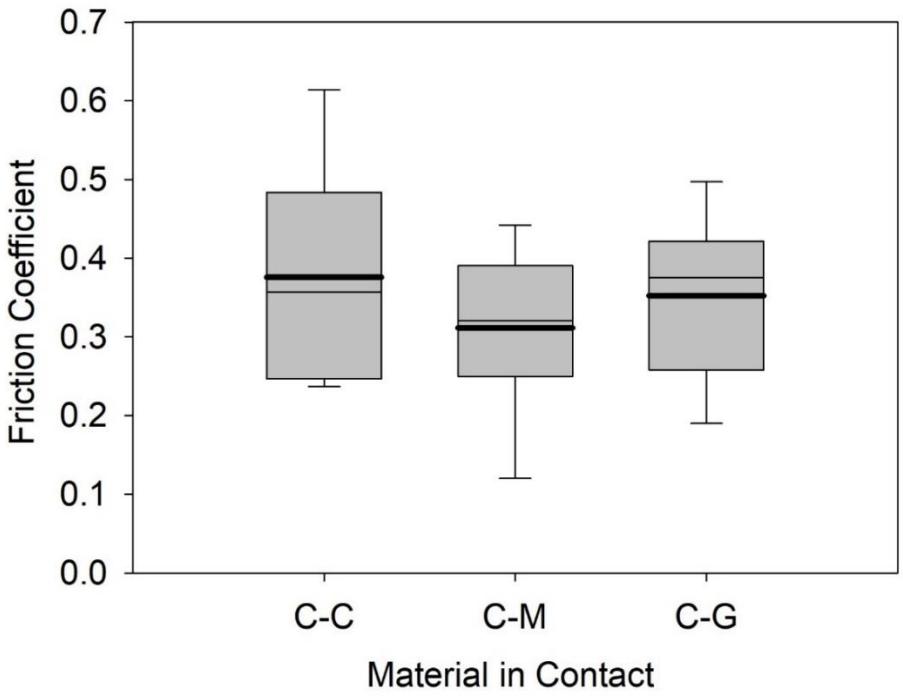

Figure 5.11: Coefficient of friction of the median from all 20-minute data set extracted for each testing scenario, across all six repeats: C-C: cartilage against cartilage test, C-M: cartilage against aluminium test and C-G: cartilage with gel biomaterial insertion against cartilage test. The dark black line represents the mean in each case, for which the median is presented as the light black line.

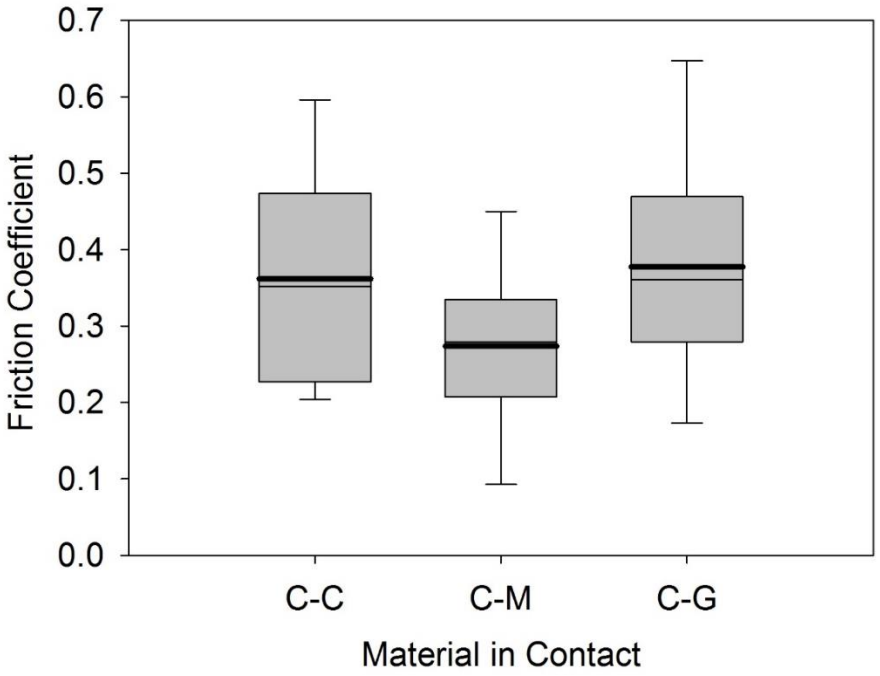

Figure 5.12: Coefficient of friction of the median from the final five-minutes of all the data set extracted for each testing scenario, across all six repeats: cartilage against cartilage test, C-M: cartilage against aluminium test and C-G: cartilage with gel biomaterial insertion against cartilage test. The dark black line represents the mean in each case, for which the median is presented as the light black line.

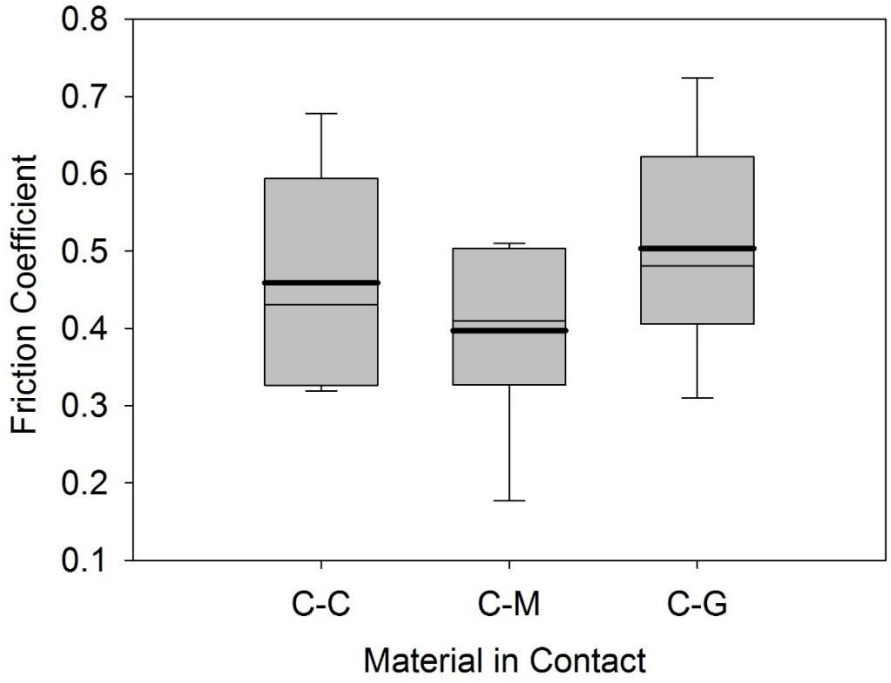

Figure 5.13: Maximum coefficient of friction extracted from the entire dataset for each testing scenario, across all six repeats: cartilage against cartilage test, C-M: cartilage against aluminium test and C-G: cartilage with gel biomaterial insertion against cartilage test. The dark black line represents the mean whilst the median is presented as the light black line.

5.7.2 Coefficient of friction with respect to sliding velocity

In this section, the friction force plotted against displacement for each testing scenario is presented. The plots represent the overlap of five successive reciprocations for the final five cycles of one test, for a single specimen. As illustrated in Figure 5.5 for each plot, the movement in the positive direction towards 2 mm represents the movement of the upper specimen across the lower specimen in the right direction, from the central starting position at 0 mm. The turn-around points in each case are identified by the vertical lines. The return stroke is identified by the movement towards the left direction at -2 mm. Figure 5.14, 5.15 and 5.16 display the individual plots for cartilage against cartilage (C-C), cartilage against aluminium (C-M) as well as cartilage/hydrogel against cartilage (C-G) testing scenarios, respectively.

Most friction vs displacement plots for the cartilage against cartilage test (Figure 5.14), have a square-like shape. In general, the two sides of the plot demonstrating the change in sliding direction, are both slanted. Particularly for specimen c, d e and f, there appears to be a small increase in friction as the velocity reaches its maximum, identified on the return stroke at the bottom edge of the loop (Figure 5.14-c; d; e; f).

Six friction vs displacement plots, representing the individual tests for the cartilage against aluminium tests (C-M), are provided in Figure 5.15(a-f). As the velocity tends toward zero, it appears a constant coefficient of friction is displayed for the predominantly square-like appearance of the friction vs displacement plots for the C-M tests. In addition, the plots demonstrate a sharp increase in friction as the sample moves from quasi-static to dynamic friction (Figure 5.15; a-f).

Six friction vs displacement plots, representing the individual tests for the cartilage with biomaterial insertion, against articular cartilage tests (C-G), are provided in Figure 5.16(a-f).

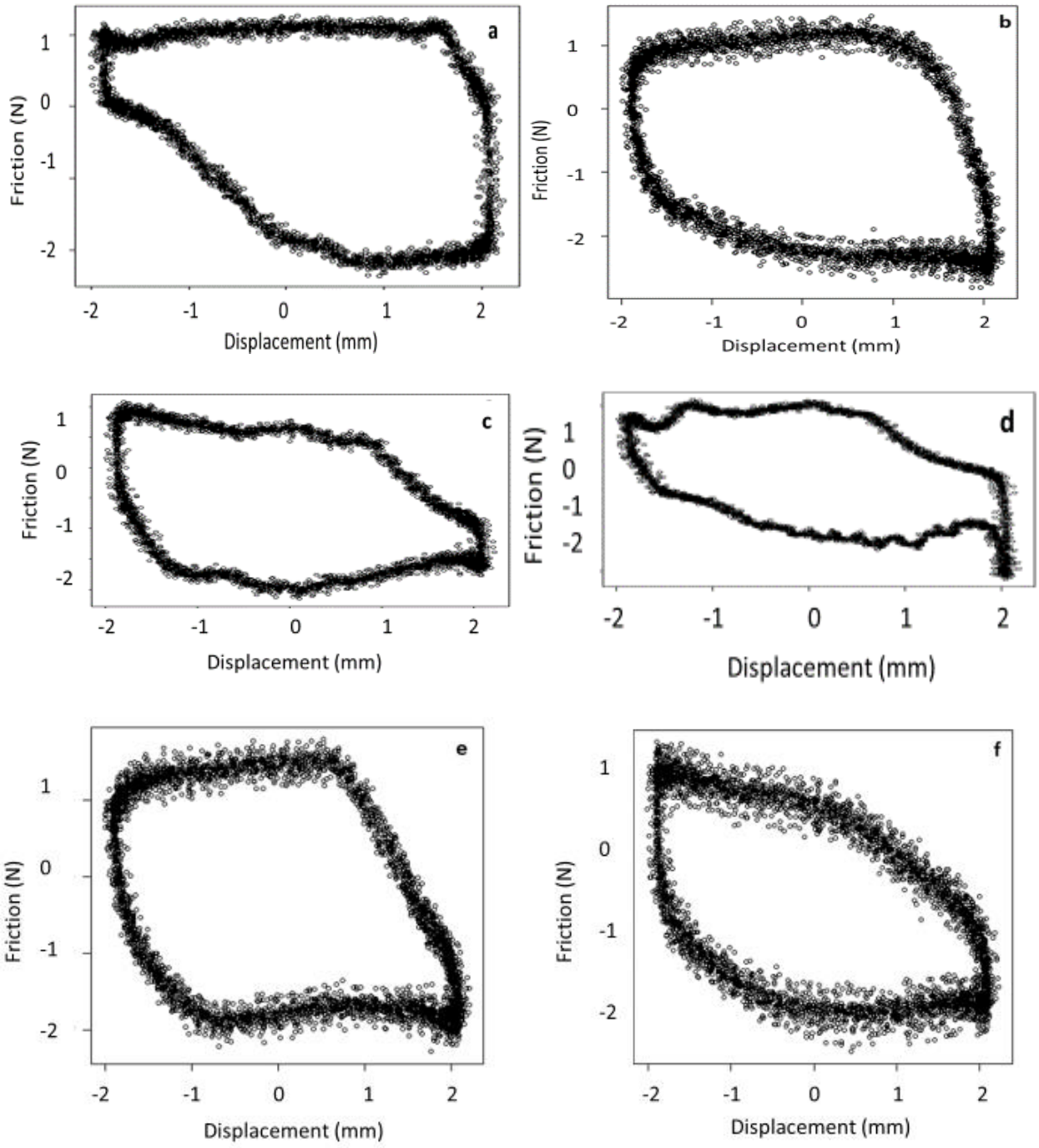

Figure 5.14: Relationship between friction and displacement presented from high speed data extraction for the cartilage against cartilage tests. Parts a-f of the figure illustrate the six individual test repeats.

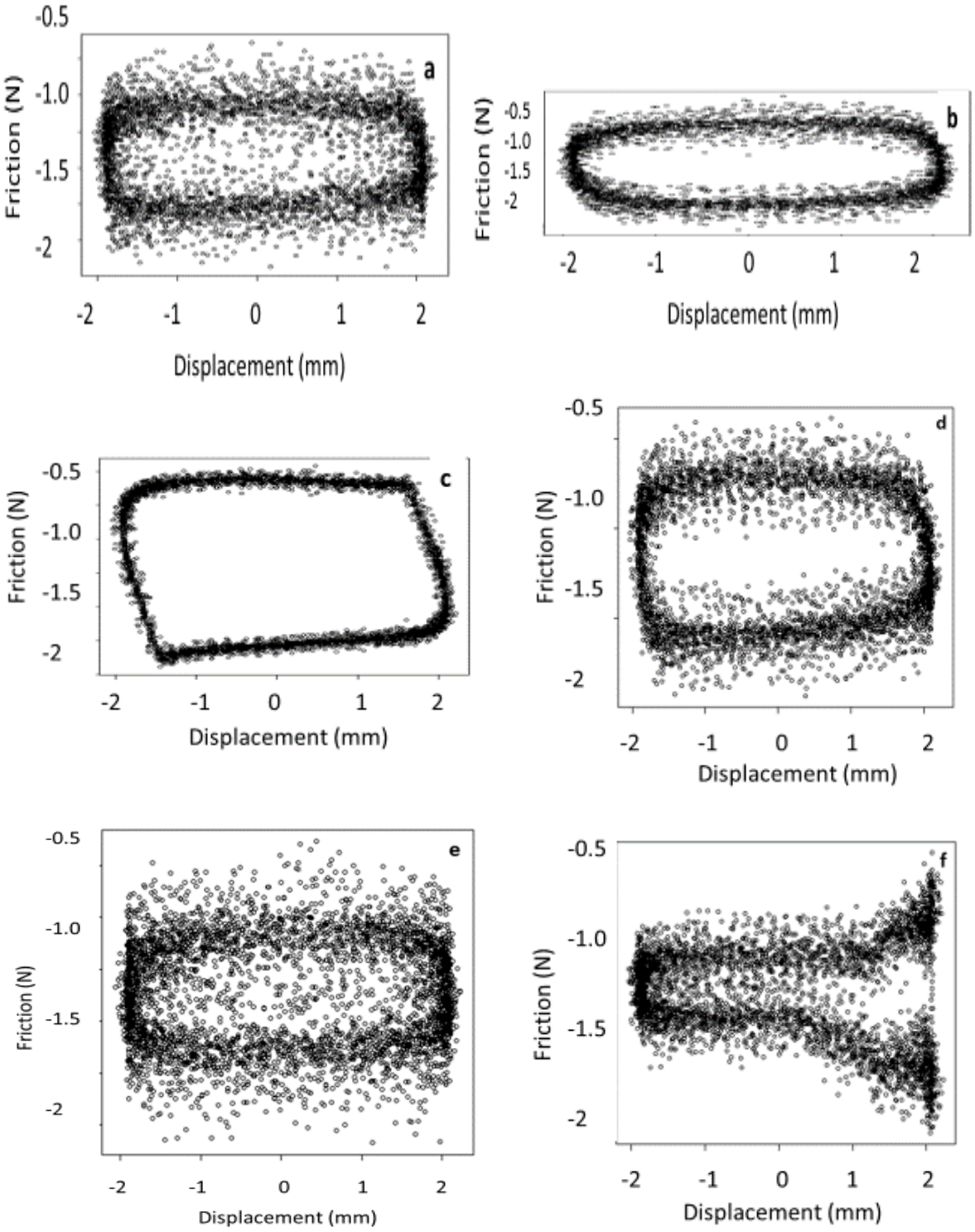

Figure 5.15: Relationship between friction and displacement presented from high speed data extraction for the cartilage against aluminium tests. Parts a-f of the figure illustrate the six individual test repeats.

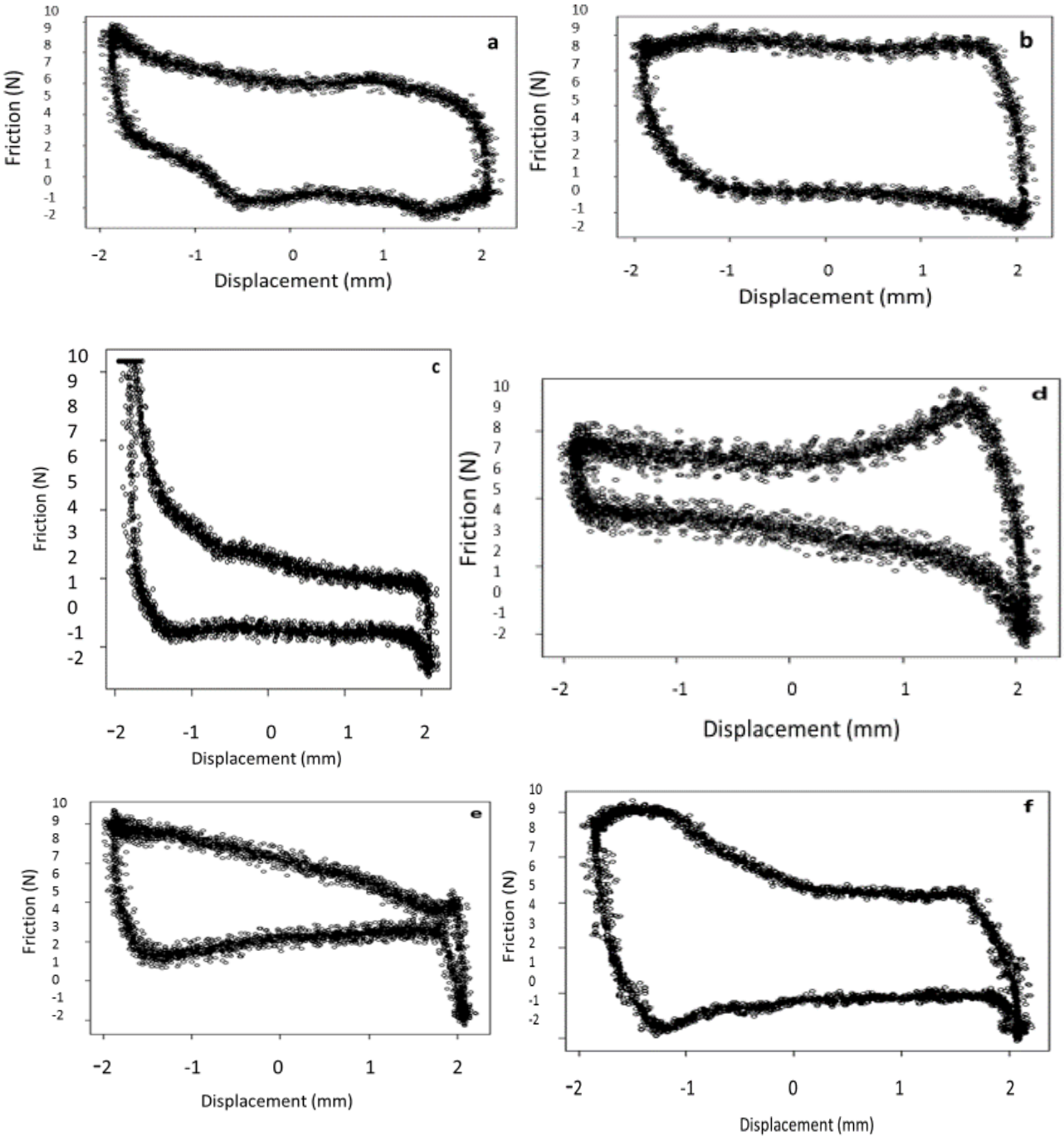

Figure 5.16: Relationship between friction and displacement presented from high speed data extraction for the cartilage/hydrogel against cartilage tests. Parts a-f of the figure illustrate the six individual test repeats.

The friction vs displacement plots for the C-G tests illustrate a different shape to C-M and C-C tests. The prominent variation is clearly identified by the large peak at the turn around points (Figure 5.16; a-f). Potential factors for the large observed variation are outlined in the discussion section of the chapter.

For further analysis to allow for a quantitative comparison across the results, the mean frictional energy was calculated for each material combination, following on from solving the integral of the friction vs displacement plot for each repeat of six per test-type. The results are shown in Figure 5.17.

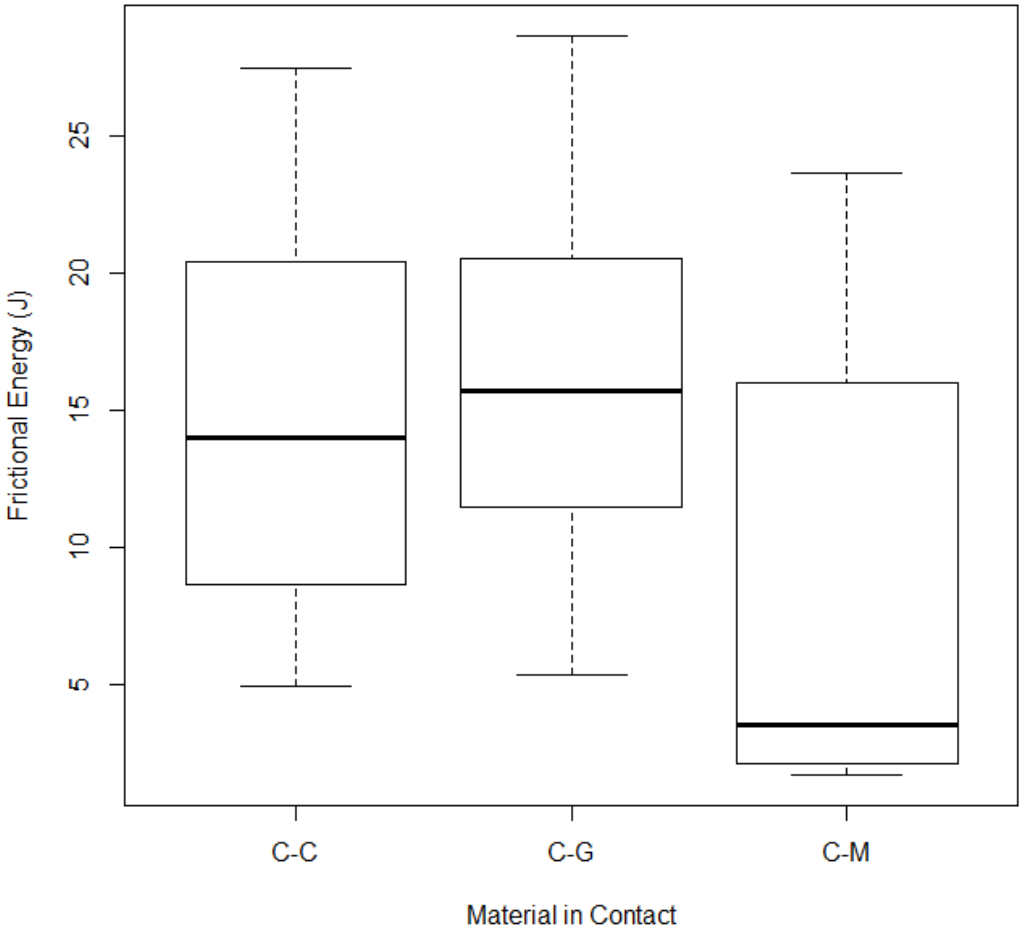

Figure 5.17: The Frictional Energy of each material combination on solving the integral of the friction versus displacement plot for each test-type repeat. C-C: cartilage against cartilage test, C-M: cartilage against aluminium test and C-G: cartilage with gel biomaterial insertion against cartilage test. The dark black line represents the mean.

5.8 Discussion

The study presented in this chapter is the first to develop a method for the assessment of the coefficient of friction of articular cartilage with incorporation of a replacement biomaterial. Hence, the principal novel aspect of the method developed in this chapter, is the introduction of the artificial defect on the cartilage surface to allow for the implantation of the biomaterial. The coefficient of friction was then assessed between the biomaterial filled defect and the articular cartilage. Thus, it is worth noting that the novelty underpins the assessment of the biomaterial, not the coefficient of friction measurement using pin-on-disc sliding, as previously demonstrated in the literature.

The work presented focuses on a hydrogel, because of its biocompatibility, hydrophilicity and permeability (Li *et al*., 2016; Spiller *et al*., 2011). Three various coefficient of friction tests have been performed, to include cartilage against cartilage, cartilage with a biomaterial insert against cartilage, as well as cartilage against aluminium. A constant induced stress of 0.06 MPa, closer towards the minimal range of average joint stress at 0.10 MPa (Brand, 2004; Li *et al*., 2016) was applied, at a frequency of 1 Hz, in a physiological body temperature testing environment at 37°. The sliding configuration used in this chapter has been referred to in previous work as the replication of physiological movements (Cilingir, 2015). In light of this, it was not the aim of the study presented in this chapter to solely replicate the physiological movements of joints, as the *in vitro* set-up confers advantage for the extraction of cartilage in a controlled experiment in tribology. What is key to note from this chapter, is that a protocol has been developed which can be used by others to assess the coefficient of friction of a potential cartilage replacement material. Future developments to the technique could further replicate physiological conditions. Such advancements to the physiological conditions could include larger contact diameters for tribological rehydration (Burris *et al*., 2019), increased sliding speeds or physiological contact stresses.

The close resemblance in the measurement of the coefficient of friction for the cartilage against cartilage test with the cartilage/hydrogel against cartilage test, demonstrates the potential of calcium alginate as an effective cartilage replacement material, from a frictional perspective. Additionally, for all assessments of the coefficient of friction in this chapter (Figure 5.11; 5.12; 5.13), the results were not significant to a 5% level, across the three test groups ($p > 0.05$) (Table 5.2). However, despite the statistically indifferent data, trends were observed.

A previous study explored the coefficient of friction of articular cartilage against stainless steel with a uni-directional testing configuration on a pin-on-plate set-up (Northwood and Fisher, 2007). After 20-minutes of testing the study presented a coefficient of friction of articular cartilage within the range of 0.22 to 0.28 (Northwood and Fisher, 2007), whilst the work in this chapter demonstrates an overall median coefficient value of 0.28, from the last five-minutes of the cartilage against aluminium test. Thus, the work in this chapter is comparable to the range attained in that study of cartilage against stainless-steel (Northwood and Fisher, 2007). The median data obtained for the cartilage against aluminium test in this chapter, is also similar to a previous study that explores the coefficient of friction of cartilage against a stainless steel, in reciprocal sliding (Oungoulian *et al.,* 2015). That study has presented a coefficient of friction of approximately 0.25 on completion of a 4-hour test period (Oungoulian *et al.,* 2015).

A previous study explored the coefficient of friction of polyvinyl alcohol (PVA) hydrogels in combination with carboxylic acid (Blum and Ovaert, 2013). On completion of friction tests in sliding, with a glass counterpart, that study identified a coefficient of friction range of 0.27 to 0.93 (Blum and Ovaert, 2013). For this chapter, the coefficient of friction for the calcium alginate biomaterial inserted within the cartilage, for sliding against cartilage, produces a maximum friction value of 0.48, whilst the median from the entire dataset and of the last five minutes, is of 0.38 and 0.36, respectively, which falls within the range of the PVA based hydrogels assessed in the previous study (Blum and Ovaert, 2013).

Previous studies assessing the coefficient of friction in sliding of the femur on the tibia have used saline as the lubricant (Mabuchi *et al.,* 1998). That work identifies a mean start-up coefficient of friction of 0.31 (Mabuchi *et al.,* 1998), whilst a further study identifies a maximum start-up coefficient of friction of cartilage against cartilage of approximately 0.30, with use of Ringer's solution as the lubricant (Forster and Fisher, 1996). Such values are comparable to the overall median extracted from the entire data set in this chapter, for cartilage against cartilage, of 0.36. Further, previous work has evaluated sliding of a cartilage pin versus a cartilage plate (Cilingir, 2015), yet that protocol performs sliding at a 10° rotated amplitude, whilst this chapter completes sliding at a linear plane. That study observes a coefficient of friction of articular cartilage of 0.26 whilst subject to sliding, under dry friction (Cilingir, 2015). Different by an order of magnitude, this chapter presents the median coefficient of friction of cartilage against cartilage, as well as of that extracted from the final five minutes, of 0.35. With the presence of phosphate buffered saline as the lubricant configuration, that study identifies a coefficient of friction of 0.08, for cartilage against cartilage in sliding (Cilingir, 2015), which is lower in comparison to our coefficient of friction for the cartilage against cartilage tests, performed in Ringer's solution.

Several factors are reported to contribute to varied measurements of the coefficient of friction, as shown in this chapter, to that of literature (Cilingir, 2015). This has been identified as the tribological circumstances (Forster and Fisher, 1999), as well as the testing protocols to include the velocity of sliding and conditions of loading (Cilingir, 2015). In fact, previous studies have further identified a higher coefficient of friction with use of Ringer's solution, as used in this chapter for the lubricant, in comparison to other lubricants. For instance, previous work identifies a greater coefficient of friction of cartilage against a PVA hydrogel with use of Ringer's solution, in comparison to hyaluronic acid (HA) solution (Li *et al*., 2016). Further, an additional study recognises a significant decline in friction of damaged articular cartilage with

use of a combined lubricant of HA with dipalmitoyl phosphatidylcholine, in comparison to Ringer's solution (Forsey *et al.,* 2006).

This leads onto the discussion of the limitation of the use of Ringer's solution in this chapter, rather than synovial fluid. It has previously been identified that the use of synovial fluid as the lubricant has shown to significantly lower the coefficient of friction, in comparison to Ringer's solution, for cartilage against cartilage contact (Forster and Fisher, 1996). However, as previously mentioned, the technique developed in this chapter acts as a baseline to which future developments could certainly incorporate further physiological conditions. Thus, a future development to address this limitation would be the use of synovial fluid. In addition, the use of human articular cartilage would provide a scenario closer to *in vivo*, enabling the coefficient of friction of the biomaterial to be directly compared to the value obtained for human cartilage. Thus, it certainly remains as a future development for the use of human articular cartilage to be incorporated into the technique.

What is key from this chapter, is that under identical testing conditions, the obtained coefficient of friction for the cartilage against cartilage test is similar to that of the cartilage/hydrogel against cartilage test. Thus, the frictional properties of calcium alginate are comparable to those of articular cartilage.

The high-speed data allowed for the coefficient of friction to be plotted against the displacement of the upper specimen. This is indicative of the variation of the coefficient of friction with the sliding velocity, as the samples are momentarily stationary (quasi-static) at the ends of the stroke and at maximum velocity at the centre. Testing articular cartilage under a sliding configuration allows for the examination of the various lubrication modes of boundary and mixed (Accardi *et al.,* 2011), hypothesised by the pressurisation of the interstitial fluid (Ateshian *et al*., 1994). The assessment of high-speed data friction loops to determine the lubrication mechanism present within the system, is applied in the study presented in this

chapter, with reference to previous work (Accardi *et al*., 2011). That study effectively explores the relationship between different lubrication regimes and sliding velocities, with respect to the Stribeck graph to correspond to a frictional joint response (Accardi *et al.,* 2011). Consequently, with reference to the Stribeck graph, the specific shape of each plot provides details on the type of lubrication mechanism present in the system (Sotres and Arnebrant, 2013; Theo and Wilfried, 2007).

The high-speed data plots as displayed in Figure 5.14 of the cartilage against cartilage test shows evidence of boundary lubrication, similar to the cartilage against aluminium test, as identified by the close-to flat upper and lower regions of the curve (Figure 5.15) (Sotres and Arnebrant, 2013; Theo and Wilfried, 2007). The observed small increase in friction as the velocity tends towards the maximum (Figure 5.14), can be attributed to the combination of the two viscoelastic materials causing a change in the contact pressure as the direction of sliding changes. Further, the slant observed on the change in sliding direction at both sides of the plot (Figure 5.14), may be an indicator of the viscoelastic properties of the materials. This characteristic is present in the cartilage against aluminium test (Figure 5.15), but it is much less pronounced.

The cartilage against aluminium test represented in Figure 5.15, demonstrates a square shape indicative of the test being boundary lubricated throughout (Theo and Wilfried, 2007). The boundary lubrication mode can be identified by the near-to flat appearance of the regions at the lower and upper segments of the curve, symbolising the sliding movements of right and left, respectively (Figure 5.15) (Sotres and Arnebrant, 2013; Theo and Wilfried, 2007). Further, the observed constant coefficient of friction until the velocity tends towards zero (Figure 5.15), indicates that the contact pressures and shear rates present in the system are not large enough to generate a lubricating film, which would otherwise induce a mixed lubrication environment (Theo and Wilfried, 2007).

As shown by the high-speed data for the cartilage/hydrogel against cartilage test, large variation exists. The observed amplified turn-around points of the cartilage/hydrogel against cartilage test (Figure 5.16), may infer either a transition from boundary lubrication to mixed lubrication (Spiller *et al*., 2011; Theo and Wilfried, 2007) or the upper specimen overlapping the gel-cartilage boundary, causing a large change in the coefficient of friction due to the change in material properties. Consequently, the cartilage against cartilage and cartilage against aluminium are both very similar in mechanism, with the cartilage/hydrogel against cartilage test either showing a formation of a lubricant film, or an interaction at the material boundaries in the lower specimen.

The frictional energy is indicative of the amount of energy absorbed by the material during each cycle. If more energy has been absorbed there is more likelihood of wear of the surface. It is expected that the cartilage against aluminium test will have a lower frictional energy than the other tests, as the aluminium is a less compliant material than the cartilage and hydrogel and so deforms less under the motion. The frictional energies of cartilage against cartilage and cartilage/hydrogel against cartilage are similar. This would suggest that the cartilage against cartilage and cartilage/hydrogel against cartilage material combinations will generate more surface damage than cartilage against aluminium. The largest frictional energy associated with the calcium alginate insertion means that the methods of lubrication are different between samples (despite a similar coefficient of friction).

As a limitation of the study presented in this chapter, the testing of articular cartilage extracted from the ligaments and tendons as *in vivo*, may contribute to a differing coefficient of friction as to when tested as its whole structure. However, as indicated in Chapter 4, it is reported that the removal of articular cartilage in this manner enables the measurement of frictional properties that of which can be extracted from a controlled experiment in tribology (Forster and Fisher, 1996). It is also worth noting the limitation of the use of aluminium as the base metal in this chapter, which is not safe for use in orthopaedic implants. However, as

outlined in the introduction, aluminium was selected based on the ease of manufacture and therefore efficiency in the incorporation into the technique presented in this chapter. Certainly, future work can involve the use of metals commonly used for orthopaedic implants, such as titanium.

A further limitation may be the potential diameter defects to the specimen, as a result of the varied lower articular cartilage specimen thickness, as well as flatness. Such defects may contribute to the measurement of the coefficient of friction. However, due to the nature of biological material this is an expected limitation, which even still, caution was exercised to ensure the articular cartilage specimens were prepared to consistent dimensions. Further, the specimens were extracted from the central region of the humeral head, ensuring maximum flatness where possible. In addition, the protocols developed to assess the coefficient of friction of the three various groups in this chapter were consistently performed, thus enabling accurate evaluations.

5.9 Chapter Summary

The conclusions determined from this chapter are detailed below:

1) The method developed in this study can be applied for future assessments of the coefficient of friction for potential replacement biomaterials of articular cartilage.
2) Statistical insignificance is observed in the coefficient of friction between all three testing groups ($p > 0.05$).
3) The chapter demonstrates the largest frictional energy for the calcium alginate insertion test. This implies the requirement of the improvement to the mechanical properties of calcium alginate for use in cartilage repair techniques.

4) The method presented in this study acts as a baseline for development in future work. Developments include the use of human articular cartilage and synovial fluid, with assessment of additional biomaterials.

6 OVERALL DISCUSSION, FUTURE WORK AND CONCLUSIONS

6.1 Overall Discussion and Conclusions

The work presented in this thesis has assessed the failure of the surface layer of articular cartilage, along with the evaluation of the surface friction of a replacement biomaterial, using novel techniques. This includes the developed new procedures for assessing surface properties of articular cartilage mimicking torque, as well as linear movement with the incorporation of a replacement biomaterial. Hence, as proof of concept for use, the potential replacement material has been evaluated using these new techniques.

Chapter 3 of this thesis examined the novel combination of the multi-factorial effect of frequency and substrate density, to mimic BMD, on associated cartilage damage. Experimentally, three varying frequencies were assessed to represent normal and above-normal gait. The results identified statistical significance between an increase in substrate density and an applied loading frequency of 10 Hz, for corresponding cartilage-off-bone damage. Chapter 4 and 5 of this thesis reported innovative techniques for the evaluation of the frictional torque, and coefficient of friction, respectively, of potential cartilage replacement biomaterials alongside that of articular cartilage. Calcium alginate was selected as the sample biomaterial for the techniques developed in Chapters 4 and 5, demonstrating a similar value in both the torque and coefficient of friction to that of articular cartilage. The work of this thesis demonstrates the importance of potential dual effects of cartilage damage factors, as well as the implementation of effective, repeatable techniques for the frictional evaluation of cartilage replacement biomaterials, in light of cartilage repair.

Chapter 3 involved two aspects to include experimental and Hertzian contact for the evaluation of the effects of substrate density on cartilage damage. Experimentally, for cartilage-off-bone, the combined effect of a frequency at 1, 10 and 50 Hz with substrate density

was examined, whilst a frequency of 1 and 10 Hz was assessed for cartilage-on-bone. The relationship observed between cartilage damage and frequency in this chapter, coincides with the frequency-independent loss modulus of articular cartilage-on-bone (Fulcher *et al*., 2009), as well as the frequency-dependent loss modulus of cartilage-off-bone (Temple *et al*., 2016). Increased damage was also observed with an increase in frequency for both on- and off-bone cartilage, from 1 to 10 Hz, as demonstrated in previous work (Sadeghi *et al.,* 2015; Sadeghi *et al*., 2017; Sadeghi *et al*., 2018).

For the first time, the results in Chapter 3 have identified the multi-factorial effect of both the frequency of loading and the density of a bone mimicking underlying substrate.

Chapter 4 presents the development of a novel technique for the determination of the frictional torque of both articular cartilage-on-bone, as well as a potential replacement biomaterial. Calcium alginate was selected as the biomaterial for assessment, based on the ease of manufacture (Wands *et al*., 2008) and previous use in cartilage repair (Focaroli *et al*., 2016; Liao *et al*., 2017). For both analysis methods, the results identified statistical significance between torque magnitude and load, for the cartilage as well as the 2 mm calcium alginate insert. This in contrast to the 10 mm calcium alginate insert, displaying statistical significance between torque magnitude and load for analysis method 1), yet not for analysis method 2). Additionally, a comparable torque magnitude range as well as the relationship between torque and rotation angle was identified, for cartilage and both calcium alginate inserts. With analysis method 1), this was shown by the torque magnitude range of 0.08 to 0.11 N m, 0.07 to 0.09 N m, and 0.08 to 0.09 N m, for cartilage and the 2 mm/10 mm calcium alginate hydrogel inserts, respectively. Similarly, with analysis method 2), comparable ranges were shown as 0.06 to 0.08 N m for articular cartilage, and 0.07 to 0.09 N m for both calcium alginate inserts.

The measurement of the frictional torque of articular cartilage has not been addressed in the literature, rather, emphasis is placed on the coefficient of friction of articular cartilage

(Burris and Moore, 2017; Drewniak *et al.,* 2012; Li *et al*., 2010; Moore and Burris, 2017). Therefore, Chapter 4 identifies the unknown measurement of the torque of cartilage in response to a load. Additionally, this Chapter has outlined the torque range as well as a linear relationship of torque in response to load, that a potential cartilage replacement biomaterial should adopt. Although the torque and coefficient are two distinct friction measurements, the results from this chapter are in line with previous work, displaying an increase in the coefficient of friction of cartilage, with time (Forster and Fisher, 1999) and under both uni- and multi-directional testing (Northwood and Fisher, 2007). This chapter has proposed a repeatable protocol for the assessment of further potential cartilage replacement biomaterials.

Chapter 5 presents an additional novel technique, for the assessment of the coefficient of friction of articular cartilage and replacement biomaterials. Friction tests were performed in sliding between three test groups. This included cartilage against cartilage, cartilage with a biomaterial insert against cartilage, as well as cartilage against aluminium. Literature is limited to the measurement of the coefficient of friction of cartilage in sliding, against biomaterials (Li *et al*., 2016; Milner *et al*., 2018; Yarimitsu *et al.*, 2016), yet not of the assessment of the biomaterial incorporated within a defect. Similar to the protocol developed in Chapter 4, calcium alginate was selected as the sample biomaterial for this chapter.

Similarities in the values obtained from Chapter 5 are shown to literature, having identified a mean start-up coefficient of friction of the femur sliding on the tibia, of 0.31 (Mabuchi *et al.*, 1998). Additionally, the literature has identified an approximate coefficient of friction of 0.25 for cartilage sliding against stainless-steel (Oungoulian *et al.,* 2015), comparable to the data obtained from the cartilage against aluminium in this chapter. For all evaluation types, the results identified no statistical difference in the coefficient of friction between all three test groups. Hence, only trends can be extracted from the data. A similarity in the coefficient of friction of the cartilage-cartilage test with the cartilage/hydrogel-cartilage test was identified.

This outcome is similar to Chapter 4, where a similar torque magnitude range is identified between that of articular cartilage and calcium alginate (Mahmood *et al*., 2020b).

Additionally, the results in Chapter 5 indicate the greatest frictional energy for the cartilage/hydrogel-cartilage test, thus conferring the greatest wear. Ultimately, the results from both Chapter 4 and 5 show that there is a requirement for the improvement to the mechanical properties of calcium alginate, for use as a cartilage replacement biomaterial.

Thus, this thesis has effectively met the study aims as presented in Chapter 1. This thesis has successfully characterised the surface failure of articular cartilage, with regards to the original potential dual effect of both bone mineral density and the frequency of loading. In addition, two novel techniques have been developed for the evaluation of both the frictional torque and coefficient of friction, of articular cartilage in accordance with a biomaterial. Considering cartilage defect repair, the techniques have been designed for the implementation of a biomaterial for assessment in line with articular cartilage.

The overall conclusions from this thesis are outlined below:

1) The application of 10 Hz in loading frequency in combination with an increase in underlying substrate density, results in a significant increase ($p < 0.05$) in the surface damage of cartilage-off-bone.
2) It is feasible to use the Frictional Torque Technique, to evaluate the frictional torque of articular cartilage and potential replacement biomaterials.
3) The frictional torque magnitude of cartilage-on-bone significantly increases with load ($p < 0.05$), of the range of 0.08 to 0.11 N m at 10 through to 100 N. The range identified is similar to that of calcium alginate of 0.07 to 0.09 N m, and 0.08 to 0.09 N m, for 2 and 10 mm calcium alginate inserts, respectively.

4) The frictional torque of an effective cartilage replacement biomaterial should adopt a linear relationship with load, whilst the torque range should coincide with that identified for articular cartilage.
5) It is feasible to use the Coefficient of Friction Technique, to evaluate the coefficient of friction of articular cartilage and potential replacement biomaterials. This technique replicates the osteochondral plug surgical procedure.
6) The coefficient of friction of cartilage sliding against cartilage is similar to that of cartilage with a calcium alginate insertion, sliding against cartilage. The results of the overall median from the entire data set are of 0.36 and 0.38, respectively. The result from the overall median from the last five minutes is of 0.35 and 0.36, respectively. The overall median obtained from the maximum coefficient of friction is of 0.43 and 0.48, respectively.

The overall limitations from this thesis are outlined below:

1) The use of bovine articular cartilage in place of human articular cartilage for all experimental chapters presented in this thesis acts as the initial limitation. This overall limitation is particularly due to the differences in morphology and proteoglycan concentration between the cartilage of the two species.
2) Limitation 1) is further demonstrated by the inability to extract information for severe osteoarthritis with use of bovine cartilage. This is due to the differences in osteoarthritic cartilage for both human and cow species. Hence, this creates limitations for the extraction of the results obtained from bovine cartilage in this thesis, to human osteoarthritic cartilage.
3) The use of Ringer's solution in place of synovial fluid for all experimental chapters presented in this thesis acts as a further limitation.

4) The linear regression statistical assessment is performed between the mean crack length and indented area, for a given substrate density, thus contributing to a low n value of 4.
5) To obtain cartilage off-bone specimens, removal occurs from the in-tact cartilage matrix, potentially weakening the sample. The removal of the subchondral bone alters the load transfer properties.
6) Disparities exist in the reproducibility of the ImageJ damage measurement technique. This is primarily due to specific requirements in the specimen positioning as well as photography environment.
7) The assessment of the curvature of the specimens prepared for Chapter 4 is limited to a qualitative visual evaluation. Surface roughness values are not measured for the specimen.
8) The curvature for specimens used in Chapter 4 may contribute to the observed reduced sensitivity to load for the biomaterial inserted specimens.
9) Specimen curvature in Chapter 4 may also contribute to misalignment error of the cartilage surface.
10) The homogenous application of stress beneath the indenter presented in the protocol for Chapter 3 and 4 is difficult to confirm
11) Diameter defects may exist for the cartilage on-bone specimen sheets prepared for use in Chapter 5
12) The extraction of the cartilage on-bone specimen from the in-tact structure as *in vivo*, may affect the measured frictional torque and coefficient of friction.
13) For the measurements of frictional torque and the coefficient of friction, the use of metal in contact with the cartilage does not represent the physiological circumstances *in vivo*.
14) The use of aluminium as the base metal incorporated into the technique presented in Chapter 5 is limited by its toxicity as an implant material.

6.2 Future Work

For all experimental chapters presented in this thesis, a common future development involves the improved replication of a physiological environment. Initially, this includes the use of human articular cartilage. The implementation of human articular cartilage would allow valuable data to be extracted from the techniques, which can be extrapolated to obtain clinical information. Both the outcome for osteoarthritic and normal cartilage can be obtained with use of human cartilage, avoiding the limitation to compare with another species. The use of human articular cartilage directly acts as a benchmark for the comparison of a potential biomaterial for cartilage replacement. A further widespread physiological improvement concerns the use of synovial fluid in replace of Ringer's solution as the lubricant.

With regards to Chapter 3, future work could involve the evaluation of the potential dual effect of further cartilage damage inducing factors, such as the effect of repeated loading (Kerin *et al*., 2003; Weightman *et al.,* 1973) in combination with an increase in BMD (Hart *et al*., 1994; Hordon *et al*., 1993). For that matter, any alternative damage inducing factors could be considered for a potential dual effect, such as dehydration (Fick and Espino, 2012) or cartilage thickness variations (Espino *et al*., 2014). In terms of future development to the experimental protocol itself, it would be useful to incorporate an intra- and inter- specimen operator study, to confirm the repeatability of the ImageJ damage assessment. Furthermore, the simple computational model has potential for future development. Advancements to the finite element analysis include the representation of the time-dependent, poro-elastic as well as fibre-reinforcement and depth dependent stiffness characteristics of articular cartilage.

The technique established in Chapter 4 acts as the baseline protocol to which further biomaterials can be assessed in future work. In addition to the use of human articular cartilage and synovial fluid as physiological advancements to the technique, there are further openings to mimic joint movement. For instance, both the rotation range as well as maximum loading

can be increased. In terms of future developments to the experimental protocol itself, surface roughness as well as surface 3D angle measurements should be introduced. This will enable the accurate assessment of the curvature and surface texture of the specimen, which can be used to confirm reliable measurements of the frictional torque.

The technique presented in Chapter 5 allows for future assessment of the coefficient of friction of potential cartilage replacement biomaterials. Alike to the opening for future work in Chapter 4, with regards to the enhanced replication of physiological characteristics, this also applies for Chapter 5. Again, aside from the incorporation of human articular cartilage and synovial fluid, additional developments include larger specimen diameters, increased sliding speeds as well as physiological contact stresses. Furthermore, metals used for orthopaedic implants could be incorporated into the technique, to replace the current aluminium base metal.

The novel techniques established in Chapter 4 and 5 replicate the osteochondral plug surgical procedure (Hattori *et al*., 2007), whereby the aim concerns the repair of a small cartilage surface defect. The field of tissue engineering provides an alternative therapy area, defined by top-down and bottom-up approaches. Top-down is illustrated by the use of cells and a scaffold, incorporated within appropriate conditions for the development of an ECM (Tamayol *et al.,* 2014). The build-up of large tissue constructs from smaller molecules describes the application of bottom-up (Tamayol *et al.,* 2014). Consequently, future work could involve the application of stem cell approaches incorporated within a scaffold and signal approach, to enable cartilage regeneration. Following on from this, the regenerated cartilage could be assessed for the resulting torque and coefficient of friction, via the developed techniques in Chapter 4 and 5, respectively.

On a wider application scale, the novel techniques developed in this thesis can be applied to clinical practice following animal testing. A further next step can involve assessing the biomaterial within a whole joint amongst a simulator set-up. Physiological conditions can

be further incorporated within the whole joint test set-up. In addition, several various biomaterials can be assessed in the whole joint test. This then acts as the baseline test to take the biomaterial to an animal model, such as rabbit or rat. On successful implementation, other larger species can be used, such as a horse or dog. Pre-clinical testing would then lead onto clinical trials of the incorporated biomaterial within a damaged articular cartilage defect.

The methods developed in the techniques are important to understand the comparison in frictional behaviour of biomaterials with articular cartilage. The results identified from this thesis indicate the need to assess further cartilage damaging factors in combination. The results for the frictional torque magnitude of articular cartilage can be used as the benchmark comparison for biomaterial assessment. Likewise, the resulting outcome of the coefficient of friction technique can be used for the comparison of biomaterials with articular cartilage. Thus, overall, the importance of the work presented in this thesis highlights the focus on repairing damaged articular cartilage with replacement biomaterials. This is in light of preventing the progression into osteoarthritis.

REFERENCES

Abdullah EY. Squeeze film characteristics in synovial hip joint. ICCEPS. 2019;571:012008

Accardi MA, Dini D, Cann PM. Experimental and numerical investigation of the behaviour of articular cartilage under shear loading - Interstitial fluid pressurisation and lubrication mechanisms. Tribol Int. 2011;44:565-78.

Ahmed EM. Hydrogel: Preparation, characterization and applications: A review. J Adv Res. 2015;6:105-21.

Akter F. Chapter 1 – What is Tissue Engineering? Tissue Eng Made Easy. 2016;1-2.

Alford JW, Cole BJ. Cartilage Restoration, Part 1: Basic Science, Historical Perspective, Patient Evaluation, and Treatment Options. Am J Sports. 2005;33:295-306

Ali AM, Yousif AE. The Role of Lubrication Mechanisms in the Knee Synovial Joints. Eng Sci NUCEJ Spatial ISSUE. 2008;11:522–35.

Alnaimat FA, Shepherd DET, Dearn K. The effect of synthetic polymer lubricants on the friction between common arthroplasty bearing biomaterials for encapsulated spinal implants. Tribol Int. 2016;98:20-25.

Amini AA, Nair LS. Injectable hydrogels for bone and cartilage repair. Biomed Mater. 2012;7.

Anderson AS, Loeser RF. Why is Osteoarthritis an Age-Related Disease? Best Pract Res Clin Rheumatol. 2010;24:15

Ansari M, Eshghanmalek M. Biomaterials for repair and regeneration of the cartilage tissue. BDM. 2019;2:41-49

Aroen A, Heir S, Loken S, Reinholt FP, Engebretsen L. Articular cartilage defects in a rabbit model, retention rate of periosteal flap cover. Acta Orthopaedica. 2005;76:220-24

Aspden RM, Jeffrey JE, Burgin LV. Letter to the Editor. Osteoarthr Cart. 2002;10:588-89

Aspden RM. Constraining the lateral dimensions of uniaxially loaded materials increases the calculated strength and stiffness: application to muscle and bone. J Mater Sci-Mater M. 1990;1:100-104

Aspden RM. India ink and cartilage. Osteoarthr Cartil. 2011;19:332.

Aspden RM. Obesity punches above its weight in osteoarthritis. Nat Rev Rheumatol. 2011;7:65-68

Ateshian GA, Lai WM, Zhu WB, Mow VC. An Asymptotic Solution for the Contact of Two Biphasic Cartilage Layers. J Biomechanics. 1994;27:1347-60.

Ateshian GA. The role of interstitial fluid pressurization in articular cartilage lubrication. J Biomech. 2009;42: 1163–76.

Athanasiou KA, Darling EM, DuRaine GD, Hu JC, Reddi AH. Articular Cartilage., first ed., New York: Taylor and Francis Group; 2013

Bader DL, Salter DM, Chowdhury TT. Biomechanical Influence of Cartilage Homeostasis in Health and Disease. Arthritis. 2011;2011

Balakrishnan B, Joshi N, Jayakrishnan A, Banerjee R. Self-crosslinked oxidized alginate / gelatin hydrogel as injectable adhesive biomimetic scaffolds for cartilage regeneration. Acta Biomater. 2014;10:3650-63.

Barker MK, Seedhom BB. The relationship of the compressive modulus of articular cartilage with its deformation response to cyclic loading: does cartilage optimize its modulus so as to minimize the strains arising in it due to the prevalent loading regime?. Rheumatology. 2001;40:274–84.

Barnes SC, Lawless BM, Shepherd DET, Espino DM, Bicknell GR, Bryan RT. Viscoelastic properties of human bladder tumours. J Mech Behav Biomed Mater. 2016;61:250-57

Barnes SC, Shepherd DET, Espino DM, Bryan RT. Frequency dependent viscoelastic properties of porcine bladder. J Mech Behav Biomed Mater. 2015;42:168-75

Basalo IM, Mauck RL, Kelly TAN, Nicoli SB, Chen FH, Hung CT, Ateshian GA. Cartilage Interstitial Fluid Load Support in Unconfined Compression Following Enzymatic Digestion. J Biomech Eng. 2013;126:779-86.

Bergink AP, Uitterlinden AG, Van Leeuwen JPTM, Hofman A, Verhaar JAN, Pols HAP. Bone mineral density and vertebral fracture history are associated with incident and progressive radiographic knee osteoarthritis in elderly men and women: The Rotterdam Study. Bone. 2005;37:446-56

Betts JG, Young KA, Wise JA, Johnson E, Poe B, Kruse DH, Korol O, Johnson JE, Womble M, DeSaix P. Anatomy and Physiology, in: Synovial Joints., Canada: Pressbooks; 2019

Bhosale AM, Richardson JB. Articular cartilage: structure, injuries and review of management. Br Med Bull. 2008;87:77-95

Bian L, Zhai DY, Tous E, Rai R, Mauck RL, Burdick JA. Enhanced MSC chondrogenesis following delivery of TGF-β3 from alginate microspheres within hyaluronic acid hydrogels in vitro and in vivo. Biomaterials. 2011;32:6425-34

Bliddal H, Leeds AR, Christensen R. Osteoarthritis, obesity and weight loss: evidence, hypotheses and horizons - a scoping review. Obes Rev. 2014;15:578-86

Blum MM, Ovaert TC. Low friction hydrogel for articular cartilage repair : Evaluation of mechanical and tribological properties in comparison with natural cartilage tissue. Mater Sci Eng C. 2013;33:4377–83.

Borrelli J, Silva MJ, Zaegel MA, Franz C, Sandell LJ. Single High-Energy Impact Load Causes Posttraumatic OA in Young Rabbits via a Decrease in Cellular Metabolism. J Orthop Res. 2008;27:347-52

Brand RA. Joint contact stress: A reasonable surrogate for biological processes? Iowa Orthop J. 2004;25:82-94.

Brennan SL, Pasco JA, Cicuttini FM, Henry MJ, Kotowicz MA, Nicholson GC, Wluka AE. Bone mineral density is cross sectionally associated with cartilage volume in healthy, asymptomatic adult females: Geelong Osteoporosis Study. Bone. 2011;49:839-44

Brittberg M, Lindahl A, Nilsson A, Ohlsson C, Isaksson O, Peterson L. Treatment of Deep Cartilage Defects in the Knee with Autologous Chondrocyte Transplantation. N Engl J Med. 1994;331:889-95

Brown DT, Shaw TD. In Vitro Contact Stress Distributions in the Natural Human Hip. J Biomech. 1983;16:373-84.

Bullough P, Goodfellow J. The significance of the fine structure of articular cartilage. J Bone Joint Surg Br. 1968;50:852-57

Burger H, van Daele PLA, Odding E, Valkenburg HA, Hofman A, Grobbee DE, Schutte HE, Birkenhager JC, Pols HAP. Association of radiographically evident osteoarthritis with higher bone mineral density and increased bone loss with age. The Rotterdam Study. Arthritis Rheumatol. 1996;39:81-86

Burgin LV, Aspden RM. A drop tower for controlled impact testing of biological tissues. Med Eng Phys. 2007;29:525-30

Burgin LV, Aspden RM. Impact testing to determine the mechanical properties of articular cartilage in isolation and on bone. J Mater Sci-Mater M. 2008;19:703-11

Burny F, Donkerwolcke M, Moulart F, Bourgois R, Puers R, Schuylenbergh KV, Barbosa M, Paiva O, Rodes F, Begueret JB, Lawes P. Concept, design and fabrication of smart orthopaedic implants. Med Eng and Phys. 2000;22:469-79

Burr DB, Schaffler MB. The involvement of subchondral mineralized tissues in osteoarthrosis: quantitative microscopic evidence. Microsc Res Tech. 1997;37:343-57

Burris DL, Moore AC. Cartilage and Joint Lubrication: New Insights Into the Role of Hydrodynamics. Biotribology. 2017;12:8-14.

Burris DL, Ramsey L, Graham BT, Price C, Moore AC. How Sliding and Hydrodynamics Contribute to Articular Cartilage Fluid and Lubrication Recovery. Tribol Lett. 2019;67:46.

Burton HE, Freij JM, Espino DM. Dynamic Viscoelasticity and Surface Properties of Porcine Left Anterior Descending Coronary Arteries. Cardiovasc Eng Tech. 2017;8:41

Caligaris M, Canal CE, Ahmad CS, Gardner TR, Ateshian GA. Investigation of the Frictional Response of Osteoarthritic Human Tibiofemoral Joints and the Potential Beneficial Tribological Effect of Healthy Synovial Fluid. Osteoarthr Cartil. 2008;17:1327-32

Canal CE, Hung CT, Ateshian AA. Two-Dimensional Strain Fields on the Cross-Section of the Bovine Humeral Head Under Contact Loading. J Biomech. 2009;41:3145–51.

Cao Y, Stannus OP, Aitken D, Cicuttini F, Antony B, Jones G, Ding C. Cross-sectional and longitudinal associations between systemic, subchondral bone mineral density and knee cartilage thickness in older adults with or without radiographic osteoarthritis. Ann Rheum Dis. 2014;73:2003-09

Cao Z, Dou C, Dong S. Scaffolding biomaterials for cartilage regeneration. J Nanomater. 2014;2014.

Charnley J. The lubrication of animal joints in relation to surgical reconstruction by arthroplasty. Ann Rheum Dis. 1960;19:10–19.

Chen CT, Burton-Wurster N, Lust G, Bank RA, Tekoppele JM. Compositional and metabolic changes in damaged cartilage are peak-stress, stress-rate, and loading-duration dependent. J Orthop Res. 1999;17:870-9

Chen WB, Lu L, Jiao YP, Zhou CR. Preparation of self-assembly scaffolds via electrostatic attachment of calcium alginate microspheres. J Clin Rehab Tissue Eng Res. 2010;14:433-37.

Chiang EH, Laing TJ, Meyer CR, Boes JL, Rubin JM, Adler RS. Ultrasonic Characterisation of In Vitro Osteoarthritic Articular Cartilage with Validation by Confocal Microscopy. Ultrasound Med Biol. 1997;23:205-13

Cilingir AC. Effect of Rotational and Sliding Motions on Friction and Degeneration of Articular Cartilage under Dry and Wet Friction. J Bionic Eng. 2015;12:464–72.

Clark JM, Huber JD. The structure of the human subchondral bone plate. J Bone Joint Surg. 1990;72-B:866-73

Cooke ME, Lawless BM, Jones SW, Grover LM. Matrix degradation in osteoarthritis primes the superficial region of cartilage for mechanical damage. Acta Biomater. 2018;78:320-28

Cooper C, Cook PL, Osmond C, Fisher L, Cawley MID. Osteoarthritis of the hip and osteoporosis of the proximal femur. Ann Rheum Dis. 1991;50:540-42

Cooper C, McAlindon T, Coggon D, Egger P, Dieppe P. Occupational activity and osteoarthritis of the knee. Ann Rheum Dis. 1994;53:90-93

Creamer P, Hochberg MC. Osteoarthritis. Lancet. 1997;350:503-09

Dabiri Y, Li LP. Influences of the depth-dependent material inhomogeneity of articular cartilage on the fluid pressurization in the human knee. Med Eng Phys. 2013;35:1591-98.

Dar FH, Aspden RM. A finite element model of an idealized diarthrodial joint to investigate the effects of variation in the mechanical properties of the tissues. Proc Inst Mech Eng H: J Eng Med. 2003;217:341-48

Darling EM, Zauscher S, Guilak F. Viscoelastic properties of zonal articular chondrocytes measured by atomic force microscopy. Osteoarthr Cartil. 2006;14:571-79

Day JS, Ding M, Van Der Linden JC, Hvid I, Sumner DR, Weinans H. A decreased subchondral trabecular bone tissue elastic modulus is associated with pre-arthritic cartilage damage. J Orthop Res. 2001;19:914-18

Dequeker J, Aerssens J, Luyten FP. Osteoarthritis and osteoporosis: Clinical and research evidence of inverse relationship. Aging Clin Exp Res. 2003;15:426-39

Dequeker J, Mbuyi-Muamba JM. Bone mineral density and bone turnover in spinal osteoarthritis. Ann Rheum Dis. 1996;55:331–4.

Drewniak EI, Jay GD, Fleming BC, Zhang L, Warman ML, Crisco JJ. Cyclic loading increases friction and changes cartilage surface integrity in lubricin-mutant mouse knees. Arthritis Rheum. 2012;64:465-73

Drury JL, Dennis RG, Mooney DJ. The tensile properties of alginate hydrogels. Biomater. 2004;25:3187-99

Drury JL, Mooney DJ. Hydrogels for tissue engineering: scaffold design variables and applications. Biomaterials. 2003;24:4337-51.

Dumond H, Presle N, Terlain B, Mainard D, Loeuille D, Netter P, Pottie P. Evidence for a key role of leptin in osteoarthritis, Arthritis Rheumatol. 2003;48:3118-29

Edelsten L, Jeffrey JE, Burgin LV, Aspden RM. Viscoelastic deformation of articular cartilage during impact loading. Soft Matter. 2010;6:5206-12

Emmerson BC, Gortz S, Jamali AA, Chung C, Amiel D, Bugbee WD. Fresh osteochondral allografting in the treatment of osteochondritis dissecans of the femoral condyle. Am J Sports Med. 2007;35:907-14

Espino DM, Shepherd DET, Hukins DWL. Viscoelastic properties of bovine knee joint articular cartilage: dependency on thickness and loading frequency. BMC Musculoskelet Disord. 2014;15:205-13.

Fell NLA, Lawless BM, Cox SC, Cooke ME, Eisenstein NM, Shepherd DET, Espino DM. The role of subchondral bone, and its histomorphology, on the dynamic viscoelasticity of cartilage, bone and osteochondral cores. Osteoarthr Cartil. 2019;27:535–43.

Fick JM, Espino DM. Articular cartilage surface failure: an investigation of the rupture rate and morphology in relation to tissue health and hydration. Proc Inst Mech Eng H: J Eng Med. 2012;226:389-96

Fick JM, Thambyah A, Broom ND. Articular Cartilage Compression: How Microstructural Response Influences Pore Pressure in Relation to Matrix Health. Connect Tissue Res. 2009;51:132-49

Flachsmann R, Broom ND, Hardy AE. Deformation and rupture of the articular surface under dynamic and static compression. J Orthop Res. 2001;19:1131-39

Flachsmann R, Kim W, Broom N. Vulnerability to Rupture of the Intact Articular Surface with Respect to Age and Proximity to Site of Fibrillation: A Dynamic and Static Investigation. Connect Tissue Res. 2005;46:159-69

Flannery CR. Lubricin and its potential as an OA therapy. Osteoarthr Cartil. 2015;23:A17-A18

Focaroli S, Teti G, Salvatore V, Orienti I, Falconi M. Calcium/Cobalt Alginate Beads as Functional Scaffolds for Cartilage Tissue Engineering. Stem Cells Int. 2016;2016:2030478

Forsey RW, Fisher J, Thompson J, Stone MH, Bell C, Ingham E. The effect of hyaluronic acid and phospholipid based lubricants on friction within a human cartilage damage model. Biomaterials. 2006;27:4581–90.

Forster H, Fisher J. The influence of continuous sliding and subsequent surface wear on the friction of articular cartilage. Proc Inst Mech Eng H: J Eng Med. 1999;213:329-45.

Forster H, Fisher J. The Influence of Loading Time and Lubricant on the Friction of Articular Cartilage. Proc Inst Mech Eng H: J Eng Med. 1996;210:109-19.

Foss MVL, Byers PD. Bone density, osteoarthrosis of the hip, and fracture of the upper end of the femur. Ann Rheum Dis. 1972;31:259–64.

Fox SAJ, Bedi A, Rodeo SA. The basic science of articular cartilage: Structure, composition, and function. Sports Health. 2009;1:461-68

Frost HM. Wolff's Law and bone's structural adaptations to mechanical usage: an overview for clinicians. Angle Orthod. 1994;64:175-88

Fulcher GR, Hukins DWL, Shepherd DET. Viscoelastic properties of bovine articular cartilage attached to subchondral bone at high frequencies. BMC Musculoskelet Disord. 2009;10:61-67.

Funayama A, Niki Y, Matsumoto H, Maeno S, Yatabe T, Morioka H, Yanagimoto S, Taguchi T, Tanaka J, Toyama Y. Repair of full-thickness articular cartilage defects using injectable type II collagen gel embedded with cultured chondrocytes in a gel model. J Orthop Sci. 2008;13:225-32

Getgood A, Gelber J, Gortz S, De Young A, Bugbee W. Combined osteochondral allograft and meniscal allograft transplantation: a survivorship analysis. Knee Surg Sports Traumatol Arthrose. 2015;23:946-53

Ghosh S, Bowen J, Jiang K, Espino DM, Shepherd DET. Investigation of techniques for the measurement of articular cartilage surface roughness. Micron. 2013;44:179-84.

Giedraitis A, Arnoczky SP, Bedi A. Allografts in Soft Tissue Reconstructive Procedures. Sports Health. 2014;6:256-64

Goldring MB. Articular Cartilage Degradation in Osteoarthritis. HSSJ. 2012;8:7-9

Gomoll AH, Minas T. The quality of healing: Articular cartilage. Wound Repair Regen. 2014;22:30-38.

Gong JP, Kurokawa T, Narita T, Kagata G, Osada Y, Nishimura G, Kinjo, M. Synthesis of hydrogels with extremely low surface friction. J Am Chem Soc. 2001;123:5582-83.

Griffin MF, Premakumar Y, Seifalian AM, Szarko M, Butler PEM. Biomechanical Characterisation of the Human Auricular Cartilages; Implications for Tissue Engineering. Ann Biomed Eng. 2016;44:3460-67

Gross AE, Shasha N, Aubin P. Long-term followup of the use of fresh osteochondral allografts for posttraumatic knee defects. Clin Orthop Relat Res. 2005;435:79-87

Guilak F, Mow VC. The mechanical environment of the chondrocyte: A biphasic finite element model of cell-matrix interactions in articular cartilage. J Biomechanics. 2001;33:1663-73

Haba Y, Skripitz R, Lindner T, Kockerling M, Fritsche A, Mittelmeier W, Bader R. Bone mineral densities and mechanical properties of retrieved femoral bone samples in relation to bone mineral densities measured in the respective patients. TSWJ. 2012;2012

Hadjidakis DJ, Androulakis II. Bone Remodelling. Ann N Y Acad Sci. 2006;1092:385-96

Hardcastle SA, Dieppe P, Gregson CL, Smith GD, Tobias JH. Osteoarthritis and bone mineral density: are strong bones bad for joints? Bonekey Rep. 2015;4:624

Hart DJ, Mootoosamy I, Doyle DV, Spector TD. The relationship between osteoarthritis and osteoporosis in the general population: the Chingford study. Ann Rheum Dis. 1994;53:158–62.

Hattori K, Uematsu K, Tanikake Y, Habata T, Tanaka Y, Yajima H, Takakura Y. Spectrocolorimetric assessment of cartilage plugs after autologous osteochondral grafting: correlations between color indices and histological findings in a rabbit model. Arthritis Res Ther. 2007;9:R88.

Haugen IK, Slatkowsky-Christensen B, Orstavik R, Kvien TK. Bone mineral density in patients with hand osteoarthritis compared to population controls and patients with rheumatoid arthritis. Ann Rheum Dis. 2007;66:1594-98

Herman BC, Cardaso L, Majeska RJ, Jepsen KJ, Schaffler MB. Activation of bone remodelling after fatigue: differential response to linear microcracks and diffuse damage. Bone. 2010;47:766-72

Hjelle K, Solheim E, Strand T, Muri R, Brittberg M. Articular cartilage defects in 1,000 knee arthroscopies. Arthroscopy. 2002;18:730-34

Hlavacek M. Squeeze-fim lubrication of the human ankle joint with synovial fluid filtrated by articular cartilage with the superficial zone worn out. J Biomech. 2000;33:1415-22.

Hodge WA, Carlson KL, Fuan RS, Burgess RG, Riley PO, Harris WH, Mann RW. Contact Pressures from and Instrumented Hip Endoprosthesis. J Bone Joint Surg. 1989;71:1378-86

Hordon LD, Stewart SP, Troughton PR, Wright V, Horsman A, Smith MA. Primary generalized osteoarthritis and bone mass. Br J Rheumatol. 1993;32:1059-61

Hou JS, Mow VC, Lai WM, Holmes MH. An analysis of the squeeze-film lubrication mechanism for articular cartilage. J Biomech. 1992;25:247-59

Houard X, Goldring MB, Berenbaum F. Homeostatic mechanisms in articular cartilage and role of inflammation in osteoarthritis. Curr Rheumatol rep. 2013;15:375

Howell DS. Pathogenesis of osteoarthritis. Am J Med.1986;80:24-28.

Hu MY, Nukavarapu S. 11- Scaffolds for cartilage tissue engineering. Handbook Tissue Eng Scaffolds. 2019;1:211-44

Hukins DWL, Aspden RM, Yarker YE. Fibre Reinforcement and Mechanical Stability in Articular Cartilage. Eng Med. 1984;13:153-56

Hukins DWL, Aspden RM. Composition and properties of connective tissues. Trends Biochem Sci. 1985;10:260-64

Hunter DJ, Guermazi A, Roemer F, Zhang Y, Neogi T. Structural correlates of pain in joints with osteoarthritis. Osteoarthr Cartil. 2013;21:1170-78

Huser CAM, Davies ME. Validation of an In Vitro Single-Impact Load Model of the Initiation of Osteoarthritis-like Changes in Articular Cartilage. J Orthop Res. 2006;24:725-32

Hyodo K, Masuda T, Aizawa J, Jinno T, Morita S. Hip, knee, and ankle kinematics during activities of daily living: a cross-sectional study. Brazilian J Phys Ther. 2017;21:159-66.

Jay GD, Waller KA. The biology of Lubricin: Near frictionless joint motion. Matrix Biol. 2014;39:17-24

Jeffrey JE, Aspden RM. The biophysical effects of a single impact load on human and bovine articular cartilage. Proc IMechE Part H: J Eng Med. 2006;220:677-86

Jeffrey JE, Gregory DW, Aspden RM. Matrix Damage and Chondrocyte Viability Following a Single Impact Load on Articular Cartilage. Arch Biochem Biophys. 1995;322:87-96

Jhon MS, Andrade JD. Water and Hydrogels. J Biomed Mater Res. 1973;7:509–22.

Jin Z, Dowson D. Bio-friction. Friction. 2013;1:100-13.

Julkunen P, livarinen J, Brama PA, Arokoski J, Jurvelin JS, Helminen HJ. Maturation of collagen fibril network structure in tibial and femoral cartilage of rabbits. Osteoarthr Cartil. 2010;18:406-15

Jurvelin JS, Buschmann MD, Hunziker EB. Optical and mechanical determination of poisson's ratio of adult bovine humeral articular cartilage. J Biomech. 1997;30:235-41

Kaab MJ, Gwynn IAP, Notzli HP. Collagen fibre arrangement in the tibial plateau articular cartilage of man and other mammalian species. J Anat. 1998;193:23-24

Kaleem B, Maier F, Drissi H, Pierce DM. Low-energy impact of human cartilage: predictors for microcracking the network of collagen. Osteoarthr Cartil. 2017;25:544-53

Karuppal R. Current concepts in the articular cartilage repair and regeneration. J Orthop. 2017;14:A1-A3

Kaufman KR, Kovacevic N, Irby SE, Colwell CW. Instrumented implant for measuring tibiofemoral forces. J Biomech. 1996;29:667-71

Kawcak CE, McIlwraith CW, Norrdin RW, Park RD, James SP. The role of subchondral bone in joint disease: a review. Equine Vet J. 2001;33:120-26

Keenan KE, Pal S, Lindsey DP, Besier TF, Beaupre GS. A Viscoelastic Constitutive Model Can Accurately Represent Entire Creep Indentation Tests of Human Patella Cartilage. J Appl Biomech. 2013;29:292-302.

Kempson GE, Muir H, Pollard C, Tuke M. The tensile properties of the cartilage in human femoral condyles related to the content of collagen and glycosaminoglycans. BBA-GEN SUBJECTS. 1973;297:456-72

Kerin AJ, Coleman A, Wisnom MR, Adams MA. Propagation of surface fissures in articular cartilage in response to cyclic loading in vitro. Clin Biomech. 2003;18:960-68.

Khan IM, Gilbert SJ, Singhrao SK, Duance VC, Archer CW. Cartilage integration: evaluation of the reasons for failure of integration during cartilage repair. A review. Eur Cell Mater. 2008;16:26-39

Kharb A, Saini V, Jain YK, Dhiman S. A review of gait cycle and its parameters. IJCEM. 2011;13:78-83

King LK, March L, Anandacoomarasamy A. Obesity & osteoarthritis. Indian J Med Res. 2013;138:185–93.

Komistek RD, Kane TR, Mahfouz M, Ochoa JA, Dennis DA. Knee mechanics: a review of past and present techniques to determine in vivo loads. J Biomechanics. 2005;38:215-28

Korhonen RK, Laasanen MS, Toyras J, Rieppo J, Hirvonen J, Helminen HJ, Jurvelin JS. Comparison of the equilibrium response of articular cartilage in unconfined compression, confined compression and indentation. J Biomech. 2002;35:903-09

Korhonen RK, Saarakkala S. Biomechanics and Modeling of Skeletal Soft Tissues, in: Theoretical Biomechanics., second ed., London: IntechOpen Limited; 2011, p. 118

Koskinen A, Vuolteenaho K, Nieminen R, Moilanen T, Moilanen E. Leptin enhances MMP-1, MMP-3 and MMP-13 production in human osteoarthritic cartilage and correlates with MMP-1 and MMP-3 in synovial fluid from OA patients. Clin Exp Rheumatol. 2011;29:57–64.

Koszowska A, Hawranek R, Nowak J. Osteoarthritis – a multifactorial issue. Rheumatologia. 2014;5:319-25.

Krishnan R, Kopacz M, Ateshian GA. Experimental verification of the role of interstitial fluid pressurization in cartilage lubrication. J Orthop Res. 2004;22:565–70.

Krishnan R, Mariner EN, Ateshian GA. Effect of dynamic loading on the frictional response of bovine articular cartilage. J Biomech. 2005;38:1665–73.

Kuroda R, Ishida K, Matsumoto T, Akisue T, Fujioka H, Mizuno K, Ohgushi H, Wakitani S, Kurosaka M. Treatment of a full-thickness articular cartilage defect in the femoral condyle of an athlete with autologous bone-marrow stromal cells. Osteoarthr Cartil. 2007;15:226-31

Kurth T, Hedbom E, Shintani N, Sugimoto M, Chen FH, Haspl M, Martinovic S, Hunziker EB. Chondrogenic potential of human synovial mesenchymal stem cells in alginate. Osteoarthr Cartil. 2007;15:1178-89

Kurz B, Jin M, Patwari P, Cheng DM, Lark MW, Grodzinsky AJ. Biosynthetic response and mechanical properties of articular cartilage after injurious compression. J Orthop Surg Res. 2001;19:1140-46

Lacourt M, Gao C, Li A, Girard C, Beuchamp G, Henderson JE, Laverty S. Relationship between cartilage and subchondral bone lesions in repetitive impact trauma-induced equine osteoarthritis. Osteoarhr Cartil. 2012;20:572-83

Lane NE, Nevitt MC. Osteoarthritis, bone mass and fractures: how are they related? Arthritis Rheumatol. 2002;46:1–4

Lawless BM, Barnes SC, Espino DM, Shepherd DET. Viscoelastic properties of a spinal posterior dynamic stabilisation device. J Mech Behav Biomed Mater. 2016;59:519-26

Lawless BM, Sadeghi H, Temple DK, Dhaliwal H, Espino DM, Hukins DWL. Viscoelasticity of articular cartilage: Analysing the effect of induced stress and the restraint of bone in a dynamic environment. J Mech Behav Biomed Mater. 2017;75:293-301.

Lee KY, Mooney DJ. Alginate: properties and biomedical applications. Prog Polym Sci. 2013;37:106–26.

Levy YD, Gortz S, Pulido PA, McCauley JC, Bugbee WD. Do fresh osteochondral allografts successfully treat femoral condyle lesions? Clin Orthop Relat Res. 2013;471:231-37

Lewis PB, McCarty LP, Kang RW, Cole BJ. Basic Science and Treatment Options for Articular Cartilage Injuries. J Orhtop Sports Phys Ther. 2006;36:717-27

Lewis PR, McCutchen CW. Experimental Evidence for Weeping Lubrication in Mammalian Joints. Nature. 1959;184:1285

Lewis RJ, MacFarland AK, Anandavijayan S, Aspden RM. Material properties and biosynthetic activity of articular cartilage from the bovine carpo-metacarpal joint. Osteoarthr Cartil. 1998;6:383-92

Li B, Aspden RM. Composition and Mechanical Properties of Cancellous Bone from the Femoral Head of Patients with Osteoporosis or Osteoarthritis. J Bone Min Res. 1997;12:641-51

Li F, Su, Y, Wang J, Wu G, Wang C. Influence of dynamic load on friction behavior of human articular cartilage, stainless steel and polyvinyl alcohol hydrogel as artificial cartilage. J Mater Sci Mater Med. 2010;21:147-54.

Li F, Wang A, Wang C. Analysis of friction between articular cartilage and polyvinyl alcohol hydrogel artificial cartilage. J Mater Sci: Mater Med. 2016;27:1-8.

Li G, Yin J, Gao J, Cheng TS, Pavlos NJ, Zhang X, Zheng MH. Subchondral bone in osteoarthritis: insight into risk factors and microstructural changes. Arthritis Res Ther. 2013;15:223-34.

Li L, Fang Y, Vreeker R, Appelqvist I. Reexamining the Egg-Box Model in Calcium - Alginate Gels with X-ray Diffraction. Biomacromolecules. 2007;8:464-68.

Li LP, Korhonen RK, Iivarinen J, Jurvelin JS, Herzog W. Fluid pressure driven fibril reinforcement in creep and relaxation tests of articular cartilage. Med Eng Phys. 2008;30:182-89

Li ZC, Dai LY, Jiang LS, Qiu S. Difference in subchondral cancellous bone between postmenopausal women with hip osteoarthritis and osteoporotic fracture: Implication for fatigue microdamage, bone microarchitecture, and biomechanical properties. Arthritis Rheum. 2012;64:3955-62

Liao JF, Wang BY, Huang YX, Qu Y, Peng JR, Qian ZY. Injectable Alginate Hydrogel Cross-Linked by Calcium Gluconate-Loaded Porous Microspheres for Cartilage Tissue Engineering. ACS Omega. 2017;2:443-54.

Linn FC, Radin EL. Lubrication of animal joints. iii. the effect of certain chemical alterations of the cartilage and lubricant. Arthritis Rheum. 1968;11:674-82.

Litwic A, Edwards M, Dennison E, Cooper C. Br Med Bull. 2013;105:185-99

Liu M, Zeng X, Ma C, Yi H, Ali Z, Mou X, Li S, Deng Y, He N. Injectable hydrogels for cartilage and bone tissue engineering. Bone Res. 2017;5.

Lizhang J, Fisher J, Jin Z, Burton A, Williams S. The effect of contact stress on cartilage friction, deformation and wear. Proc Inst Mech Eng Part H: J Eng Med. 2010;225:461-75.

Loening AM, James IE, Levenston ME, Badger AM, Frank EH, Kurz B, Nuttall ME, Hung HH, Blake SM, Grodzinsky AJ, Lark MW. Injurious mechanical compression of bovine articular cartilage induces chondrocyte apoptosis. Arch Biochem Biophys. 2000;381:205-12

Loeser RF, Goldring SR, Scanzello CR, Goldring MB. Osteoarthritis. A disease of the joint as an organ. Arthritis Rheumatol. 2012;64:1697-1707

Lu XL, Su DD, Guo XE, Chen FH, Lai WM, Mow VC. Indentation Determined Mechanoelectrical Properties And Fixed Charged Density of Articular Cartilage. Ann Biomed Eng. 2004;32:370–79.

Mabuchi K, Ujihira M, Sasada T. Influence of loading duration on the start-up friction in synovial joints: measurements using a robotic system. Clin Biomech. 1998;13:492-94.

Mahmood H, Eckold D, Stead I, Shepherd DET, Espino DM, Dearn KD. A method for the assessment of the coefficient of friction of articular cartilage and a replacement biomaterial. J Mech Behav Biomed Mater. 2020a;103:103580.

Mahmood H, Shepherd DET, Espino DM. Surface damage of bovine articular cartilage-off-bone: the effect of variations in underlying substrate and frequency. BMC Musculoskelet Disord. 2018;19:384-94.

Mahmood H, Shepherd DET, Espino DM. A technique for measuring the frictional torque of articular cartilage and replacement biomaterials. Med Eng Phys. 2020b. Unpublished results

Mak AF, Lai WM, Mow VC. Biphasic indentation of articular cartilage – I. Theoretical analysis. J Biomechanics. 1987;20:703-14

Malekipour F, Whitton C, Oetomo D, Lee PV. Shock absorbing ability of articular cartilage and subchondral bone under impact compression. J Mech Behav Biomed Mater. 2013;26:127-35

Mang T, Dresel W. Lubricants and Lubrication, 2nd, Completely Revised and Extended Edition., Germany: Wiley-VCH; 2007, p.14

Mansfied J, Yu J, Attenburrow D, Moger J, Tirlapur U, Urban J, Cui Z, Winlove P. The elastin network: its relationship with collagen and cells in articular cartilage as visualized by multiphoton microscopy. J Anat. 2009;215:682-91

Mansfield JC, Bell JS, Winlove CP. The micromechanics of the superficial zone of articular cartilage. Osteoarthr Cartil. 2015;23:1806-16

McCrae F, Shouls J, Dieppe P, Watt I. Scintigraphic assessment of osteoarthritis of the knee joint. Ann Rheum Dis. 1992;51:938-42

McCulloch PC, Kang RW, Sobhy MH, Hayden JK, Cole BJ. Prospective evaluation of prolonged fresh osteochondral allograft transplantation of the femoral condyle: minimum 2-year follow-up. Am J Sports Med. 2007;35:411-20

McCutchen CW. Mechanism of Animal Joints: Sponge-hydrostatic and Weeping Bearings. Nature. 1959;184:1284-85

McCutchen CW. The frictional properties of animal joints. Wear. 1962;5:1-17.

Mcilwraith CW, Frisbie DD, Kawcak CE, Weeren RV. Joint Disease in The Horse, second ed., Missouri: Elsevier; 2016; p. 10

McNary SM, Athanasiou KA, Reddi AH. Engineering Lubrication in Articular Cartilage. Tissue Eng Part B Rev. 2012;18:88-100

Merkle TP, Beckmann N, Bruckner T, Zeifang F. Shoulder joint replacement can improve quality of life and outcome in patients with dysmelia: a case series. BMC Musculoskeletal Disord. 2016;17:185

Milner PE, Parkes M, Puetzer JL. Chapman R, Stevens MM, Cann P, Jeffers JRT. A low friction, biphasic and boundary lubricating hydrogel for cartilage replacement. Acta Biomater. 2018;65:102-11.

Moghadas P, Mahomed A, Hukins DWL, Shepherd DET. Friction in metal-on-metal total disc arthroplasty: Effect of ball radius. J Biomech. 2012;45:504-9.

Moghadas P, Mahomed A, Hukins DWL. Effect of lubricants on friction in laboratory tests of a total disc replacement device. Proc Inst Mech Eng H: J Eng Med. 2013;227:988-93.

Moore AC, Burris DL. Tribological rehydration of cartilage and its potential role in preserving joint health. Osteoarthr Cartil. 2017;25:99-107.

Morris BA, D'Lima DD, Slamin J, Kovacevic N, Arms SW, Townsend CP, Colwell CW. e-Knee: evolution of the electronic knee prosthesis. Telemetry technology development. J Bone Joint Surg Am. 2001;83-A Suppl 2(Pt 1):62-6

Mow VC, Edward GX. Mechano-Electrochemical Properties of Articular Cartilage: Their Inhomogeneities and Anisotropies. Ann Rev Biomed Eng. 2002;4:175-209

Mow VC, Gibbs MC, Lai WM, Zhu WB, Athanasiou KA. Biphasic indentation of articular cartilage – II. A numerical algorithm and an experimental study. J Biomechanics. 1989;22:853-61

Murakami T, Higaki H, Sawae Y, Ohtsuki N, Moriyama S, Nakanishi Y. Adaptive multimode lubrication in natural synovial joints and artificial joints. Proc Inst Mech Eng Part H: J Eng Med. 1998;212:23-35.

Na Y, Shi Y, Liu W, Jia Y, Kong L, Zhang T, Han C, Ren Y. Is Implantation of autologous chondrocytes superior to microfracture for articular cartilage defects of the knee? A systematic review of 5-year follow-up data. Int J Sur. 2019;68:56-62

Nevitt MC, Lane NE, Scott JC, Hochberg MC, Pressman AR, Genant HK, Cummings SR. Radiographic osteoarthritis of the hip and bone mineral density. Arthritis Rheumatol. 1995;38:907–16

Nguyen D, Hagg DA, Forsman A, Ekholm J, Nimkingratana P, Brantsing C, Kalogeropoulos T, Zaunz S, Concaro S, Brittberg M, Lindahl A, Gatenholm P, Enejder A, Simonsson S. Cartilage Tissue Engineering by the 3D Bioprinting of iPS Cells in a Nanocellulose/Alginate Bioink. Scientific Reports. 2017;7:658

Nia HT, Han L, Li Y, Ortiz C, Grodzinsky A. Poroelasticity of cartilage at the nanoscale. Biophys J. 2011;101:2304-13

Nickien M, Heuijerjans A, Ito K, Donkelaar CCV. Comparison between in vitro and in vivo cartilage overloading studies based on a systematic literature review. J Orthop Res. 2018;36:2076-86.

NIH Consensus Development Panel. Osteoporosis Prevention, Diagnosis, and Therapy. JAMA. 2001;285:785-95

Northwood E, Fisher J. A multi-directional in vitro investigation into friction, damage and wear of innovative chondroplasty materials against articular cartilage. Clin Biomech. 2007;22:834–42.

O'Brien FJ. Biomaterials & scaffolds for tissue engineering. Mater Today. 2011;14:88-95

Oegema TR, Carpenter RJ, Hofmeister F, Thompson RC. The Interaction of the Zone of Calcified Cartilage and Subchondral Bone in Osteoarthritis. Microsc Res Tech. 1997;37:324-32

Oungoulian SR, Durney KM, Jones BK, Ahmad CS, Hung CT, Ateshian GA. Wear and damage of articular cartilage with friction against orthopedic implant materials. J Biomech. 2015;48:1957–64.

Outerbridge RE. The Etiology of Chondromalacia Patellae. J Bone Joint Surg. 1961;43-B:752-57

Park H, Choi B, Hu J, Lee M. Injectable chitosan hyaluronic acid hydrogels for cartilage tissue engineering. Acta Biomater. 2013;9:4779-86

Park S, Hung CT, Ateshian GA. Mechanical response of bovine articular cartilage under dynamic unconfined compression loading at physiological stress levels. Osteoarthr Cartil. 2004;12:65-73

Parsons JR, Black J. The viscoelastic shear behaviour of normal rabbit articular cartilage. J Biomech. 1977;10:21-9

Patel PSD, Shepherd DET, Hukins DWL. Compressive properties of commercially available polyurethane foams as mechanical models for osteoporotic human cancellous bone. BMC Musculoskelet Disord. 2008;9:137

Paterson SI, Amin AK, Hall AC. Airflow accelerates bovine and human articular cartilage drying and chondrocyte death. Osteoarthr Cartil. 2015;23:257-65

Pauli C, Whiteside R, Heras FL, Nesic D, Koziol J, Grogan SP, Matyas J, Pritzker KPH, D'Lima DD, Lotz MK. Comparison of cartilage histopathology assessment systems on human knee joints at all stages of osteoarthritis development. Osteoarthr Cartil. 2012;20:476-85

Pearle AD, Warren RF, Rodeo SA. Basic Science of Articular Cartilage and Osteoarthritis. Clin Sports Med. 2005;24:1-12

Pearson B, Espino DM. Effect of hydration on the frequency-dependent viscoelastic properties of articular cartilage. Proc Inst Mech Eng H: J Eng Med. 2013;227:1246-52

Peters AE, Comerford EJ, Macaulay S, Bates KT, Akhtar R. Micromechanical properties of canine femoral articular cartilage following multiple freeze-thaw cycles. J Mech Behav Biomed Mater. 2017;71:114-21

Philp AM, Davis ET, Jones SW. Developing anti-inflammatory therapeutics for patients with osteoarthritis. Rheumatol. 2017;56:869-81

Portalatin-Vazquez N, Kilmer CE, Panitch A, Liu JC. Characterisation of Collagen Type I and II Blended Hydrogels for Articular Cartilage Tissue Engineering. Biomacromolecules. 2016;17:3145-52

Radin EL, Parker HG, Pugh JW, Steinberg RS, Paul IL, Rose RM. Response of joints to impact loading - III. Relationship between trabecular microfractures and cartilage degeneration. J Biomech. 1973;6:51-54

Radin EL, Paul IL, Rose RM. Role of Mechanical Factors in Pathogenesis of Primary Osteoarthritis. Lancet. 1972;56:869-81

Radin EL, Paul IL, Tolkoff MJ. Subchondral bone changes in patients with early degenerative joint disease. Arthritis Rheumatol. 1970;13:400–5.

Radin EL, Rose RM. Role of subchondral bone in the initiation and progression of cartilage damage. Clin Orthop Relat Res. 1986;213:34–40

Ramachandran M. Basic Orthopaedic Sciences, in: Lubrication., New York: Taylor and Francis Group; 2017, p.153

Rawal BR, Ribeiro R, Chouksey M, Tripathi K. Biomaterials for Cartilage Repair: A Review. J Med Sci. 2013;13:615-20.

Rieppo J, Halmesmaki EP, Siitonen U, Laasanen MS, Toyras J, Kiviranta I, Hyttinen MM, Jurvelin JS, Helminen HJ. Histological differences of human, bovine and porcine cartilage. 49th Annual Meeting of the Orthopaedic Research Society. 2002;57:1998

Riff AJ, Yanke AB, Shin JJ, Romeo AA, Cole BJ. Midterm results of osteochondral allograft transplantation to the humeral head. J Shoulder Elbow Surg. 2017;26:E207-15

Rutgers M, Van-Pelt MJP, Dhert WJA, Creemers LB, Saris DBF. Evaluation of histological scoring systems for tissue-engineered, repaired and osteoarthritic cartilage. Osteoarthr Cartil. 2010;18:12-23

Ryan JA, Eisner EA, DuRaine G, You Z, Reddi AH. Mechanical Compression of Articular Cartilage Induces Chondrocyte Proliferation and Inhibits Proteoglycan Synthesis by Activation of the Erk Pathway: Implications for Tissue Engineering and Regenerative Medicine. J Tissue Eng Regen Med. 2009;3:107-16

Sadeghi H, Espino DM, Shepherd DET. Fatigue strength of bovine articular cartilage-on-bone under three-point bending: the effect of loading frequency. BMC Musculoskelet Disord. 2017;18:142

Sadeghi H, Lawless BM, Espino DM, Shepherd DET. Effect of frequency on crack growth in articular cartilage. J Mech Behav Biomed Mater. 2018;77:40-46.

Sadeghi H, Shepherd DET, Espino DM. Effect of the variation of loading frequency on surface failure of bovine articular cartilage. Osteoarthr Cartil. 2015;23:2252-58.

Sánchez-Téllez DA, Téllez-Jurado L, Rodríguez-Lorenzo LM. Hydrogels for cartilage regeneration, from polysaccharides to hybrids. Polymers. 2017;9:1-32

Sandell LJ, Aigner T. Articular cartilage and changes in arthritis. An introduction: Cell biology of osteoarthritis. Arthritis Res. 2001;3:107-13.

Schenau GJVI. From rotation to translation: Constrains on multi-joint movements and the unique action of bi-articular muscles. Hum Mov Sci. 1989;8:301-37

Schmidt TA, Gastelum NS, Nguyen QT, Schumacher BL, Sah RL. Boundary lubrication of articular cartilage: Role of synovial fluid constituents. Arth Rheum. 2007;56:882-91

Schmidt TA, Sah RL. Effect of synovial fluid on boundary lubrication of articular cartilage. Osteoarthr Cartil. 2007;15:35-47

Sen R, Hurley JA. Osteoarthritis. StatPearls Publishing. 2019

Shang W, Liu Y, Wan W, Hu C, Liu Z, Wong CT, Fukuda T, Shen Y. Hybrid 3D printing and electrodeposition approach for controllable 3D alginate hydrogel formation. Biofabrication. 2017;9.

Shen Y, Zhang YH, Shen L. Postmenopausal women with osteoporosis and osteoarthritis show different microstructural characteristics of trabecular bone in proximal tibia using high-resolution magnetic resonance imaging at 3 tesla. BMC Musculoskelet Disord. 2013;15:136

Shepherd DET, Seedhom BB. A technique for measuring the compressive modulus of articular cartilage under physiological loading rates with preliminary results. Proc Inst Mech Eng H: J Eng Med. 1997;211:155-65.

Shepherd DET, Seedhom BB. Thickness of human articular cartilage in joints of the lower limb. Ann Rheum Dis. 1999;58:27-34

Shetty N, Bendall S. Understanding the gait cycle, as it relates to the foot. Orthop Trauma. 2011;25:236-40

Singh N. Synovial Joints and Lubrication mechanisms. IJCAM. 2017;12:29-33

Sotres J, Arnebrant T. Experimental Investigations of Biological Lubrication at the Nanoscale: The Cases of Synovial Joints and the Oral Cavity. Lubricants. 2013;1:102-31.

Sowers MF, Hochberg M, Crabbe JP, Muhich A, Crutchfield M, Updike S. Association of bone mineral density and sex hormone levels with osteoarthritis of the hand and knee in premenopausal women. Am J Epidemiol. 1996;143:38-47

Sowers MF, Lachance L, Jamadar D, Hochberg MC, Hollis B, Crutchfield M, Jannausch ML. The associations of bone mineral density and bone turnover markers with osteoarthritis of the hand and knee in pre-and perimenopausal women. Arthritis Rheumatol. 1999;42:483–9.

Spiller KL, Maher SA, Lowman AM. Hydrogels for the Repair of Articular Cartilage Defects. Tissue Eng Part B Rev. 2011;17:281-99.

Steadman JR, Rodkey WG, Briggs KK. Microfracture. Cartilage. 2010;1:78-86

Steinert AF, Ghivizzani SC, Rethwilm A, Tuan RS, Evans CH, Noth U. Major biological obstacles for persistent cell-based regeneration of articular cartilage. Arthritis Res Ther. 2007;9:213

Stewart HL, Kawcak CE. The Importance of Subchondral Bone in the Pathophysiology of Osteoarthritis. Front Vet Sci. 2018;5:178

Suponenkovs A, Platkajis A, Glazs A. Development of methods for analysis of knee articular cartilage degeneration by magnetic resonance imaging data. J Phys Conf Ser. 2017;818:012001

Swann AC, Seedhom BB. The stiffness of normal articular cartilage and the predominant acting stress levels: Implications for the aetiology of osteoarthritis. Rheumatol. 1993;32:16-25

Szarko M, Muldrew K, Bertram JEA. Freeze-thaw treatment effects on the dynamic mechanical properties of articular cartilage. BMC Musculoskelet Disord. 2010;11:231-38.

Szeparowicz P, Popko J, Sawicki B, Wolczynski S. Is the repair of articular cartilage lesion by costal chondrocyte transplantation donor age-dependent? An experimental study in rabbits. Folia Histochem Cytobiol. 2006;44:201-06

Tamayol A, Akbari M, Annabi N, Paul A, Khademhosseini A, Juncker D. Fiber-Based Tissue Engineering: Process, Challenged and Opportunities. Biotechnol Adv. 2014;31:669-87

Tanner RI. An Alternative Mechanism for the Lubrication of Synovial Joints. Phys Med Biol. 1966;11:119-27.

Tarafder S, Lee CH. Synovial Joint: In Situ Regeneration of Osteochondral and Fibrocartilaginous Tissues by Homing of Endogenous Cells. In Situ Tissue Regeneration, New York: Elsevier Inc; 2016, p. 253-267.

Taylor B. Tutorial – Hertz Contact Stress. OPTI521. 2016

Teichtahl AJ, Wang Y, Wluka AE, Strauss BJ, Proietto J, Dixon JB, Jones G, Cicuttini FM. Associations between systemic bone mineral density and early knee cartilage changes in middle-aged adults without clinical knee disease: a prospective cohort study. Arthritis Res Ther. 2017;19:98

Teichtahl AJ, Wluka AE, Wijethilake P, Wang Y, Zadeh AG, Cicuttini FM. Wolff's law in action: a mechanism for early knee osteoarthritis. Arthritis Res Ther. 2015;17:207

Temple DK, Cederlund AA, Lawless BM, Aspden RM, Espino DM. Viscoelastic properties of human and bovine articular cartilage: a comparison of frequency-dependent trends. BMC Musculoskelet Disord. 2016;17:419-26.

Theo M, Wilfried D. Lubricants in the Tribological System, in: Lubricants and Lubrication, second ed., Germany: Wiley-VCH; 2007, p. 14

Thomas DP, King B, Stephens T, Dingle JT. In vivo studies of cartilage regeneration after damage induced by catabolin/interleukin-1. Ann Rheum Dis. 1991;50:75-80

Tiku ML, Sabaawy HE. Cartilage regeneration for treatment of osteoarthritis: a paradigm for nonsurgical intervention. Ther Adv Musculoskelet Dis. 2015;7:76-87

Tong L, Hao Z, Wan C, Wen S. Detection of depth-depend changes in porcine cartilage after wear test using Raman spectroscopy. J Biophotonics. 2018;11:e201700217

Umberger BR. Stance and swing phase costs in human walking. J R Soc Interface. 2010;7:1329-40

Unsworth A, Dowson D, Wright V. Some new evidence on human joint lubrication. Ann Rheum Dis. 1975;34:277-85

Vazquez KJ, Andreae JT, Henak CR. Cartilage-on-cartilage cyclic loading induces mechanical and structural damage. J Mech Behav Biomed Mater. 2019;98:262-67

Venkatesan J, Bhatnagar I, Manivasagan P, Kang KH, Kim SK. Alginate composites for bone tissue engineering: A review. Int J Bio Macro. 2015;72:269-81

Verteramo A, Seedhom BB. Effect of a single impact loading on the structure and mechanical properties of articular cartilage. J Biomech. 2007;40:3580-9

Wands I, Shepherd DET, Hukins DWL. Viscoelastic properties of composites of calcium alginate and hydroxyapatite. J Mater Sci: Mater Med. 2008;19:2417–21.

Wang CC, Yang KC, Lin KH, Liu YL, Liu HC, Lin FH. Cartilage regeneration in SCID mice using a highly organised three-dimensional alginate scaffold. Biomater. 2012;33:120-7

Wang H, Ateshian GA. The normal stress effect and equilibrium friction coefficient of articular cartilage under steady frictional shear. J Biomech. 1997;30:771-6

Warnecke D, MeBemer M, Roy LD, Stein S, Gentilini C, Walker R, Skaer N, Ignatius A, Durselen L. Articular cartilage and meniscus reveal higher friction in swing phase than in stance phase under dynamic gait conditions. Sci Rep. 2019;9:5785.

Warner MD, Taylor WR, Clift SE. Finite element biphasic indentation of cartilage: A comparison of experimental indenter and physiological contact geometries. Proc Inst Mech Eng Part H: J Eng Med. 2001;215:487-96

Weightman BO, Freeman MAR, Swanson SAV. Fatigue of articular cartilage. Nature. 1973;244:303-04

Whitney GA, Jayaraman K, Dennis JE, Mansour JM. Scaffold-free cartilage subjected to frictional shear stress demonstrates damage by cracking and surface peeling. J Tissue Eng Regen Med. 2017;11:412-24

Whitney GA, Mansour JM, Dennis JE. Coefficient of Friction Patterns Can Identify Damage in Native and Engineered Cartilage Subjected to Frictional-Shear Stress. Ann Biomed Eng. 2015;43:2056-68

Wright V, Dowson D. Lubrication and cartilage. J Anat. 1976;121:107-18

Yang G, Ma J, Carlson BE, Wang HP, Atabaki MM, Kovacevic R. Decreasing the surface roughness of aluminium alloy welds fabricated by a dual beam laser. Mater Des. 2017;127:287-96.

Yao JQ, Seedhom BB. Mechanical conditioning of articular cartilage to prevalent stresses. Br J Rheumatol. 1993;32:956–65.

Yarimitsu S, Sasaki S, Murakami T, Suzuki A. Evaluation of lubrication properties of hydrogel artificial cartilage materials for joint prosthesis. Biosurface and Biotribology. 2016;2:40-47.

Yousif AE, Al-allaq AA. The hydrodynamic squeeze film lubrication of the ankle joint. IJMEA. 2013;1:34-42

Zhang Y, Hannan MT, Chaisson CE, McAlindon TE, Evans SR, Aliabadi P, Levy D, Felson DT. Bone mineral density and risk of incident and progressive radiographic knee osteoarthritis in women: the Framingham study. J Rheumatol. 2000;27:1032–7

Zhao L, Weir MD, Xu HHK. An injectable calcium phosphate-alginate hydrogel-umbilical cord mesenchymal stem cell paste for bone tissue engineering. Biomaterials. 2010;31:6502-10.

Appendix A - Preliminary Experiments for Chapter 3

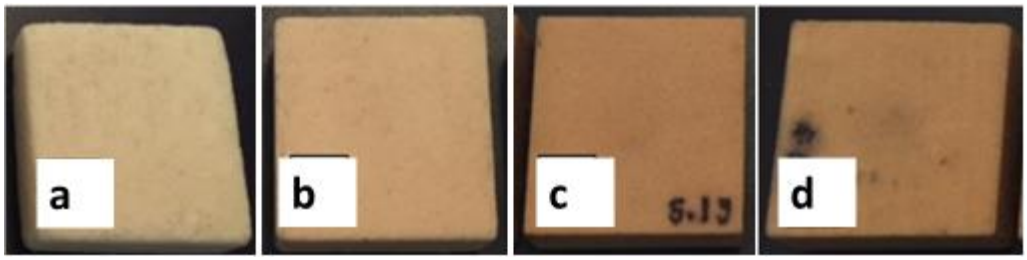

Figure 3.5: The four substrates utilised for this investigation presented in the chapter. a-d represents the substrate with the lowest to highest density, relating to substrate 1-4, respectively.

In order to achieve a suitable mechanical testing protocol for the evaluation presented in Chapter 3, preliminary tests were conducted. The data obtained from preliminary tests was essential to guide a final testing protocol with appropriate frequencies at loading, as well as the selection of the range of the induced mechanical load. The range was identified based on the most effective load to apply for damage inducing to both on- and off-bone cartilage. A pre-load for all tests of 0.2 N was initially applied to the cartilage specimen, to ensure the indenter was in contact with the specimen prior to and throughout testing. A load from 9 to 30 N was applied to cartilage off-bone, in load-control, as shown in Figure part a).

Additionally, a load of 6 to 160 N was applied to cartilage on-bone, illustrated in Figure part b). The range of loads tested in each case were based upon results from preliminary tests of the minimum and maximum loads to accommodate for both cartilage on- and off-bone. Thus, following on from the preliminary tests, the force region of 5-50 N was chosen as the suitable range to investigate for both on- and off-bone cartilage. This range was selected in light of preventing unnecessary compression to the cartilage off-bone, whilst testing cartilage on-bone to a higher load. The unnecessary compression could otherwise have caused an effect on the resulting damage observed.

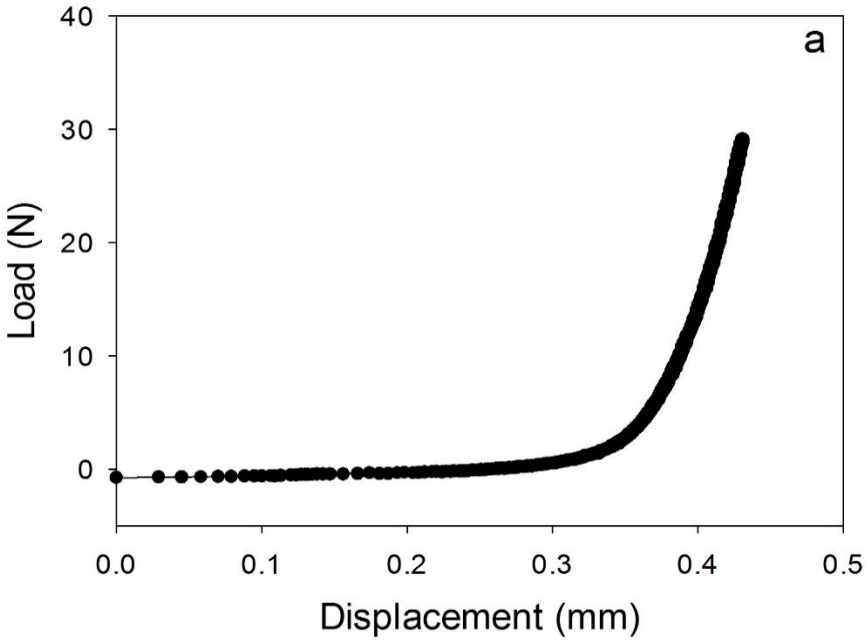

Load vs Displacement for cartilage off-bone

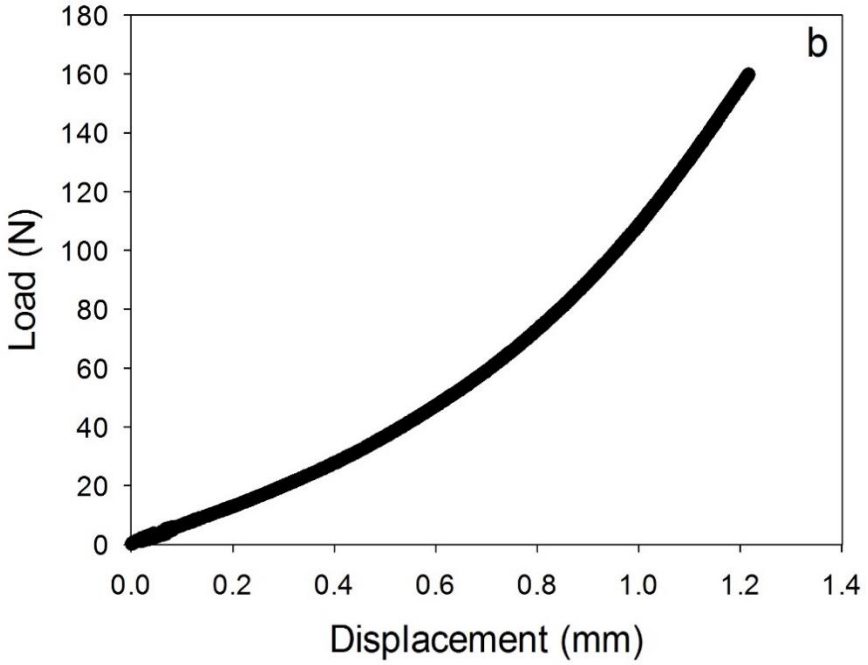

Load vs Displacement plot for cartilage on-bone

Appendix B – Cartilage off-bone Experimental Results for Chapter 3

Articular cartilage images captured prior to, and post testing, following the confirmation of damage absence with India ink are displayed in this appendix section; B for off-bone and C for on-bone cartilage. All results are displayed with respect to the four substrates at the corresponding frequency tested. Before images at each repeat of six for every test type are displayed at the upper segment, whilst images captured post-test are displayed as its counterpart, in the lower segment.

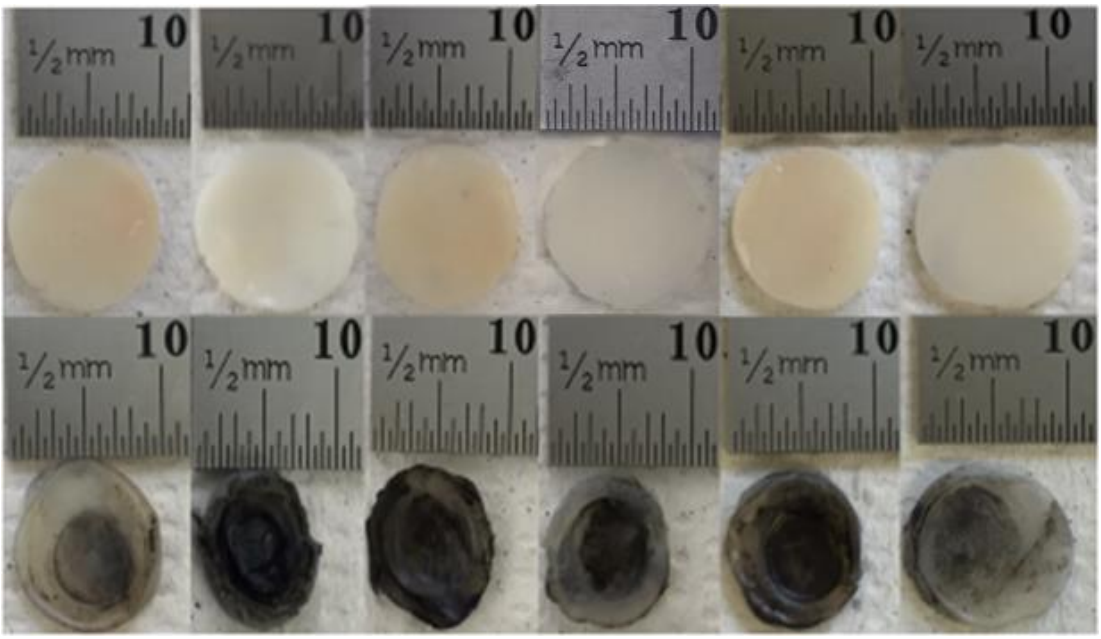

Results for off-bone cartilage at 1 Hz of testing on substrate one.

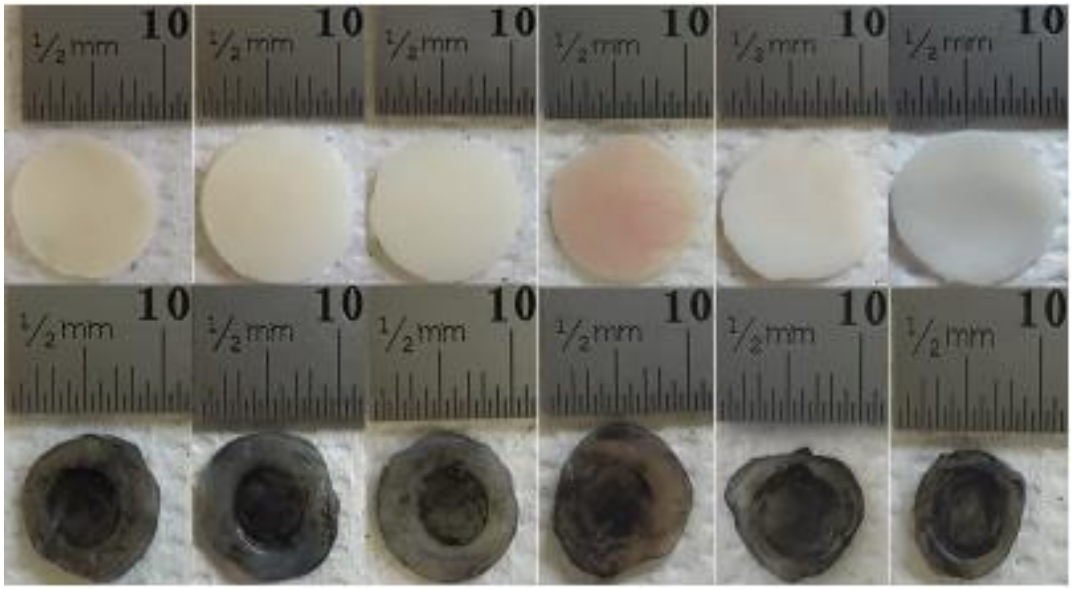

Results for off-bone cartilage at 1 Hz of testing on substrate two.

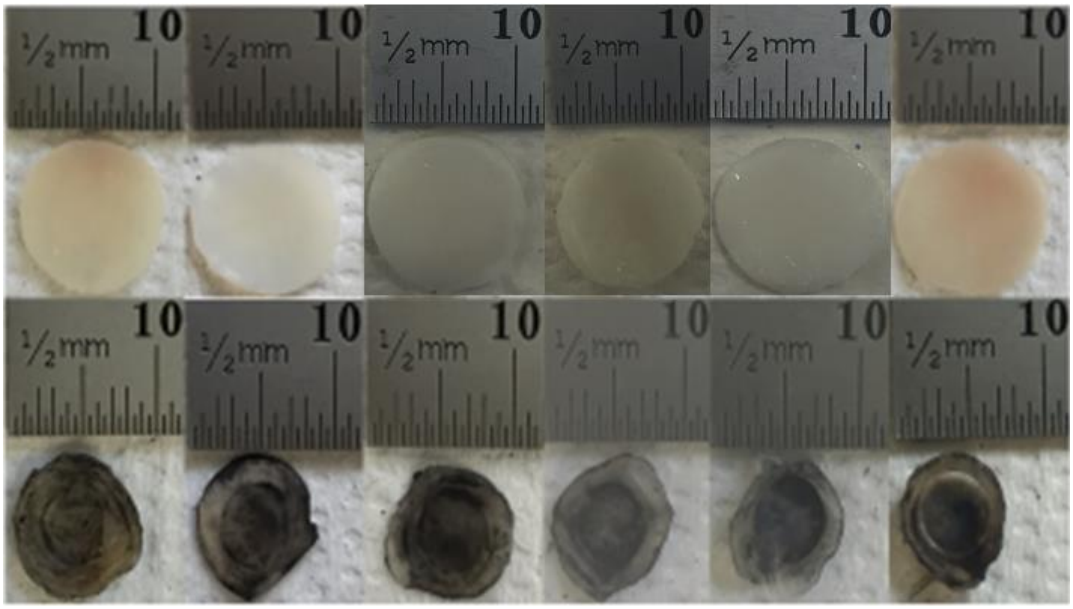

Results for off-bone cartilage at 1 Hz of testing on substrate three.

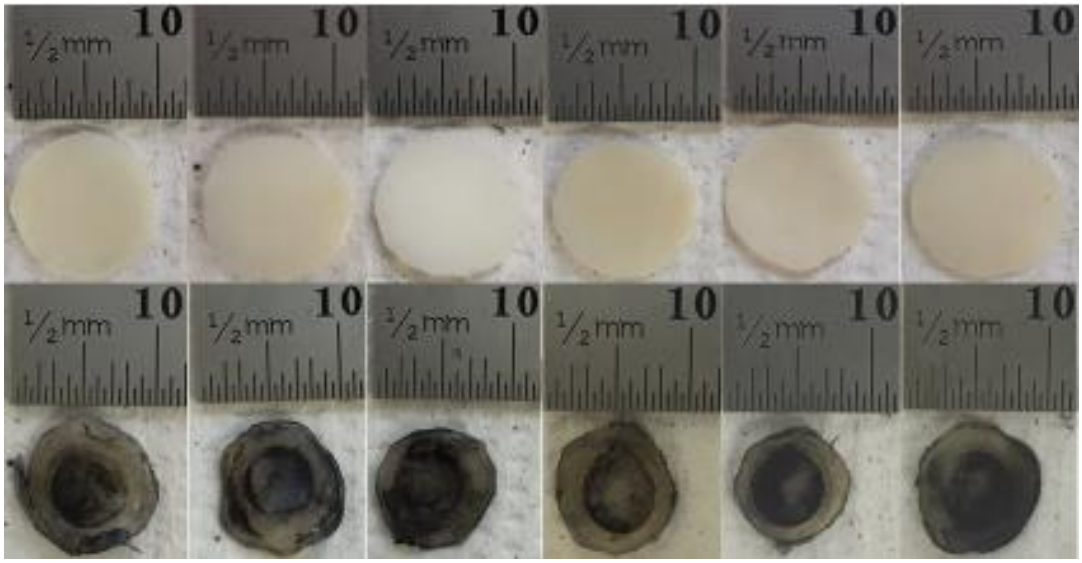

Results for off-bone cartilage at 1 Hz of testing on substrate four.

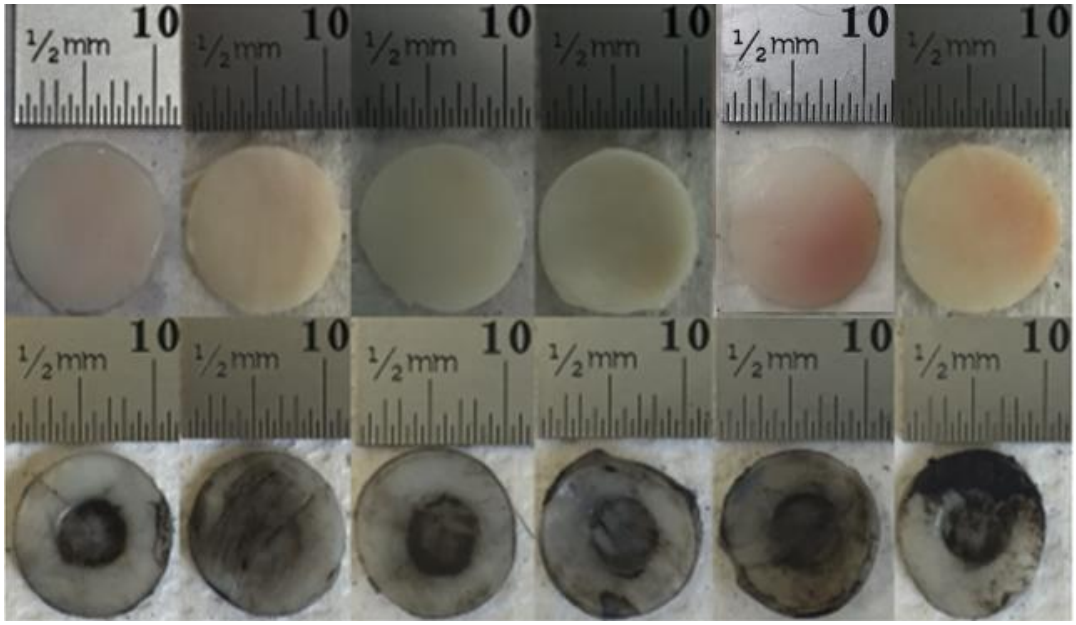

Results for off-bone cartilage at 10 Hz of testing on substrate one.

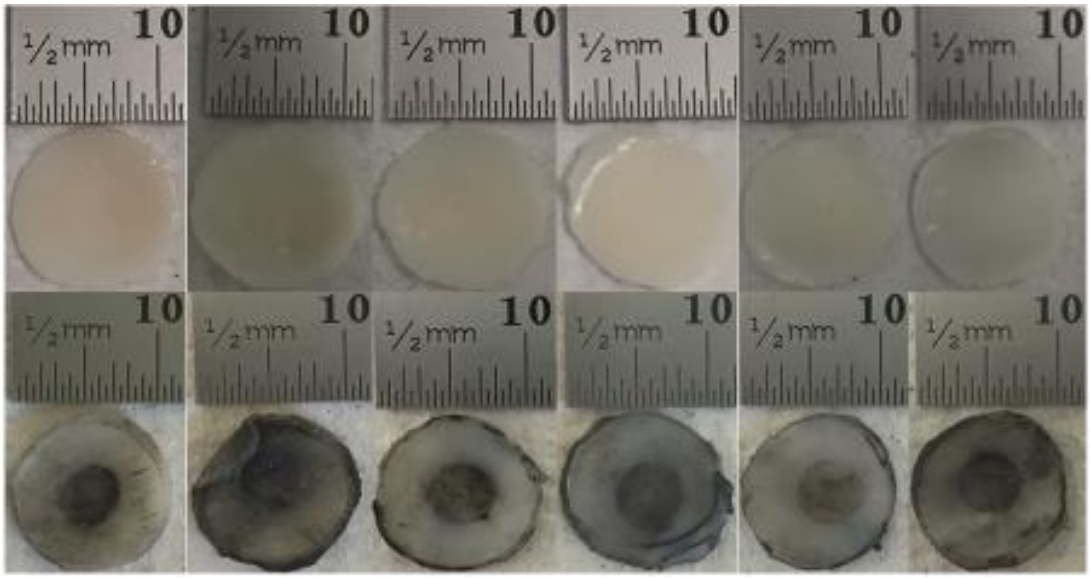

Results for off-bone cartilage at 10 Hz of testing on substrate two.

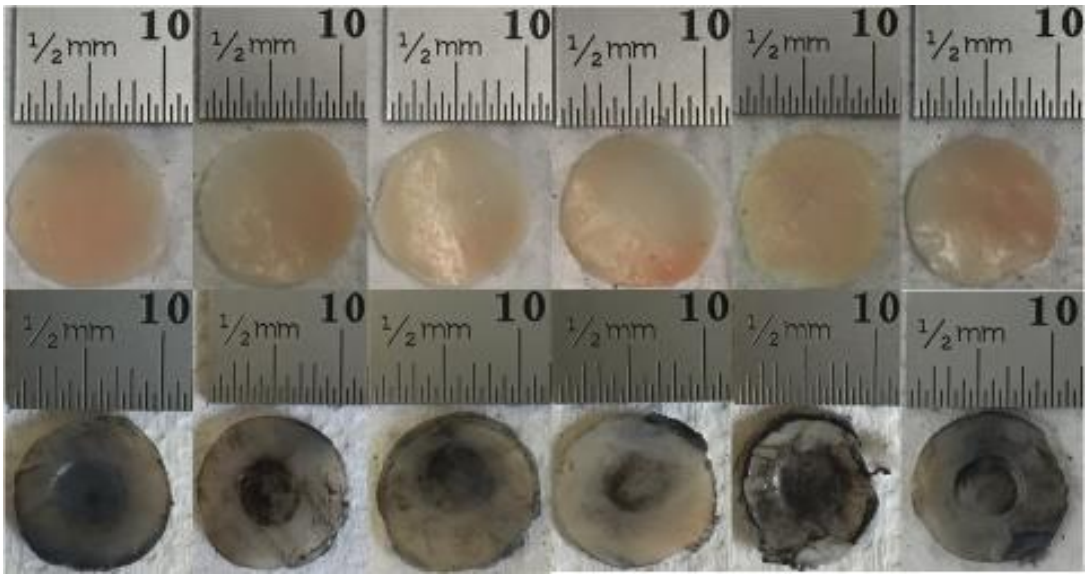

Results for off-bone cartilage at 10 Hz of testing on substrate three.

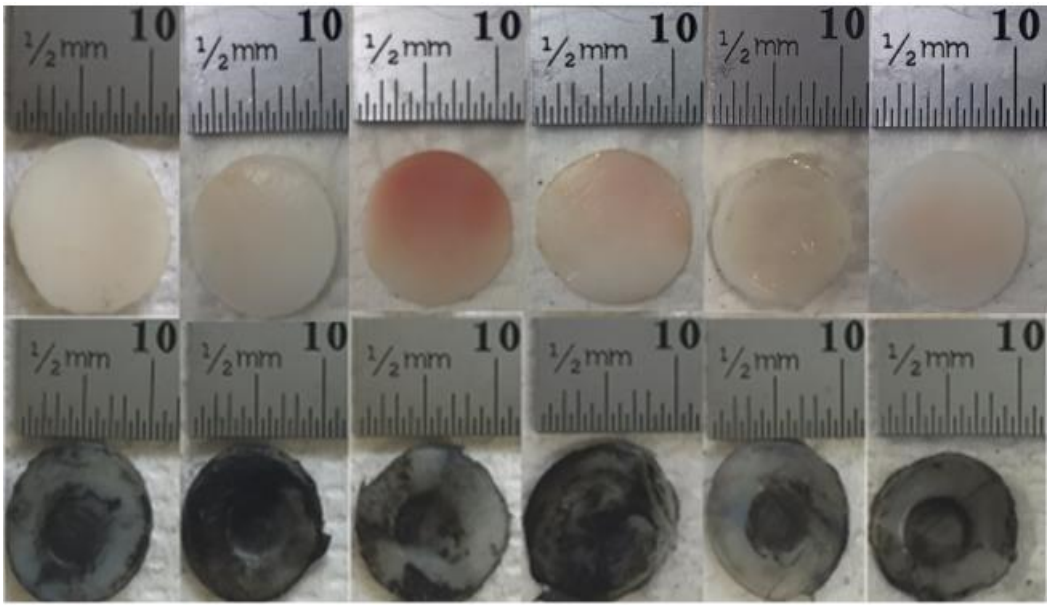

Results for off-bone cartilage at 10 Hz of testing on substrate four.

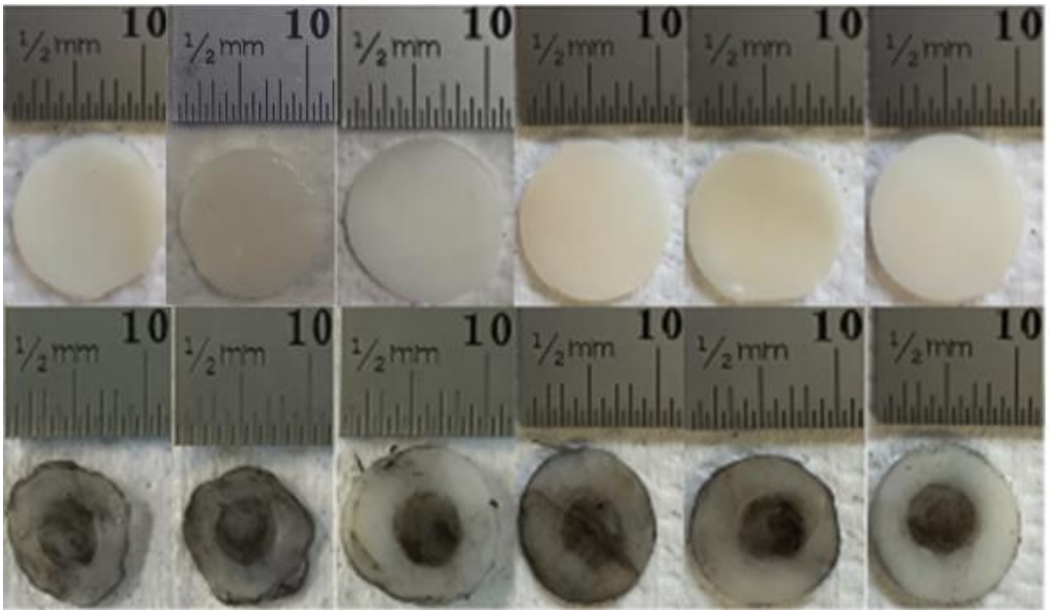

Results for off-bone cartilage at 50 Hz of testing on substrate one.

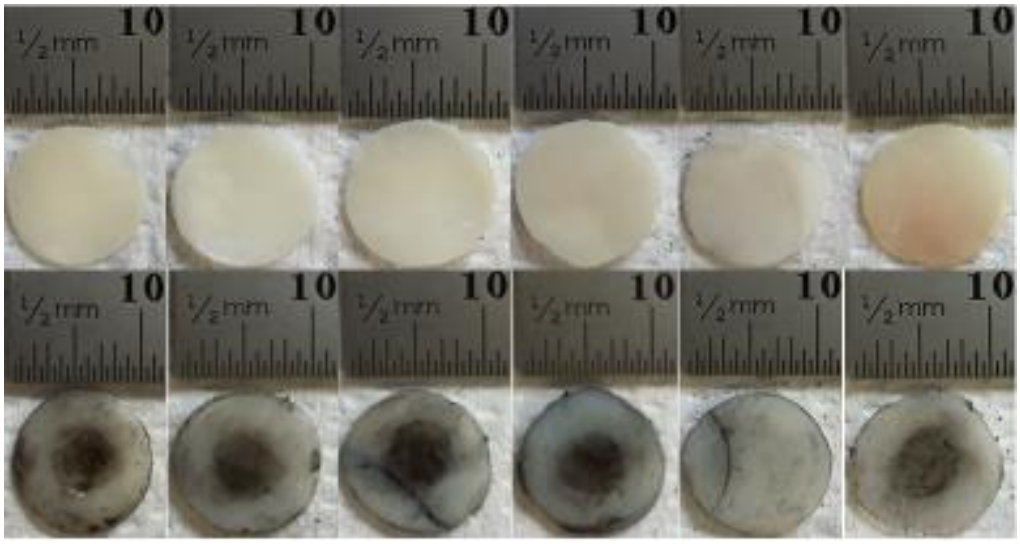

Results for off-bone cartilage at 50 Hz of testing on substrate two.

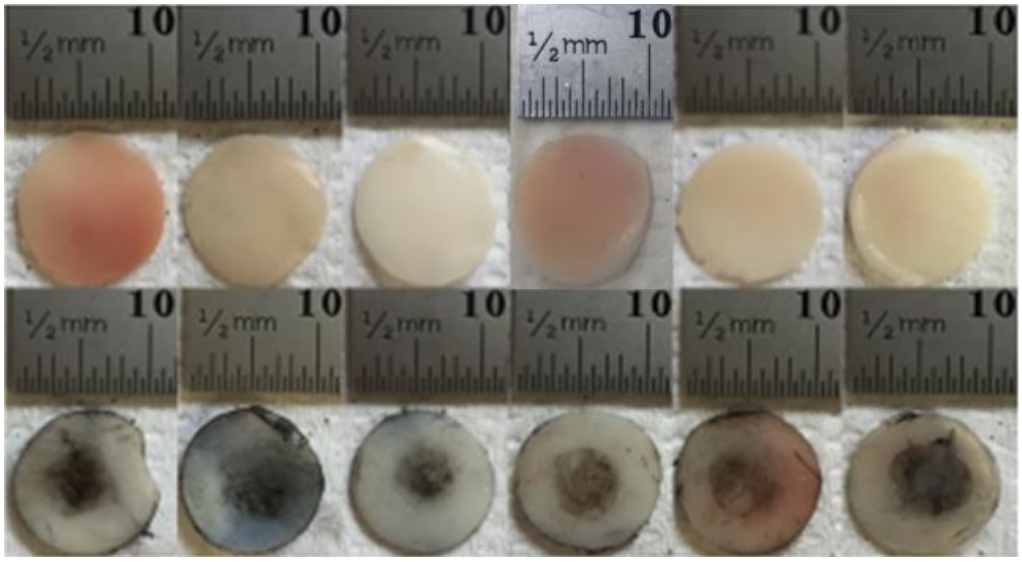

Results for off-bone cartilage at 50 Hz of testing on substrate three.

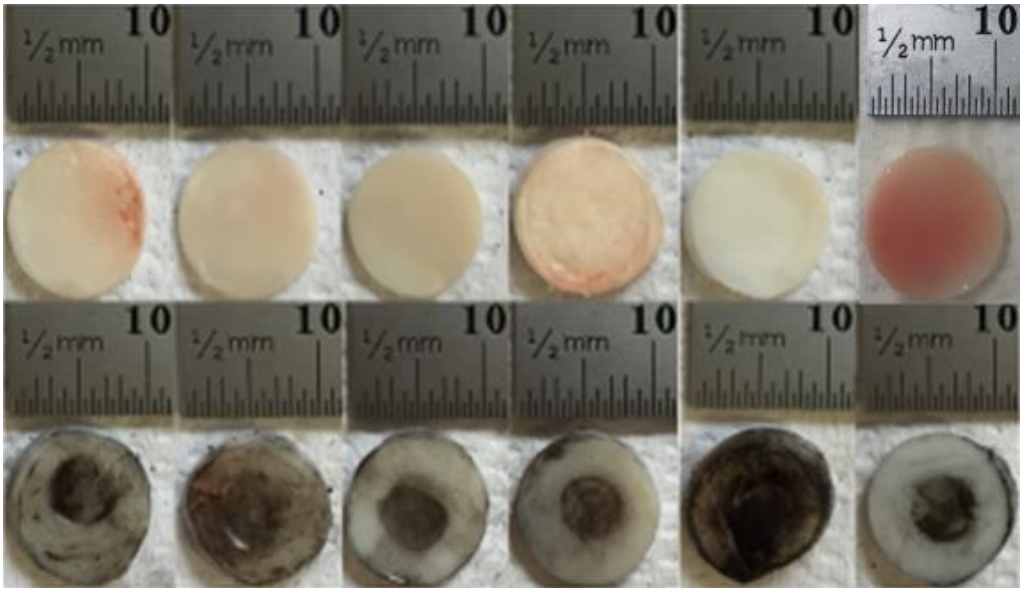

Results for off-bone cartilage at 50 Hz of testing on substrate four.

Appendix C – Cartilage on-bone Experimental Results for Chapter 3

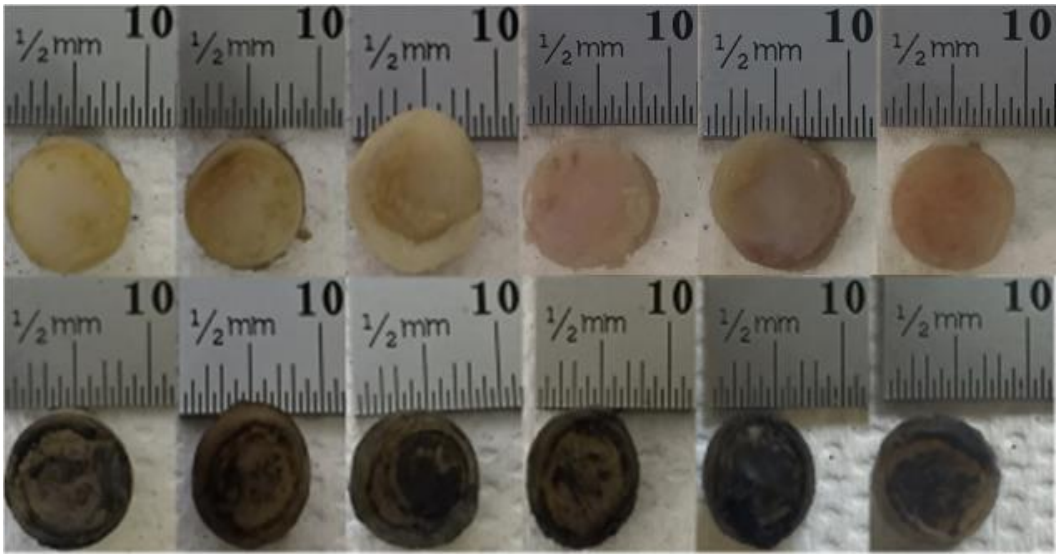

Results for on-bone cartilage at 1 Hz of testing on substrate one.

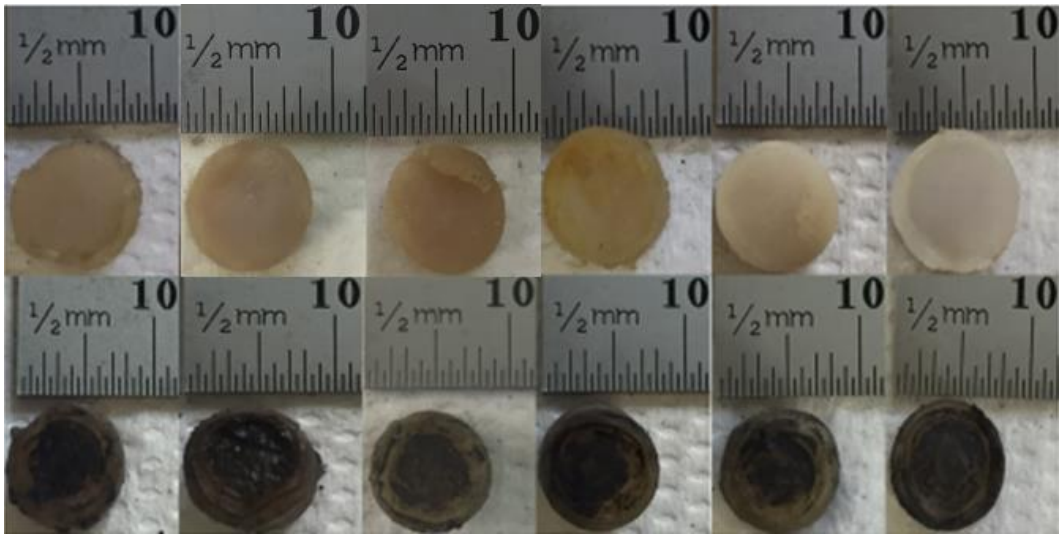

Results for on-bone cartilage at 1 Hz of testing on substrate two.

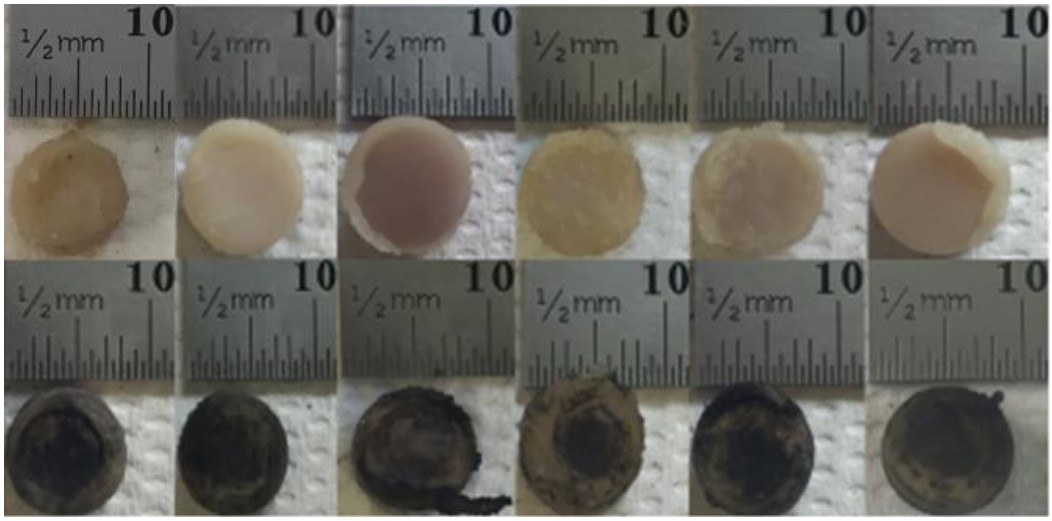

Results for on-bone cartilage at 1 Hz of testing on substrate three.

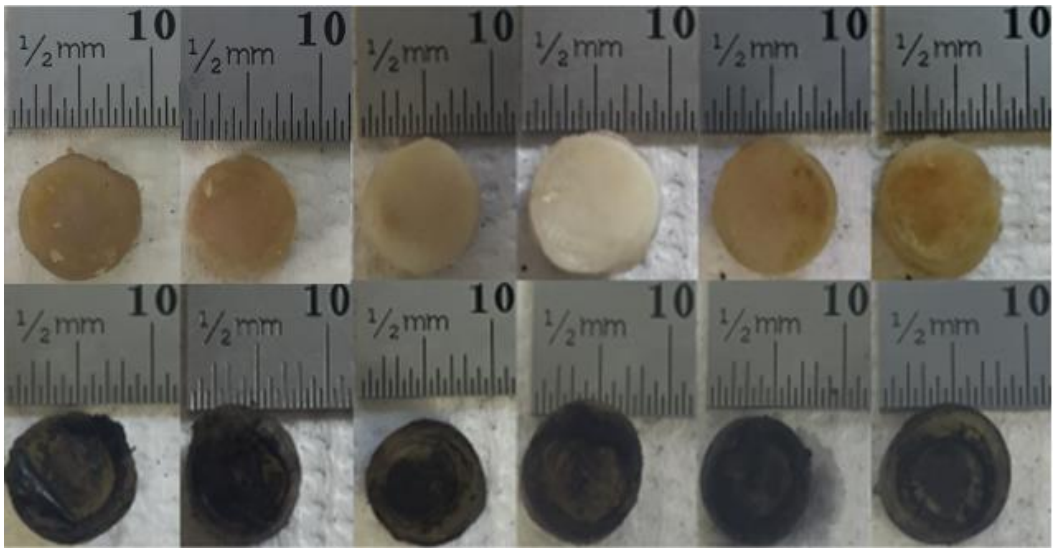

Results for on-bone cartilage at 1 Hz of testing on substrate four.

Results for on-bone cartilage at 10 Hz of testing on substrate one.

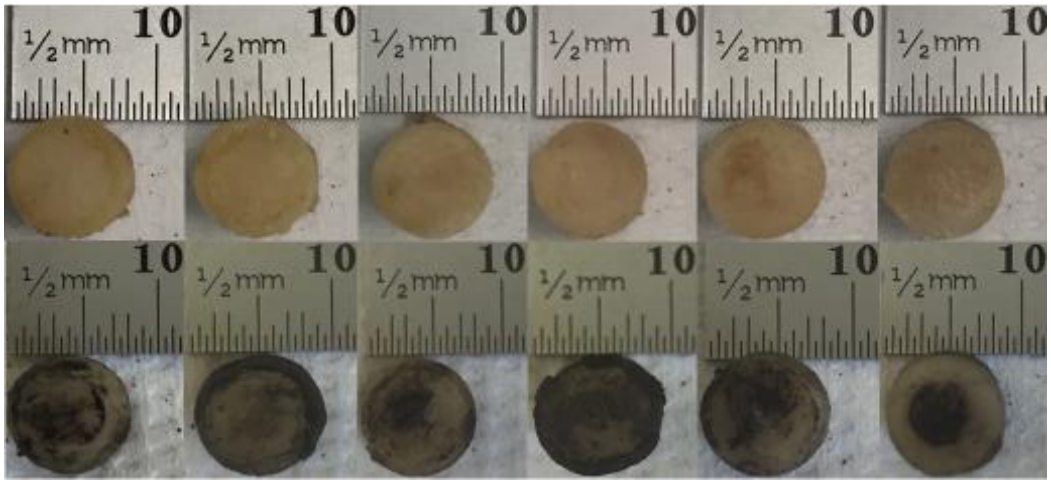

Results for on-bone cartilage at 10 Hz of testing on substrate two.

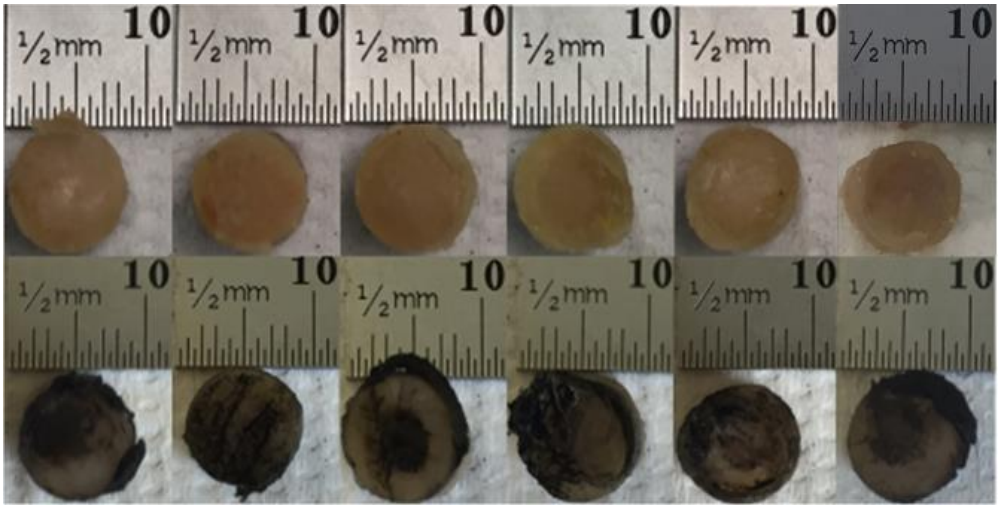

Results for on-bone cartilage at 10 Hz of testing on substrate three.

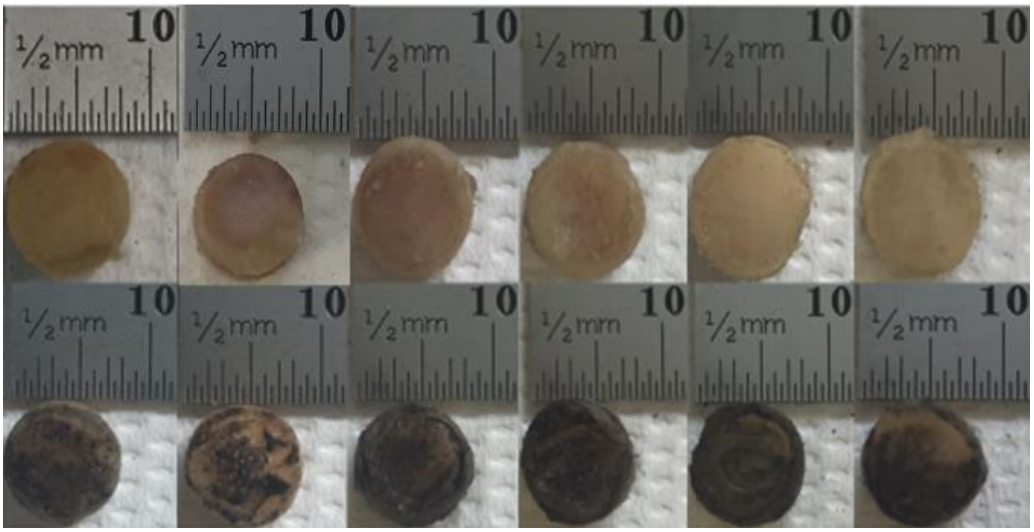

Results for on-bone cartilage at 10 Hz of testing on substrate four.

Appendix D – Hertzian Contact Calculations for Chapter 3

Substrate 1 and off-bone cartilage contact:

= $\left[\frac{1}{E^*} = \frac{1-(0.44^2)}{10} + \frac{1-(0.30^2)}{407.33}\right]$ therefore $\boldsymbol{E^* = 12.07\ MPa}$

= $a = \left(\frac{3.50.(5.5)}{4.(12.07)}\right)^{\frac{1}{3}}$ **therefore** $\boldsymbol{a = 2.58\ mm}$

= $P_o = \frac{3.50}{2\pi 2.58^2}$ **therefore** $\boldsymbol{P_o = 3.59\ MPa}$

Substrate 2 and off-bone cartilage contact:

= $\left[\frac{1}{E^*} = \frac{1-(0.44^2)}{10} + \frac{1-(0.30^2)}{930.04}\right]$ therefore $\boldsymbol{E^* = 12.25\ MPa}$

= $a = \left(\frac{3.50.(5.5)}{4.(12.25)}\right)^{\frac{1}{3}}$ **therefore** $\boldsymbol{a = 2.56\ mm}$

= $P_o = \frac{3.50}{2\pi 2.56^2}$ **therefore** $\boldsymbol{P_o = 3.64\ MPa}$

Substrate 3 and off-bone cartilage contact:

= $\left[\frac{1}{E^*} = \frac{1-(0.44^2)}{10} + \frac{1-(0.30^2)}{2090.87}\right]$ therefore $\boldsymbol{E^* = 12.33\ MPa}$

= $a = \left(\frac{3.50.(5.5)}{4.(12.33)}\right)^{\frac{1}{3}}$ **therefore** $\boldsymbol{a = 2.56\ mm}$

= $P_o = \frac{3.50}{2\pi 2.56^2}$ **therefore** $\boldsymbol{P_o = 3.64\ MPa}$

Substrate 4 and off-bone cartilage contact:

= $\left[\frac{1}{E^*} = \frac{1-(0.44^2)}{10} + \frac{1-(0.30^2)}{3310.22}\right]$ therefore $\boldsymbol{E^* = 12.36\ MPa}$

= $a = \left(\frac{3.50.(5.5)}{4.(12.36)}\right)^{\frac{1}{3}}$ **therefore** $\boldsymbol{a = 2.56\ mm}$

= $P_o = \frac{3.50}{2\pi 2.56^2}$ **therefore** $\boldsymbol{P_o = 3.64\ MPa}$

Appendix E – Simple Computational Model for Chapter 3

Overall methods

A simplified two-dimensional finite element model of cartilage was generated using COMSOL Multiphysics software (version 5.3, COMSOL Inc., Burlington, USA). The cartilage was modelled as resting on a substrate, with the stainless-steel indenter positioned above the cartilage to simulate the application of 50 N to match the maximum force utilised in the experimental work. This was set as a force per unit area boundary load onto the surface of the cartilage, applied as 2.35 MPa. The layered approach is similar to a finite element model previously designed to represent a synovial joint (Dar and Aspden, 2003). The model was solved with a steady-state solver. Cartilage was modelled as a homogenous elastic material with a Young's modulus of 10 MPa, which is comparable to literature (Barker and Seedhom, 2001; Edelsten *et al*., 2010; Shepherd and Seedhom, 1999). The Poisson's ratio of articular cartilage was taken as 0.44, as an average from the range stated in literature of 0.37 - 0.50 (Jurvelin *et al*., 1997). The subchondral bone was modelled with a Young's modulus of 5700 MPa (Mente and Lewis, 1994). The material properties utilised for the components of both the off- and on-bone cartilage model are summarised in the Table below. See Table 3.1 in Chapter 3 for the material details of each substrate utilised for the construction of the finite element analysis. The sides of the substrate, bone and cartilage were free to move, whilst the base of the substrate was fixed in all directions (see Figures in this section). No boundary conditions associated with contact were applied between the cartilage-bone, bone-substrate nor cartilage-substrate interfaces. A free triangular mesh of size extra fine was utilised. The mesh details are shown in the Table in this section.

Table to summarise the material properties utilised for the indenter and cartilage off- and on-bone components to generate the finite element analysis on COMSOL Multiphysics software

Material Property	Indenter	Cartilage off-bone	Cartilage on-bone
Poisson's ratio	0.30	0.44	0.44
Young's modulus (MPa)	200000	10	10
Density (g/cm^3)	7.87	1.05	1.33

Table to summarise the details on the mesh size utilised for the off- and on-bone cartilage finite element analysis on COMSOL Multiphysics software

Mesh Size	Cartilage off-bone	Cartilage on-bone
Triangular elements	1061	1215
Mesh vertices	601	685

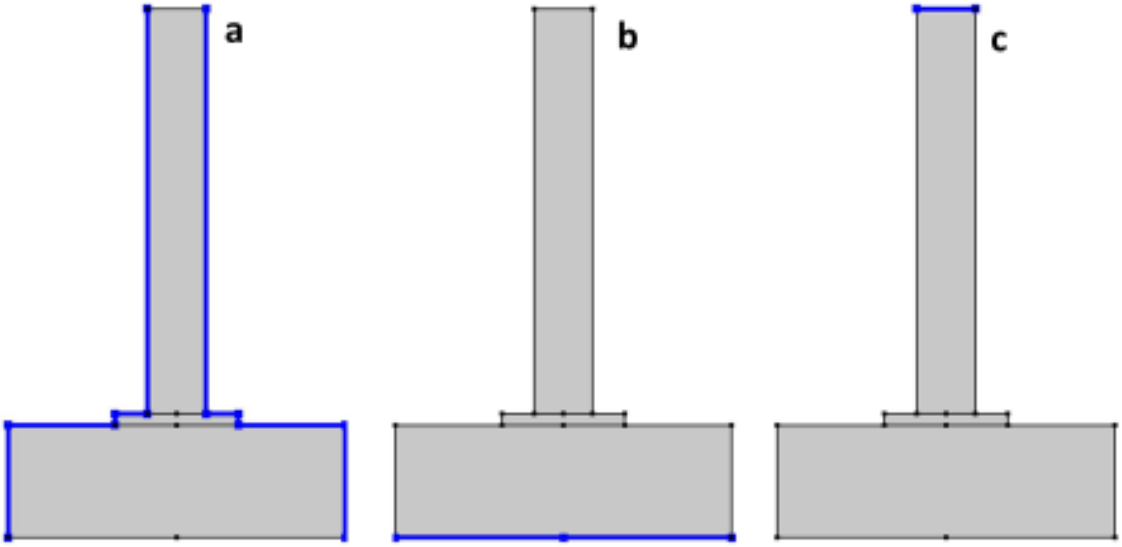

The boundary conditions associated with the cartilage off-bone model extracted from COMSOL Multiphysics software. a) free, b) fixed constraint and c) boundary load

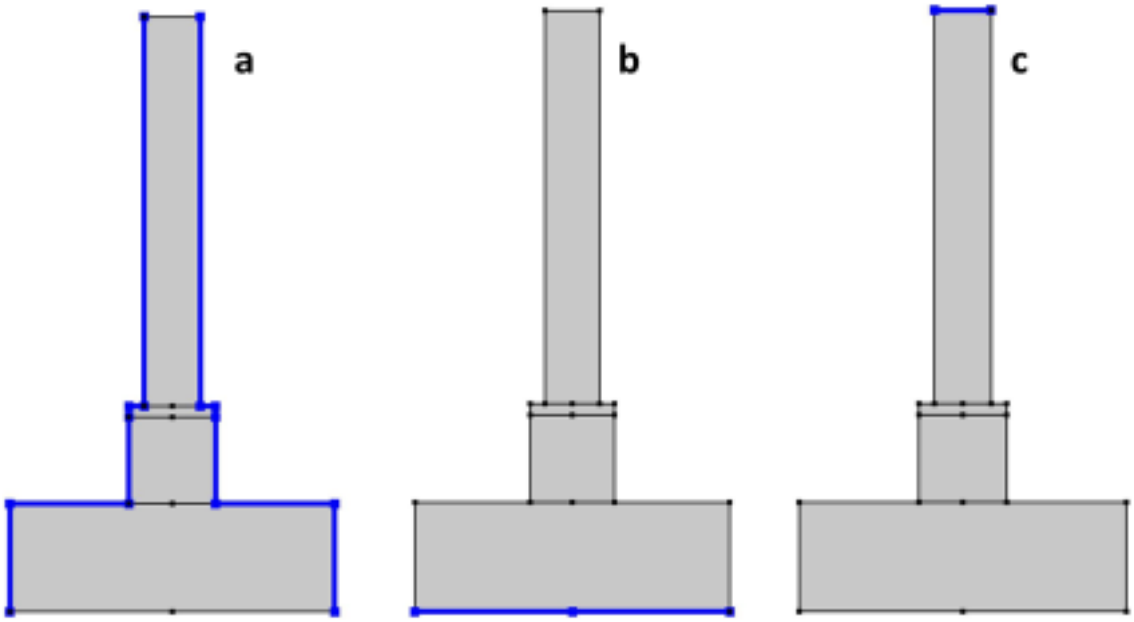

The boundary conditions associated with the cartilage on-bone model extracted from COMSOL Multiphysics software. a) free, b) fixed constraint and c) boundary load

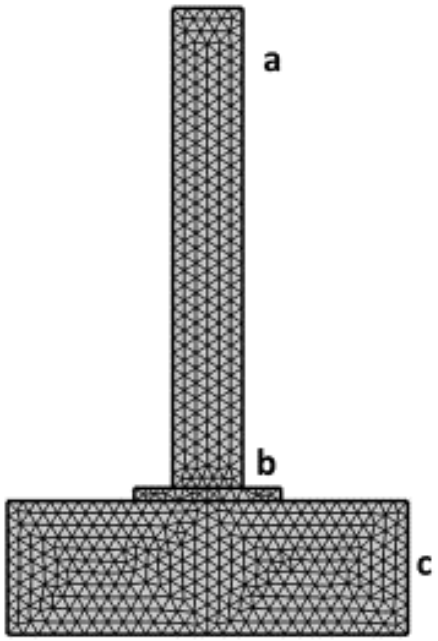

The free triangular mesh of size extra fine used for the finite element analysis of the cartilage off-bone model extracted from COMSOL Multiphysics Software. a) indenter, b) cartilage off-bone specimen and c) substrate

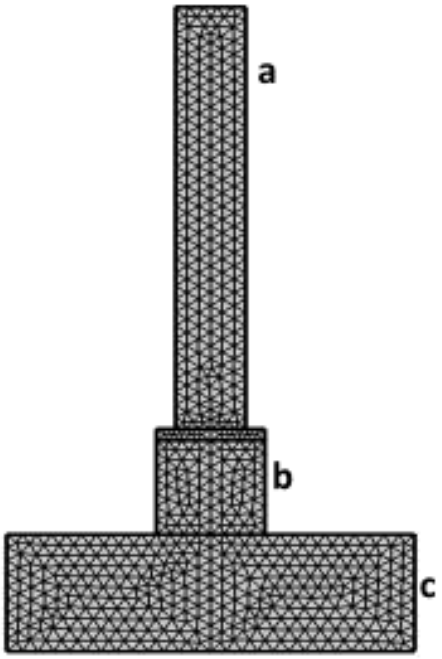

The free triangular mesh of size extra fine utilised for the finite element analysis of the cartilage on-bone model extracted from COMSOL Multiphysics Software. a) indenter, b) cartilage on-bone specimen and c) substrate

The maximum values for von Mises stress were analysed at the upper central position of the off- and on-bone cartilage, as highlighted by the position of the red dot on the Figure below. This area was specifically selected for the consistent identification of the maximum value across both the off- and on-bone cartilage models, with respect to the direct effect of substrate density. The extracted results are displayed in the Table shown later in this section. Additionally, analysis of the displacement across a cut-through of the cartilage; off- and on-bone, including the underlying substrate was computed.

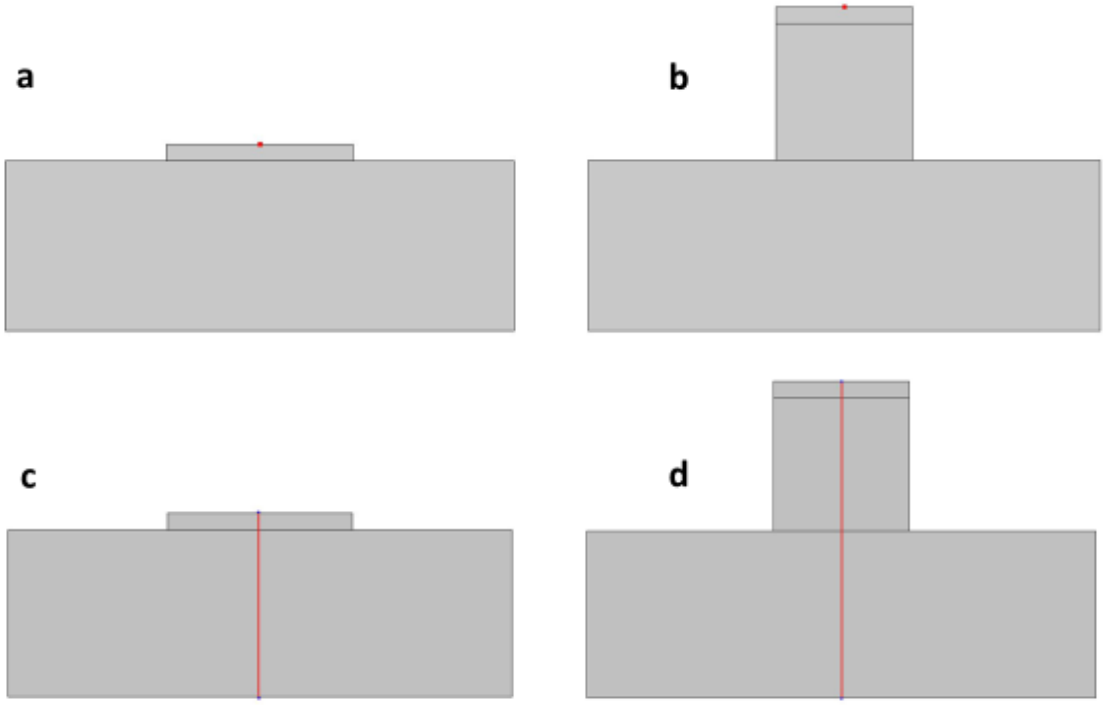

The method of extraction of the von Mises stress at the upper central position of the off- and on-bone cartilage, is shown in parts a) and b), respectively. The representation of the method of extraction of the displacement at a central cut-through for the off- and on-bone cartilage, is shown in parts c) and d), respectively.

Computational Results

The maximum von Mises stress generated from COMSOL Multiphysics software at the upper central position of the off-bone cartilage was found to increase by 4.08 %, from 0.49 to 0.51 MPa, with an increase in substrate density. At all substrates investigated, the region of higher stress within the cartilage was observed beneath the position of contact with the indenter, to include the observation of peak stress concentration towards the left-hand side of this area. The minimal computed stress is observed within the outer regions of the cartilage, the region exempt from the load applied with the indenter. The total maximum von Mises stress computed within the substrate was found to decrease by 1.93 %, from 2.07 to 2.03 MPa, as substrate density increase. The observed maximum stress in the substrate is directly beneath the off-bone cartilage, below which the stress is then shown to decline through the depth of the substrate. Minimal stress within the substrate was observed surrounding the outer region. This trend within the substrate was observed for all substrate densities investigated.

For cartilage on-bone, the von Mises stress computed at the upper central position was found to remain at a constant 0.18 MPa, as substrate density increases. The maximum region of stress was predicted at the corners of the interface between the indenter and the on-bone cartilage. Minimal stress was observed beyond this region throughout the on-bone cartilage. These observations are demonstrated with respect to all substrate densities investigated. The total maximum von Mises stress computed within the substrate was found to decrease by 5.28 %, from 2.84 to 2.69 MPa, as substrate density increases. The observed maximum stress in the substrate was located at the corners of the interface with the subchondral bone. Minimal stress within the substrate was observed beneath this region as well as amongst the outer surrounding area. This trend within the substrate was observed for all substrate densities investigated.

The total maximum von Mises stress computed within the bone was observed to be greater than both the on-bone cartilage as well as the substrate. This has shown to reduce by 31.31 %, from 4.95 to 3.40 MPa, as substrate density increases. The region of the minimal stress within the bone was observed at the interface region with the overlying cartilage.

From the results obtained, it can, therefore, be identified that an increase in substrate density leads to a greater maximum von Mises stress within the off-bone cartilage, located at the upper central point. This result was in contrast to a constant von Mises stress generated at this location at the on-bone cartilage, with an increase in substrate density. For the instance of on-bone cartilage, the absence of the effect of the substrate can be linked towards the presence of the underlying subchondral bone that takes presidence over the substrate, as demonstrated by a greater maximum von Mises stress within the bone, in comparison to both the on-bone cartilage as well as substrate. In addition, the increase in the von Mises stress within the off-bone cartilage as substrate density increases, can be linked towards the decline in the maximum von Mises stress computed within the substrate, beneath the off-bone cartilage specimen itself, as the density increased.

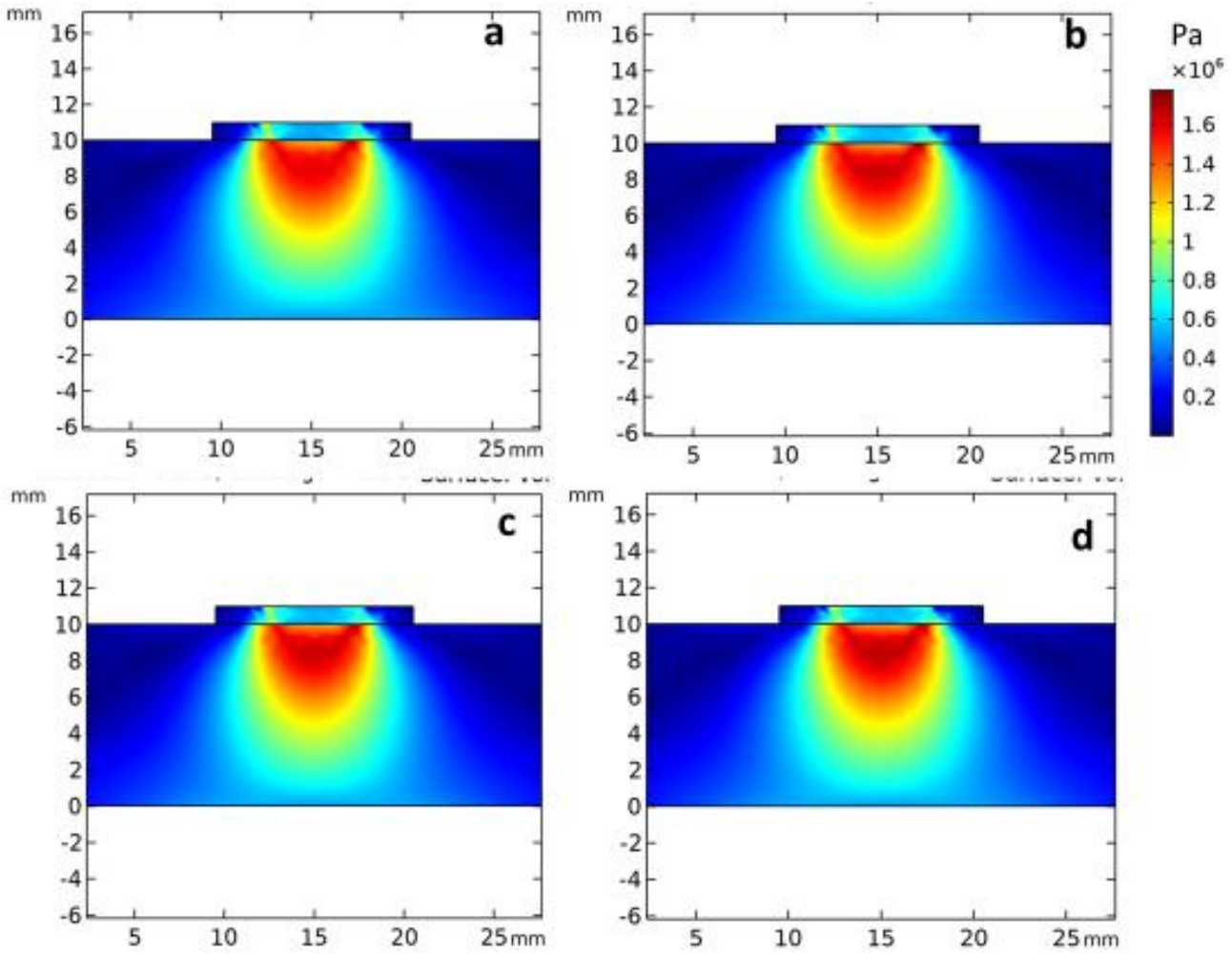

Finite element analysis result computed for the internal von Mises stress of cartilage off-bone with respect to all substrates evaluated; a) substrate one, b) substrate two, c) substrate three and d) substrate four. The coloured scale bar on the right-hand side extracted from COMSOL Multiphysics software displays the extent of the von Mises stress presented in Pa. The substrate is modelled from a thickness of 0-10 mm; the cartilage at 10-11 mm. Model generated with a deformation scale of 0.

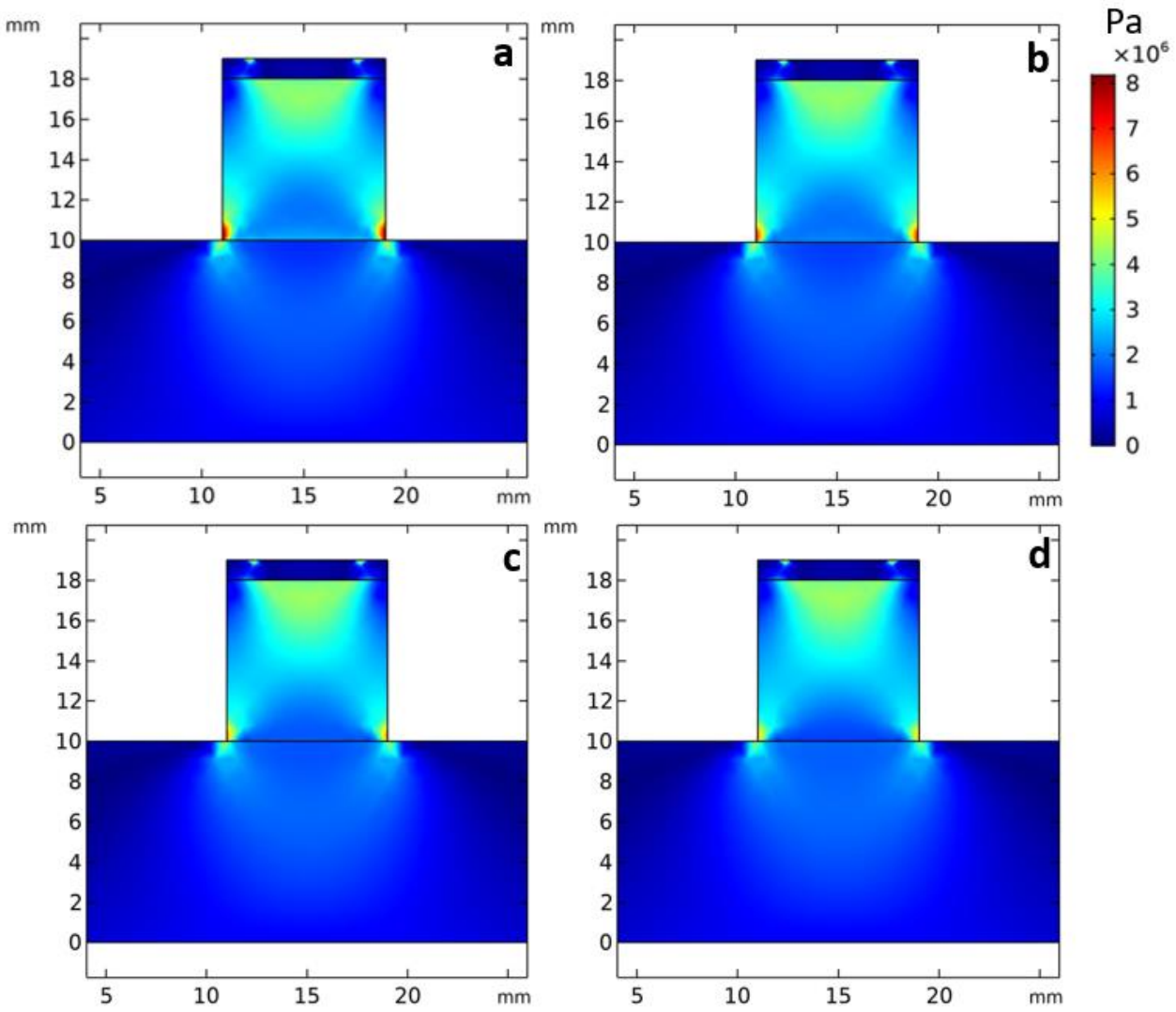

Finite element analysis result computed for the internal von Mises stress of cartilage on-bone with respect to all substrates evaluated; a) substrate one, b) substrate two, c) substrate three and d) substrate four. The coloured scale bar on the right-hand side extracted from COMSOL Multiphysics software displays the extent of the von Mises stress presented in Pa. The substrate is modelled from a thickness of 0-10 mm, the subchondral bone at 10-18 mm and the cartilage at 18-19 mm. Model generated with a deformation scale of 0.

Values for the von Mises stress extracted at the upper central point on the cartilage, both on- and off-bone. Values are presented in MPa.

Analysis at upper central position on cartilage on- and off-bone taken as maximum value	**von Mises stress (MPa)**	
Substrate	**Off-bone**	**On-bone**
1	0.49	0.18
2	0.50	0.18
3	0.50	0.18
4	0.51	0.18

The maximum von Mises stress values extracted at the underlying substrate, for both on- and off-bone cartilage with respect to all substrates investigated. All stresses are presented in MPa.

	Maximum von Mises stress at substrate surface (MPa)	
Substrate	**On-bone**	**Off-bone**
1	2.84	2.07
2	2.81	2.05
3	2.74	2.04
4	2.69	2.03

The maximum von Mises stress values extracted at the subchondral bone, with respect to all substrates investigated. All stresses are presented in MPa.

Substrate	Maximum von Mises stress at bone surface (MPa)
1	4.95
2	4.36
3	3.71
4	3.40

The maximum displacement predicted within both the off- and on-bone cartilage was shown to decline by 27.27 %, from 0.11 to 0.08 mm, as substrate density increased. The region of the maximum displacement within both the off- and on-bone cartilage was observed at the upper surface in contact with the indenter. Minimal displacement was observed within the regions not in contact with the indenter. For the case of cartilage on-bone, the minimum displacement was predicted to decline from 0.02 to 0.00 mm, with an increase in substrate density. For off-bone cartilage, a reduction from 0.01 to 0.00 mm was observed as substrate density is increased. Displacement within the cartilage was, therefore, at its maximum at the substrate with the lowest density, and at the least for the substrate with the highest density.

Graphical results for the cut-through of the displacement through the centre of the surface of the cartilage off- and on-bone, are also shown in this section. The off- and on-bone cartilage are represented from 0-1 mm arc length, followed by the substrate beyond this region in part ‘a’ for the off-bone cartilage model. In the instance of on-bone cartilage, part ‘b’, the subchondral bone is shown from 1-9 mm arc length, followed by the underlying substrate beyond this region. Substrate one, that of the lowest density, was represented by the dark blue

line, following through to substrate four, that of the highest density, represented by the light blue coloured line. Displacement for off-bone cartilage is observed from 0 to 0.103 mm; -whilst a range of 0 to 0.10 mm is observed for on-bone cartilage. For the case of both off- and on-bone cartilage, similar to the result of the maximum displacement observed to decline within the cartilage as the substrate density increased; the cut-through displacement is also observed to reduce with an increase in substrate density.

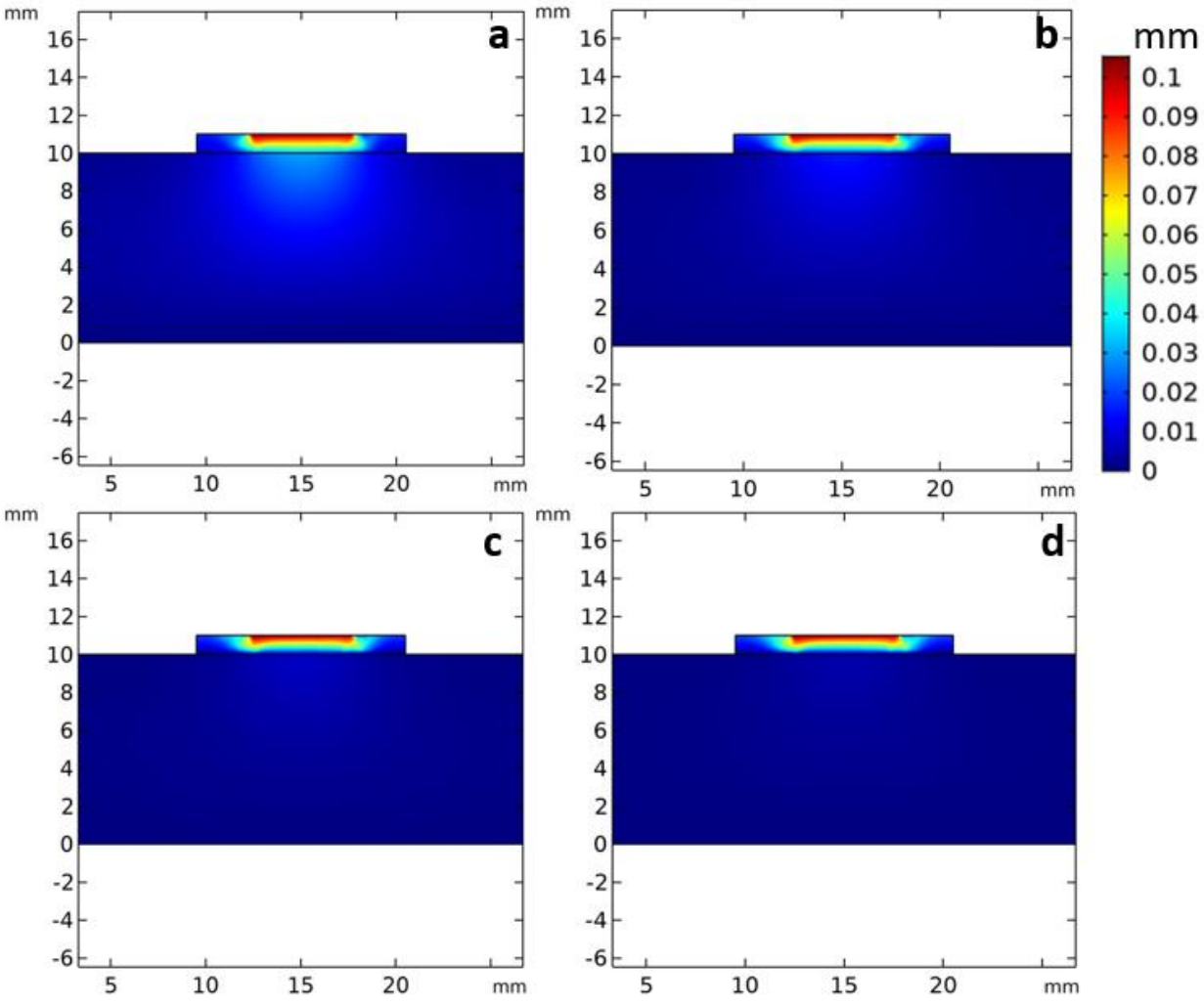

Finite element analysis result computed for the internal displacement of cartilage off-bone with respect to all substrates evaluated; a) substrate one, b) substrate two, c) substrate three and d) substrate four. The coloured scale bar on the right-hand side extracted from COMSOL Multiphysics in displays the extent of the displacement presented in mm. The substrate is modelled from a thickness of 0-10 mm and the cartilage at 10-11 mm. Model generated with a deformation scale of 0.

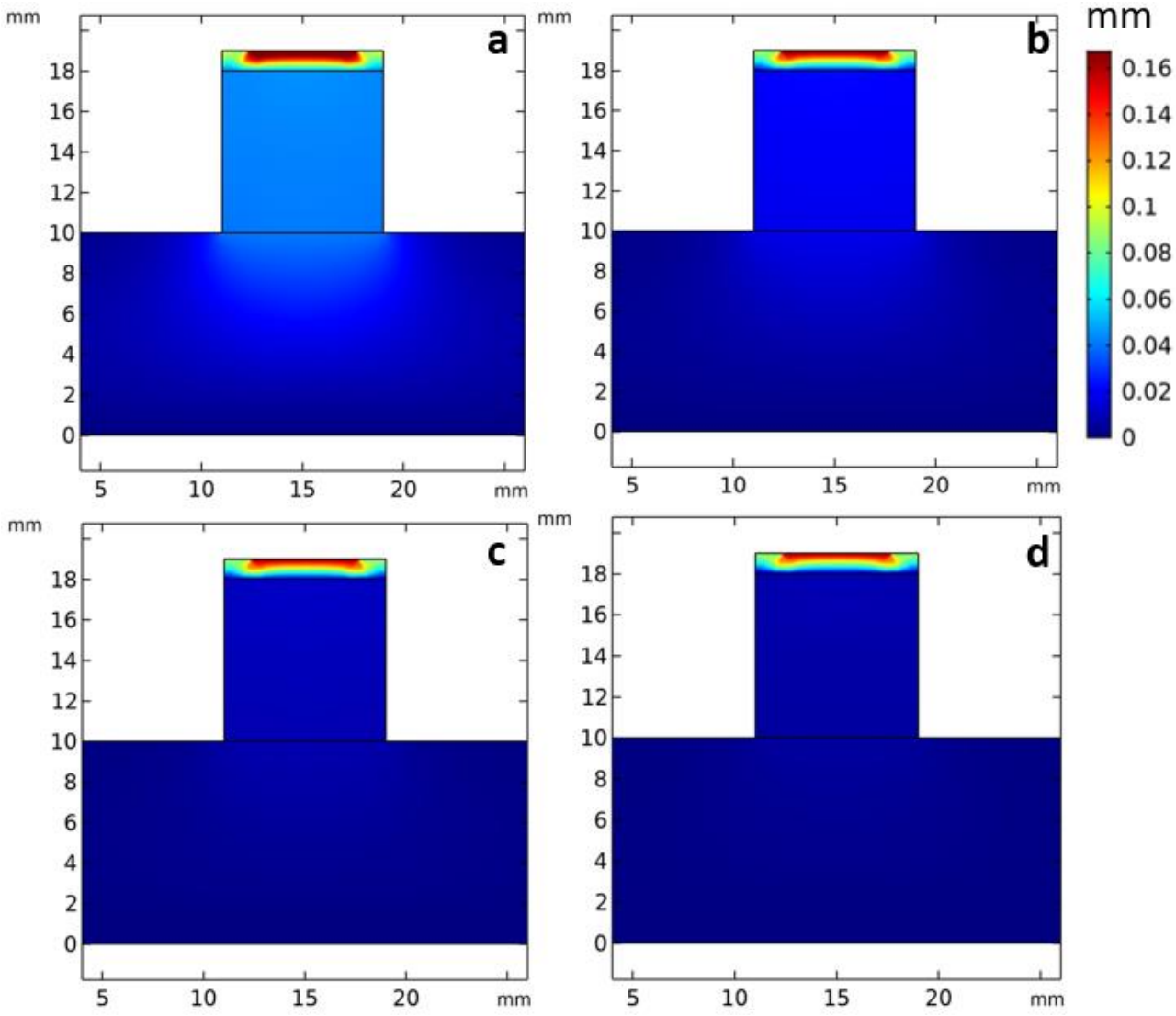

Finite element analysis result computed for the internal displacement of cartilage on-bone with respect to all substrates evaluated; a) substrate one, b) substrate two, c) substrate three and d) substrate four. The coloured scale bar on the right-hand side extracted from COMSOL Multiphysics software displays the extent of the displacement presented in mm. The substrate is modelled from a thickness of 0-10 mm, the subchondral bone at 10-18 mm and the cartilage at 18-19 mm. Model generated with a deformation scale of 0.

The displacement values extracted at the cartilage surface for both on- and off-bone cartilage with respect to all substrates investigated. All values are presented in mm

	Maximum total displacement at cartilage surface (mm)		**Minimum total displacement at cartilage surface (mm)**	
Substrate	**On-bone**	**Off-bone**	**On-bone**	**Off-bone**
1	0.11	0.11	0.02	0.01
2	0.09	0.09	0.01	0.00
3	0.09	0.08	0.01	0.00
4	0.08	0.08	0.00	0.00

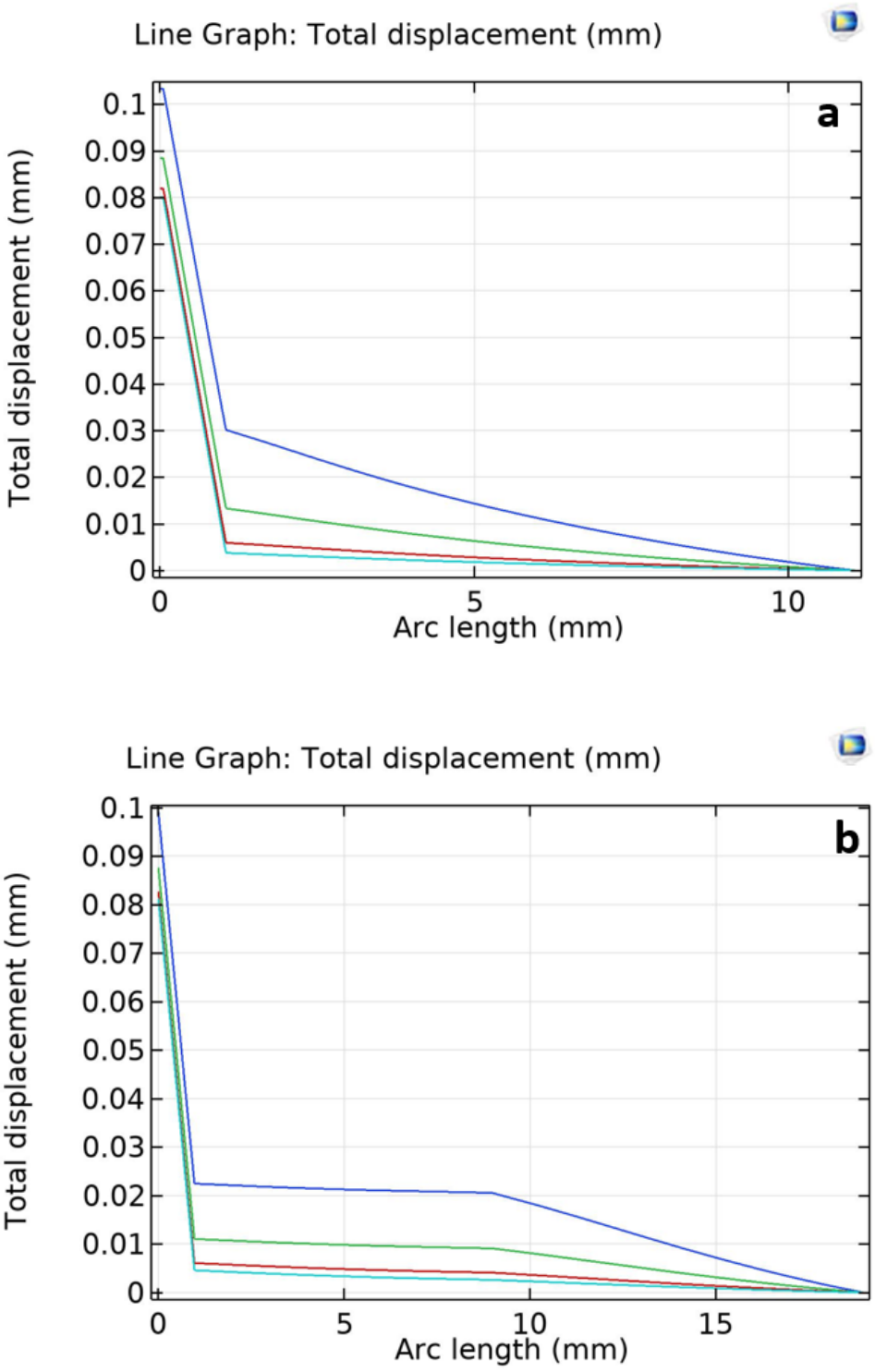

Graphical illustration generated from COMSOL Multiphysics software for the resulting cut-through to investigate total displacement. a) cut-through displacement at cartilage off-bone model, with the cartilage at arc length 0-1 mm, and the underlying substrate at the arc length beyond this. b) cut-through displacement at cartilage on-bone model, with the cartilage at arc length 0-1 mm, the subchondral bone at arc length 1-9 mm and the underlying substrate at the arc length beyond this. Each substrate is represented by the coloured lines as follows: substrate one = dark blue, substrate two = green, substrate three = red and substrate four = light blue

Appendix F - Preliminary Experiments for Chapter 4

Initial preliminary tests involved the evaluation of the frictional torque of ten different articular cartilage specimens, one specimen per load. On maximum load application of 100 N, surface depressions observed on the articular cartilage were reversible with addition of Ringer's solution, hence, not categorised as damage, but rather creep behaviour. Thus, based on preliminary tests, 100 N was identified as the suitable maximum load of testing. Corresponding to the 1:10 relationship as used for the protocol in Chapter 3, a load range of 10 - 100 N was adopted, for the torque test of both the articular cartilage as well as the biomaterial, to enable a comparable evaluation. The rotation of 2° is representative of internal hip movements, thus an interesting range to examine for the articular cartilage/hydrogel specimens presented in the chapter.

A representative plot of the last ten cycles to represent the torque with respect to time is displayed in the Figure below. For analysis, the maximum point highlighted as '*a*' and the minimum point annotated as '*b*', were extracted across all ten curves from the plot, and a torque average calculated. This procedure was applied for each plot produced for all repeats of the preliminary tests performed on individual articular cartilage specimens. Thus, an overall mean value was extracted from the procedure repeats, per load. The mean maximum and minimum torque were then plotted against the load, as represented in part a) and b) of the following two Figures, respectively.

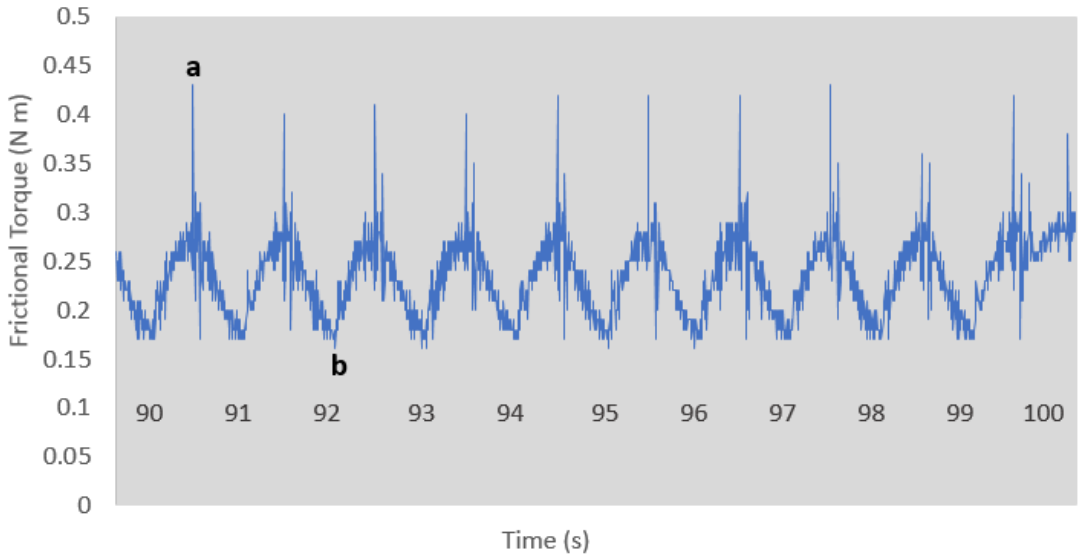

Preliminary protocol illustration for the assessment of the frictional torque: the maximum and minimum torque were extracted as points ‘a’ and ‘b’ respectively, from each curve of the last 10 curves, to represent the last 10 cycles from the test. The mean value was then calculated and the process repeated per load, for every specimen repeat.

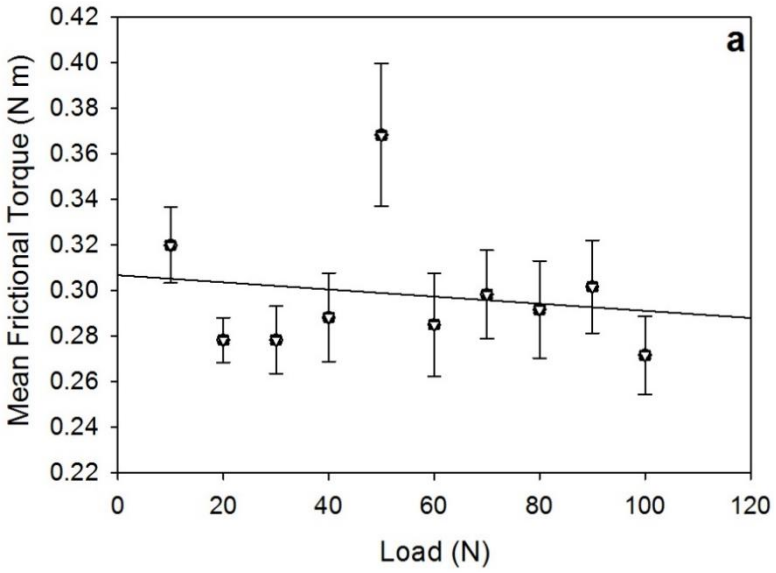

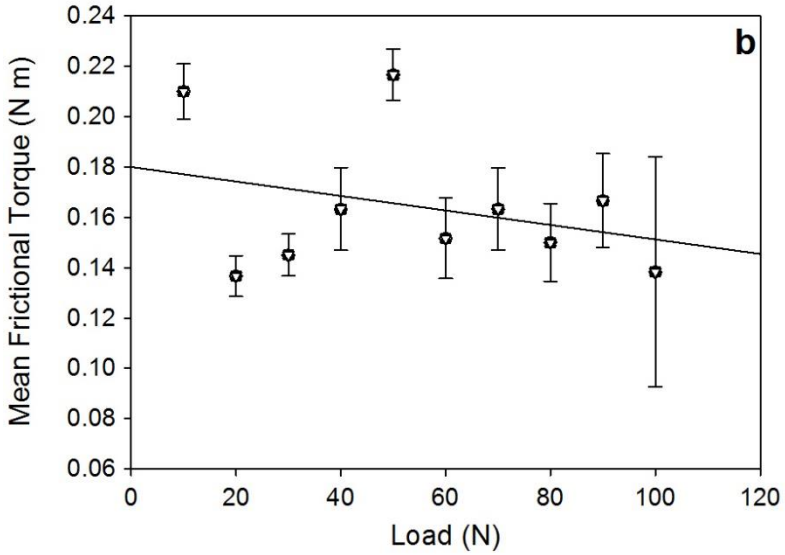

The plots represent the overall mean calculated across ten different specimens, where each specimen is subject to loads 10-100 N. a) mean maximum frictional torque and b) mean minimum frictional torque, extracted from the last 10-cycle period of the test. Error bars represent standard deviations.

There were large variations above and below the linear regression line to represent the torque with respect to load, for both the maximum and minimum torque of the Figure parts a) and b), respectively. This is therefore due to the use of a different cartilage specimen, for a given load. In addition, based on the concept of friction, it is an expected outcome for the frictional torque to increase with load. However, the preliminary tests performed in this manner did not produce such an outcome, rather, as displayed by the Figure of parts a and b, a decline in the torque was observed with load. Consequently, for the final protocol of the cartilage/cartilage-hydrogel/hydrogel specimens, it was decided to perform the repeated torque test on a single specimen, across all ten loads, from which the overall mean is extracted. In addition, the 'noise' amongst the torque against time plot created ambiguity in the extraction of the torque for final analysis. Thus, this indicated the need for the development of a consistent torque calculation method, as detailed in Chapter 4.

Appendix G - Specimen Surface Evaluation for Chapter 4

A photographic image of a representative cartilage on-bone specimen post-test is presented in this section of the Appendix. The impacted region due to contact with the indenter is identified with a red arrow, and as can be observed, this region appears darker in tone than its surrounding articular cartilage. The microscopic image of this specimen is presented next to this image, with the region in contact with the indenter outlined with the red dashed-line circumference. It appears that most of the impact has occurred at the left- and right-hand side of the indenter region, identified by the darkest tone regions, highlighted by the red circles.

As shown by the next Figure in this section, following axial rotation the 2 mm hydrogel insert indicated by the red arrow appears to display an inconsistent roughening of the surface, in comparison to the surrounding articular cartilage. This is due to the hydrogel structure that appears to have damaged and torn across the surface, as a result of subjection to the impact via the indenter. For the evaluation of the hydrogel alone, surface damage as can be observed visually in the third Figure of this section, displays a broken structure due to teared regions. This damage is identified by the black patch regions outlined by the red circles in the microscopic image.

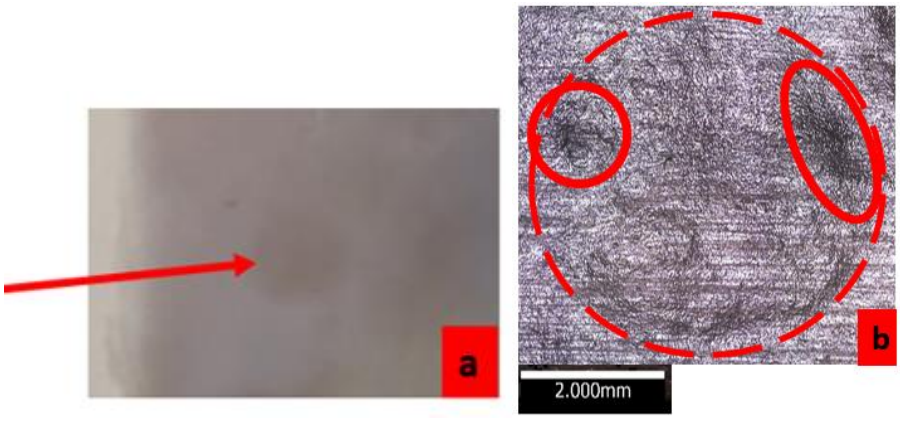

Cartilage on-bone specimen post-test imaging. Part a) photographic image captured with iPhone to illustrate the resulting indent on the surface of the specimen highlighted by the red arrow. This region is darker than the surrounding articular cartilage specimen not in contact with the indenter for testing. Part b) displays the microscopic imaging performed at a scale bar of 2 mm and magnification 5X of the specimen represented in part a). The indented region post-test on the microscopic image is outlined with the red dashed-line zone. The red circles indicate the maximum impacted regions at either side of the indented zone.

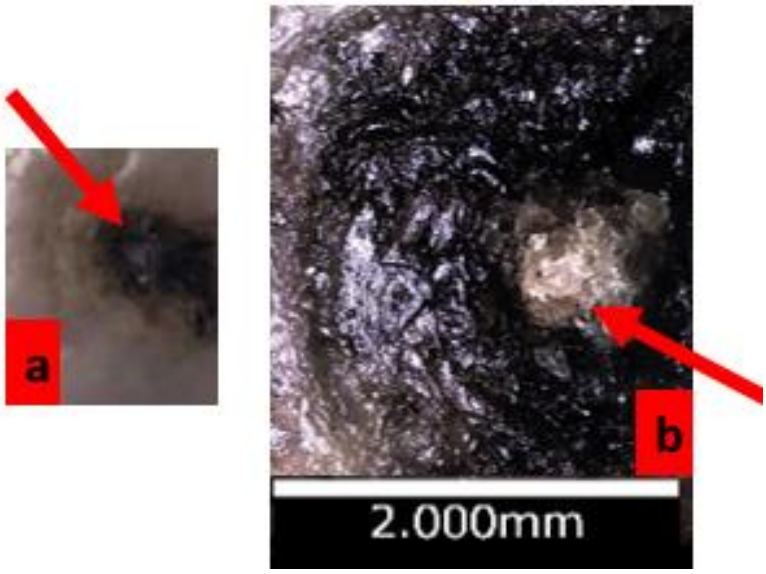

Cartilage on-bone specimen with 2 mm calcium alginate insert post-test imaging. Part a) photographic image captured with iPhone to illustrate the 2 mm hydrogel insert highlighted by the red arrow. A microscopic image of this region is displayed in part b) highlighted by the red arrow, at a scale bar of 2 mm and magnification 5X. The calcium alginate biomaterial is damaged, and broken above the cavity surface as displayed in the microscopy image of part b. The black staining surrounding is of India ink utilised for identifying the location of the indenter in contact with the specimen surface, to enable detection of the region to insert the biomaterial for testing.

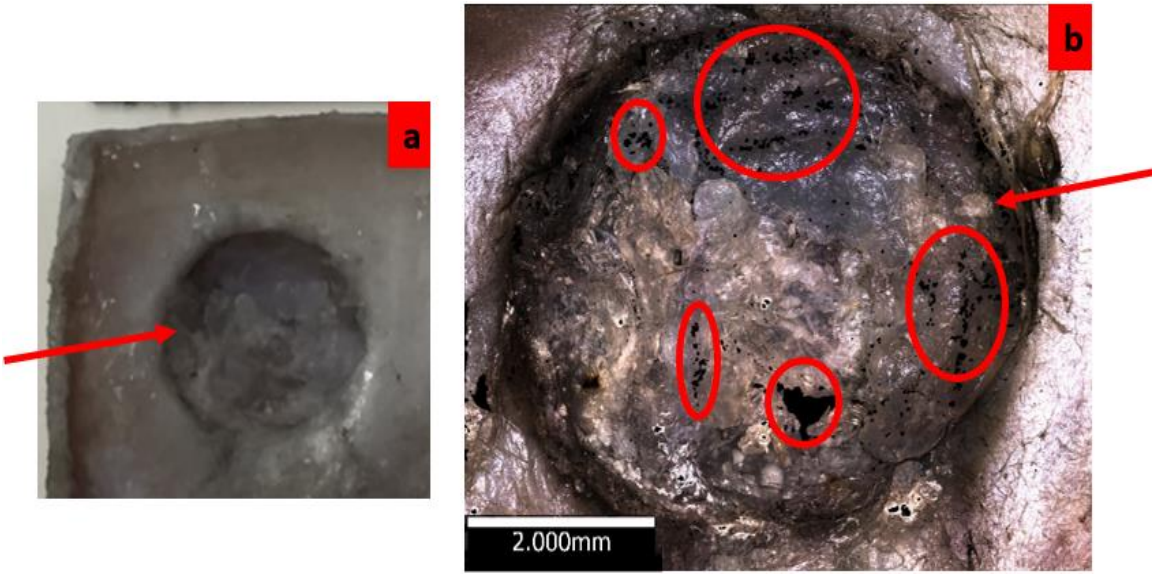

10 mm calcium alginate insert post-test imaging. Part a) photographic image captured with iPhone to illustrate the hydrogel indicated by the red arrow. The insertion is pushed within the cavity, as well as subject to surface tears. Damage is also apparent via the irregular surface structure. Part b) represents the microscopic image of the 10 mm calcium alginate specimen insert displayed in part a) at a scale bar of 2 mm and magnification 5X. Red regions highlighted on part b) represent the damage regions observed visually in part a) illustrated as black shaded zones where the microscope did not capture material due to tears.

Appendix H - Preliminary Experiments for Chapter 5

For the development of the protocol for insertion of the biomaterial within a cartilage surface defect, two hydrogel sythesis methods were initially conducted. Firstly, aluminium rectangular test rigs were manufactured as shown below.

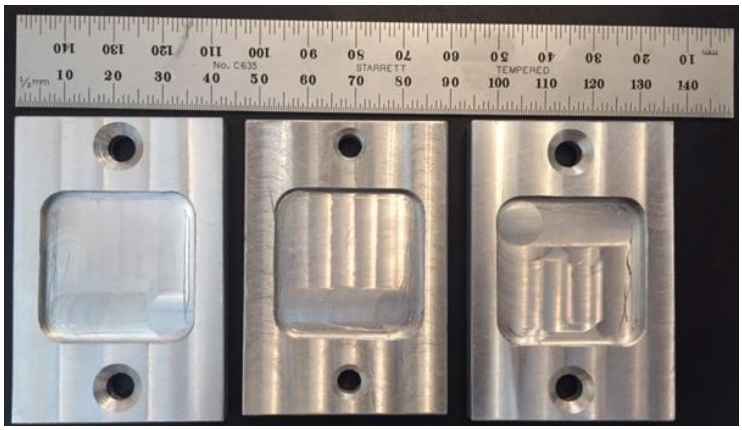

Customised aluminium test-rig manufacture to contain hydrogel for preliminary testing

Method i) consists of synthesising the calcium alginate hydrogel within the aluminum test-rig. As shown in part ‘a’, both the sodium alginate and calcium chloride dihydrate solutions were inserted within the well of the rig. Part ‘b’ illustrates the mixed solutions covered with cling-film prior to setting. The final calcium alginate hydrogel is shown in part ‘c’, post setting. It is clear from part ‘c’ the formed hydrogel adopts an inconsistent configuration, thus, proving difficult as a lower specimen for friction tests in sliding. This led onto method ii) for hydrogel synthesis.

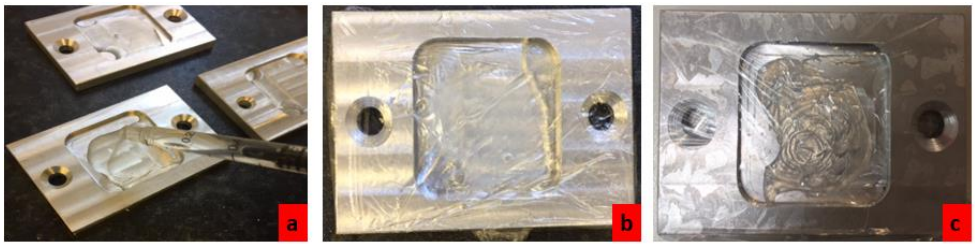

Method i) biomaterial synthesis procedure. a) synthesis of biomaterial, b) pre-setting and c) post-setting of biomaterial

Method ii) is illustrated in the Figure below. The sodium alginate and calcium chloride dihydrate solutions are combined on an aluminum sheet, shown in part ‘a’. A second aluminum sheet is placed ontop of this formed solution, to allow for the compression of the two sheets via securing in a vice (part ‘b’). Post-setting, the synthesised biomaterial is displayed in part ‘c’, from which a square segment is cut out and glued to the well of the aluminum test-rig (part ‘d’). Following preliminary friction tests of a upper cartilage core sliding against the lower biomaterial (part ‘d’), the end result identified a tear amongst the central region of the biomaterial, indictaed by the red arrow in part ‘e’. Thus, both method i) and ii) failed to produce sufficient biomaterial counterparts adequate for friction tests in sliding. This led onto the development of the procedure for the articular cartilage to contain the biomaterial, demonstrated via the insertion into an ariifical surface defect.

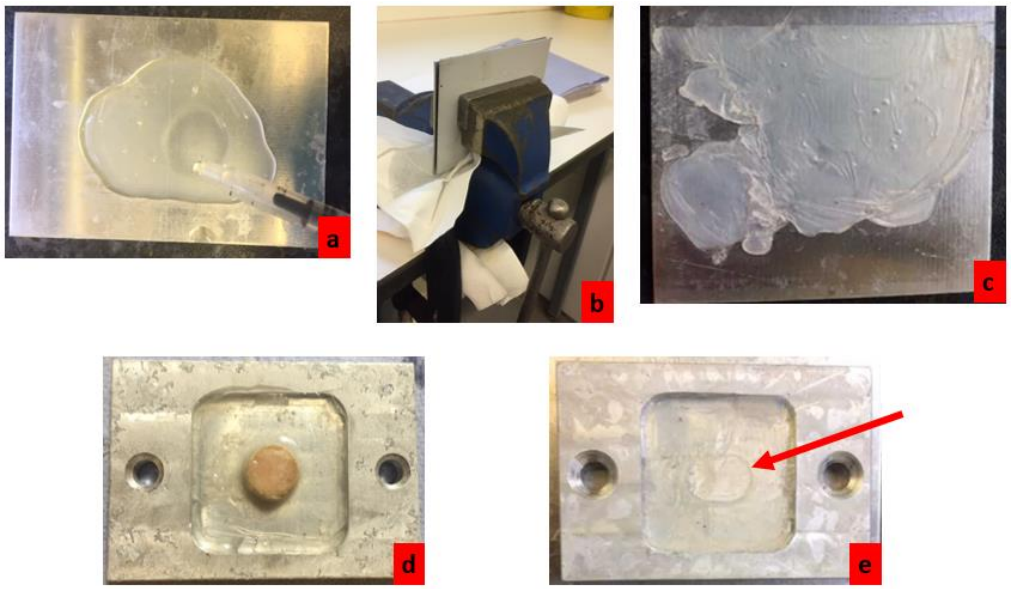

Method ii) biomaterial synthesis procedure. a) biomaterial synthesis to allow for compression setting with additional aluminium plate in vice, shown in part b). The formed biomaterial post-setting is displayed in part c) followed by the preliminary test set-up of upper cartilage core in position on lower biomaterial for friction in sliding, shown in part d). The end-result displays tearing of the biomaterial indicated by the red arrow in part e).

For determination of the most suitable load to apply for the coefficient of friction tests performed in Chapter 5, calcium alginate hydrogel was subject to compression testing to identify the point of failure. Part ‘a’ of the figure below demonstrates a load of approximately 4.4 N to result in failure, whilst a repeat test displayed in part ‘b’ identifies a higher continuous load threshold at 7 N. Thus, a load value of 5 N was selected as appropriate for conduction of the final experiments.

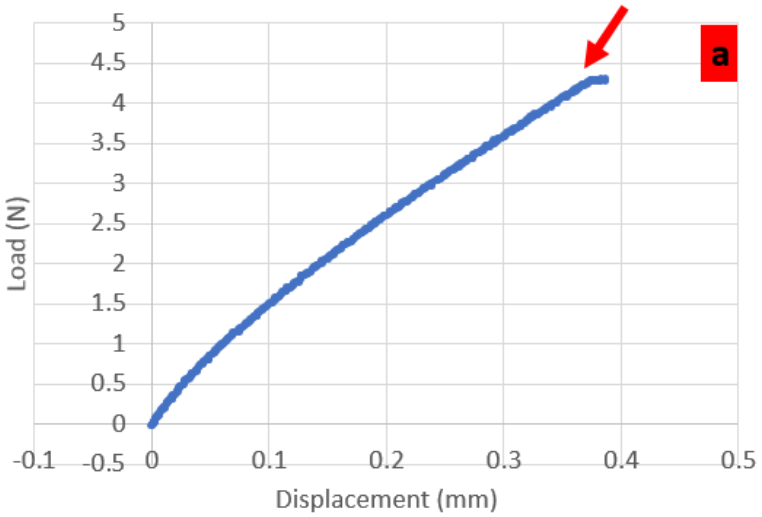

Result of compression test on calcium alginate hydrogel to display failure at approximately 4.4 N, identified by red arrow

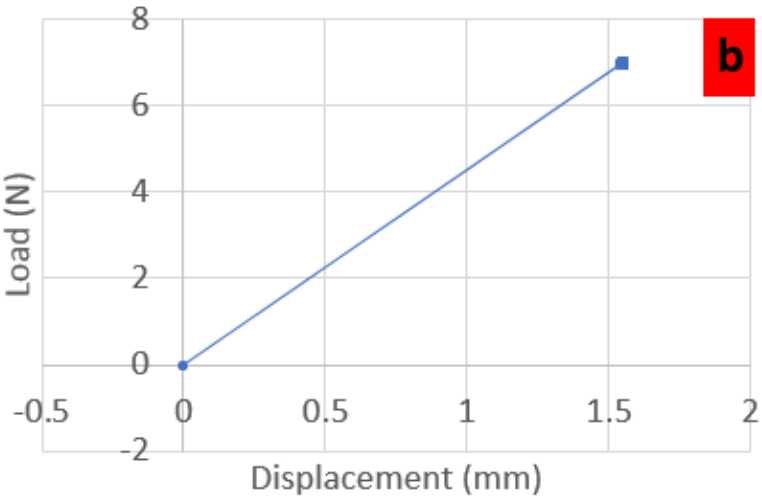

Result of compression test on calcium alginate hydrogel to display continued compression at 7 N

Preliminary friction sliding tests of cartilage against the biomaterial were initially performed at a stroke length of 12.5 mm. An example plot is represented in part ‘a’ Figure below. The large variation indicated the requirement to reduce the stroke length. Thus, a suitable stroke length was selected as 3.832 mm for the final friction experiments. An example plot is shown in part ‘b’ Figure below. A clear improvement to the consistency in the measured coefficient of friction is identified.

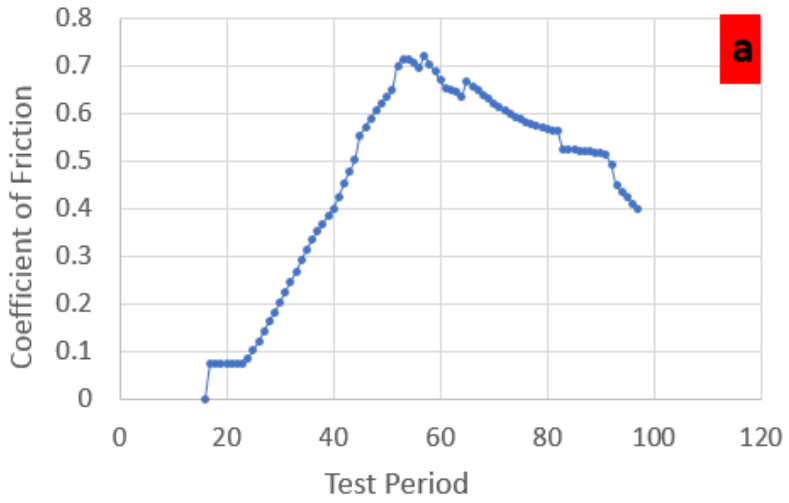

Coefficient of friction plot for preliminary testing of cartilage sliding against hydrogel at stroke length of 12.5 mm

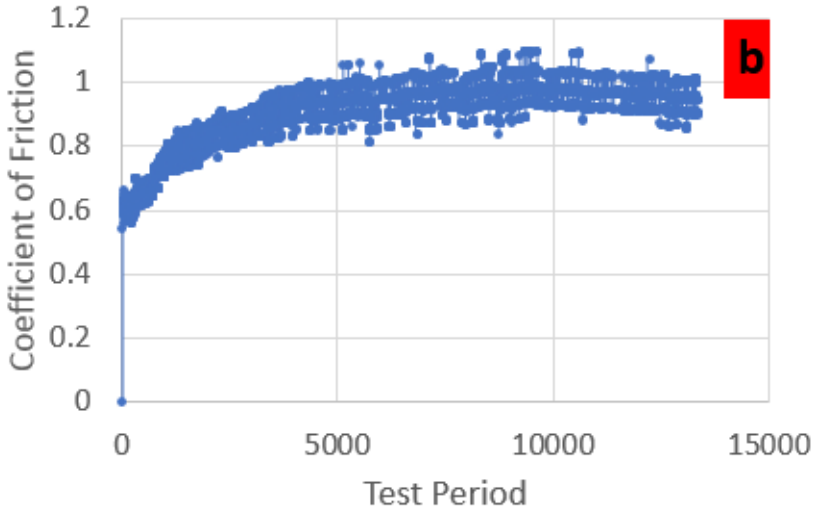

Coefficient of friction plot for revised testing of biomaterial inserted within cartilage defect at stroke length of 3.832 mm